Fire Behaviour of Pultruded Composites

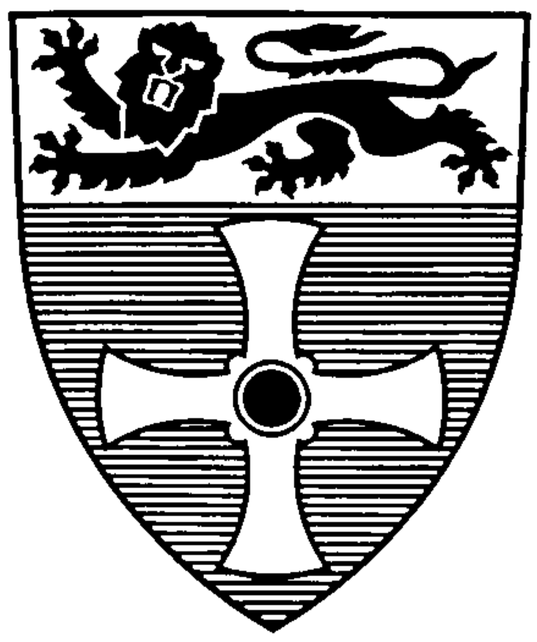

Thesis submitted in accordance with the requirements of the University of Newcastle upon Tyne for the degree of Doctor of Philosophy.

R. C. Easby

Centre for Composite Materials Engineering,
School of Mechanical & Systems Engineering,
University of Newcastle upon Tyne.

May 2007

Acknowledgements

Firstly I would like to express my gratitude to my supervisor, Professor A. G. Gibson, who has provided me with continual support and guidance throughout my studies. I would also like to acknowledge the integral part Dr. Yongshu Wu has played, providing answers to endless questions. Similarly I would like to thank Mr. Ron Jensen for dealing with all of my last minute requests and ideas with good humour, and professionalism.

I also wish to thanks my sponsors, the EPSRC and Fiberline Composites, in particular Mr. Anders Korsgarrd for his constant assistance throughout this project.

Finally I would like to acknowledge the assistance, support and endless patience of my colleagues, family and friends and of course Deb.

Abstract

This thesis describes the development of a model to predict the failure response of loaded pultruded composites in fire. The model takes an existing thermal model [1-9] capable of describing temperature evolution and residual resin content as functions of time through a pultrusion for fires with heat-fluxes up to and including 125kWm^{-2}. Experiments were developed to determine how tensile and compressive strength (σ_T and σ_C), and longitudinal and transverse stiffness (E_1 and E_2) of the composites varied with temperature. This required specialised equipment to be designed and fabricated. The mechanical property data were recorded as functions of temperature and combined with the thermal model and classical laminate theory. The resulting failure model, outputs tensile and compressive strength of the pultrusion as a function of time for fires with heat- fluxes up to and including 125kWm^{-2}. ***A***, ***B***, ***D*** matrix evolution as a function of time is also produced.

The modelling procedure was carried out for polyester and phenolic glass fibre-reinforced pultrusions subjected to a 50kWm^{-2} heat-flux and verified by a series of propane burner tests. The modelled tensile and compressive results match the data from the propane burner tests to a reasonable degree of accuracy. It was shown that the materials were more susceptible to compressive failure rather than tensile failure, when subjected to a fire.

Work on the model was supplemented by a series of larger scale fire tests on box and 'I' sections, including flexure tests in a pool fire and temperature controlled furnace. In both tests it was found that failure occurred on the compressive side of the section, with a failure time in the order of 100 seconds. Compression tests were also carried out on short box columns to investigate the effect various fire protections systems had on failure time of the columns, when surrounded by a heat-flux of 50kW^{-2}. It was found that protecting the loaded section inside an insulating sleeve proved the most successful approach.

ACKNOWLEDGEMENTS 1

ABSTRACT 2

NOMENCLATURE 7

1. INTRODUCTION 9

1.1. Introduction to Composite Materials 9

1.2. Reinforcement Material 9

1.3. Reinforcement Architecture 10
1.3.1. Unidirectional 10
1.3.2. Chopped Strand Mat/Needle Weave 10

1.4. Matrix Material 11
1.4.1. Polyester 11
1.4.2. Phenolic 11

1.5. Pultrusion 11

1.6. Fire Reaction & Fire Resistance 13
1.6.1. Fire Reaction 13
1.6.2. Fire Resistance 13

1.7. Test Procedures 14
1.7.1. Cone Calorimeter (including atmosphere controlled) 15
1.7.2. OSU Heat Release Rate Technique 15
1.7.3. Limiting Oxygen Index (LOI) Test 16
1.7.4. Radiant Panel Test 17
1.7.5. Flame Propagation & Spread Tests 17
1.7.6. Smoke Density 18
1.7.7. Single Burning Item (SBI) Test 19
1.7.8. Room Fire Test 19
1.7.9. Furnace Tests 20
1.7.10. Pool-fire Tests 21
1.7.11. Burner Tests 22
1.7.12. Jet-fire Tests 22

1.8. Thesis Overview 24

1.9. Chapter Summary 25

2. LITERATURE REVIEW 26

2.1. The 'Slow Burn-Through' Effect 26

2.2. Fire Resistance Modelling 27
2.2.1. Response of Composites to Fire 28
2.2.2. 1-D Heat Conduction Model 30
2.2.3. Henderson Model 31
2.2.4. Simplified Henderson Model 32

2.3. Fire Behaviour under Load 32

2.4. Chapter Summary 34

3. THERMAL MODELLING 36

3.1. 1-D Thermal Model 36

3.2. Thermogravimetric Analysis (TGA) Parameters 37

3.3. Propane Burner Test 40

3.4. Rear Face Temperature Profile 42

3.5. Chapter Summary 42

4. MECHANICAL PROPERTIES 44

4.1. Materials 44

4.2. Tensile Strength at Elevated Temperatures 46

4.3. Compressive Strength at Elevated Temperatures 47

4.4. Longitudinal (E_1) & Transverse (E_2) Stiffness at Elevated Temperatures 48

4.5. Chapter Summary 49

5. FIRE TESTING UNDER LOAD 51

5.1. Tensile Tests in Fire 51

5.2. Compression Tests in Fire 52

5.3. Pool Fire Test under Load 55

5.4. Furnace Test under Load 57

5.5. Columns under Compression in Fire 59

5.6. Chapter Summary 61

6. RESULTS 63

6.1. Mechanical Properties 63
- 6.1.1. Problems arising from the Material Cross Section 64
- 6.1.2. Tensile Strength 65
- 6.1.3. Compressive Strength 69
- 6.1.4. Longitudinal (E_1) and Transverse (E_2) Stiffness 71
- 6.1.5. Mechanical Properties vs. Temperature 71

6.2. Fire Testing under Load 78
- 6.2.1. Tensile and Compressive Tests 78
- 6.2.2. Pool Fire test under Load 79
- 6.2.3. Furnace test under Load 81

6.2.4. Columns under compression 82

6.3. Experimental reliability **84**
6.3.1. Mechanical properties at elevated temperatures 84
6.3.2. Fire testing under load 86
6.3.3. Pool fire test under load 87
6.3.4. Furnace test under load 87

7. MODELLING BEHAVIOUR UNDER LOAD 89

7.1. Laminate Constitutive Equations **89**

7.2. Input of Mechanical Properties vs. Temperature **91**
7.2.1. Mechanical Properties of CSM Skins 91

7.3. Results **94**
7.3.1. A, B, D Matrix Evolution 94
7.3.2. Strengths Modelling 99
7.3.3. Tensile Strength Prediction 101
7.3.4. Buckling and Compressive Strength Prediction 103

8. CONCLUSIONS 108

8.1. Propane burner test **108**

8.2. Thermal modelling **108**

8.3. Mechanical properties as a function of temperature **108**

8.4. Fire testing under Load **108**
8.4.1. Tension 108
8.4.2. Compression including intumescents 109
8.4.3. Pool fire test 109
8.4.4. Furnace test 109
8.4.5. Columns including coatings 110

8.5. Modelling **110**
8.5.1. A, B, D Matrix Evolution 110
8.5.2. Tensile Strength Prediction 111
8.5.3. Compressive and Buckling Strength Prediction 111

9. FUTURE WORK 112

9.1. Thermally Induced Deformations **112**

9.2. Modelling of fire protective coatings **112**

9.3. Sandwich panels **112**

9.4. Buckling Response **113**

9.5. Structures **113**

REFERENCES 115

PUBLICATIONS **122**

APPENDIX **123**

Visual Basic Code **123**
ABD Matrix calculation (Polyester) 123
Tensile and Compressive strengths as functions of time (Polyester) 132
Stress strain curve modelling (Polyester) 136
ABD Matrix calculation (Phenolic) 138
Tensile and Compressive strengths as functions of time (Phenolic) 147
Stress strain curve modelling (Phenolic) 151

Thermal Model Outputs **153**

Engineering Drawings **164**

Nomenclature

A_i	pre-exponential factor
$\tilde{A}$	A matrix
$\tilde{A}'$	inverted A matrix
b	breadth
$\tilde{B}$	B matrix
$\tilde{B}'$	inverted B matrix
c	buckling constant
C_P	specific heat capacity
C_{Pg}	specific heat of volatile gases
$\tilde{D}$	D matrix
$\tilde{D}'$	inverted D matrix
E	flexural modulus
E	Young's Modulus
$E(T)$	longitudinal modulus as a function of temperature
E_1	longitudinal flexural modulus
E_2	transverse flexural modulus
E_{45}	modulus at 45° to the longitudinal
E_{CSM}	flexural modulus of the skin material
E_{Full}	flexural modulus of the full section of material
E_i	activation energy
E_{UD}	flexural modulus of the core material
G_{12}	shear modulus
h	enthalpy of the solid phase
h_C	enthalpy of the composite
h_g	enthalpy of volatile gases
I	second moment of area
k	relaxation constant (used in the context of mechanical properties as function of temperature)
k_x, k	thermal conductivity in the through thickness direction
$\tilde{k}$	mid plane curvatures
$\tilde{k}^T$	thermally induced curvatures
l	span length
m	instantaneous mass
M	mass
m_0	initial mass
m_f	final mass
$\dot{m}_g, \dot{M}_G$	mass flux of volatile gases
$\tilde{M}$	bending moment matrix
n	loading constant
n_i	order of reaction
$\tilde{N}$	normal load matrix
P	property value at any temperature
P_R	relaxed property value

P_U	unrelaxed property value
Q_i	heat of decomposition
Q_P	endothermic decomposition energy
$\tilde{Q}$	Q matrix
R	universal gas constant (8.3144 $Jmol^{-1}K^{-1}$)
R	resin content (used in the context of mechanical properties as function of temperature)
t	time
T	temperature
t	thickness
t_1	thickness of the core material
t_2	thickness of the full section
T_g	glass transition temperature
V_f	fibre volume fraction
W	applied load

Greek letters

δ	deflection
ε	applied strain
ε_f	failure strain
$\tilde{\varepsilon}_0$	mid plane strains
$\tilde{\varepsilon}_0^T$	thermally induced strains
ν	Poisson's ratio
ρ	density
$\sigma(T)$	material strength as a function of temperature
σ^*	failure strength of the composite
σ^*_f	failure strength of the fibres
σ'_m	stress in the matrix at the failure strength of the fibres
σ_{App}	applied stress
$\sigma_{buckling}$	buckling strength
σ_{C1}	longitudinal compressive strength
σ_f	failure strength
σ_{max}	exaggerated strength value
σ_{T1}	longitudinal tensile strength

1. Introduction

1.1. Introduction to Composite Materials

Composite materials have a high strength-to-weight ratio when compared to metals, making them a desirable structural material. In its most basic form, a composite material consists of at least two elements, which when combined, form one single material with mechanical properties greater than its components.

Most composites consist of a bulk material called the matrix, combined with a reinforcement material, to increase strength and stiffness of the matrix. The most common composite materials are fibre reinforced plastics (FRP). These generally consist of a polymer matrix reinforced with glass, carbon or aramid fibres.

The mechanical properties of a composite will vary according to the proportions of matrix and reinforcement used. This proportionality is defined by the fibre volume fraction. The larger the fibre volume fraction, the stiffer and stronger the composite.

1.2. Reinforcement Material

In FRP's, reinforcement material can be glass fibre, aramid fibre or carbon fibre. This thesis is concerned with E-glass fibre reinforcement. On its own, E-glass exhibits high tensile and compressive strengths and high stiffness properties. It is one of the cheapest reinforcements available, making it a common choice for general engineering applications, accounting for around 90% of the reinforcement used in structural reinforced plastic applications[10].

Table 1.1. Typical properties of E-glass [11].

	Specific gravity	Young's Modulus (GPa)	Poisson's ratio	Tensile Strength (MPa)
E-glass	2.55	72	0.2	2400

1.3. Reinforcement Architecture

1.3.1. Unidirectional

Unidirectional (UD) reinforcement consists of fibres running in the same direction (0° direction). The main benefit of using UD reinforcement is that fibres can be oriented in the exact position to allow any forces to pass along the fibre, thereby take up any loading the component would experience in service. This is advantageous when designing structural components. The downside of having all the fibres laying in the same direction is that all the stiffness and strength is associated with that direction. There is very little strength or stiffness in other directions. Loads acting parallel to the fibre are easily dealt with, whereas any acting in other directions cause problems.

1.3.2. Chopped Strand Mat/Needle Weave

Chopped Strand mat (CSM)/Needle weave is a random in plane reinforcement material. It differs from simple CSM by the way that mat is 'needled' together. This provides the material with additional strength. This enables the material to be pultruded (see Section 1.5), since the strength is sufficient to resist the tractive forces associated with the process.

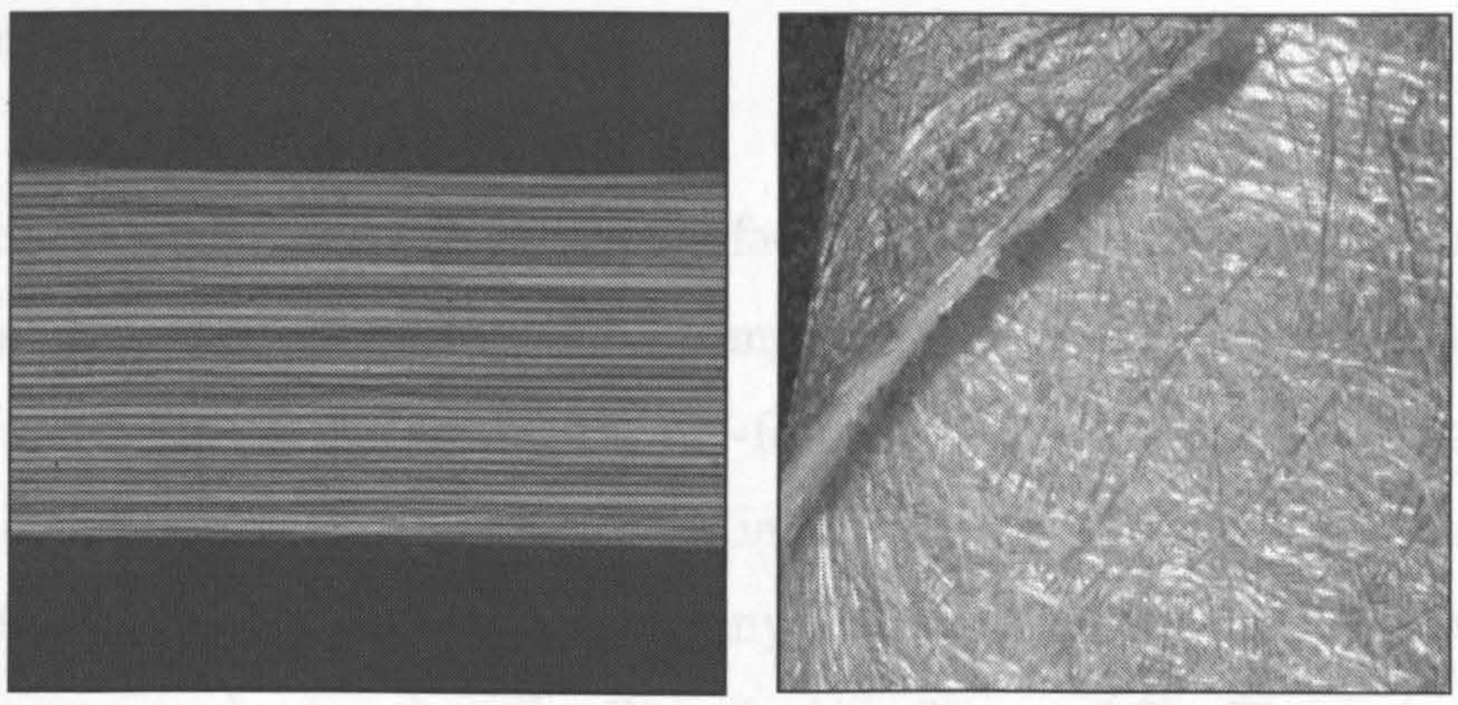

(i) (ii)

Figure 1.1. Unidirectional glass fibre reinforcement (i) [12] and CSM/Needle Weave glass fibre reinforcement (ii) [13].

1.4. Matrix Material

1.4.1. Polyester

Thermosetting polyester is the most widely used matrix material due to its ease of use, low cost and good all round mechanical properties.

1.4.2. Phenolic

Phenolic resin is used as a matrix when improved fire resistance is required. Phenolic based composites retain their properties at higher temperatures.

Table 1.2. Typical properties of polyester and phenolic resins [11].

Matrix Material	Specific Gravity	Young's Modulus (GPa)	Poisson's ratio	Tensile Strength (MPa)	Compressive Strength (MPa)
Polyester	1.21	3.6	0.36	60	130
Phenolic	1.15	3.0	-	50	-

1.5. Pultrusion

Pultrusion is a manufacturing process by which many composites with structural applications are made.

The process can vary according to manufacturer but is essentially the same. The pultrusions manufactured by Fiberline Composites begin as spools of unidirectional reinforcement which is fed through a pre-former. The material then passes into a heating and curing chamber where resin is injected under pressure. The cured profile emerges at the other end to be sawn into any required length. The material is pulled through the process by a series of pulling devices (Figure 1.2). The end product has a constant cross section. A variation of the process called 'pulforming' is used to produce components with slight changes in section.

Often an enveloping layer of chopped strand mat (CSM) needle weave mat is applied to protect the unidirectional core from damage. A surface-veil is usually applied to the surface of the profile to give a high quality surface finish.

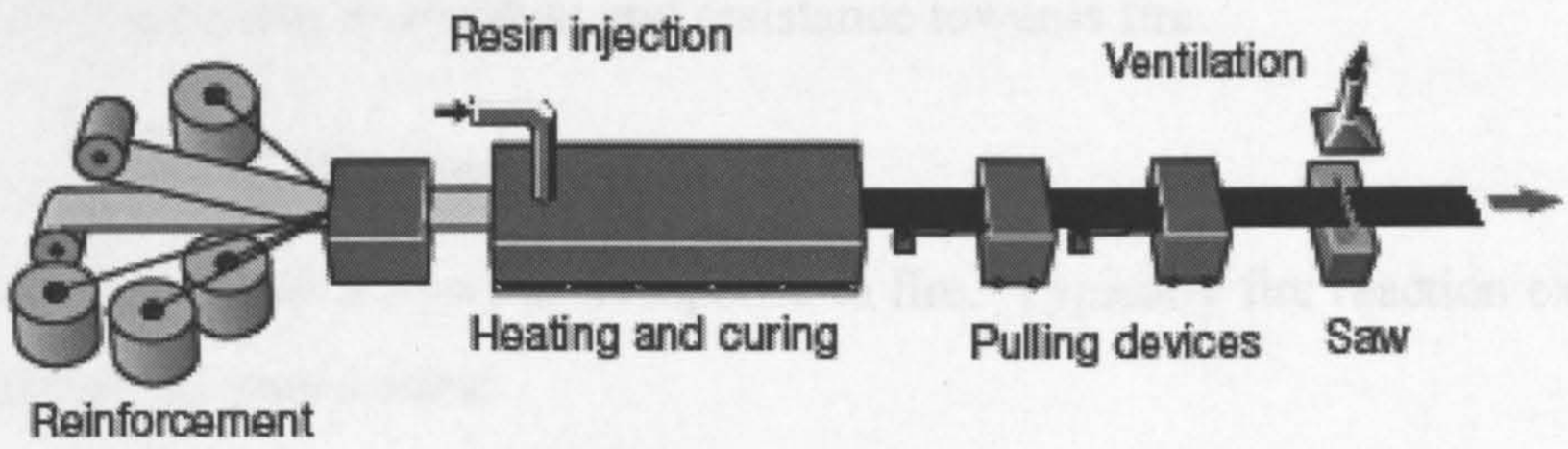

Figure 1.2. The pultrusion process [14].

Typical applications for pultruded sections include drive shafts, ladders, walkways, handles etc. Several large structures have been constructed using pultruded sections as the main load bearing component including road bridges, foot bridges and medium sized buildings. The greatest advantage of pultrusion is the low cost of manufacture associated with continuous processes (Table 1.3).

Table 1.3. Advantages and disadvantages of the pultrusion process.

Advantages	**Disadvantages**
Very fast and economical	Limited to constant/near constant cross section
Resin content can be accurately controlled	High die costs
High fibre volume fractions can be obtained	
Resin impregnation area is minimised, reducing volatile emissions	

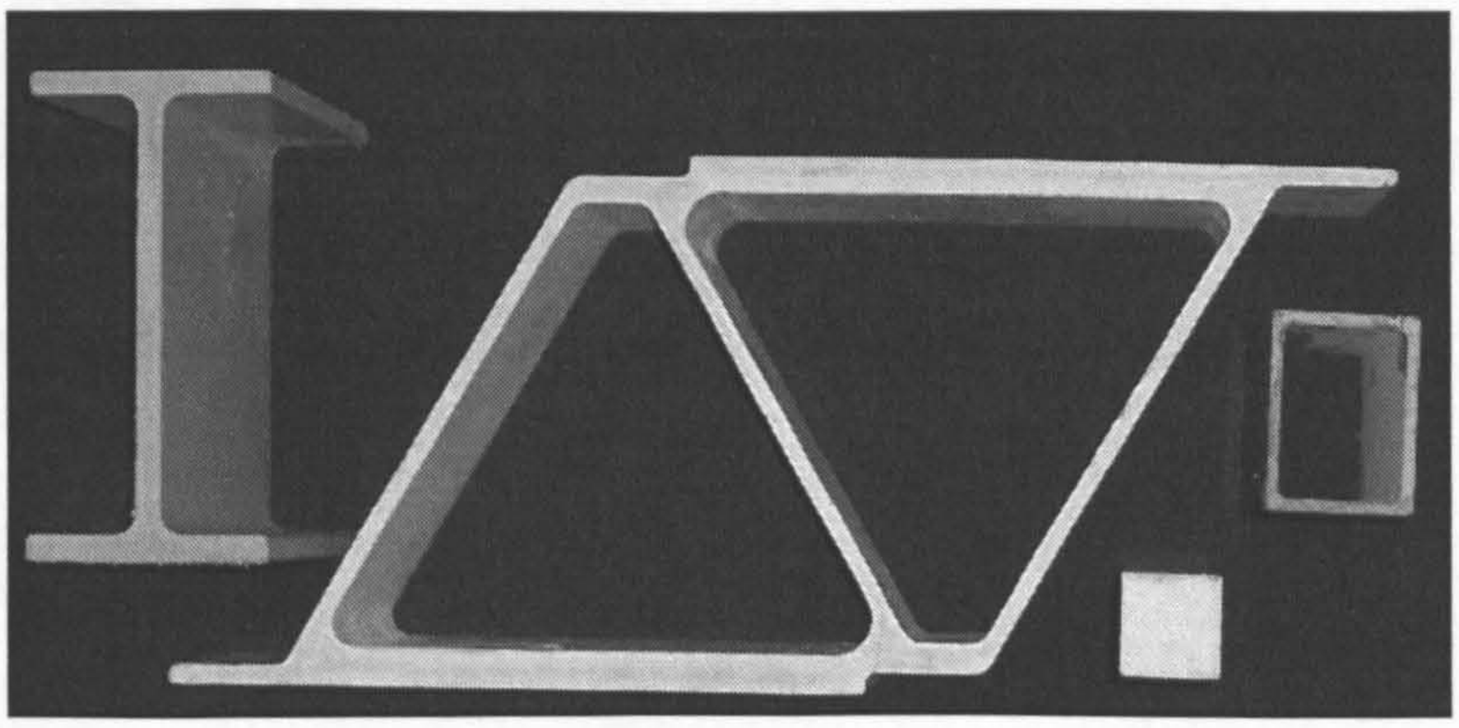

Figure 1.3. Typical pultruded profiles. The large profile in the centre was used in the construction of a road bridge.

1.6. Fire Reaction & Fire Resistance

In order for a material to be used in a fire risk application it must conform to a series of standards regarding its reaction and resistance towards fire.

1.6.1. Fire Reaction

Fire reaction concerns a material's response to fire. Typically fire reaction examines the following key parameters:

- **Ignitibility.** Time-to-ignition (TTI) is a very important fire reaction property since it defines the onset of combustion.
- **Heat release.** Heat release rate (HRR) is the single most important fire reaction property[15] because the heat released by burning material can provide the additional thermal energy required for the growth and spread of fire. Heat release is defined as the thermal energy produced per unit area of surface, when inflammable decomposition products ignite and burn in the vicinity of a material in fire, or subjected to a heat flux.
- **Surface spread of flame.** The speed of flame-spread across the surface of combustible materials is an important factor in fire growth.
- **Smoke and toxicity.** Smoke reduces visibility which is of great concern in a fire situation. Smoke can also be highly toxic, which obviously poses serious health hazards.

1.6.2. Fire Resistance

Fire resistance describes the ability of a material or structure to restrict the spread of fire and to retain mechanical and physical integrity. Key fire resistance parameters include heat transfer, burn-through resistance and structural integrity.

1.7. Test Procedures

There are several fire tests in existence, each of which is used to test materials to determine whether they conform to one standard or another. An area of concern for the materials industry is that there is not a single common approach to determine the fire response of composites[16], and it is often necessary to use a combination of tests to sufficiently describe the behaviour of a composite material or structure in fire.

Fire tests vary in scale, from small bench-scale procedures to large-scale room tests. Fire resistance tests tend to be towards the large end of this scale. The most popular fire reaction tests are bench scale tests because they are quick, inexpensive and will usually yield reproducible data. Bench-scale tests are limited because they ignore the effect due to fire growth, indeed it is said that they only relate to a 'snapshot' of the overall fire behaviour [17]. Heat release rates, air movements and the oxygen/fuel ratio that exist in a real fire, are often very different to those in bench-scale tests. These can affect the measured fire reaction properties [18]. One further drawback of bench-scale testing is that the entire test sample is consumed. This may not be the case in a real fire scenario due to the reduced oxygen levels in enclosed, unventilated spaces [19].

Intermediate-scale tests provide a link between the bench-scale tests and the more expensive large-scale tests. They can overcome some of the shortcomings of bench scale-testing as they lean more towards real fire scenarios, usually involving a scale model or part-section of the structure under investigation.

Large-scale tests are expensive and complex with long set-up times. For these reasons they are performed rarely and only when it is unavoidable. For instance, if there is any uncertainty with scaling up data from an intermediate-sized test. Large-scale tests also have a commercial role in demonstrating the fire performance of new materials and methods.

The size and type of test (fire reaction or fire resistance) for the most common fire tests are detailed in Table 1.4. The most common fire tests are as follows:

1.7.1. Cone Calorimeter (including atmosphere controlled)

The cone calorimeter is a versatile fire reaction test capable of measuring most fire reaction properties with the exception of flame spread. It forms the basis of many fire standards, placing it in high regard with universities and research institutes across the world. The test involves exposing a small sample to a heat flux and igniting any evolved gases. These gases are then analysed. The sample is also placed on a load cell to record any change in mass. Some cone calorimeters have the facility to control the combustion atmosphere, namely the level of oxygen. Conventional cone calorimeters can only provide data in atmospheric conditions (i.e. 21% oxygen). Atmosphere controlled apparatus are not so common due to the high cost involved, and because fire reaction properties are usually required under atmospheric conditions, simulating a material's response in a real fire scenario.

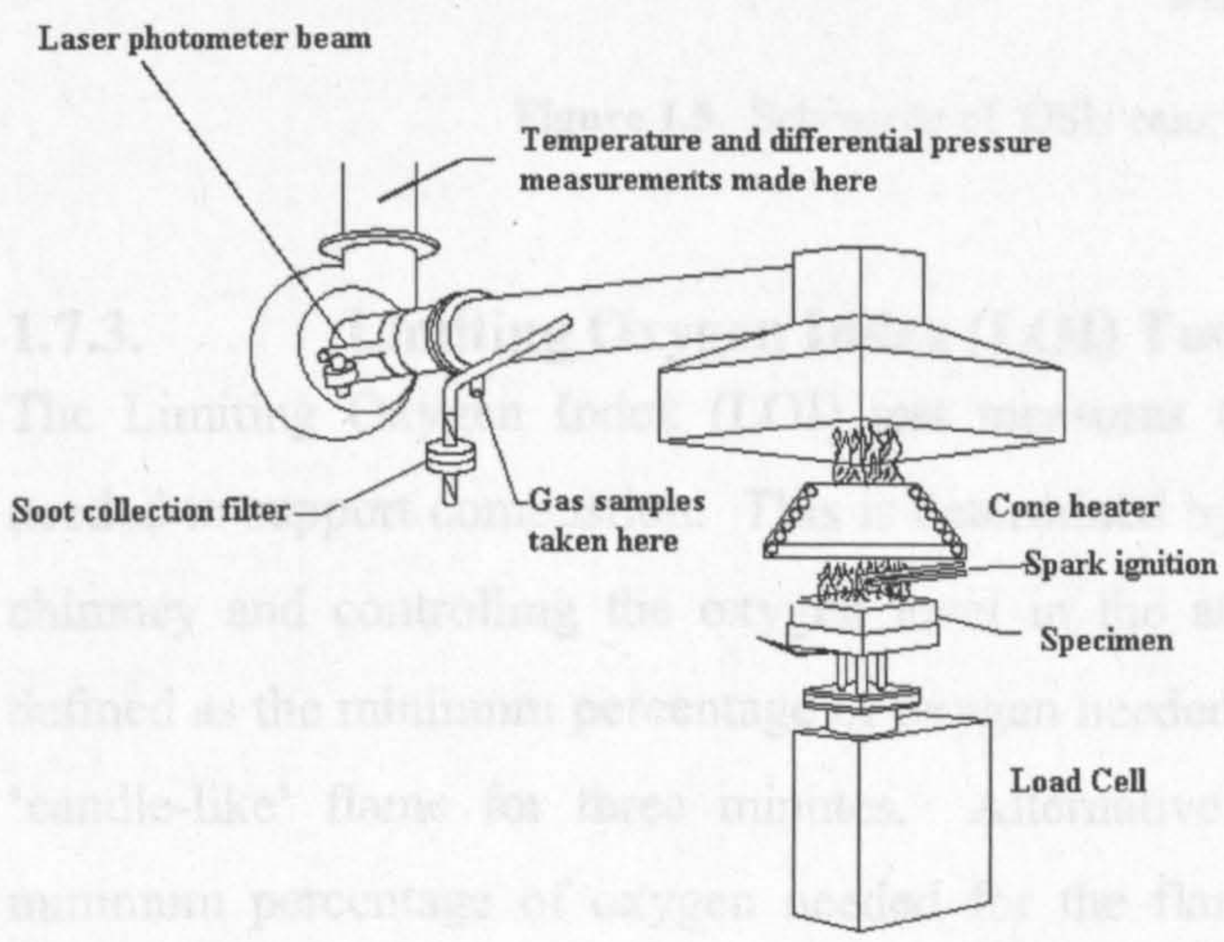

(i)

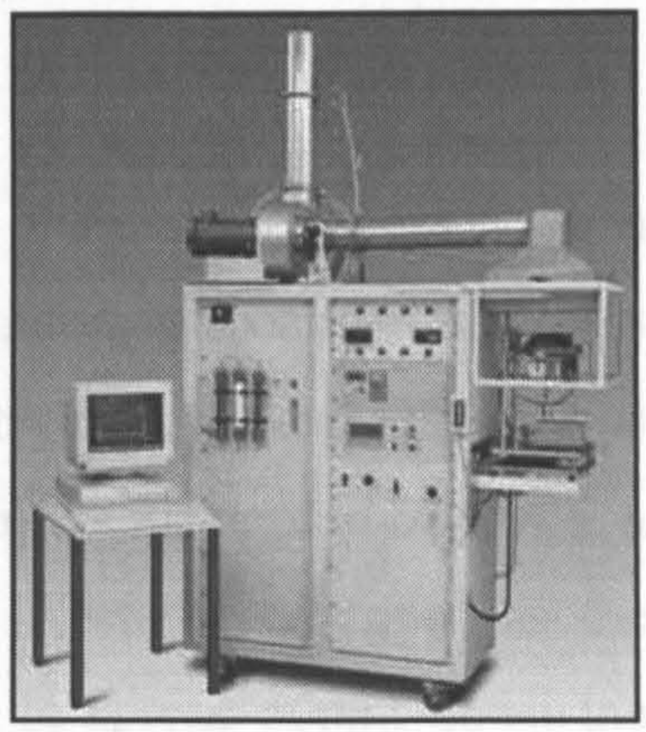

(ii)

Figure 1.4. Schematic (i) [20] and general view (ii) [21] of a cone calorimeter. The prefix 'cone' comes from the shape of the heater.

1.7.2. OSU Heat Release Rate Technique

The Ohio State University (OSU) heat release rate technique consists of an adiabatic chamber into which a sample is placed and exposed to a constant heat flux ranging

from 35-100 kWm^{-2}. The specimen is ignited using a high temperature flame, then heat release rate is monitored and on occasion, smoke release. This method is not as common as the cone calorimeter since it has been shown to be prone to a greater error than the cone calorimeter. Moreover it cannot measure mass loss.

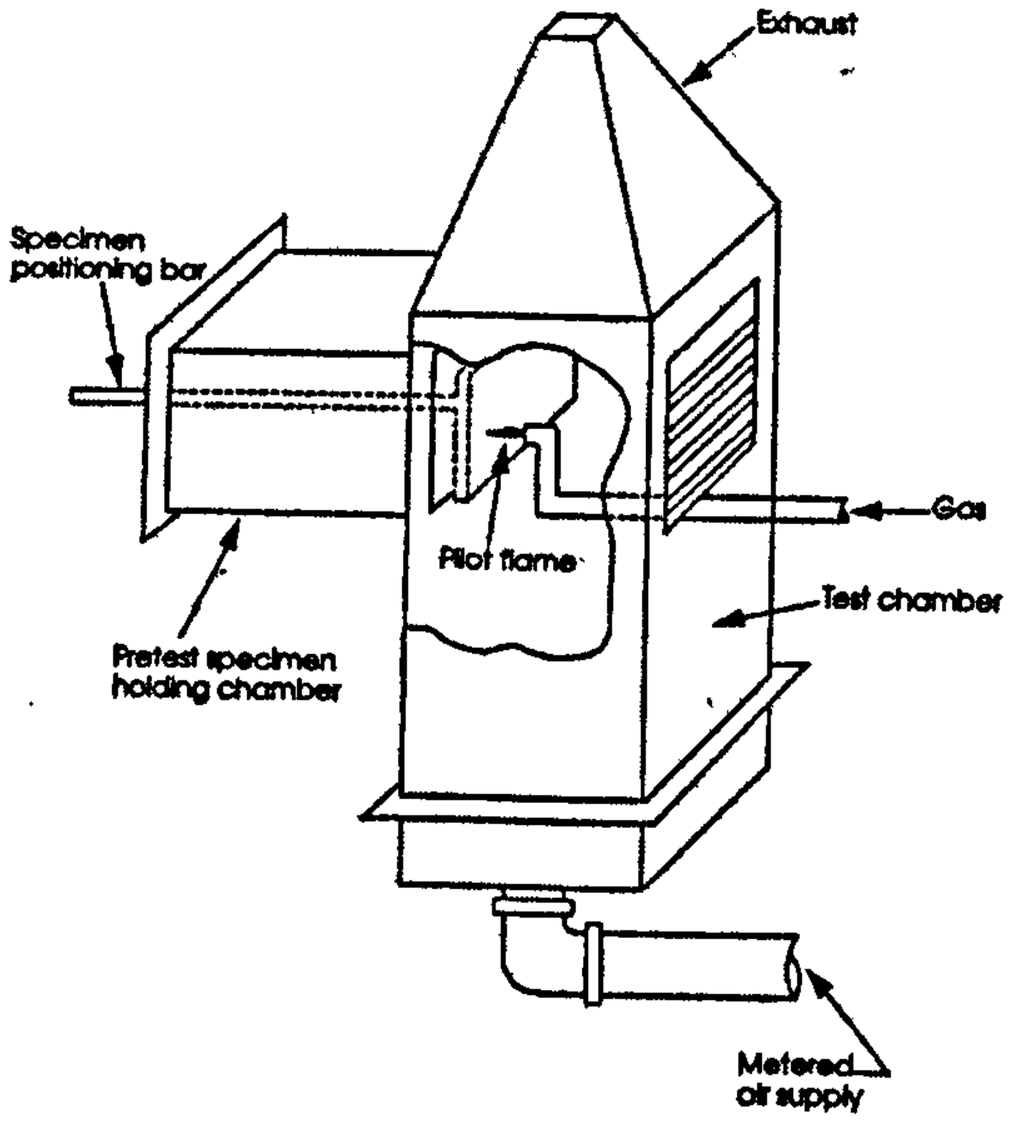

Figure 1.5. Schematic of OSU calorimeter[22].

1.7.3. Limiting Oxygen Index (LOI) Test

The Limiting Oxygen Index (LOI) test measures the minimum level of oxygen needed to support combustion. This is determined by igniting a specimen in a glass chimney and controlling the oxygen level in the atmosphere. The LOI index is defined as the minimum percentage of oxygen needed for the material to burn with a 'candle-like' flame for three minutes. Alternatively it can be described as the minimum percentage of oxygen needed for the flame to spread 50mm down the sample. The apparatus consists of an oxygen-nitrogen mixing system and analysis equipment.

The value of the LOI test has been questioned by many since it bears little resemblance to a real fire scenario[15]. Despite this it used in the polymer industry as a method of describing inflammability.

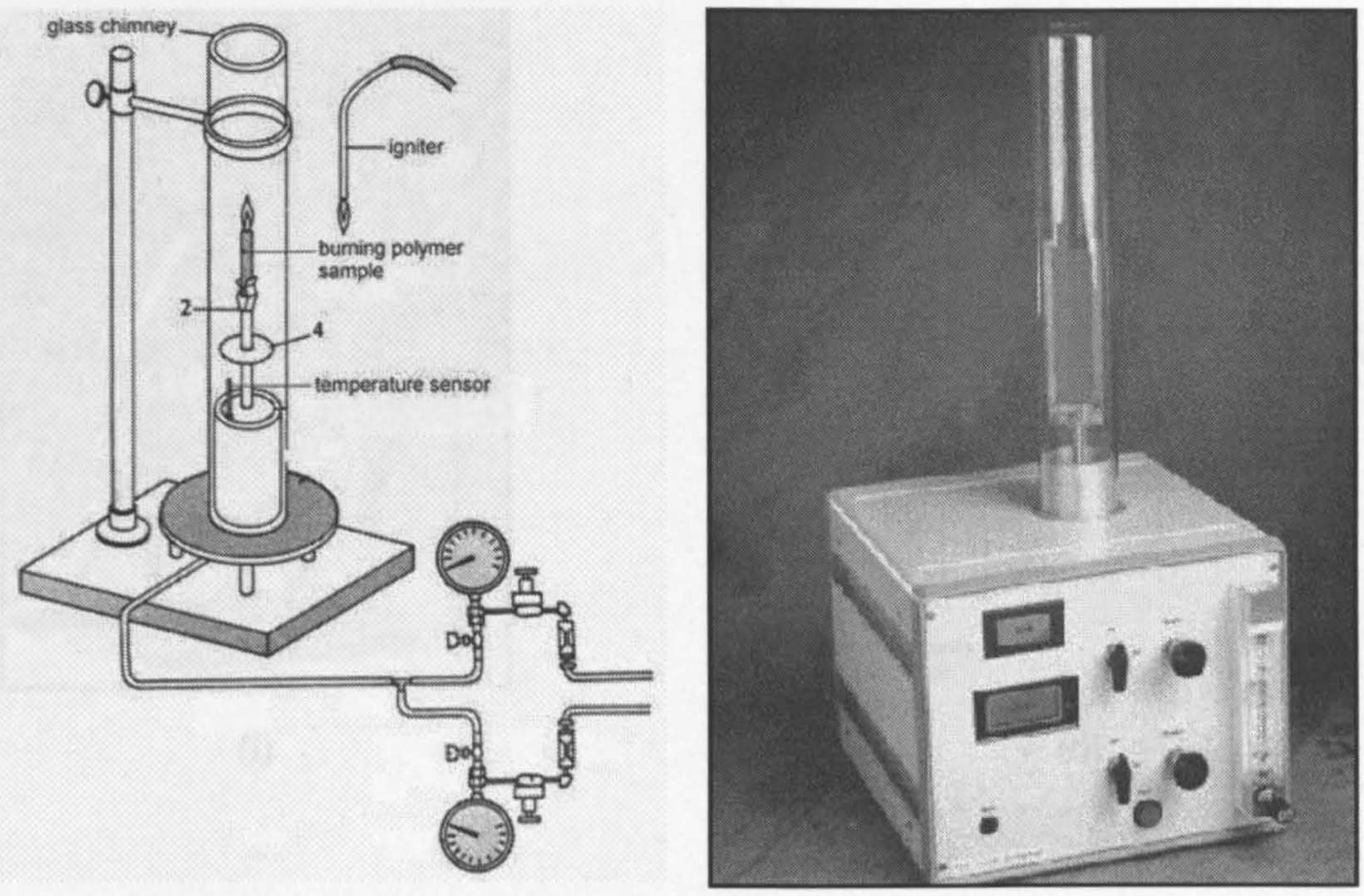

(i) (ii)

Figure 1.6. Schematic (i) [23] and general view (ii) [21] of LOI test.

1.7.4. Radiant Panel Test

The radiant panel test involves subjecting a panel of the test material to a known heat flux. The panel itself is angled at 45° to the heater, directed at the panel's top edge. During the test, the rate at which the flame travels down the panel along with the temperature rise are recorded. From these a Flame Spread Index is determined and used to compare the material with others. This method has been criticised, because like the LOI test the direction of flame spread is downwards. This is deemed unrealistic of a real fire where flame spread is predominately upwards, and therefore more rapid.

1.7.5. Flame Propagation & Spread Tests

Many other flame spread tests are in existence although not as common as the radiant panel test. NASA has developed an Upward Flame Propagation Test which subjects a sample to a heat flux of 75 kWm^{-2}. The average flame spread rate is determined by dividing the length of flame travel by the burn time. A sample is deemed to have passed if this number is less than 6.12 mms^{-1}. Other tests include the lateral flame spread method and the fire tunnel test.

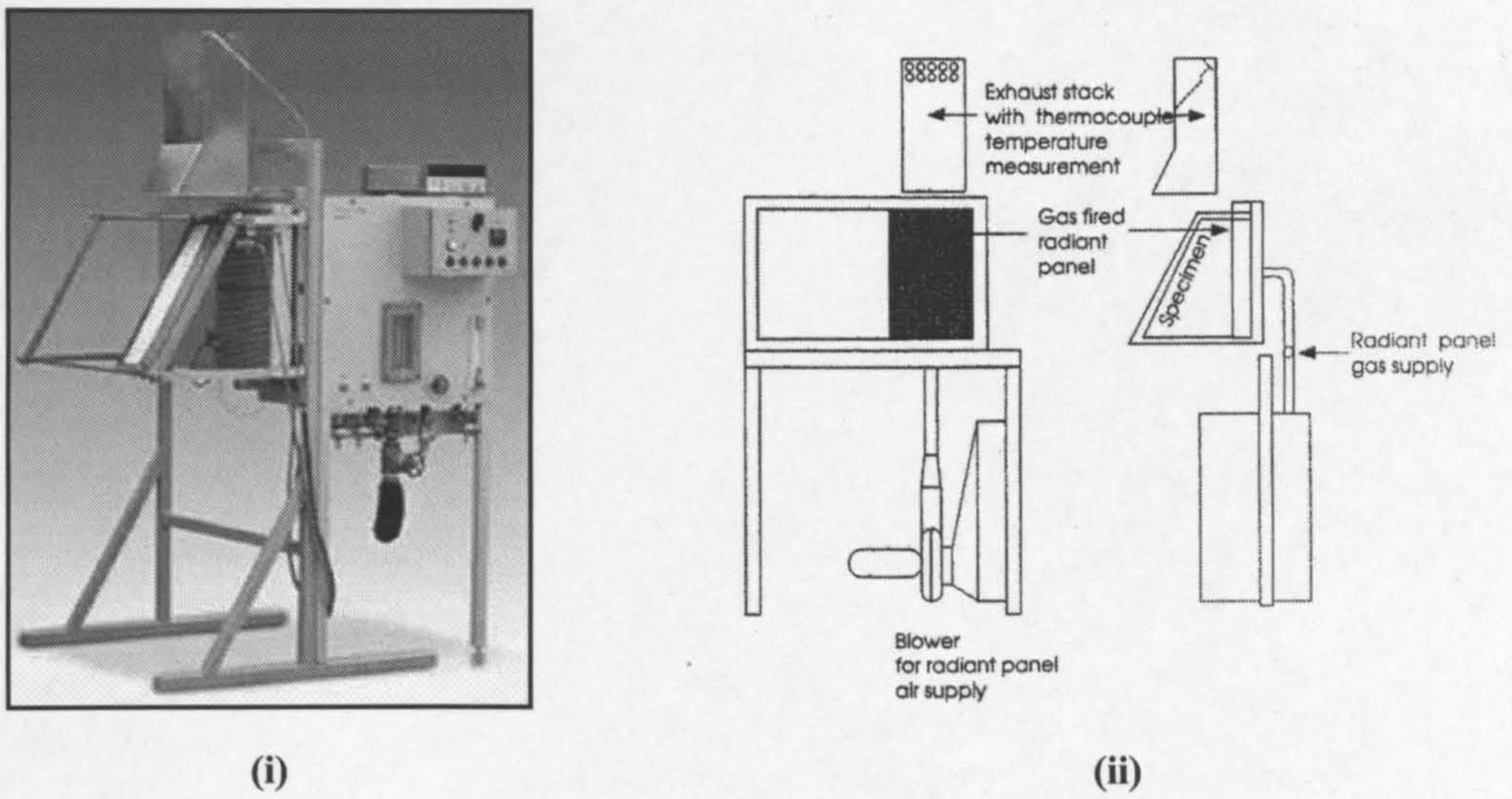

(i) (ii)

Figure 1.7. General view (i) [21] and schematic view (ii) [24] of the radiant panel test. Note the top edge of the specimen angled towards the heater.

1.7.6. Smoke Density

The most widely used smoke density test is the NBS (National Board of Standards) smoke chamber. This operates by subjecting a sample to a known heat flux, usually 25 kWm^{-2}, and measuring the density of the generated smoke. This involves using a monochromatic light (a photometric system) to determine light transmission. This in turn is used to determine the specific optical density which is inversely related to the visibility of the smoke.

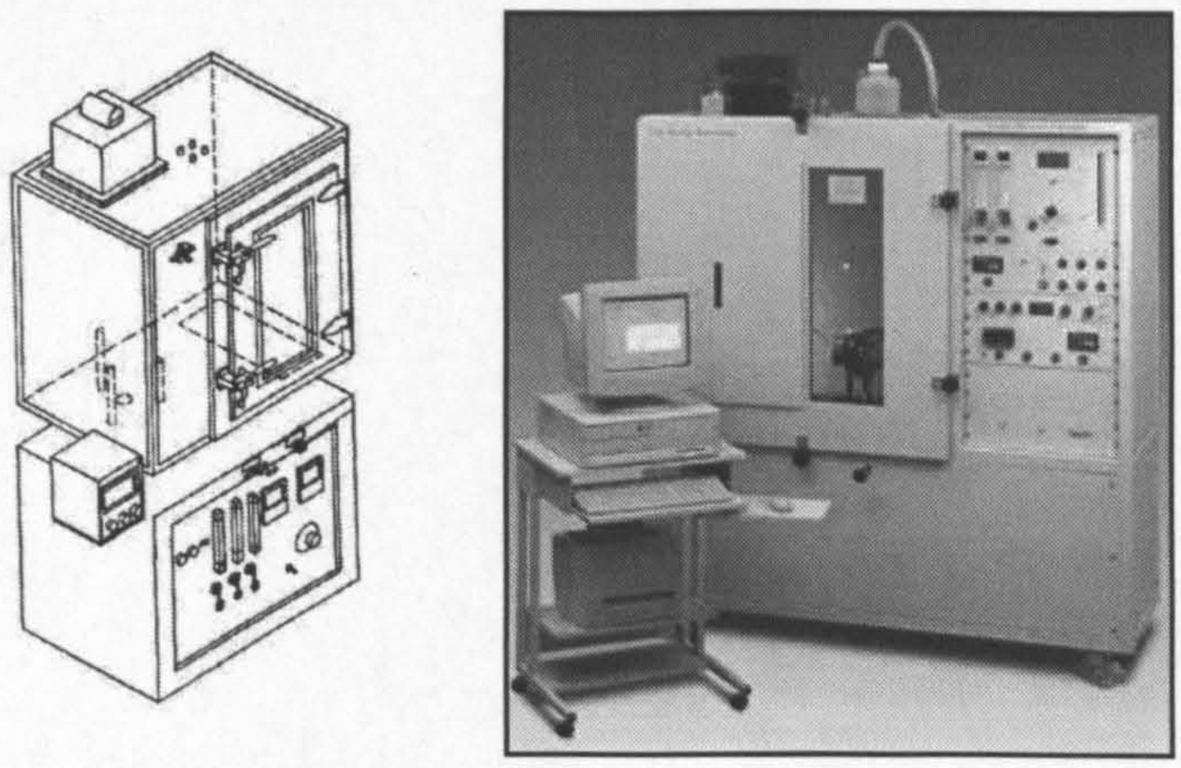

(i) (ii)

Figure 1.8. Schematic (i) [24] and general view (ii) [21] of a NBS smoke chamber.

1.7.7. Single Burning Item (SBI) Test

The SBI test simulates a burning waste receptacle (the burning item) in a room corner. It is essentially an intermediate-scale room corner test (see section 1.7.8), consisting of two wall panels made of the test material. The burning waste receptacle is simulated by a triangular-shaped propane burner generating a heat flux of approximately 50kWm^{-2}. The test is performed inside a fire room with a fume extraction system in the ceiling. Heat, smoke and gases released from the burning walls are extracted and analysed, giving data on temperature, heat release rate, smoke density, O_2 and CO_2 concentrations.

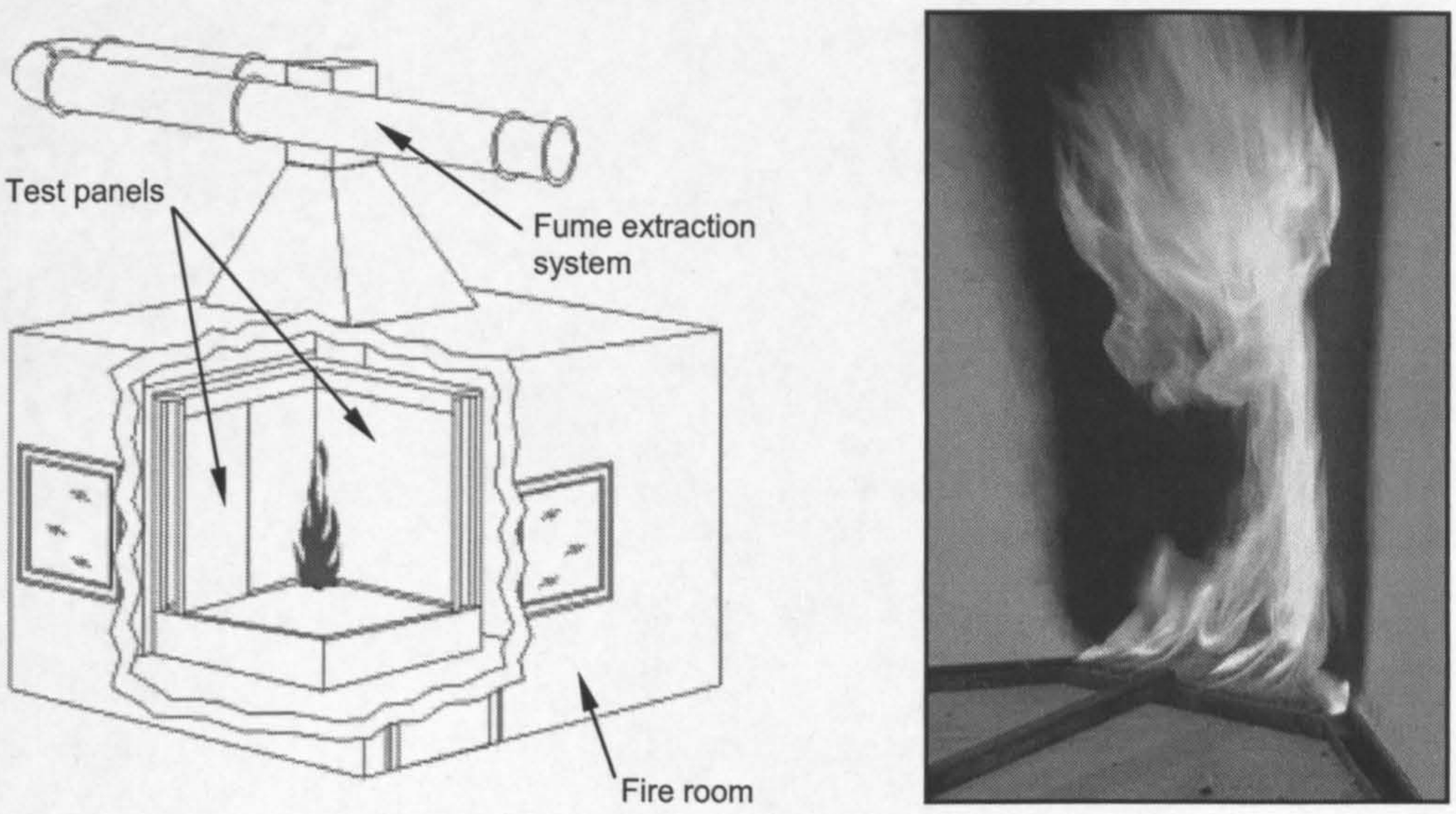

Figure 1.9. Schematic (i) [21] and close up (ii) of SBI test [25].

1.7.8. Room Fire Test

There are several intermediate to full scale room fire tests in existence. These are used to establish the fire behaviour of composites for use in buildings and ship compartments. The simplest of these is the room corner test, which is essentially a slightly larger SBI test. In this case though, the heat source is a 30 litre pan of hexane fuel.

The largest room fire test is the room calorimeter test. This consists of a room with a doorway at one end. The ceiling, both side walls, and the end wall without the

doorway are clad in the material to be tested. The test material is installed in the end-use condition, with all joints, fixtures and surface coatings applied. The fire source is a propane burner placed in one of the rear corners. A fume extraction hood is positioned over the open doorway in the end wall to remove any fumes for analysis (see Figure 1.10).

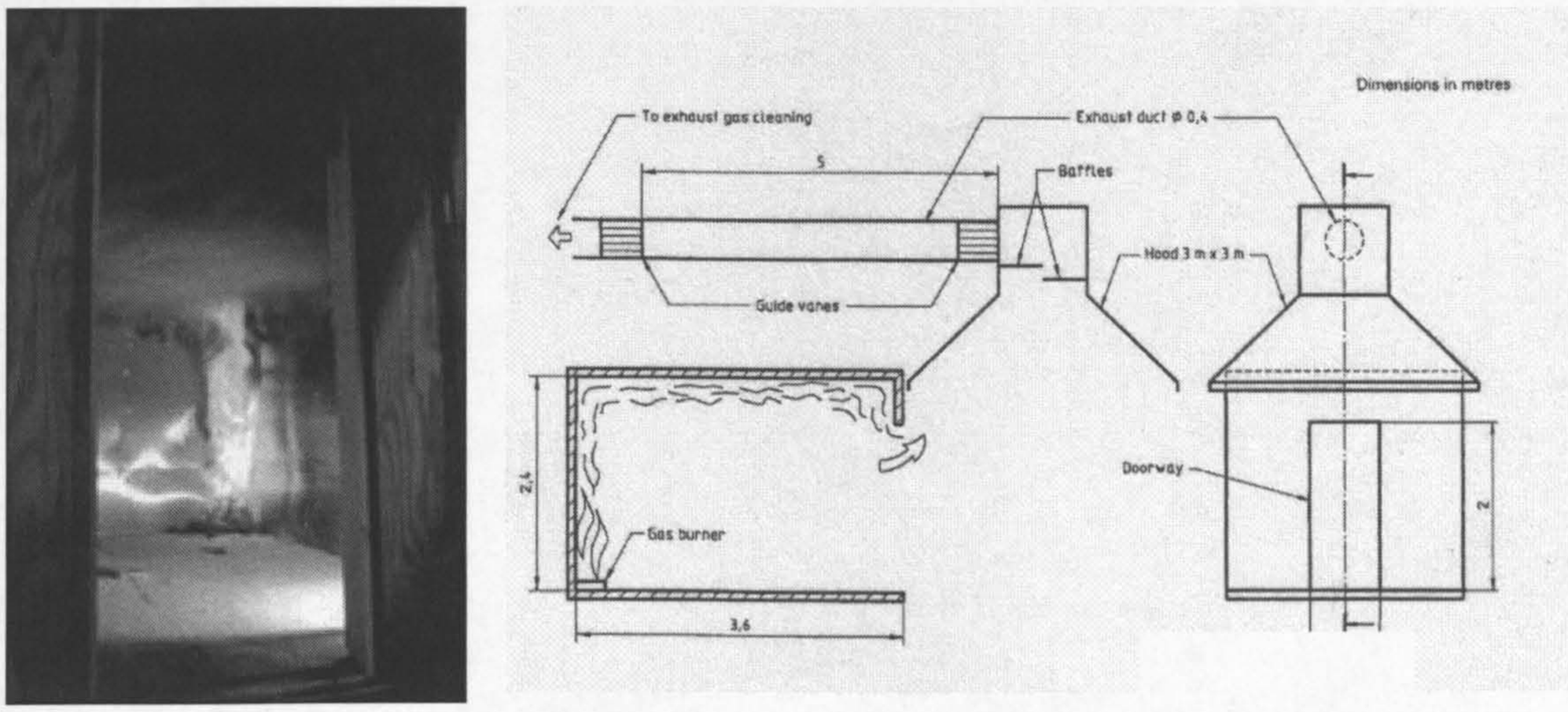

(i) (ii)

Figure 1.10. Room corner test (i) [26] and schematic of the room calorimeter test (ii) [27].

This test can provide information on a number of fire reaction properties, including time-to-ignition, heat release rate, smoke density, toxic gas emission and flame spread [19]. In addition, certain fire resistance properties can be determined including, heat penetration through the walls, burn-through rate and structural response to fire.

1.7.9. Furnace Tests

The most commonplace resistance test consists of a structural sample in the form of a panel, one side of which is subjected to the temperature profile of the furnace. Panels measuring from $1m^2$ to $10m^2$ can be tested, depending on the size of the furnace. Fire resistance is defined by the time taken for the cool side of the panel to reach 140°C above ambient or for a hotspot of 180°C above ambient to appear. Furnace tests offer a high level of repeatability compared to other reaction tests provided they are carried out using the same furnace, since variability between

furnaces exists. This variation can be brought on by having different lining materials, different thermocouple positions and different insulating materials in the furnace walls.

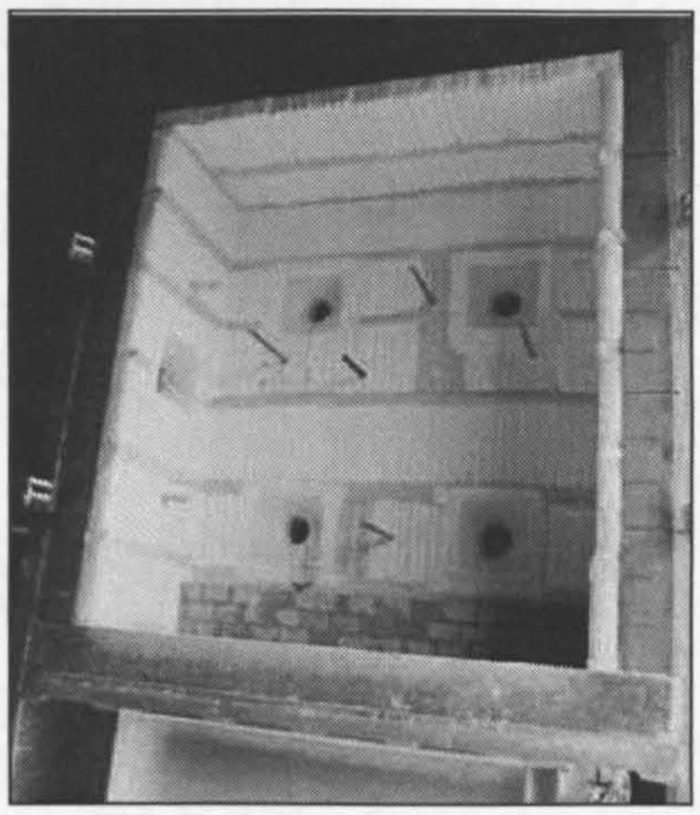

Figure 1.11. General view of a large scale furnace with the test panel removed [28].

1.7.10. Pool-fire Tests

Pool fire tests consist of placing a section, sometimes under load, over a tray of a highly inflammable liquid, depending on the application. Heat transfer and structural integrity are measured throughout the test. The fire is often subject to convection currents and air streams, making repeatability an issue

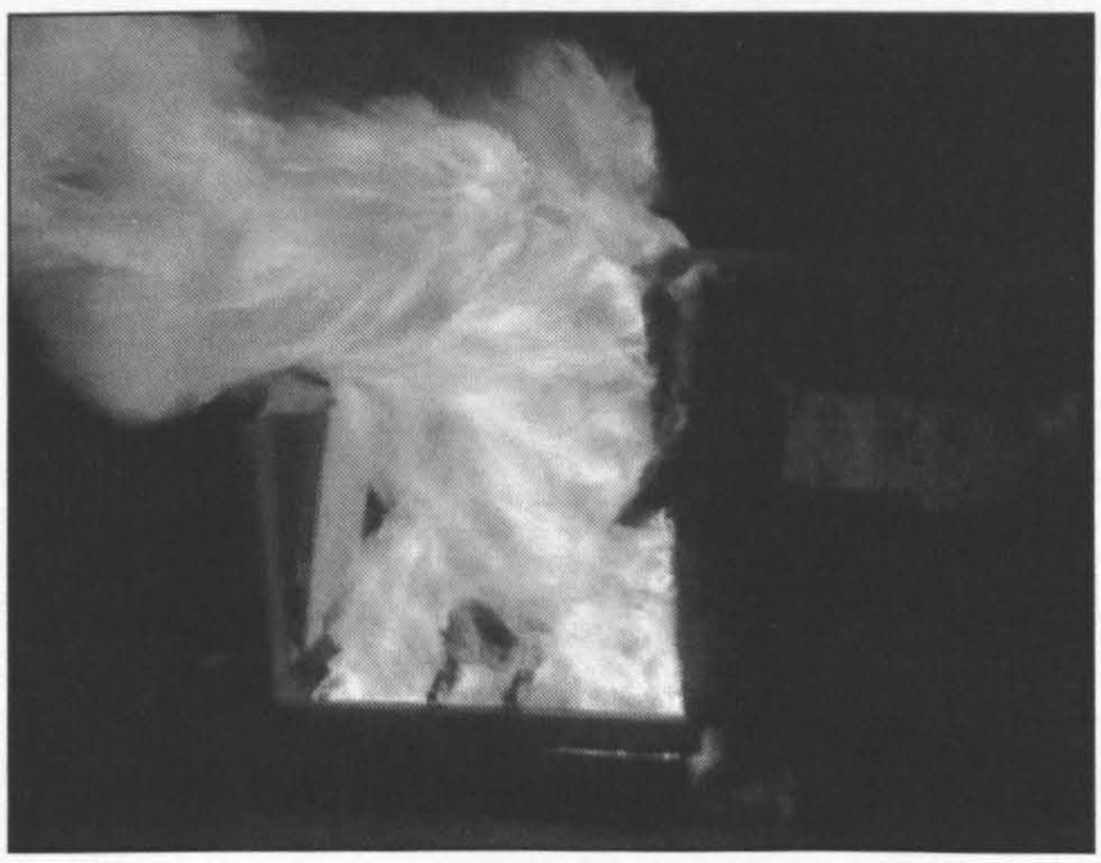

Figure 1.12. Typical pool fire test. In this instance a pultruded composite section is under constant flexural strain whilst in the fire. The point at which the photograph was taken, the pool fire has reached the point of secondary flashover.

Furthermore, it has been found that pool fires can exhibit two distinct flashovers. An initial low temperature flashover is followed by a much hotter secondary flashover, when the heat of the fire begins to reflect back on itself, rapidly heating the remaining fuel.

1.7.11. Burner Tests

Burner tests provide a less expensive option for resistance testing. One such technique consists of testing samples in the region of 100 x 100 square millimetres, subjected to a constant heat flux. In addition to measuring the integrity of composite laminates in fire, it can also be used to measure heat flux transmitted to an underlying substrate. Furthermore it has been demonstrated that it can be used to test loaded structures [29].

1.7.12. Jet-fire Tests

A jest fire consists of a high velocity jet of flame directed towards a specimen. Jet-fires are a very severe test due to the high heat flux they generate and the erosive nature of the jet itself. A small number of jet-fire rigs exist in the United Kingdom, United States and Norway. They are designed principally for testing pipes, vessels and structures, with or without passive fire protection, under conditions relevant to the oil and gas industries. The largest of these rigs is operated by British Gas at their Spadeadam facility. This rig is capable of directing a 20 metre horizontal flame of burning natural gas onto a test specimen, subjecting it to heat flux of ~300kWm^{-2} and a jet velocity of ~50ms^{-1}. The specimen is exposed to the fire for a fixed length of time, and subsequently assessed for burn-through and functionality.

Jet-fire tests are very expensive to carry out due their large scale. Small to medium scale tests have been developed, capable of subjecting test specimens to high heat fluxes and gas velocities, but without the high operating costs[29-31].

A British Standard for determining the resistance of passive fire protection materials towards jet fires is currently under evaluation.

Figure 1.13. Jet-fire test underway at the British Gas Spadeadam Facility [32]. The rig shown has the ability to direct a 20 metre horizontal flame, equivalent to a heat flux of ~300kWm^{-2} at a velocity of ~50ms^{-1}.

Table 1.4. Details of the scale and type of the most common fire tests.

		Test Size		
Test type	**Test name**	**Small 'bench-scale'**	**Intermediate-scale**	**Large-scale**
Fire Reaction				
	Cone calorimeter	✓		
	OSU technique	✓		
	LOI test	✓		
	Radiant panel test	✓		
	NBS smoke chamber	✓		
	SBI test		✓	
	Room fire test		✓	✓
Fire Resistance				
	Room fire test		✓	✓
	Furnace test	✓	✓	
	Burner test	✓		
	Pool-fire test			✓
	Jet-fire test			✓

The problem with fire resistance of GFRP (glass fibre reinforced plastics) is seen by many as the most significant factor hindering the expansion of the material in many engineering applications, particularly those with strict guidelines for performance in fire.

1.8. Thesis Overview

This thesis describes the development of a model capable of predicting failure times of pultruded GFRP when exposed to fire, under load. This is achieved by building on existing fire resistance models[1-8, 33] with laminate theory and data describing mechanical properties as functions of temperature. This model is explained in Figure 1.14 below and is described in detail in chapter 7. The failure model was verified by a series of fire tests on the pultruded material, loaded in tension and compression.

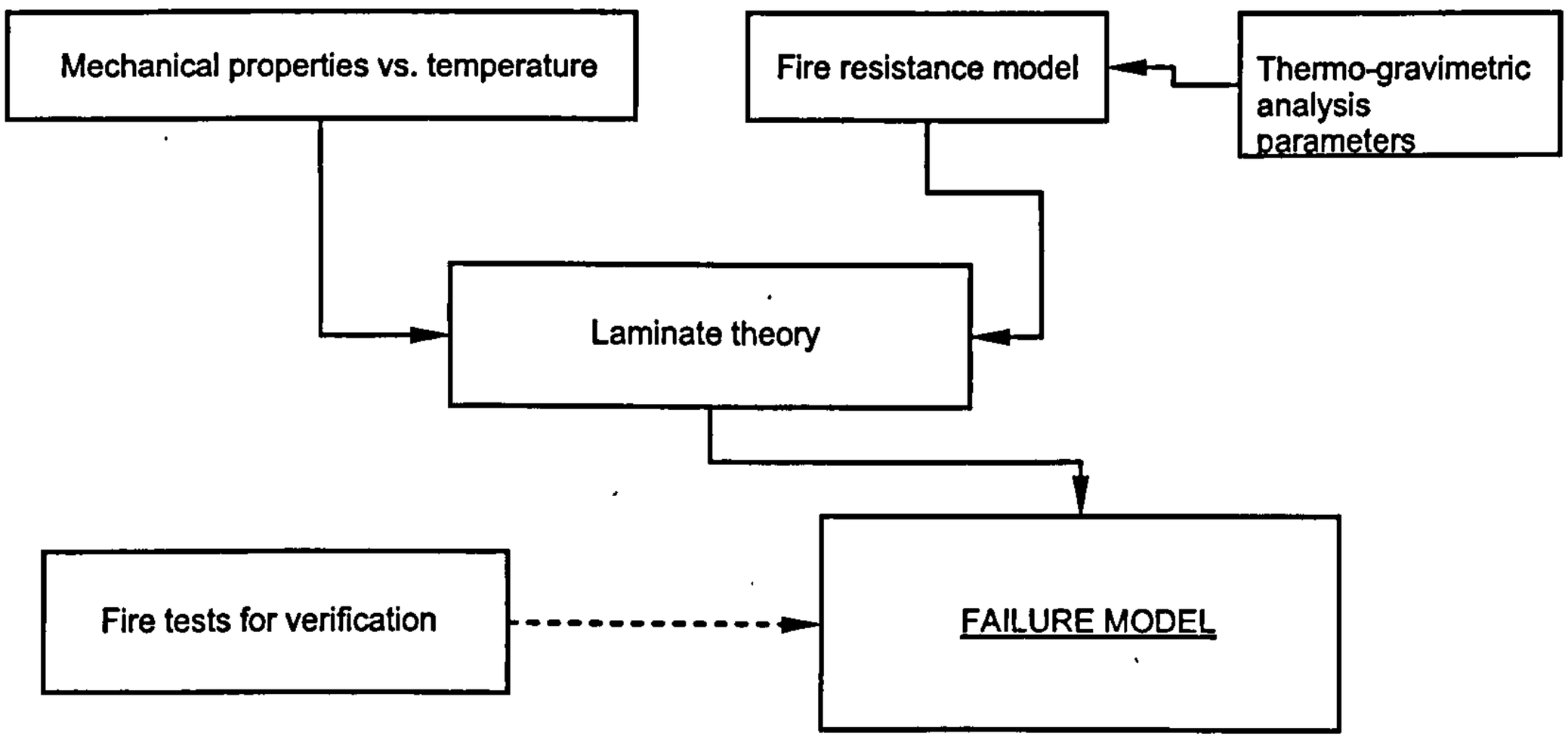

Figure 1.14. Overview of the failure model developed in this thesis.

Data describing mechanical properties as functions of temperature are unavailable in the literature so experiments needed to be designed and carried out. This is described in Chapter 4. The fire tests carried out to verify the model are detailed in Chapter 5 and results of both the fire tests and the mechanical property tests are discussed in Chapter 6.

Further to this failure model, investigative work was also carried out to prolong the failure time of pultruded sections. This work involved flexing pultruded sections in pool fires and a furnace, as well as carrying out compression tests on columns subjected to heat and flames from a propane burner. These experiments are described in Chapter 5 and the results discussed in Chapter 6.

1.9. Chapter Summary

Composites are used in many industries in a variety of applications utilising their high strength –to-weight ratio. Due to their organic matrix material, they are usually highly flammable, prompting a great deal of research into their reaction and resistance to fire.

Many fire reaction and resistance tests exist, ranging in scale and cost from the small scale laboratory tests like the cone calorimeter test, to the large scale, high cost jet fire resistance test (see section 1.7). As of yet there is no standard fire reaction or fire resistance test, there is instead a selection of tests that are recognised by the fire and composites industries.

2. Literature Review

2.1. The 'Slow Burn-Through' Effect

Concerns have been raised about the fire reaction and fire behaviour of composites, brought on by the combustibility of the organic polymer matrix[34]. In spite of the inflammable nature of composite materials, they exhibit some interesting and potentially useful properties in fire. The most important of these properties is the 'slow burn-through' effect. In composites above a certain critical thickness, the burn through rate is greatly reduced, as are heat release and heat transmission through the material. These result in increased fire integrity of the composite, increasing their potential for use in fire protection applications[35].

The factors contributing to the 'slow burn-through' effect are:

- **Transport properties of the laminate.** Thermal conductivity and diffusivity of the laminate is low when compared to steel.
- **Transport properties of the residual glass.** The reinforcement depleted of any resin material, has a lower thermal conductivity and diffusivity than that of the laminate.
- **Endotherm due to decomposition and vaporisation.** Resin decomposition and vaporisation are highly endothermic and therefore temporarily delay heat conduction through the laminate.
- **Convection of volatiles.** As the gaseous decomposition products diffuse through the laminate towards the hot surface, they can be expected to produce a cooling effect[35].

The response of composites in fire is discussed in greater detail later in this chapter.

Findings like the slow burn through effect have enabled performance led design procedures to replace the more conservative approach of relying heavily on regulations[36]. This new attitude towards material selection has led to composites

being used in fire risk situations, provided they can be qualified and their behaviour predicted[2].

2.2. Fire Resistance Modelling

Thermal decomposition of fibre reinforced composites is very complex, combining thermal, chemical and physical processes. The thermal processes involved include heat conduction through the material, heat absorbed through decomposition, heat generated from the ignition of any inflammable reactant gases, and any convective heat loss from the reactant gases and any water vapour flowing through and out of the material. Chemical processes include melting, pyrolysis and volatilisation of the matrix and fibres, and the growth and oxidation of char. The physical processes occurring may include, thermal softening, thermal expansion and contraction, internal pressure build-up caused by the formation of volatile gases and vapours, thermally-induced strains, delamination damage, matrix and surface cracking, and the softening, melting and fusion of fibres. In order to appreciate how composite materials respond to fire, it is important to understand these processes and how they interact.

The need for reliable models capable of predicting the thermal, thermal-physical and thermal-mechanical response of composites was recognised in the 1970s when carbon fibre composites began to be used for aerospace applications. Composites of all types are now being used in more industries and in more applications, increasing demand for reliable fire models.

Accurately modelling the fire response of composites is beneficial in several ways. Firstly, models can rapidly assess the fire resistance of new materials for composite products. This can reduce the number of expensive fire tests that need to be conducted. Reliable models can also help improve our understanding of the fire behaviour of composites, and further the development of new fire-safe materials.

There are several mathematical models describing the fire response of composites, varying in complexity from the simple where only heat conduction is considered, to

the very complex where several processes described earlier are considered. However, before any of theses models are discussed it is useful to describe the sequence of events that occur when a composite material is exposed to fire.

2.2.1. Response of Composites to Fire

When a heat flux typical of a high temperature fire is applied to one side of a composite material, the first event to take place is heat conduction into the material. The rate of heat conduction through the material is governed by the incident heat flux and the thermal diffusivity of the material. Thermal diffusivity is low for most composites particularly in the through thickness direction. This results in a steep temperature gradient between the hot front face and the cold rear face. The process of heat conduction is complicated by the anisotropic nature of the material, giving it different values for thermal conductivity in different directions. It is further complicated by the fact that thermal conductivity and specific heat of composites vary with temperature. Although a large amount of work has been carried out on the thermal conductivity of composites [37-46], a theoretical model capable of predicting it as a function of temperature is not yet available. This is also true of specific heat [47].

Heat conduction through a laminate will cause it to expand. Due to the thermal gradient in the through thickness direction, this expansion will be non-uniform. It will be greatest in the hot face, decreasing towards the cold face.

At temperatures below the decomposition temperature of the matrix material, heat transfer occurs largely by conduction. When the temperature rises above the decomposition temperature, the matrix and fibres degrade endothermically, yielding gaseous products. These reaction volatiles flow through the char layer to the surface. If the temperature reaches above 100-150°C, then any moisture present in the matrix is vaporised. The endothermic reactions have the effect of temporarily delaying conduction through the material.

The reaction volatiles and moisture vapour are initially trapped in the material due to the low gas permeability of composites. This leads to a rapid rise in internal pressure causing the material to expand further. At this point the matrix is heated well above its glass transition temperature (T_g), making it soft and compliant. This allows the formation of gas filled pores, and delaminations and matrix cracks to occur.
Eventually the matrix will become sufficiently cracked and porous to allow volatiles and moisture vapour to escape to the surface through the degraded region of the composite. This process has the effect of delaying conduction.

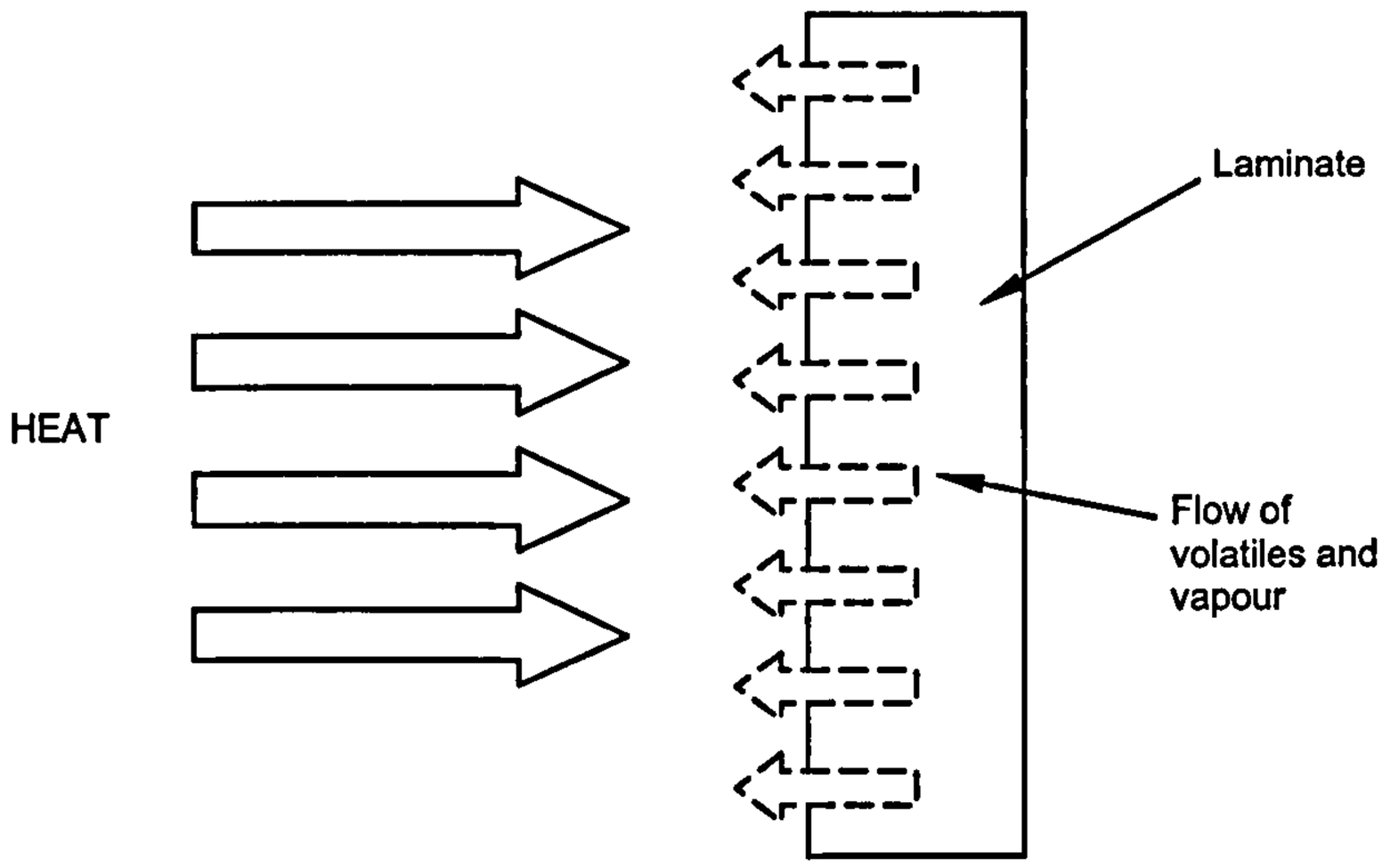

Figure 2.1. Schematic detailing the flow of volatiles and vapour to the hot face of a composite laminate, subjected to heat.

Decomposition continues until the reaction zone reaches the rear face where the last of the combustible material is turned to char and volatiles. The decomposition process is usually complete at this point unless the temperature is high enough to induce pyrolysis reactions between the char and silica network of the degraded reinforcement (in excess of 1000°C). If this is the case, then considerable mass loss can occur [48]. Ablation can also occur at high temperatures, which is accelerated by high velocity air flow over the surface.

All of the processes described are listed in Table 2.1.

Table 2.1. Summary of the main processes occurring when a composite is exposed to fire.

Anisotropic heat conduction through virgin material and char
Thermally induced strains
Decomposition of polymer matrix and organic fibres
Pressure rise due to formation of combustion gases and vaporisation of moisture
Flow of gases from the reaction zone through the char zone
Formation of delamination and matrix cracks
Reactions between char and fibre reinforcement
Ablation

Complex models [2, 8, 35, 49-64] consider many of the processes laid out in Table 2.1. The majority of mathematical models are all based on one-dimensional heat conduction.

2.2.2. 1-D Heat Conduction Model

In the study of heat transfer it is usual to consider the three modes of thermal energy transfer: conduction, convection and radiation. For simplicity of analysis, nearly all mathematical models for composites only consider conduction.

The simplest model is a 1-D approach that considers heat conduction through a composite in the through-thickness (x) direction when heated from one side. The model assumes that the composite is a thick slab with a uniform in-plane temperature distribution. The rear face is also assumed to be adiabatic. The 1-D heat conduction [65] is expressed as:

$$\rho C_P \frac{\partial T}{\partial t} = \frac{\partial}{\partial x}\left[k_x \frac{\partial T}{\partial x}\right] \qquad (2.1)$$

where T is the temperature, t is the time and x is the distance below the hot surface in the through thickness direction. ρ and C_P are the density and specific heat of the composite, respectively, and k_x is the thermal conductivity of the composite in the through-thickness direction. ρ, C_P and k_x are assumed to be independent of temperature, although this is not strictly the case.

2.2.3. Henderson Model

The latest mathematical models owe a lot to Henderson [7, 8, 50-54]. This work was based on the theory of the fire response and decomposition of wood, particularly that of Kung [66] and Kansa et al.[67]. Henderson's 1-D equation is expressed as:

$$\rho C_P \frac{\partial T}{\partial t} = k\frac{\partial^2 T}{\partial x^2} + \frac{\partial k}{\partial x}\frac{\partial T}{\partial x} - \dot{m}_g C_{Pg}\frac{\partial T}{\partial x} - \frac{\partial \rho}{\partial t}(Q_i + h - h_g) \qquad (2.2)$$

where i equals 1 and 2 for the matrix decomposition and carbon-silica reactions, respectively, and k is taken to be the through thickness thermal conductivity. The first term on the right hand side of the equation considers heat conduction. This is also the case for the second term, although this considers the influence of changes in the rate of heat conduction brought on by variation in the transverse thermal conductivity. As it is not possible to model the change in thermal conductivity, this is based on an empirical relationship. The third term on the right hand side of the equation considers the effect of volatiles flowing through and out of the damaged material. The cooling effect of this makes this a negative term. The final term on the right hand side relates to the heat generation or consumption resulting from matrix decomposition and any char glass reactions, where Q_i, h and h_g are the heat of decomposition, enthalpy of the solid phase, and enthalpy of the volatile gas, respectively. This term is negative for endothermic reactions, and positive for exothermic reactions. In this final term the decomposition reaction rates are determined from the mass loss rate from the Arrhenius kinetic rate equation:

$$\frac{\partial m}{\partial t} = -A_i m_0 \left[\frac{m - m_f}{m_0}\right]^{n_i} e^{\frac{E}{RT}} \qquad (2.3)$$

where A_i, E and n_i are the pre-exponential factor, activation energy and order of the reaction. These parameters are determined through thermo-gravimetric analysis. R is the universal gas constant; m_0, m_f and m are the initial, final and instantaneous mass of the material, respectively.

2.2.4. Simplified Henderson Model

A simplified version of the Henderson model was developed by Gibson et al.[35]. In this case it is assumed that glass-char reactions do not occur, making in inapplicable to heat fluxes above ~125kWm^{-2} (1000°C). As the majority of real fires are in the region of 50-75kWm-2 this simplification is justified. This is reflected in the fact that the tests described in section 1.7 are designed to function in this region. Further simplifications assume that thermal and gas transport properties are constant during the decomposition of the matrix. The thermal conductivity and specific heat properties of the composite are assumed to remain constant. This is expressed as:

$$\rho C_P \frac{\partial T}{\partial t} = \frac{\partial}{\partial x}\left(k\frac{\partial M}{\partial x}\right) - \rho A\left[\frac{m-m_f}{m_0}\right]^n e^{\frac{E}{RT}}(Q_P + h_C - h_G) - \dot{M}_G \frac{\partial}{\partial x} h_G \qquad (2.4)$$

The three terms on the right hand side of the equation relate respectively to heat conduction through the material, endothermic resin decomposition, and transportation of heat to the hot face by volatile convection.

Much like the Henderson model, no account is taken for char formation, believed to be beneficial in prolonging integrity, nor does it take into account fibres falling away from the hot surface after a prolonged exposure to fire. In spite of this the model has proven accurate in determining the fire performance of many types of composite systems [2, 4, 35, 64, 68].

2.3. Fire Behaviour under Load

Gibson et al. developed a failure model[6] based on a two layer model developed by Mouritz et al.[34, 69, 70]. This assumes the laminate consists of two explicit layers. The first is the thermally affected region and is assumed to have zero mechanical properties. The second layer is the undamaged region consisting of untouched, virgin material with room temperature mechanical properties (see Figure 2.2).

A major shortcoming of this approach is that it fails to take into account the progressive change in mechanical properties of a material as temperature increases; it simply assumes a step change. This need for accurate material property data has been highlighted by other workers[71, 72]. Further work has been carried out to try and achieve this[73] resulting in better understanding of how material properties vary with temperature.

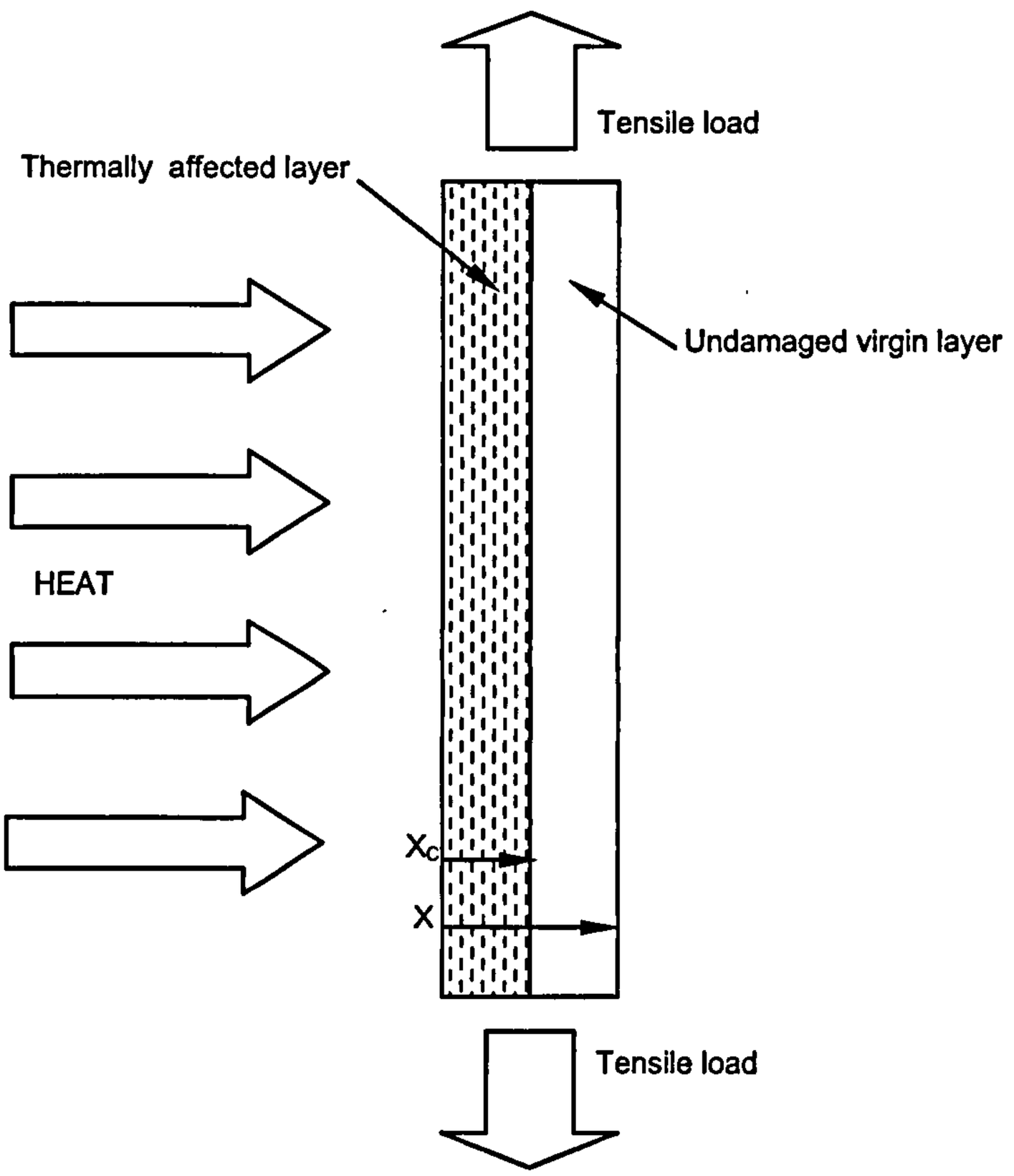

Figure 2.2. Schematic of a composite sample described using the two layer approach. The sample is undergoing tensile loading whilst subjected to a one-sided heat flux (x denotes depth of laminate, x_C denotes depth of char layer).

Large scale testing has been carried out to determine the fire response of large pultruded structures[74-76]. The main findings of this work are that pultruded decking when loaded, is capable of maintaining structural integrity provided that the heat source is on the tensile side of the beam[75]. Further work has investigated the effect internal water-cooling has on extending failure time of composite flooring[74].

Again in this case the fire attacked the tensile side of the structure, highlighting the ability to maintain structural integrity if in tension.

2.4. Chapter Summary

In spite of being inherently combustible they exhibit some interesting properties in fire, particularly the 'slow burn-through' effect. In composites above a certain critical thickness, the burn through rate is greatly reduced, as are heat release and heat transmission through the material. These result in increased fire integrity of the composite, increasing their potential for use in fire protection applications.

Thermal decomposition of fibre reinforced composites is very complex, combining thermal, chemical and physical processes. These are detailed in Table 2.1.

In the study of heat transfer it is usual to consider the three modes of thermal energy transfer: conduction, convection and radiation. For simplicity of analysis, nearly all mathematical models for composites only consider conduction. The simplest of these is a 1-D approach that considers heat conduction through a composite in the through-thickness direction when heated from one side (equation 2.1).

The latest mathematical models are based on Henderson's 1-D equation (equation 2.2) which considers heat conduction through the laminate, as well as the effect of volatiles flowing through the damaged laminate, and any decomposition effects.

A simplified version of Henderson's equation was developed, suitable for fires with heat fluxes less than ~125kWm^{-2} (1000°C).

There has also been some investigative work into the fire behaviour of composites whilst under load. A two layer model was developed that assumes the composite has two explicit layers. The first is the thermally affected region and is assumed to have zero mechanical properties. The second layer is the undamaged region consisting of untouched, virgin material with room temperature mechanical properties (see Figure

2.2). Large scale testing has been carried out to determine the fire response of large pultruded structures. The main findings of this work are that pultruded decking when loaded, is capable of maintaining structural integrity provided that the heat source is on the tensile side of the beam.

3. Thermal Modelling

3.1. 1-D Thermal Model

Heat flowing through a laminate can be described by a modified version of Laplace's equation[1-9]. In its one-dimensional form this relationship based on the Henderson equation gives,

$$\rho C_P \frac{\partial T}{\partial t} = \frac{\partial}{\partial x}\left(k\frac{\partial M}{\partial x}\right) - \rho\frac{\partial M}{\partial t}(Q_P + h_C - h_G) - \dot{M}_G\frac{\partial}{\partial x}h_G \qquad (3.1)$$

where T, t and x are temperature, time and through thickness co-ordinates, respectively. ρ, C_P and k are the density, specific heat and conductivity of the composite. $\dot{M}_G$ is the mass flux of volatiles, h_C and h_G are the respective enthalpies of the composite and the evolved gas. Q_P is the endothermic decomposition energy. The three terms on the right hand side of the equation relate respectively to heat conduction through the laminate, endothermic resin decomposition, and transportation of heat to the hot face by volatile convection.

Thermal decomposition of the matrix material can be approximated by a single reaction with Arrhenius temperature dependence,

$$\frac{\partial m}{\partial t} = -A\left[\frac{(m - m_f)}{m_0}\right]^n e^{(-E/RT)} \qquad (3.2)$$

where m, t and T are the mass, time and temperature variables respectively, A, E and n are the rate constant, activation energy and order of the reaction. R is the gas constant (8.3144 $Jmol^{-1}K^{-1}$). Polyester resin (and indeed many others) can be described in this way, whereby after decomposition a relatively small proportion of solid material is left behind (char), after all the volatiles have burnt off. Phenolic resin decomposes in a more complex manner. This takes place in two distinct stages,

an initial primary condensation (often producing water), followed by char formation at a much higher temperature.

In each case, the decomposition parameters need to be determined by thermo-gravimetric analysis (TGA), based upon a mass loss curve for the resin as it heated at a constant heating rate.

3.2. Thermogravimetric Analysis (TGA) Parameters

In order to use the thermal model (equation 3.1), kinetic inputs are required (see Figure 1.14.). The necessary kinetic parameters are;

A, the rate factor (s^{-1})

E, the activation energy ($Jmol^{-1}K^{-1}$)

These parameters were obtained from the literature and are detailed in Table 3.1 and Table 3.2 for polyester and phenolic respectively.

Table 3.1. TGA parameters for polyester resin [77].

Parameter	Value
A	$1.29 \times 10^{13}\ s^{-1}$
E	$2 \times 10^{5}\ Jmol^{-1}k^{-1}$

Table 3.2. TGA parameters for phenolic resin [2]. Note that phenolic resin decomposes in two distinct phases, requiring two sets of parameters. A percentage of remaining mass is also needed to define the boundary between the two phases.

Parameter	Value
A (Phase 1)	$5\ s^{-1}$
E (Phase 2)	$27200\ Jmol^{-1}k^{-1}$
A (Phase 2)	$68\ s^{-1}$
E (Phase 2)	$65200\ Jmol^{-1}k^{-1}$
Mass remaining after Phase 1	87 %

A finite difference model based upon the simplified Henderson equation (equation 3.1) was used to produce data describing the temperature evolution and resin decomposition through laminates of the pultrusions (Figure 3.2 and Figure 3.3). The model has a time step of 0.04056 seconds and records one in every 76 times steps. Typical input data is detailed in Table 3.3.

Table 3.3. Typical input data for the thermal finite difference model. This data would be for an 8mm polyester pultrusion.

Input	Value
Resin type	Polyester
Duration of test	13 mins
Thickness of 3 layers	1.00 mm, 6.00 mm, 1.00 mm
Fibre volume fractions	0.311, 0.527, 0.311
Room Temperature	21°C
Constant heat flux	50 kWm^{-2}
Gas constant	0.8431 $Jmol^{-1}K^{-1}$
A	1.29 $10^{13}s^{-1}$
E	2 x 10^{5} $Jmol^{-1}k^{-1}$
H	2344600 Jkg^{-1}
Resin density	1200 kgm^{-3}
Fibre density	2560 kgm^{-3}
Fibre thermal conductivity	1.09 $Wm^{-1}K^{-1}$
Resin thermal conductivity	0.19 $Wm^{-1}K^{-1}$
Fibre specific heat	760 $Jkg^{-1}C^{-1}$
Resin specific heat	1600 $Jkg^{-1}C^{-1}$
Specific heat of gases	2386.5 $Jkg^{-1}C^{-1}$

The model predicts a universal temperature rise through the pultrusion. Higher temperatures are reached nearer the hot face for a fixed time period, similarly temperature increases at a greater rate nearer the hot face. Residual resin content decreases at a greater rate nearer the hot face, corresponding with the higher temperatures.

The model splits the laminate into the 50 discrete layers with a node at the boundary of each layer making up a total of 51 nodes (1 to 51). Boundary nodes exist between the 2 different reinforcement materials, occurring at nodes 5 and 47 (Figure 3.1). For each time step, the model outputs a resin content and temperature for 7 pre-determined nodes. Typical output files for an 8mm thick polyester pultrusion are detailed in the appendix (Tables A and B). Files for both the residual resin content and temperature evolution are shown.

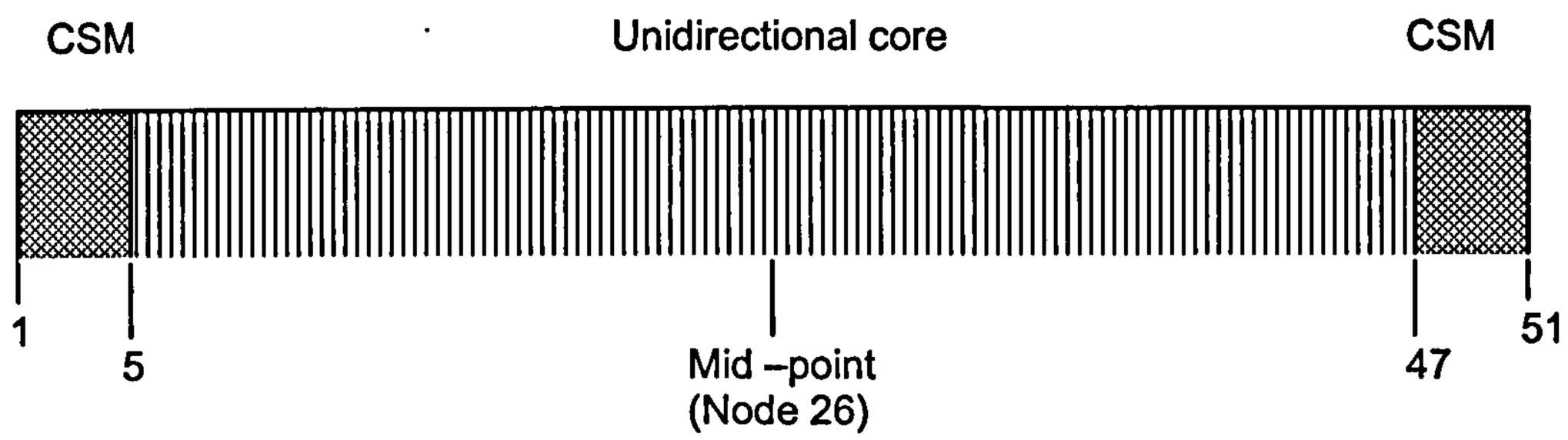

Figure 3.1. Section through a pultrusion highlighting the boundary nodes between the different reinforcement materials.

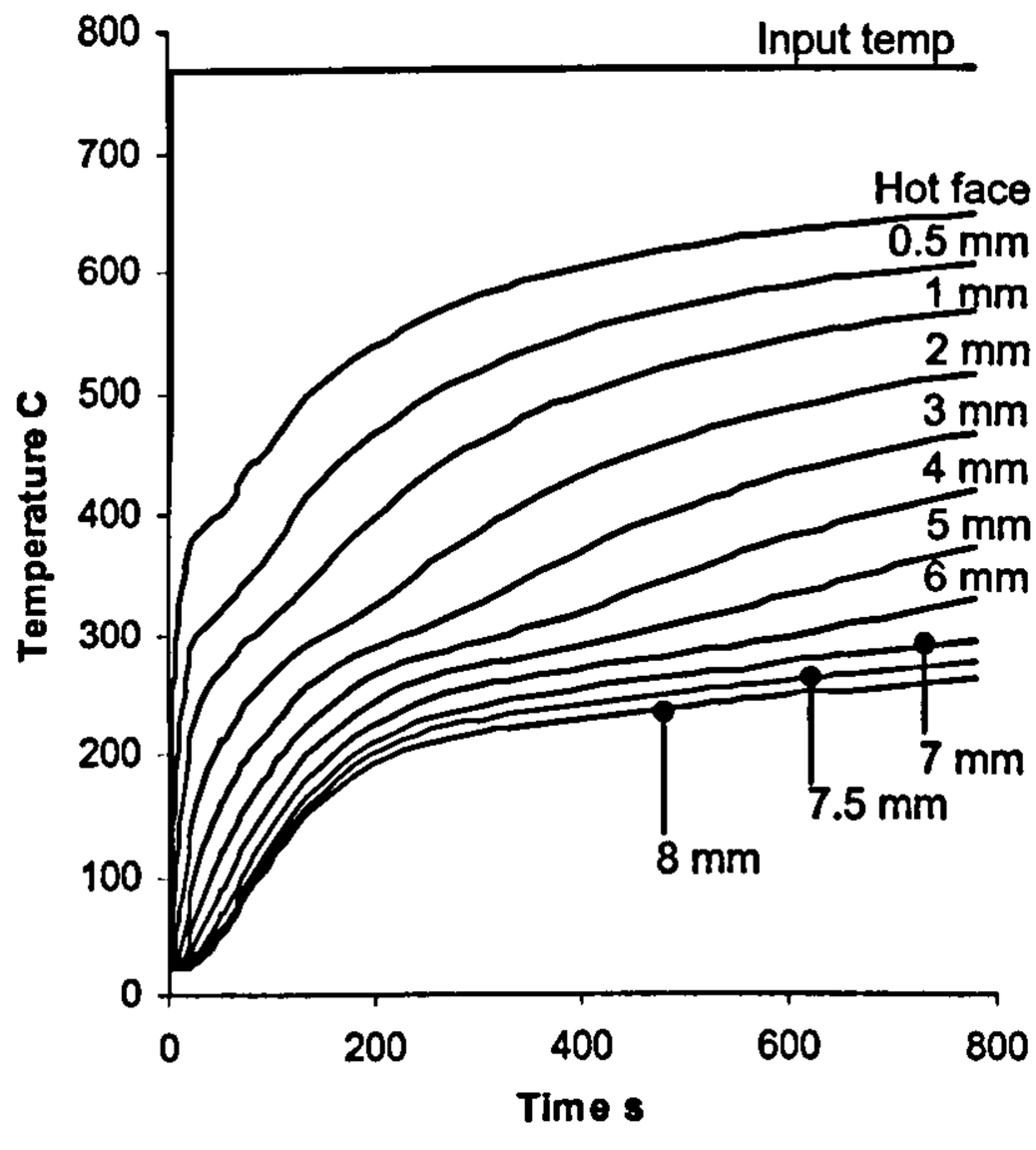

(i)

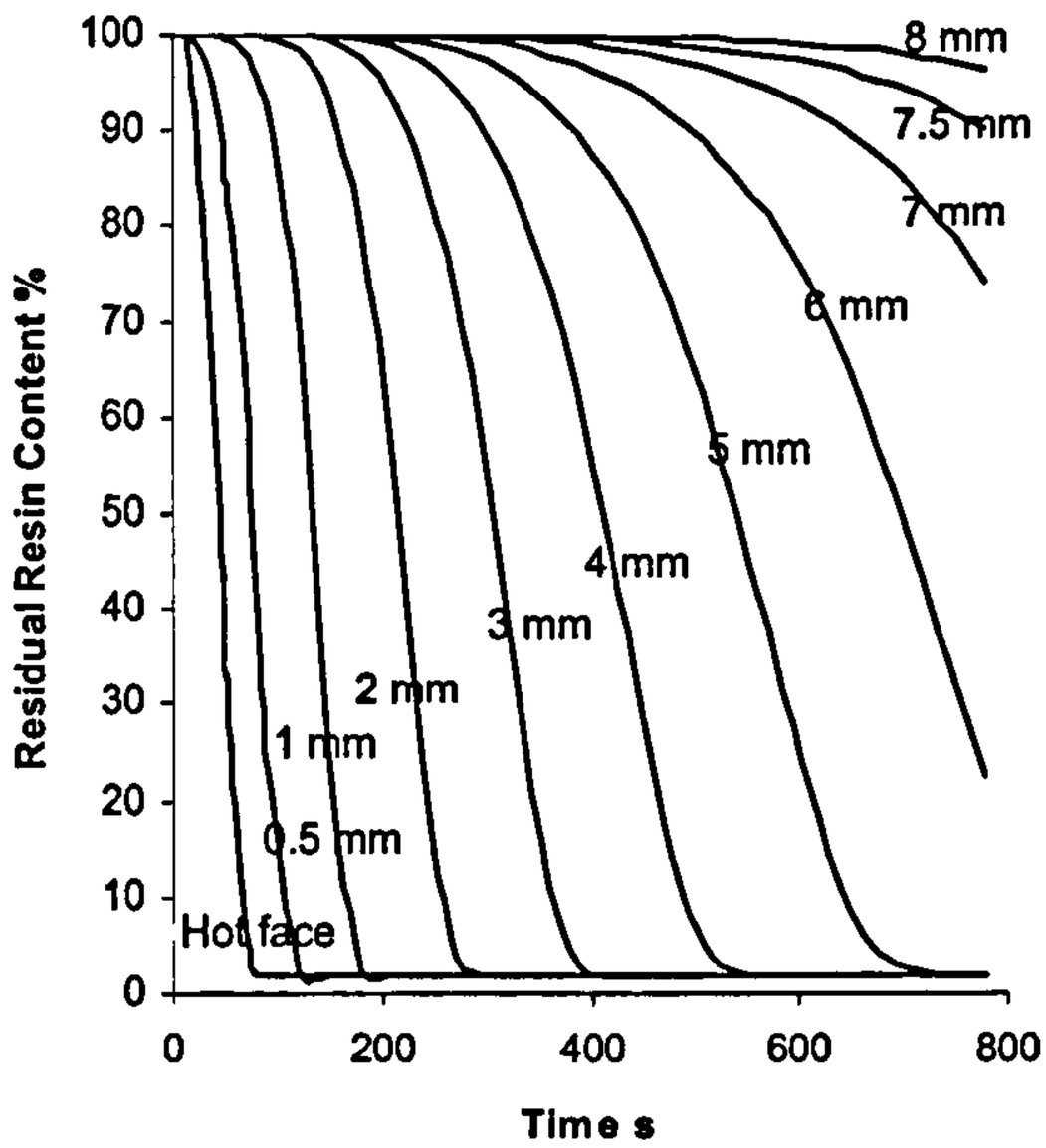

(ii)

Figure 3.2. Temperature evolution (i) and Residual Resin Content (RRC) (ii) for a polyester pultrusion subject to a 50kWm^{-2} heat flux.

The model curves describing residual resin content for the phenolic pultrusion exhibit a kink in the curves corresponding to 87% resin content. This is the point that distinguishes between the two different phases of decomposition associated with phenolic resins

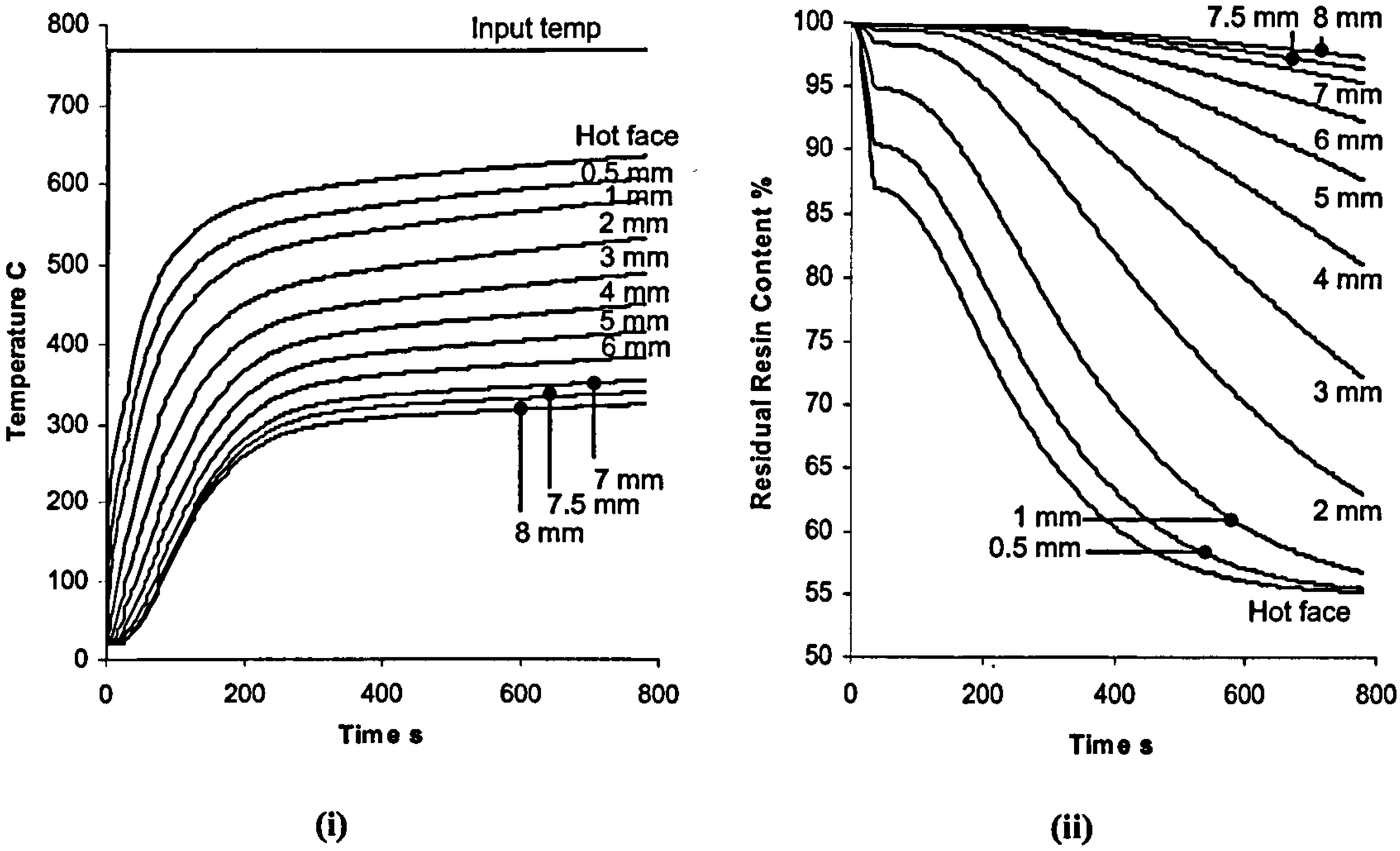

Figure 3.3. Temperature evolution (i) and Residual Resin Content (RRC) (ii) for a phenolic pultrusion subject to a 50kWm^{-2} heat flux.

The accuracy of this model needed to be verified. This was carried out by comparing the calculated cold face temperature of the laminate with a measured thermal response. This thermal response was obtained by using a propane burner test.

3.3. Propane Burner Test

A small scale fire resistance test was developed[29] using a calibrated propane burner[77] capable of producing a constant heat flux. This is directed towards the sample, which measures 110mm x 110mm, and is held vertically in a steel frame, leaving an area of 100mm by 100mm exposed to the burner flame (Figure 3.4). The material is insulated from the frame by a 5mm layer of Kaowool. This minimised heat conduction through the frame and prevented any volatiles escaping and burning at the edge of the sample.

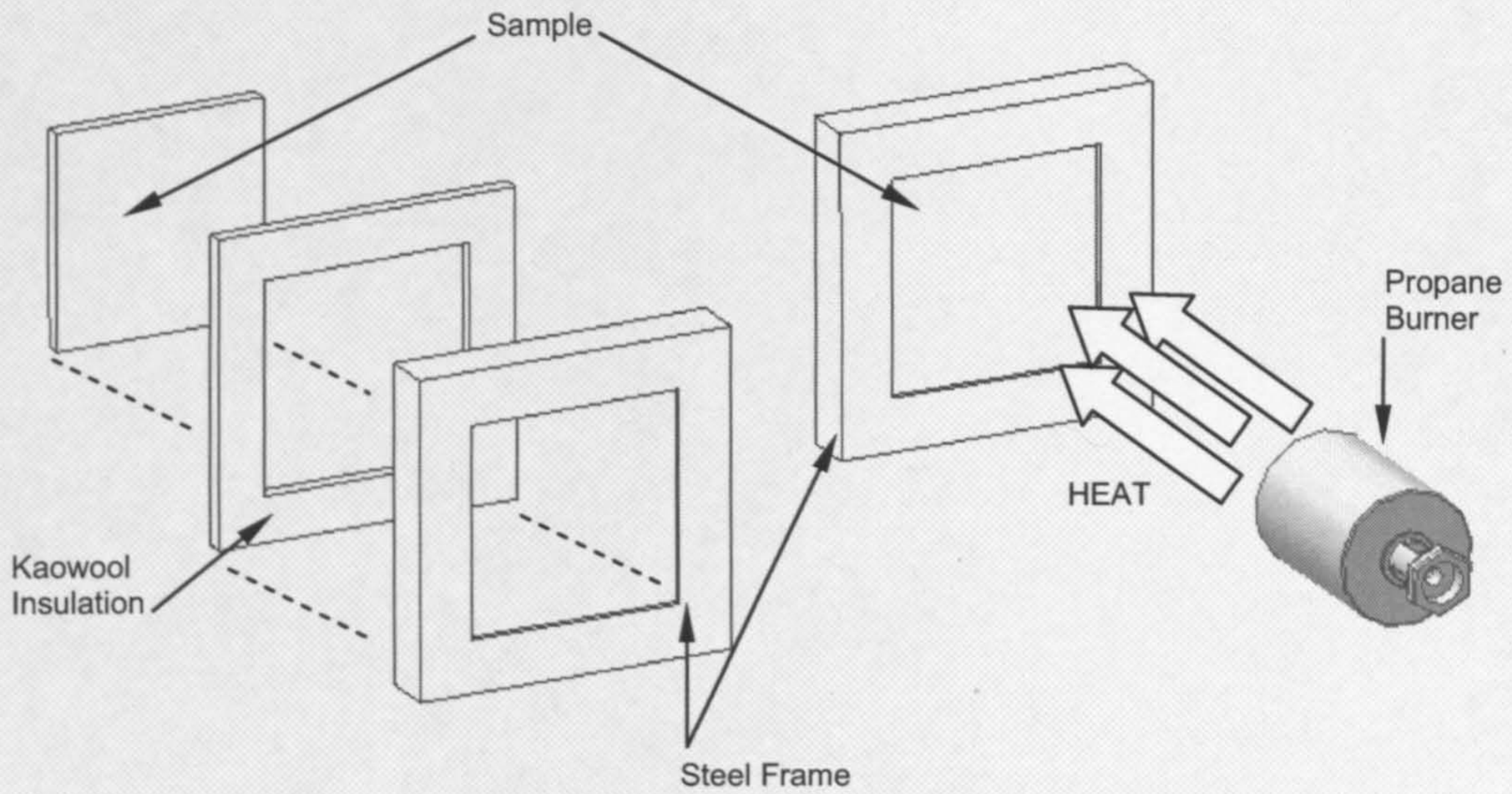

Figure 3.4. Propane burner test. Note the insulation used to minimise heat conduction through the steel frame.

A thermocouple was used to measure an indicative field temperature 10mm from the front of the sample. It was decided to use a constant incoming heat flux throughout the test. This would address any problems caused by material flash-over. Flash-over usually occurred after about 60 seconds and would increase field temperature by 50-100°C.

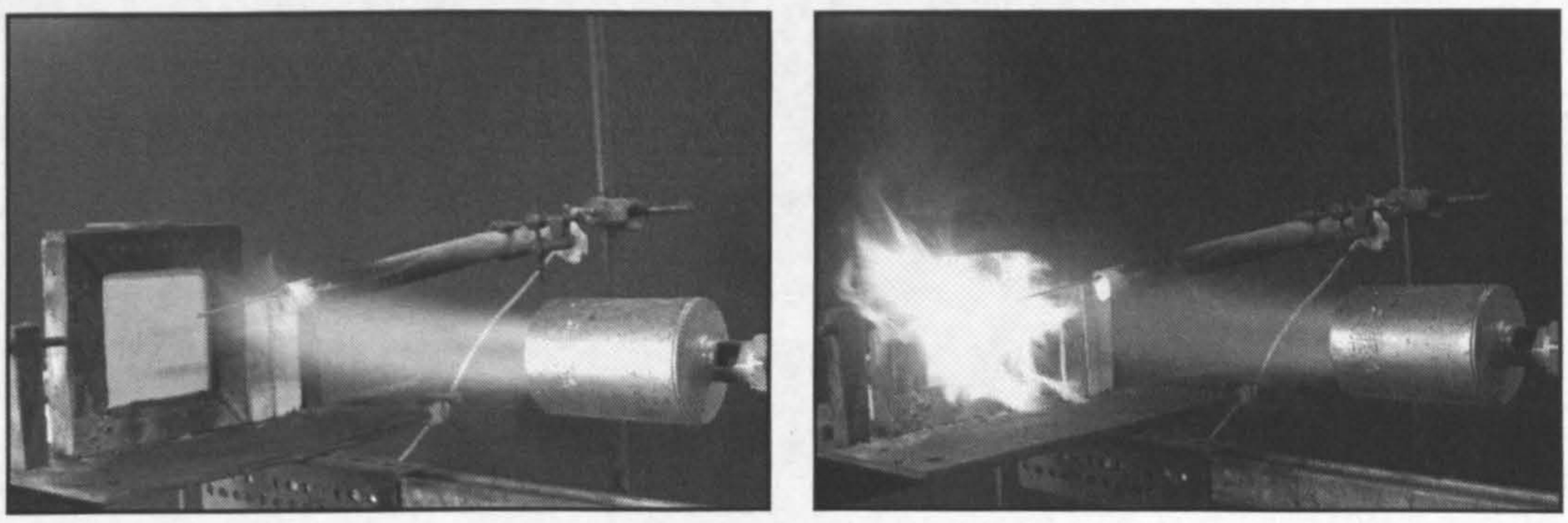

(i) **(ii)**

Figure 3.5. Propane burner test underway, (i) before and (ii) during material flashover.

Thermocouples attached to the rear face of the sample, monitored cold face temperature. The cold face response data is subsequently compared with temperature evolution data calculated from equation 3.1. If the two profiles sufficiently matched

then the material constants used in the thermal modelling can be regarded as acceptable.

3.4. Rear Face Temperature Profile

The cold face responses of the samples tested with the burner were compared to the modelled response. In both cases the modelled response matches the measured cold face response to a reasonable degree of accuracy (Figure 3.6).

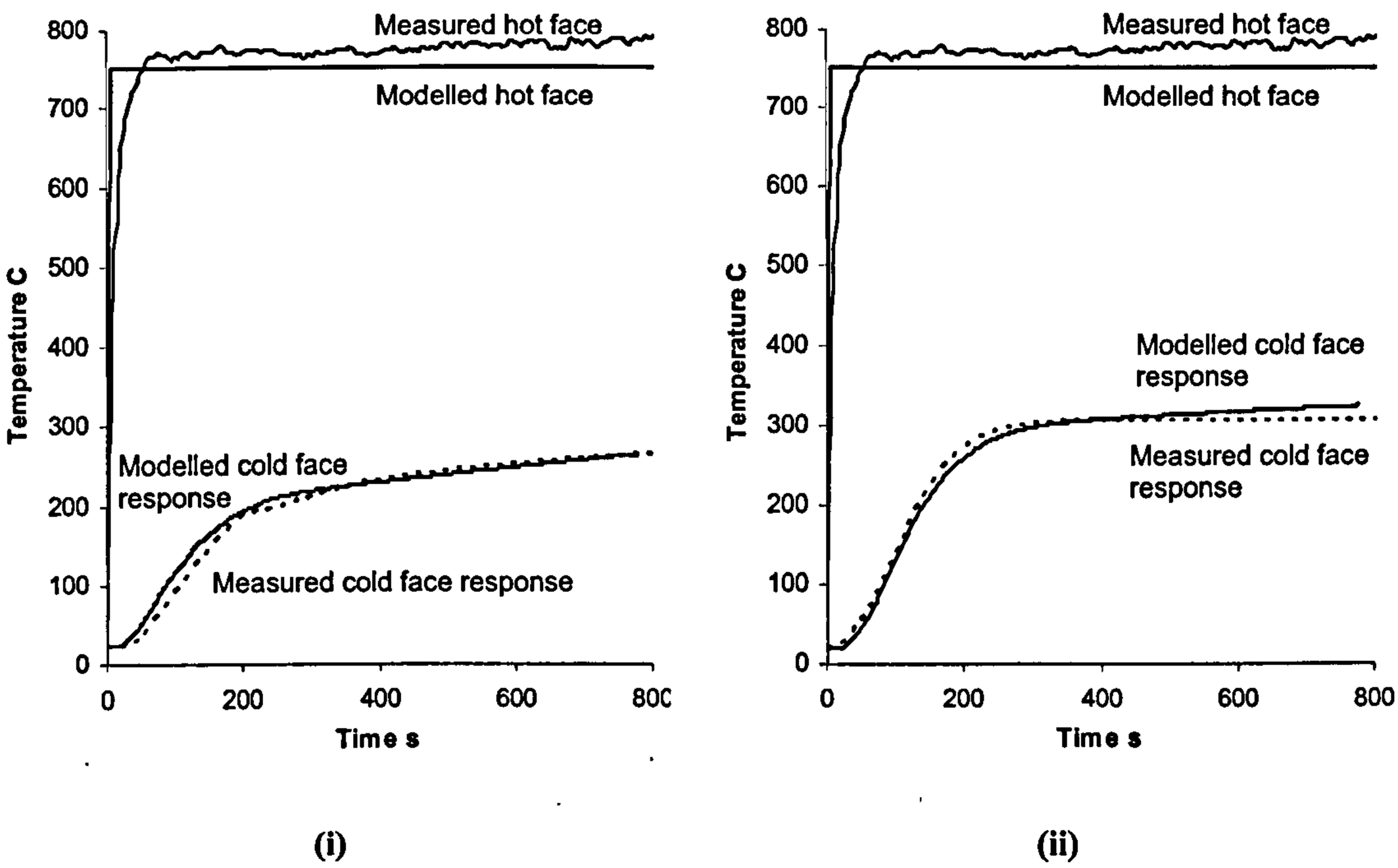

Figure 3.6. Comparison of the real cold face response (dotted line) with the modelled response (solid line) for both polyester (i) and phenolic (ii) pultrusions. In both cases the material was subject to a 50kWm^{-2} heat flux, the temperature profile of which is also shown.

3.5. Chapter Summary

A finite difference model based upon the simplified Henderson equation (equation 3.1) was used to produce data describing the temperature evolution and resin decomposition through laminates of the pultrusions (Figure 3.2 and Figure 3.3). This model uses TGA data taken from literature.

A propane burner test was developed to verify the model's accuracy where the modelled rear face response can be compared with the measured response form the test.

4. Mechanical Properties

To model the structural behaviour of a composite material in fire, material elastic constants and strengths as functions of temperature are needed. However data in this area are scarce in the literature. Consequently a series of experiments were developed and carried out to deliver this information. These are detailed in this chapter. Fitting a temperature dependent relationship to the subsequent data is discussed in chapter 6.

4.1. Materials

Pultrusions were provided by Fiberline Composites, and supplied in box and 'I' sectioned beams. Simple plate sections were also cut from these profiles. The sections were manufactured from E-glass with both a polyester and a phenolic matrix. Material was made up of a unidirectional (UD) core with a CSM needle weave surface layer. The UD core made up 60% of the material thickness, although this did vary slightly from section to section (see Figure 4.1). Details of mechanical properties were provided by the manufacturer (see Table 4.1).

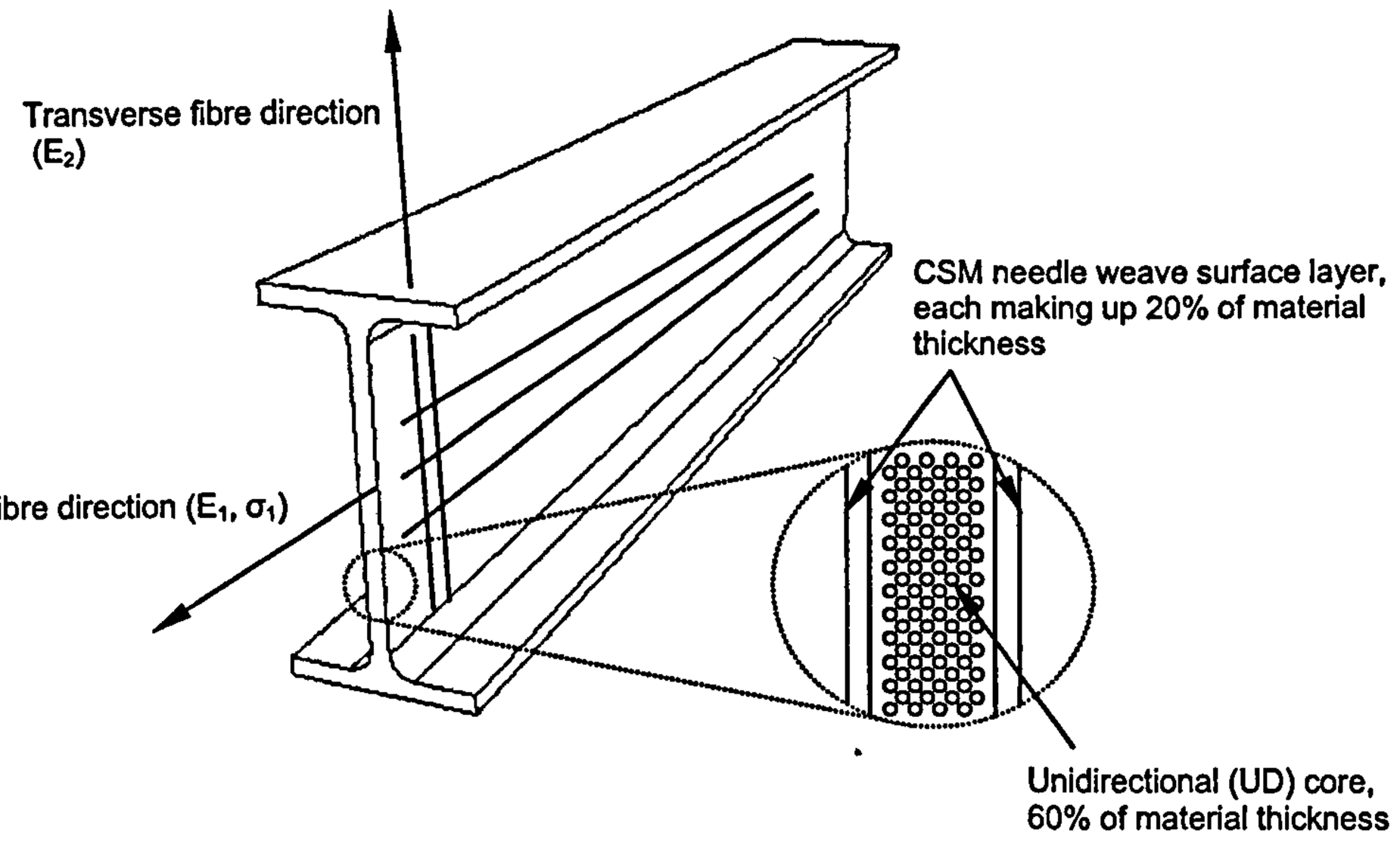

Figure 4.1. Detail view of an 'I' beam highlighting the different layers through the section. Primary fibre directions are also shown. All of the supplied material was constructed with this 3-layer system.

Table 4.1. Material specifications supplied by Fiberline Composites.

Material	UTS (MPa)	Comp. Strength (MPa)	Longitudinal Stiffness E_1 (GPa)	Transverse Stiffness E_2 (GPa)
Polyester (PE)	240	240	23	8.5
Phenolic (Ph)	216	216	18.4	6.8

The fibre volume fraction of each layer was also determined alongside matrix and void content (see Table 4.2).

Table 4.2. Volume fraction data.

Material	Fibre volume fraction %	Matrix volume fraction %	Void volume fraction %
Polyester UD	52.7	42.1	5.1
Polyester CSM weave	31.1	63.5	5.3
Phenolic UD	36.1	38.9	24.8
Phenolic CSM weave	31.1	63.5	5.3

4.2. Tensile Strength at Elevated Temperatures

Pultruded material was milled into a 'dog-bone' shape (see Appendix) for tensile testing. Tests were carried out over a range of temperatures from room temperature up to 400°C. A uniform temperature of the gauge length was maintained through a temperature controlled, aluminium heating jacket (see Figure 4.2). Once the desired temperature was reached, an increasing tensile load was applied until failure occurred. Data were recorded and stress-strain curves were plotted.

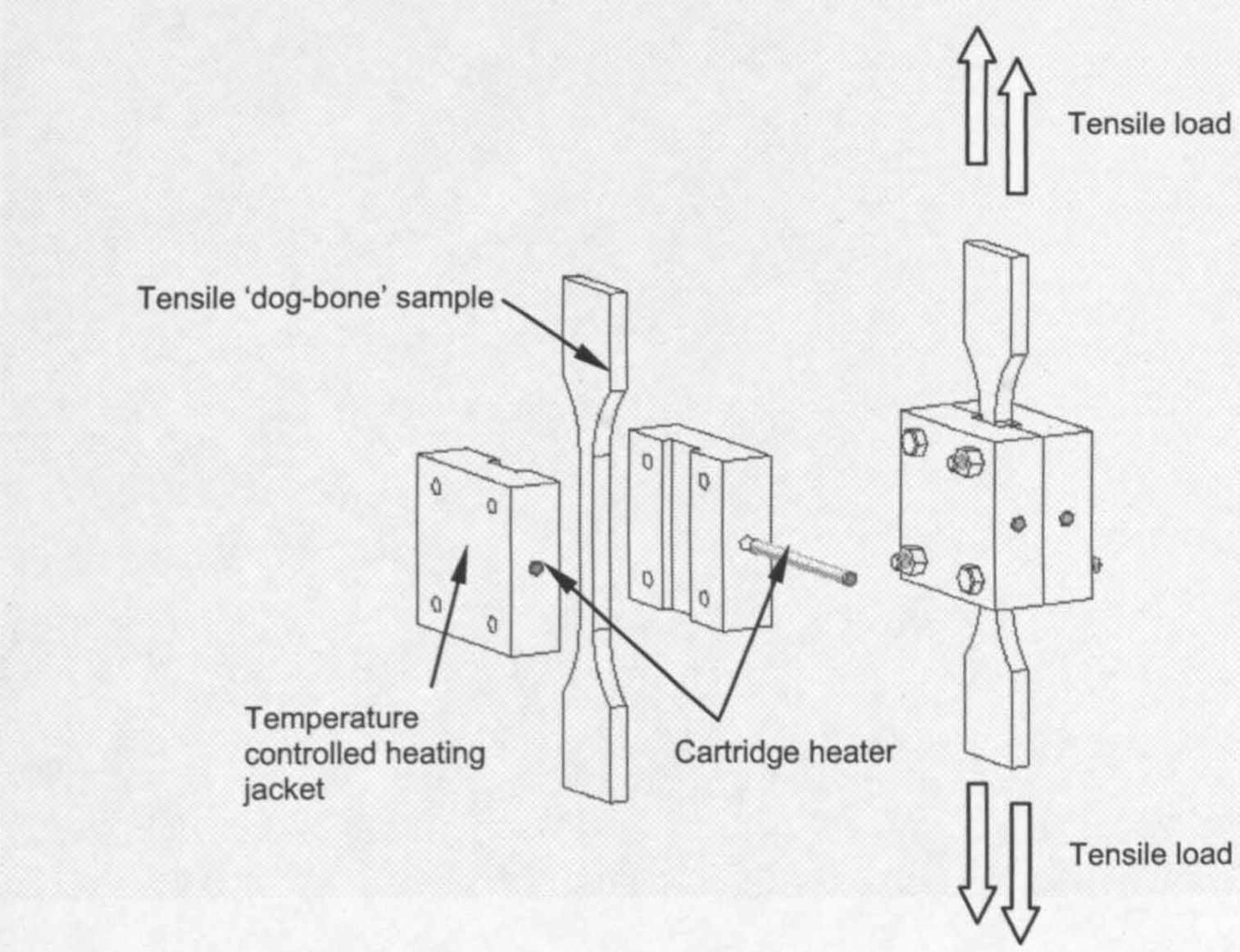

Figure 4.2. Tensile heating rig assembly. Note that heating only takes place in the gauge length of the sample to prevent the material slipping in the grips of the test frame.

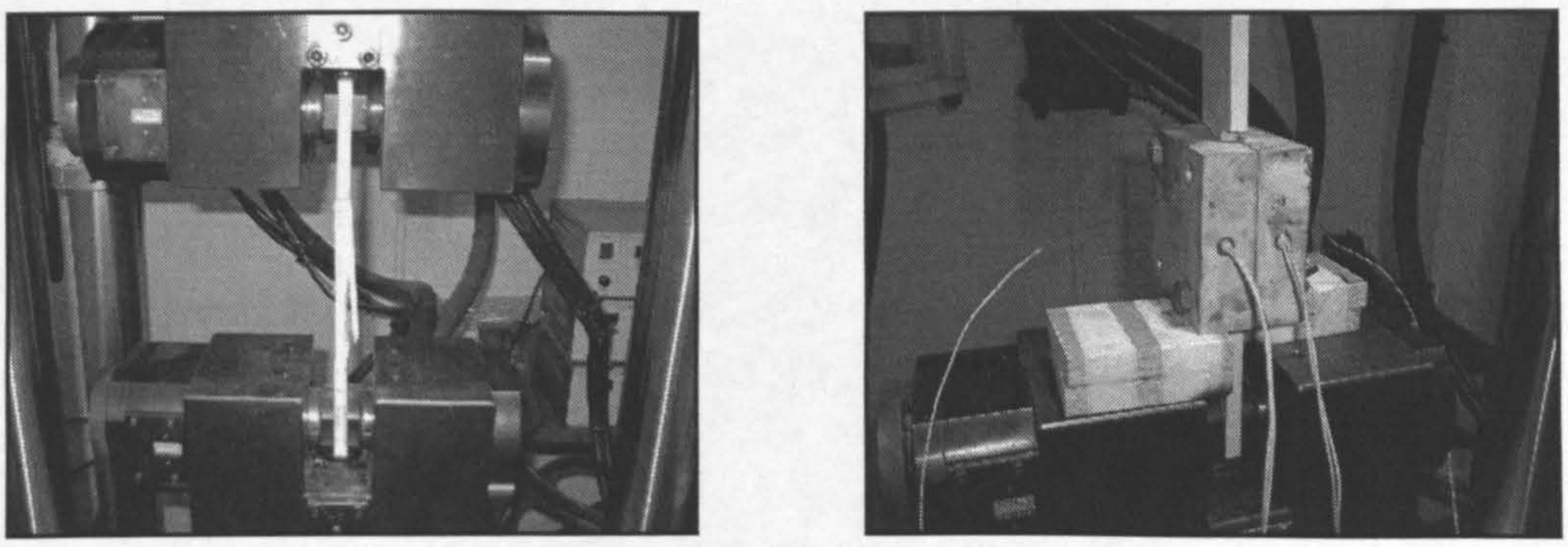

(i) **(ii)**

Figure 4.3. Tensile test carried out at room temperature on a polyester sample (i), and a view of the assembly with external insulation removed (ii).

4.3. Compressive Strength at Elevated Temperatures

Material was cut to size (see Appendix) and positioned in a compressive testing rig designed to both suppress buckling, and provide uniform heating (see Figure 4.4). The rig and sample were heated to the desired temperature. Once up to temperature, an increasing compressive load was applied until failure occurred. This was carried out for temperatures ranging from room temperature up to 400°C. Data were recorded and stress strain curves were plotted.

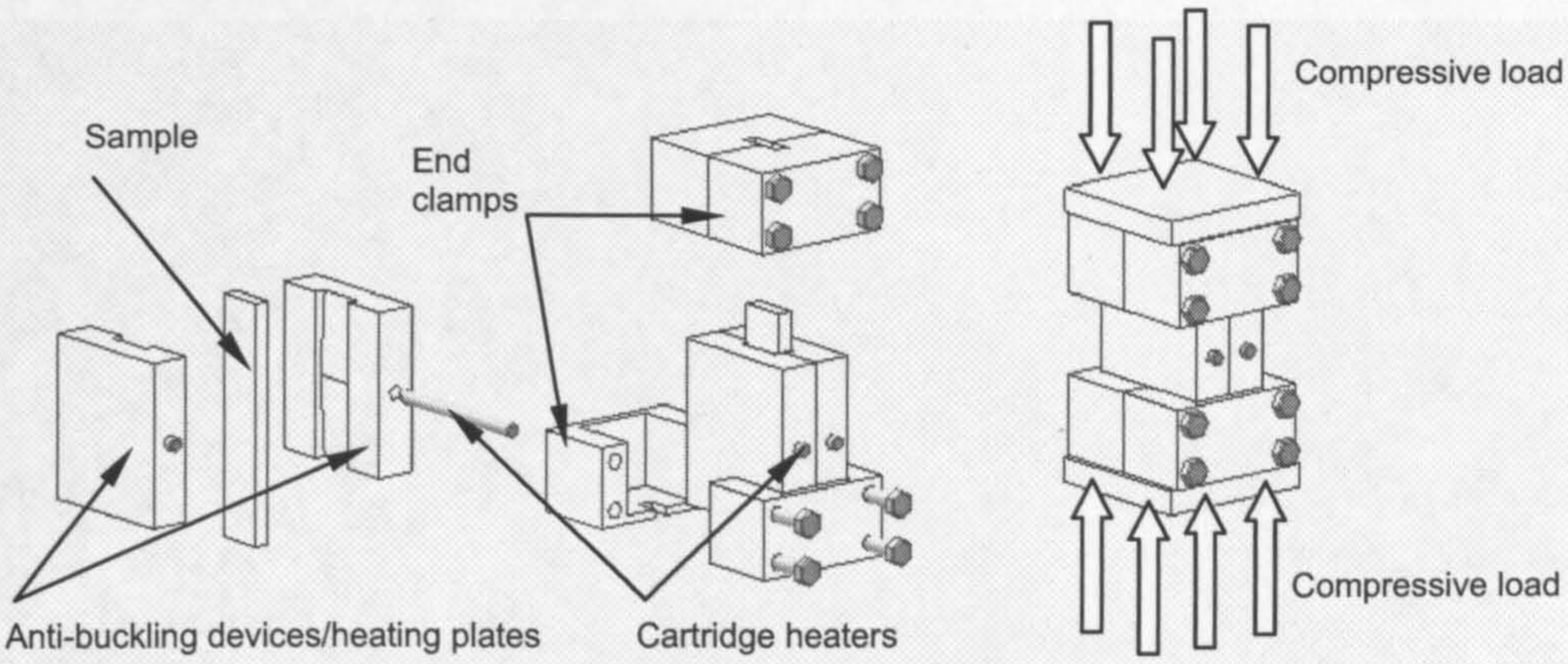

Figure 4.4. Compression rig assembly. Note the anti-buckling devices, designed to suppress the first mode of global-buckling, and also heat up the sample.

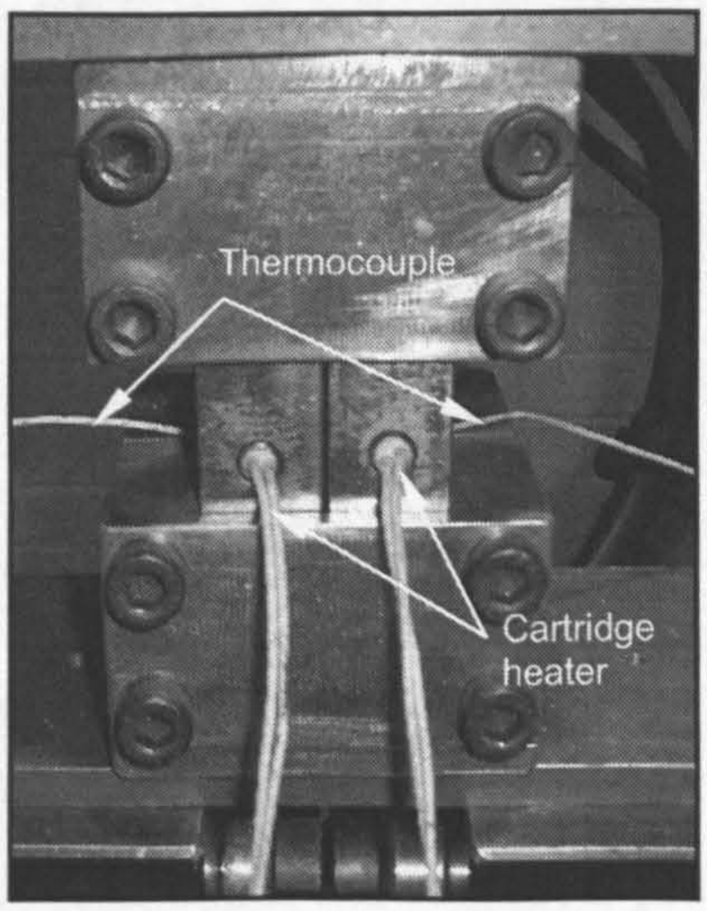

Figure 4.5. View of the compression rig with external insulation removed for clarity. Note the thermocouples used to monitor and control the cartridge heaters.

4.4. Longitudinal (E_1) & Transverse (E_2) Stiffness at Elevated Temperatures

Stiffness measurements were carried out according to BS EN ISO 14125: 1998. A 3-point-bend with a span to thickness ratio of 16:1 [78]. For these tests the bend rig was thermally insulated and temperature controlled (see Figure 4.6). Tests were carried out over a range of temperatures. Once the desired temperature was reached, load was applied in the form of a dead weight (100g). The temperature and load were maintained for a period of 10 seconds, during which deflection data were recorded at 1 and 10 seconds after the load was applied.

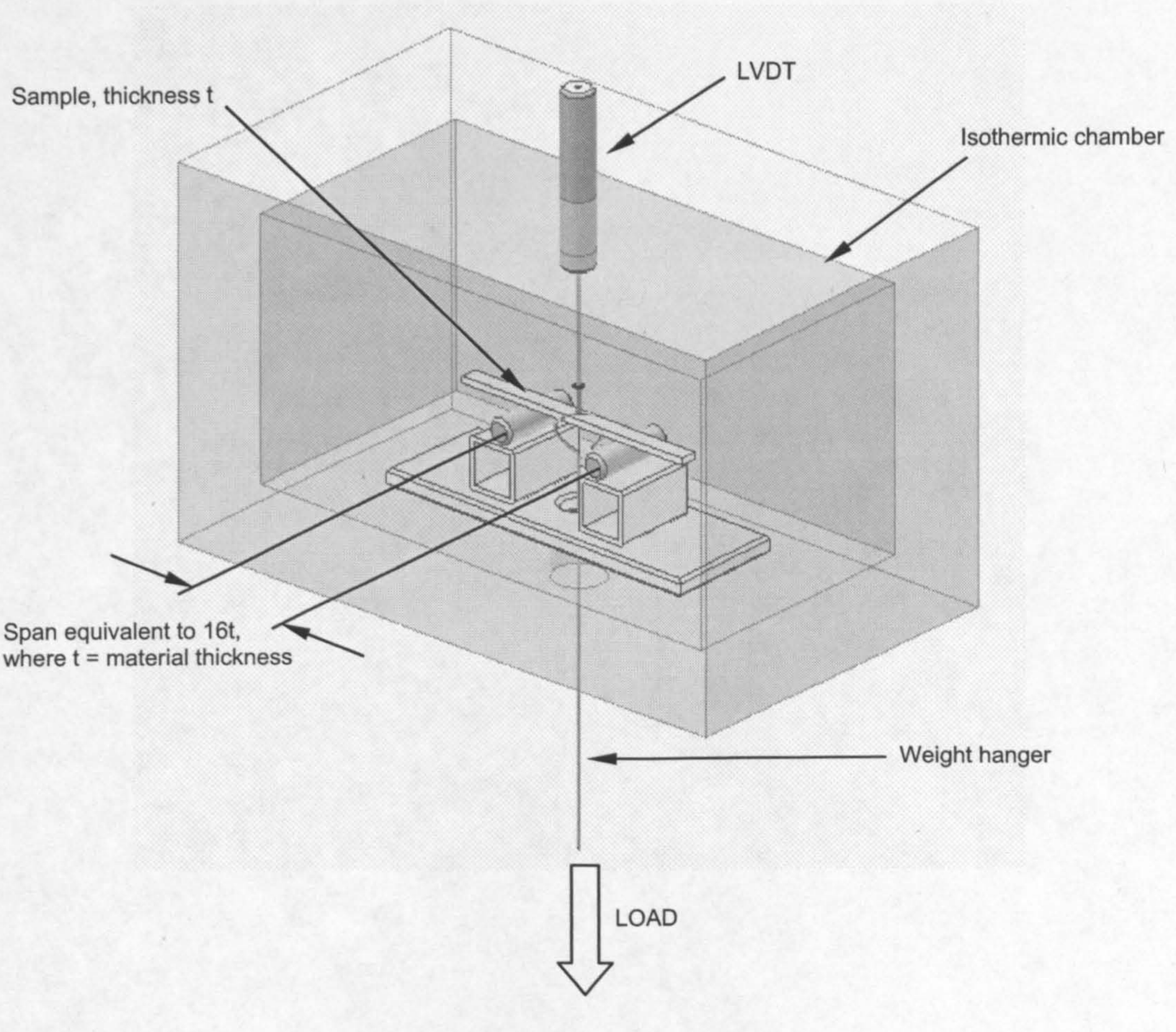

Figure 4.6. Longitudinal and transverse stiffness testing rig. Note the span-to-thickness ratio of 16:1, and the isothermic chamber to allow tests to be carried out at constant temperatures.

Deflection data were converted to provide stiffness values (GPa) over the temperature range by using the equation,

$$E = \frac{Wl^3}{48I\delta} \qquad \textbf{(4.1)}$$

where E is the flexural modulus, W the applied load, l the length of span, I the second moment of area and δ the measured deflection. Once 10s was reached and the data recorded, the load was removed and the sample relaxed. After a short period the temperature of the rig was slowly increased to the next desired value and the procedure repeated. The procedure was repeated for transverse modulus, E_2.

The mechanical properties E_1, E_2, σ_{T1} and σ_{C1} as functions of temperature were all used in the construction of a failure model (see Chapter 7).

4.5. Chapter Summary

To model the structural behaviour of a composite material in fire, material elastic constants and strengths as functions of temperature are needed. However data in this area are scarce in the literature. Consequently a series of experiments were developed and carried out to deliver this information. They consisted of temperature controlled heating rigs, designed to maintain a constant test sample temperature.

The material tested in this thesis was provided by Fiberline Composites, and supplied in box and 'I' sectioned beams. Simple plate sections were also cut from these profiles. The sections were manufactured from E-glass with both a polyester and a phenolic matrix. Material was made up of a unidirectional (UD) core with a CSM needle weave surface layer. The UD core made up 60% of the material thickness,

although this did vary slightly from section to section (see Figure 4.1). Details of mechanical properties were provided by the manufacturer (see Table 4.1).

5. Fire Testing Under Load

The simplest method of assessing the fire resistance of a composite system under load is to carry out small scale tests equivalent to stress-rupture tests[3, 34, 70, 71, 79]. Although they cannot be used for qualification purposes, they can provide useful indications of failure modes, and also provide information about the effectiveness of fire protection, without the expense and complexity of a larger scale test.

5.1. Tensile Tests in Fire

Tensile samples were fabricated measuring 500mm x 75mm with the long side being cut in the longitudinal direction. The samples were loaded with a constant tensile load and subjected to a flame from a propane burner (Figure 5.1). The heat flux of the burner was calibrated to 50kWm^{-2} based on hot face temperature and distance from the front of the burner to the front of the sample. The heat flux was kept constant throughout the test by monitoring the temperature from the 'hot-face' thermocouple. The time taken for the sample to fail from the moment the burner was turned on (time to failure) was recorded for several loads. Ultimate tensile strength was determined also, and recorded with a failure time of 1 second.

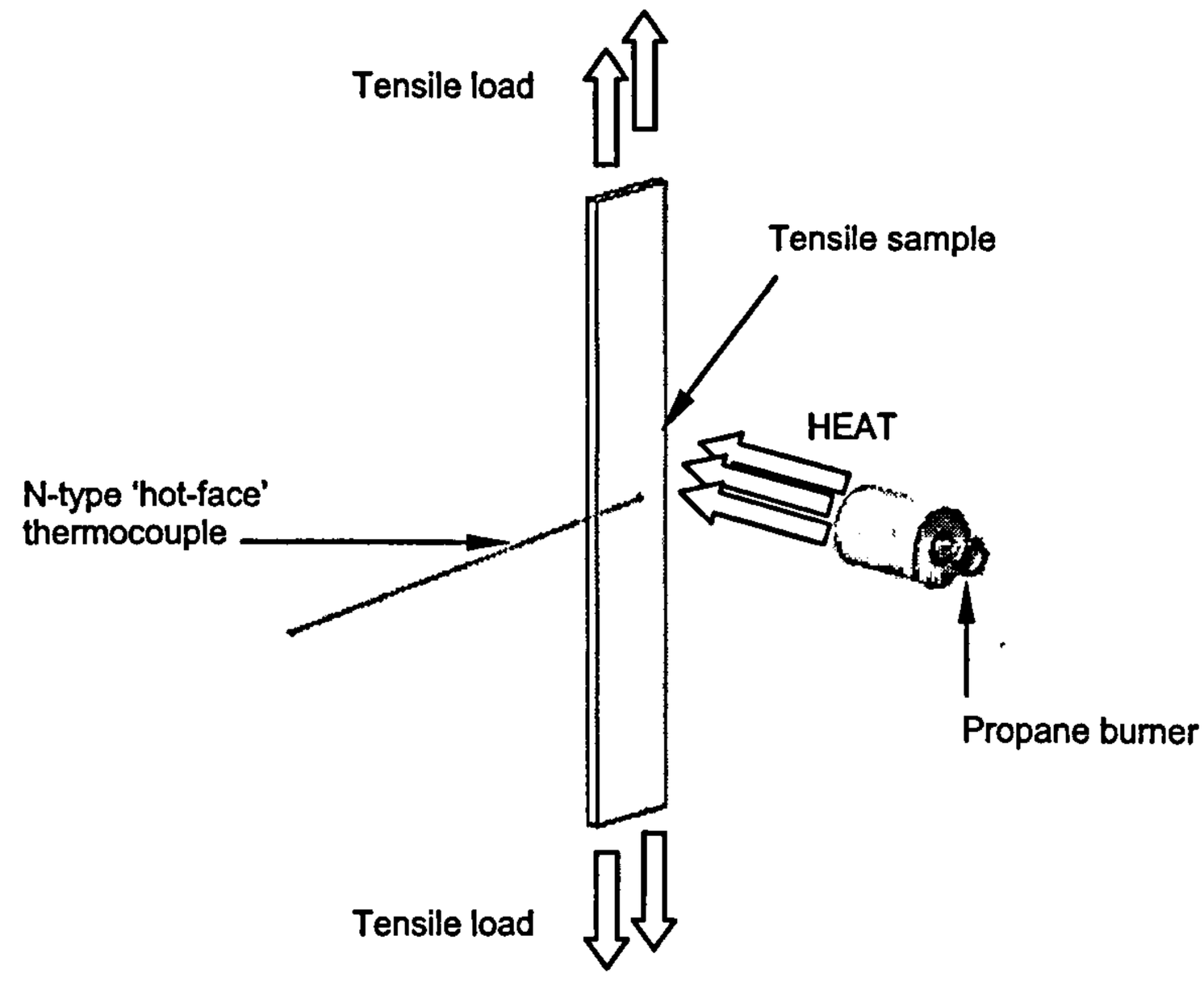

Figure 5.1. Arrangement for tensile fire test using a propane burner as a heat source.

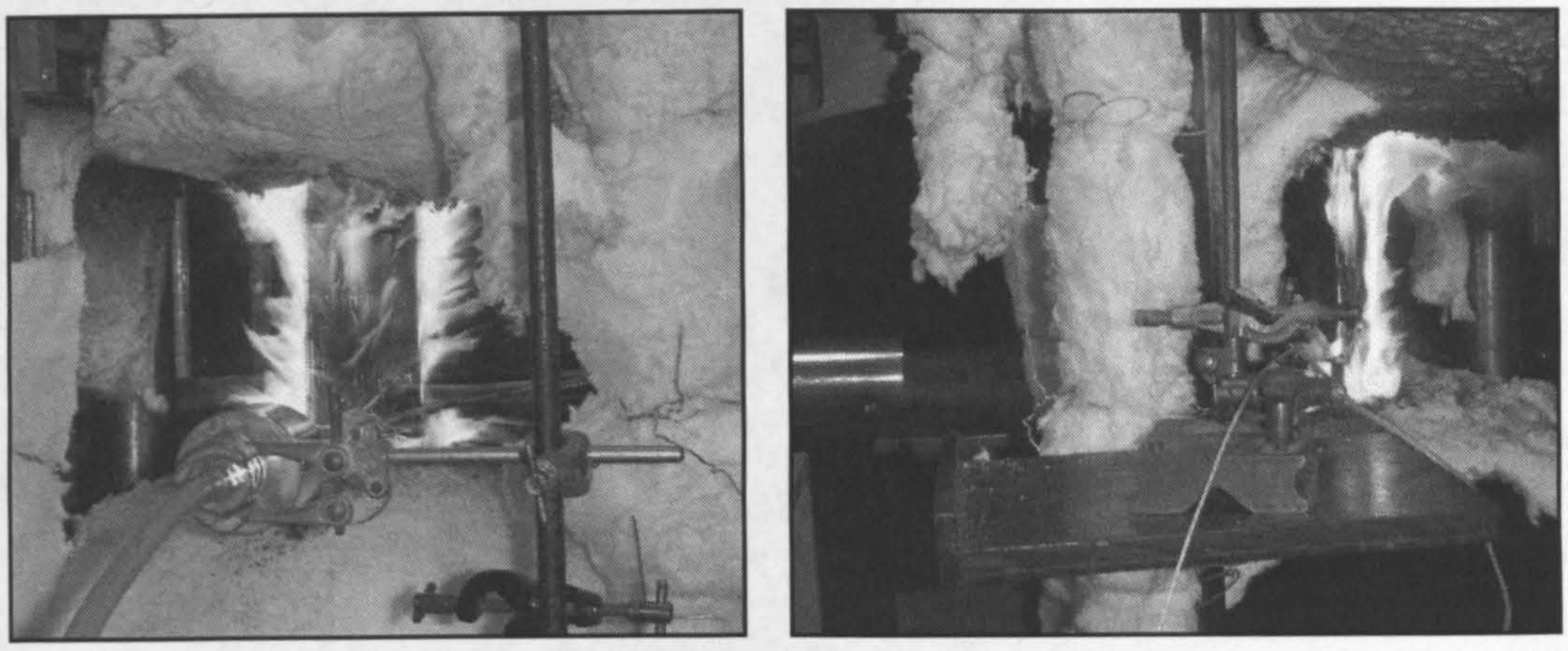

(i) (ii)

Figure 5.2. Front view (i) and side view (ii) of a polyester pultrusion undergoing a tensile test whilst subjected to a 50kWm^{-2} heat flux.

5.2. Compression Tests in Fire

Compressive samples were fabricated measuring 120mm x 100mm again with the long side being cut in the longitudinal direction. The samples were held in a constrained compression rig in principle with the Boeing compression after impact test frame[80]. This was to suppress global buckling of the samples during testing (Figure 5.3), while at the same time allowing samples of a large surface area to be tested. Once in place the samples were loaded with a constant compressive load, and subjected to a flame from a propane burner, the heat flux of which was monitored and maintained as before. Time to failure was recorded for several loads. Ultimate compressive strength was also determined and recorded with a failure time of 1 second. The failure event, when it occurred, was very rapid and with little warning. This test was repeated for the two materials with an intumescent coating applied to the hot face.

The intumescent material was supplied by Clariant, details of which are found in Table 5.1.

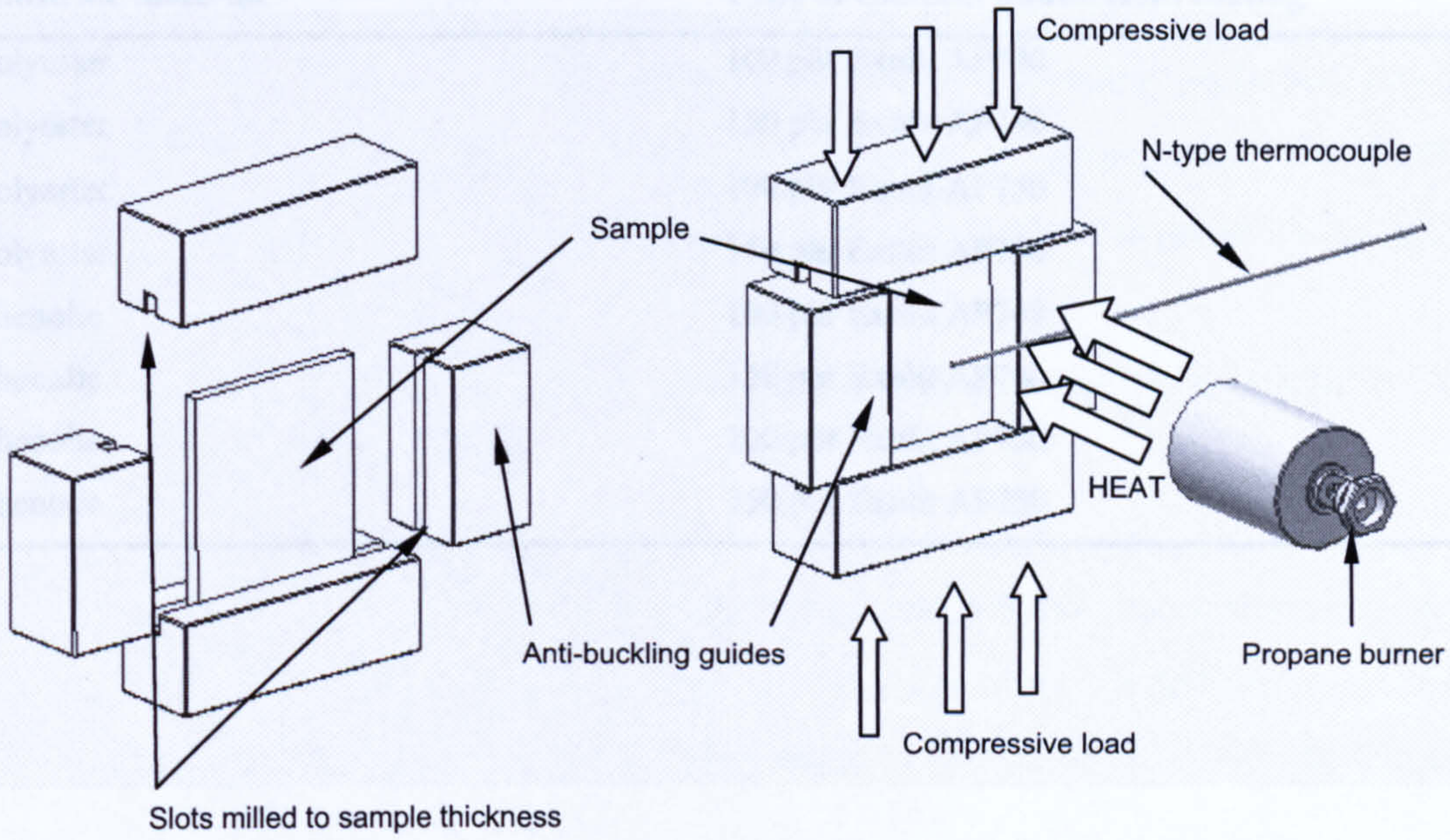

Figure 5.3. Arrangement for compression fire test using a propane burner as a heat source. Note the use of anti-buckling guides. These suppress global buckling allowing samples with a large surface area to be tested.

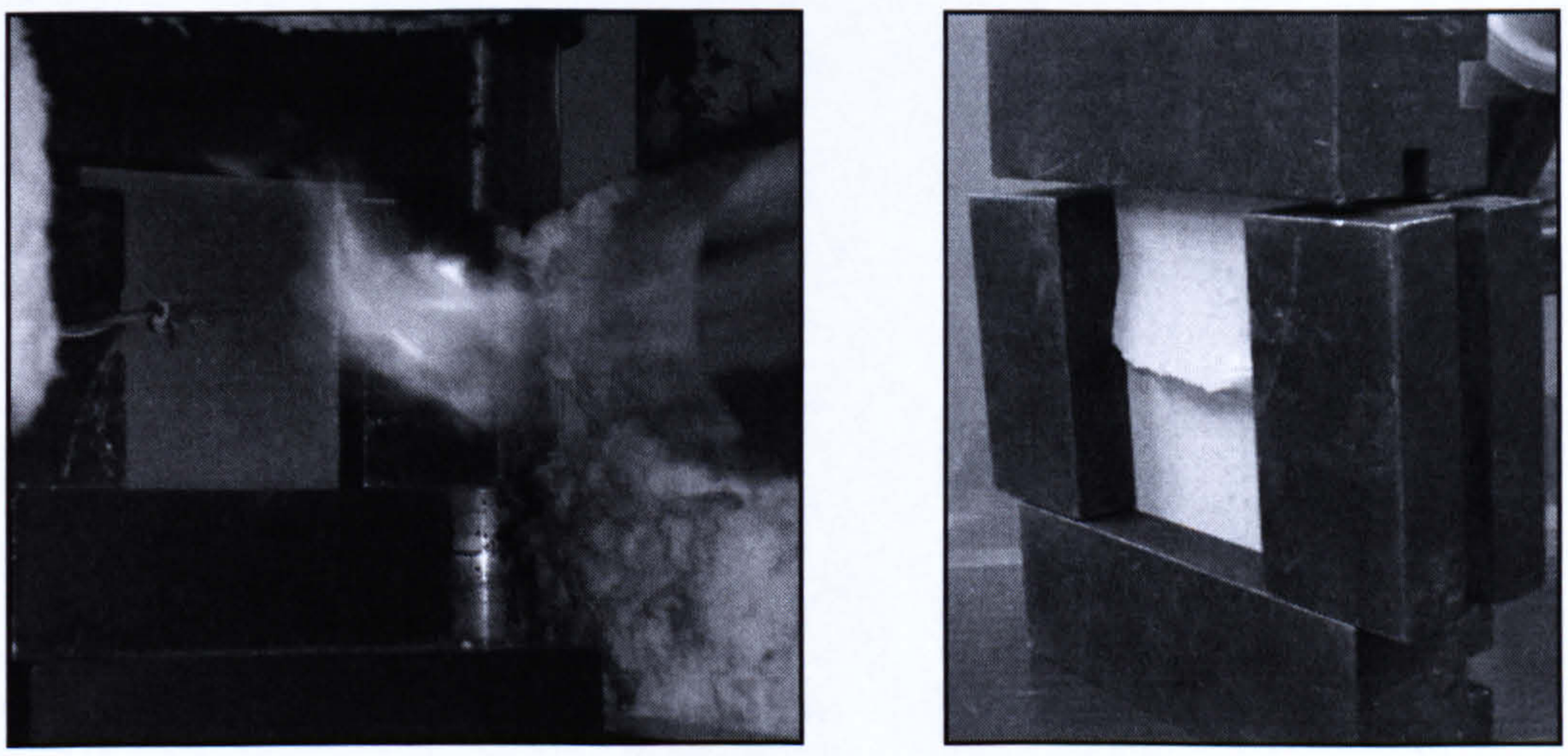

(i) **(ii)**

Figure 5.4. Phenolic pultrusion undergoing a compression test whilst subjected to a 50kWm^{-2} heat flux (i), and a polyester pultrusion after undergoing a compression test without to fire (ii). The purpose of such a test was to establish a value for ultimate compressive strength, recorded as a failure occurring after 1 second of exposure to fire.

Table 5.1. Details of the type of Clariant intumescent systems tested using the compression fire test. All systems were tested on both polyester and phenolic pultrusions

Substrate material	Type of Clariant intumescent coating
Polyester	100 phr Exolit AP740
Polyester	150 phr Exolit AP740
Polyester	100 phr Exolit AP750
Polyester	150 phr Exolit AP750
Phenolic	100 phr Exolit AP740
Phenolic	150 phr Exolit AP740
Phenolic	100 phr Exolit AP750
Phenolic	150 phr Exolit AP750

5.3. Pool Fire Test under Load

A rig was designed to flex beam sections (I and box) to their maximum design curvature whilst in a pool fire (see Figure 5.5). Load was applied using a hydraulic cylinder. The hydraulics and sensitive measuring equipment were protected by metal shielding
(not shown). Load was monitored with a load cell and change in stroke of the cylinder with and LVDT.

The section under test was clamped at each end between the assemblies as shown, leaving a gauge length of 1m. The section was then flexed to its design curvature.(see Figure 5.6). This corresponded to a bend ratio of 1:100 (deflection: gauge length).

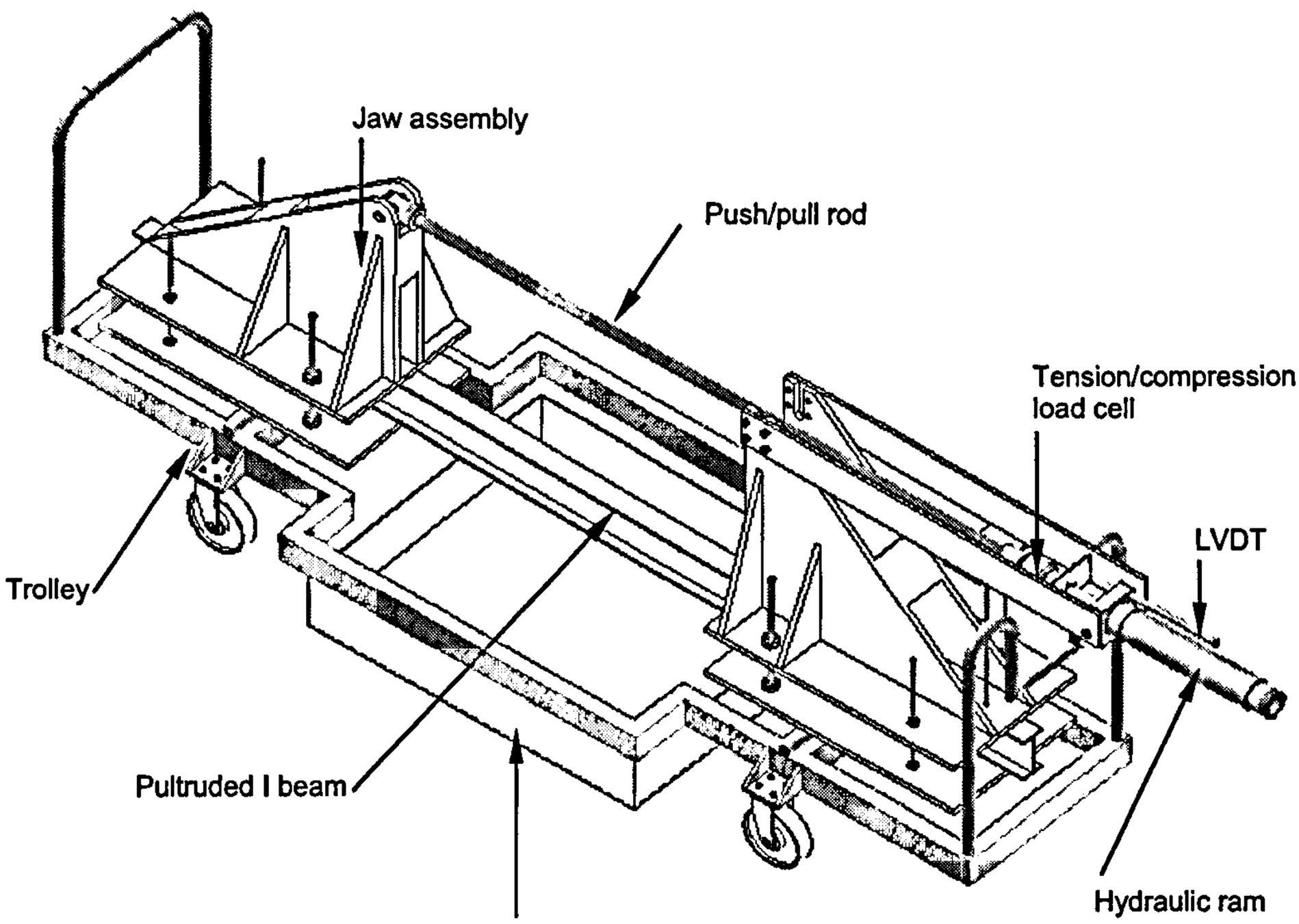

Figure 5.5. Pool-fire bending rig.

Once the necessary load was reached the pool fire was lit. This consisted of 9 litres of paraffin in a tray with an effective area of 0.69m^2. The load was kept constant during the test and time to failure was recorded alongside load and deflection, δ.

Temperature was also recorded along the gauge length of the section to determine how hot the fire was, and how it varied. Failure was sudden, usually in the order of 100s.

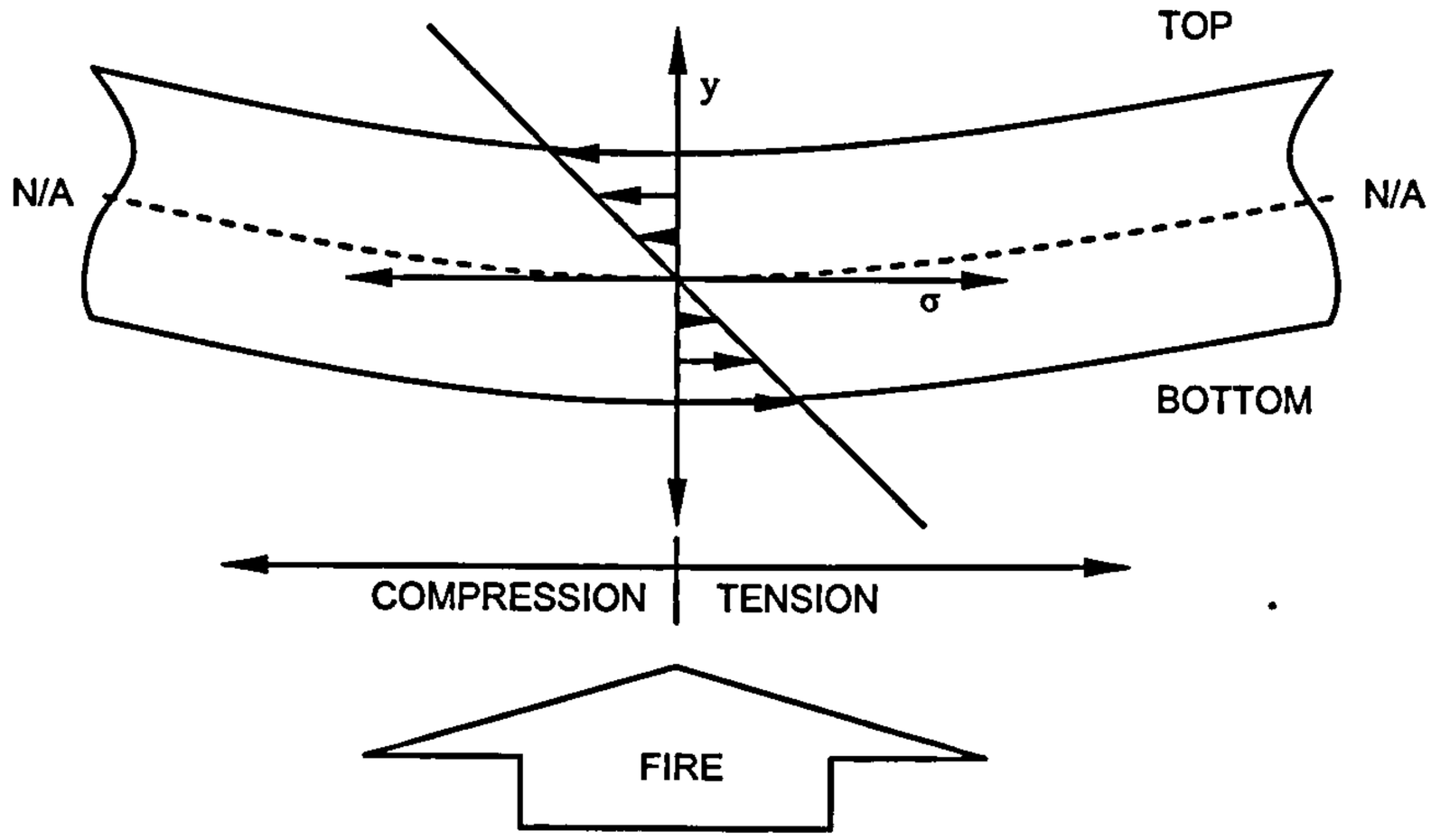

Figure 5.6. Details of the type of bend each section was subjected to. The top skin is in compression, and the bottom in tension. (N/A = Neutral axis).

Maintaining a steady temperature proved difficult. The pool-fire would exhibit an initial flash-over reaching approximately 100°C. This would then cause the un-burnt paraffin to heat up sufficiently to cause the much larger, secondary flashover (see Figure 5.7).

Figure 5.7. Typical temperature profile of a pool-fire. Note the initial flash-over followed by the much larger one.

5.4. Furnace Test under Load

A smaller bending rig was designed and fabricated (Figure 5.9) to fit around a furnace. The furnace in question was capable of following the SOLAS fire curve (see Figure 5.8), therefore overcoming the problem of repeatability experienced with the pool fire.

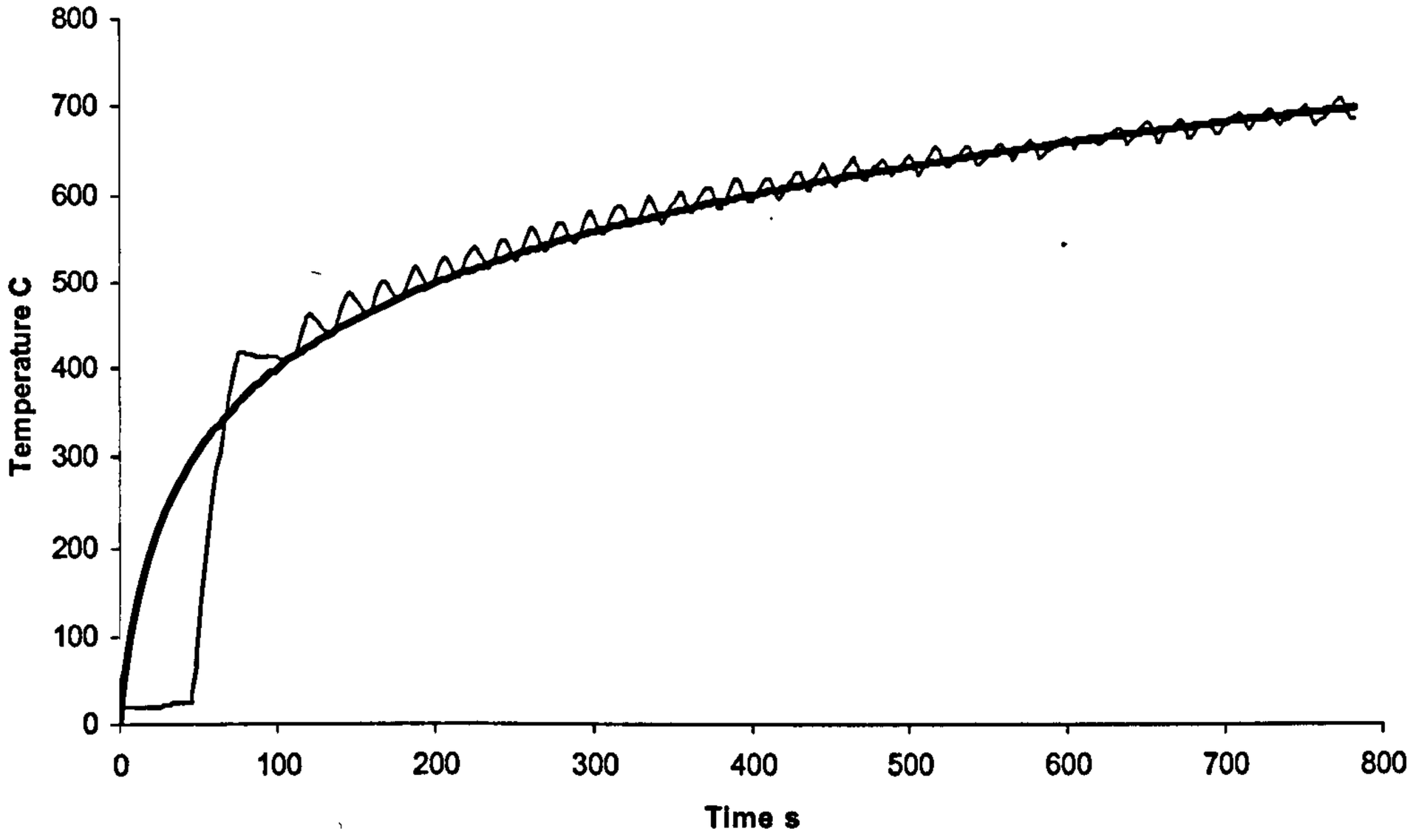

Figure 5.8. SOLAS curve (thick line) compared with furnace temperature (thin line).

The test section was positioned through the centre of the oven with both ends clamped as shown. It was ensured that the beam's central axis lined up with that of the lever arms. Once in place the load was slowly applied until the bend ratio of 1:100 was achieved.

The load was controlled by applying a torque to a threaded shaft as shown. As soon as the load had stabilised the furnace was ignited. Throughout the test the load was kept constant. Time to failure was recorded.

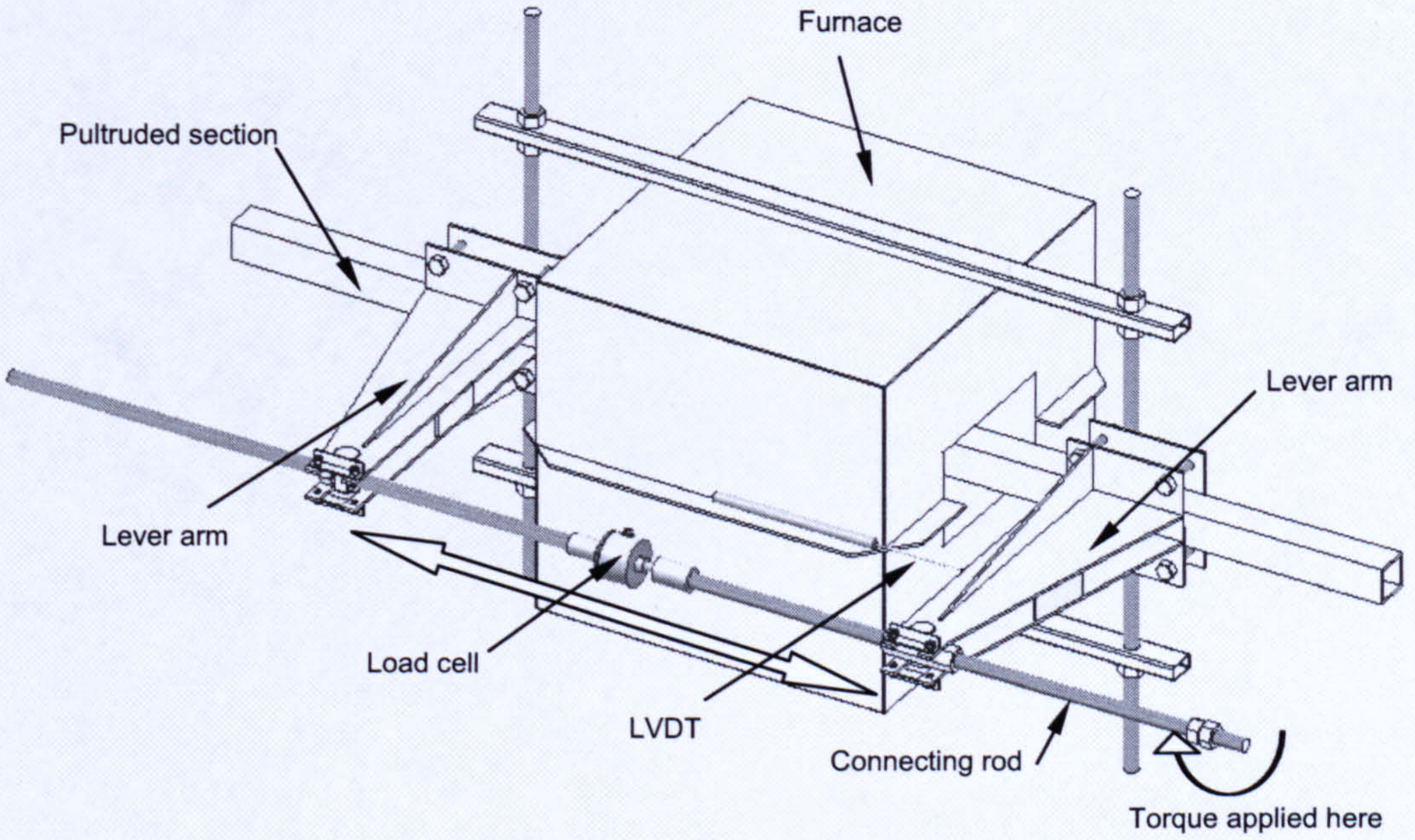

Figure 5.9. SOLAS furnace bending rig. The pultruded section is loaded by applying a torque to the threaded connecting rod.

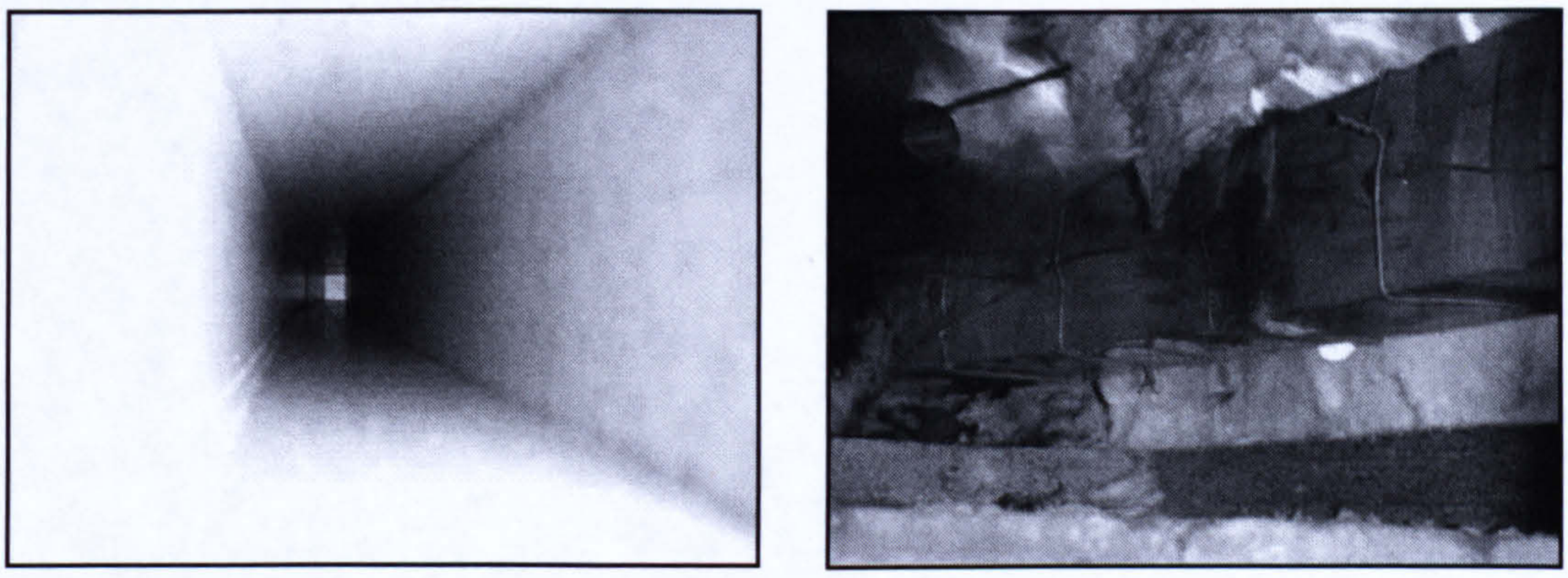

(i) **(ii)**

Figure 5.10. View through the inside of a section flexed to its design curvature (i), highlighting the flexibility of the section. View of a section undergoing furnace testing (ii).

5.5. Columns under Compression in Fire

Results from the pool-fire and furnace tests demonstrated that all sections fail in the region of 100 seconds when flexed to their maximum design curvature. A new experiment was designed with the intention of overcoming this problem by extending failure time. The new test took the form of a compression test involving short columns, coated with various fire barriers and systems. The basis of the test was to see if each coating/system would prolong failure time compared to the virgin material, when subjected to an enveloping heat flux. Compression was chosen over flexing as the loading method because it meant that a smaller section of material needed to be prepared with the relevant fire protection. Compression was also the failure mechanism in all of the beams tested in flexure,

Sections of 60x60x5mm columns were cut to a length of 90mm. These were then placed between two platens. The assembly was put under constant compression and compressed to a designated load. Whilst under compression, the column was subjected to a surrounding heat flux from a pair of opposing propane burners (see Figure 5.11). The burners were set to 50kWm^{-2} and monitored and maintained as in the tensile and constrained compression tests before. Time to failure at several loads was recorded.

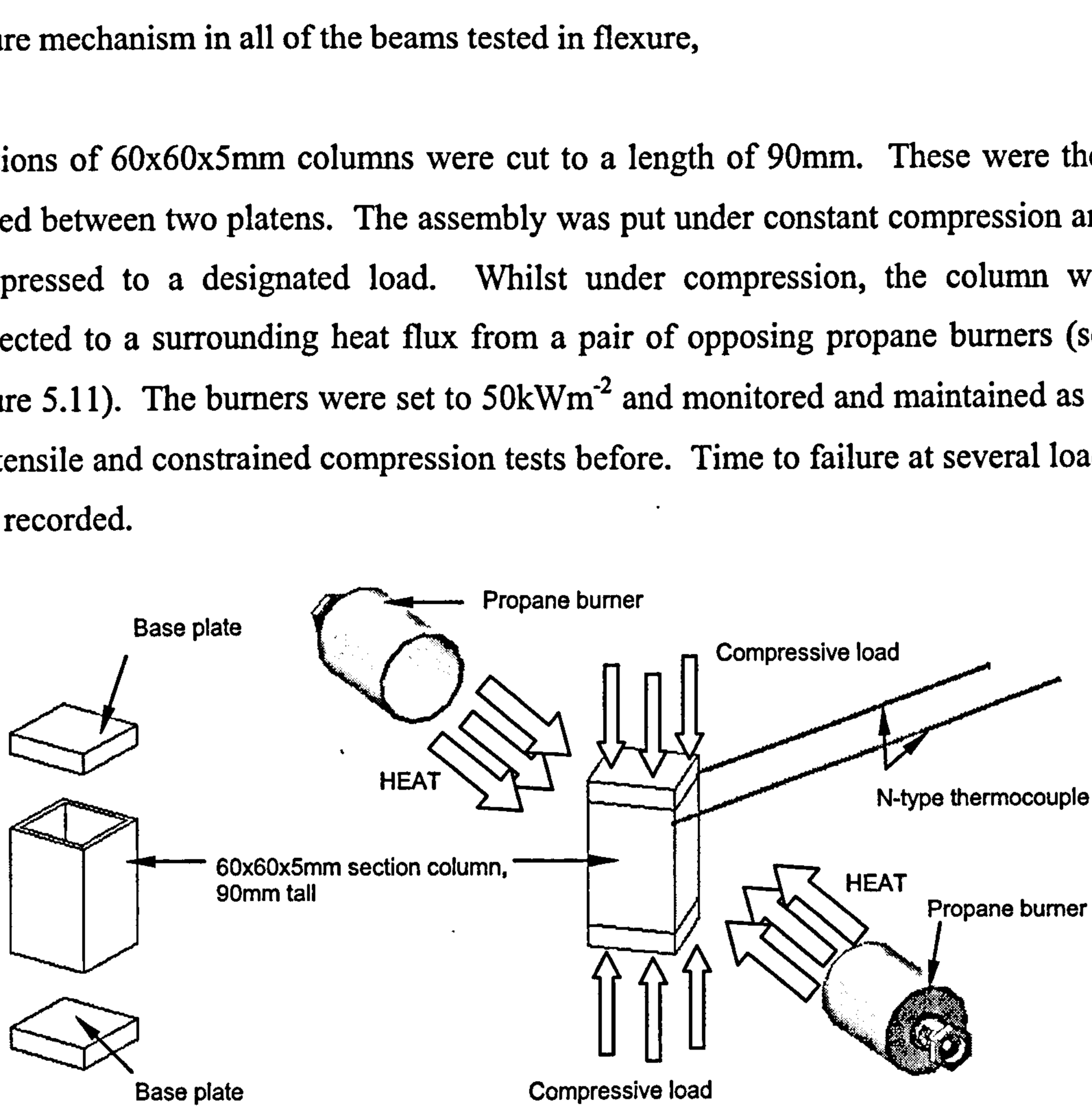

Figure 5.11. Arrangement for column compression test using a pair of propane burners as a heat source. Note the opposing burner flames, providing an enveloping heat.

Ultimate compressive strength was also determined and recorded with a failure time of 1 second. When failure occurred, it was rapid and with little warning particularly at higher loads. The columns provided useful basis for testing fire coatings and insulations. The test was repeated for columns with fire protective coatings/systems applied. (see Figure 5.12).

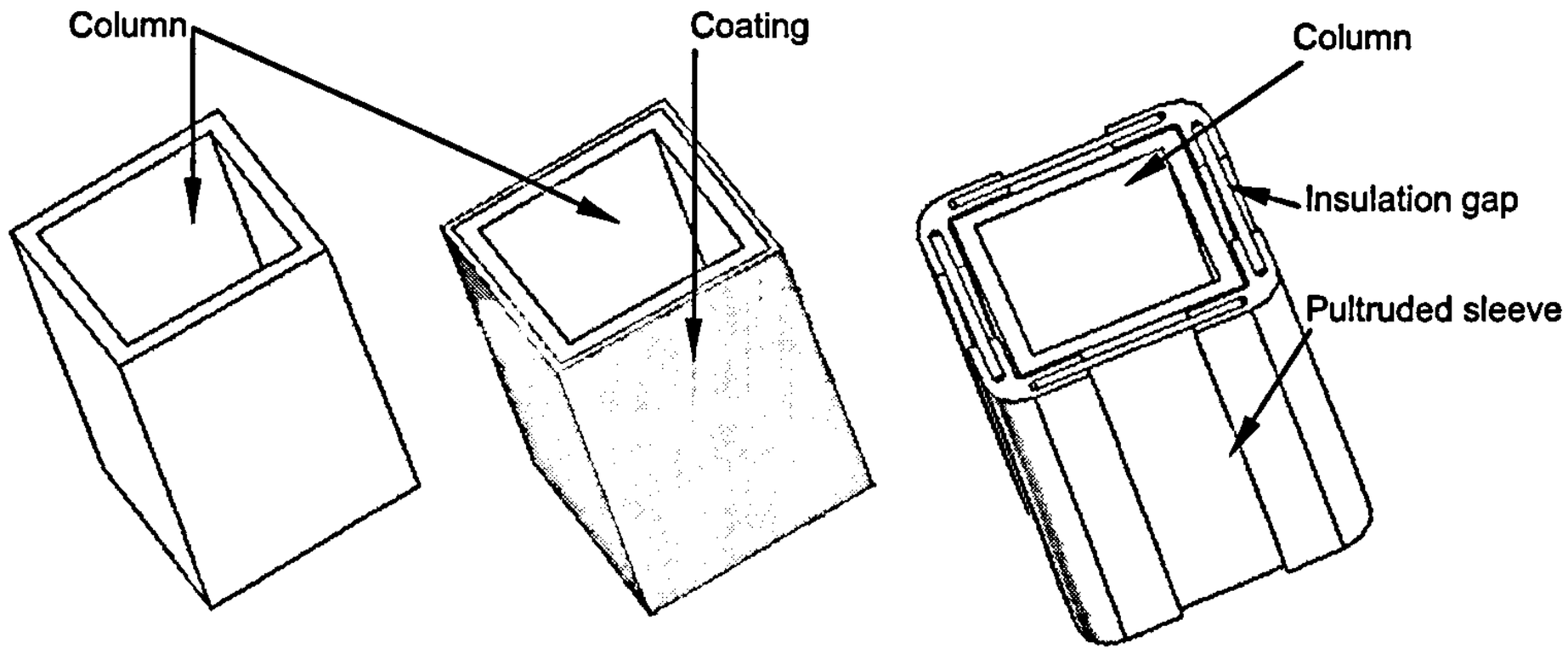

Figure 5.12. Details of column coatings and systems tested, ranging from simple coated columns to more complex systems involving a pultruded sleeve.

Table 5.2. Details of type of fire protection tested on the pultruded columns.

Column Material	Type of protection system	Description
Polyester	Coating	Clariant intumescent
Polyester	Coating	Kerin, ceramic based
Polyester	Coating	Geo-polymer
Polyester, Phenolic	Coating	'Tinned'
Polyester	'Boxed column'	Air insulation
Polyester	'Boxed column'	Kaowool

The 'boxed columns' included an insulating layer. Both air and Kaowool were tested as insulation. K-type thermocouples were attached at key interfaces on the 'boxed columns', as well as on the inside of the column (see Figure 5.13). Temperature evolution at these points was recorded for the duration of the test.

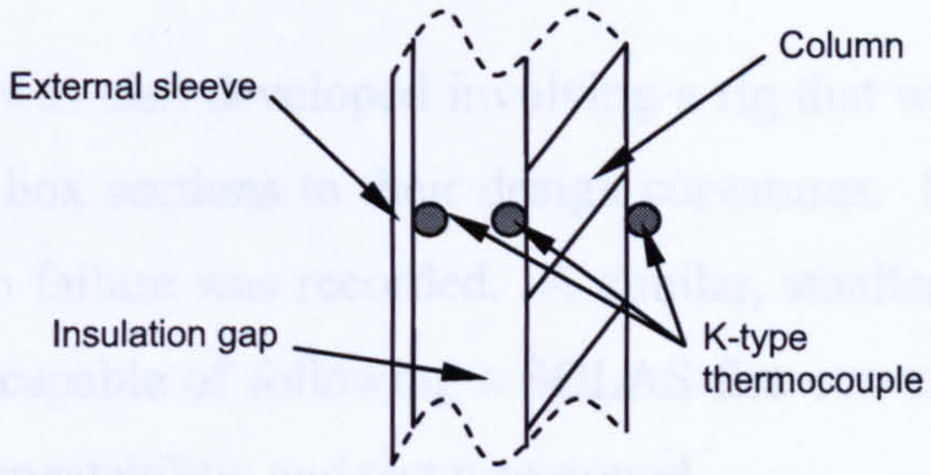

Figure 5.13. Top down view of a section through a 'boxed column', highlighting the position of the thermocouples.

(i) **(ii)**

Figure 5.14. View of an unprotected polyester column prior to fire testing (i). Note the opposing burner arrangement. A coated column undergoing fire testing (ii). Note the area where a section of the fire protective coating has fallen away, exposing the column beneath.

5.6. Chapter Summary

Several fire tests were developed to assess the fire resistance of a composite system under load. Tensile and compressive samples were subjected to a heat flux of $50kWm^{-2}$ from a propane burner whilst loaded in a test frame. Time to failure was recorded in each case, for different tensile and compressive loads. Intumescent coatings were also tested on the compressive samples.

Short columns of the same material were also tested in a similar way. These too, provided a basis for testing a series of coatings including supplementary fire protection.

A pool fire test was also developed involving a rig that was capable of flexing long 'I' sections and box sections to their design curvatures. Several beams were tested and their time to failure was recorded. A similar, smaller scale test was developed using a furnace capable of following a SOLAS fire curve. This improved upon the pool fire test's repeatability, and test turnaround.

6. Results

6.1. Mechanical Properties

To investigate high temperature applications of composites, particularly how they perform mechanically in a fire, it is useful to be able to express the elastic constants and strengths as a function of temperature. Finding data in this form proved very difficult. Therefore a series of high temperature mechanical property tests were carried out. Once the results were obtained it was a case of fitting a suitable temperature dependent relationship. This was made easier by the fact that thermosetting resins only go through a single transition phase before the resin begins to decompose. This occurs at the glass transition temperature T_g. This meant that a suitable temperature dependent relationship only really needed to fit this region.

A polynomial in temperature can be used to describe the variation of an elastic constant in this transition region[9, 81]. This method often requires a polynomial of order 6 to accurately describe the relationship across the whole transition region. This method is flawed, since the relationship only behaves reliably within the fitted region of the data.

For this thesis it was decided to use a function based on the hyperbolic tan function (tanh),

$$P(T) = P_R + \left[\frac{P_U + P_R}{2}\right]\left\{1 - \tanh\left[k(T - T_g)\right]\right\} \qquad \textbf{(6.1)}$$

where P_U and P_R are the un-relaxed and relaxed property values respectively, k is a constant describing the breadth of relaxation, T the absolute temperature, and T_g the absolute temperature of the mechanical glass transition (where P is equivalent to the mean of P_U and P_R). This is detailed in Figure 6.1.

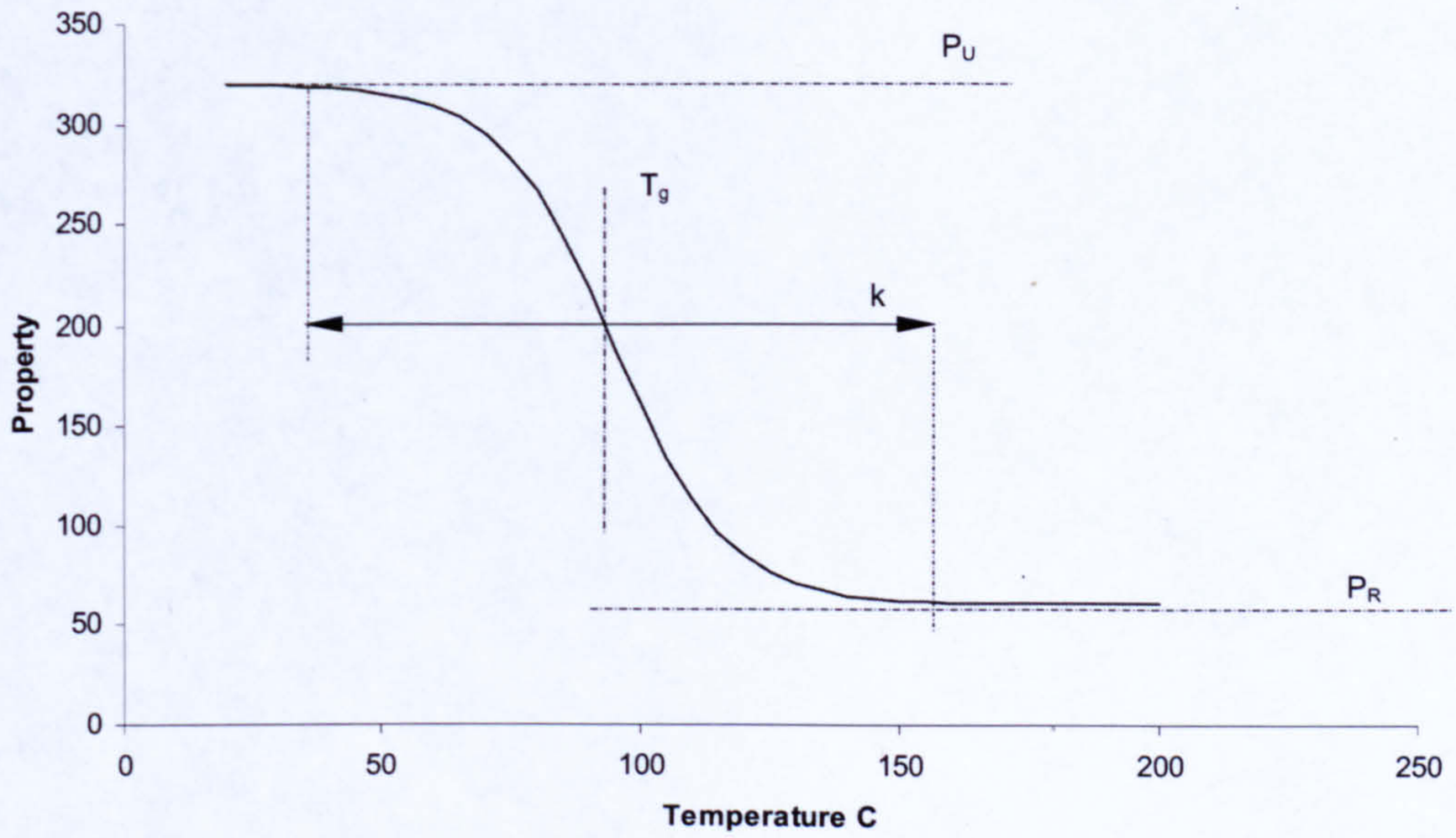

Figure 6.1. Property variation with respect to temperature described with a 4 parameter relationship.

6.1.1. Problems arising from the Material Cross Section

The pultruded material in this thesis consisted of a unidirectional core, with CSM needles weave outer layers (described in Figure 4.1 and Figure 6.2).

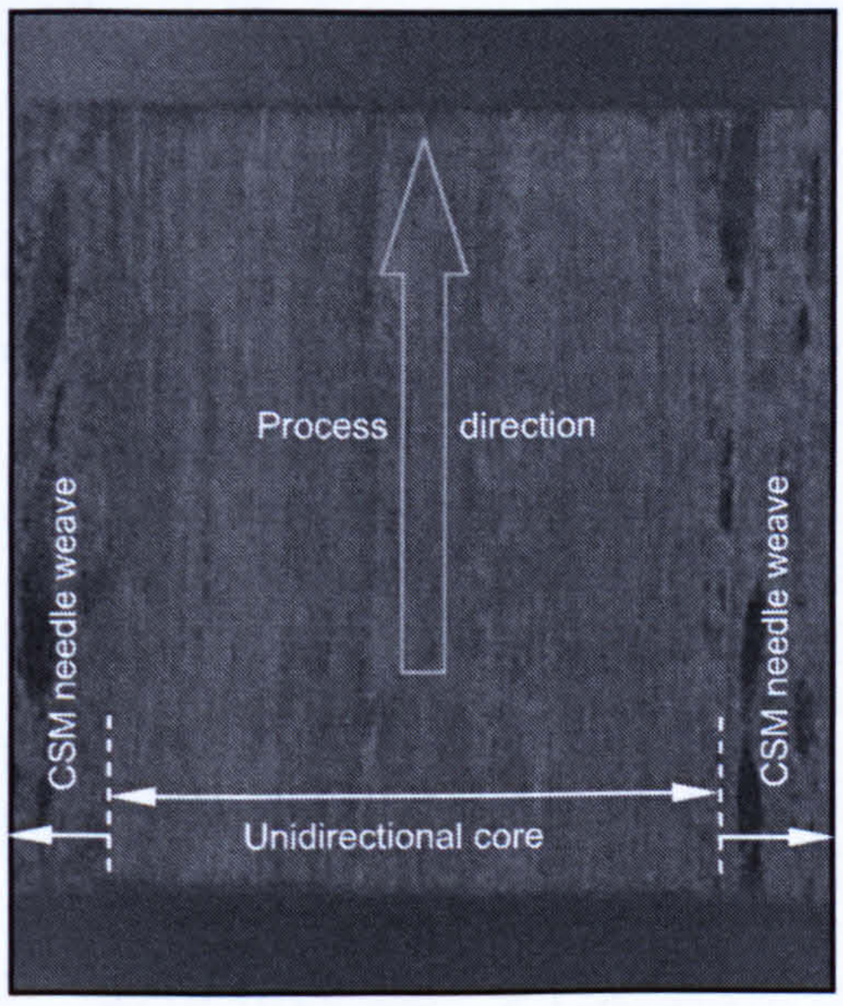

Figure 6.2. Close-up of a section of pultruded polyester, highlighting the three separate layers.

This caused problems during the tensile testing phase. The unidirectional material had a tendency to pull through the CSM needle weave outer layers (Figure 6.3). It was decided to overcome this problem by carrying out tensile tests on the unidirectional material too, to supplement those for the full section of material.

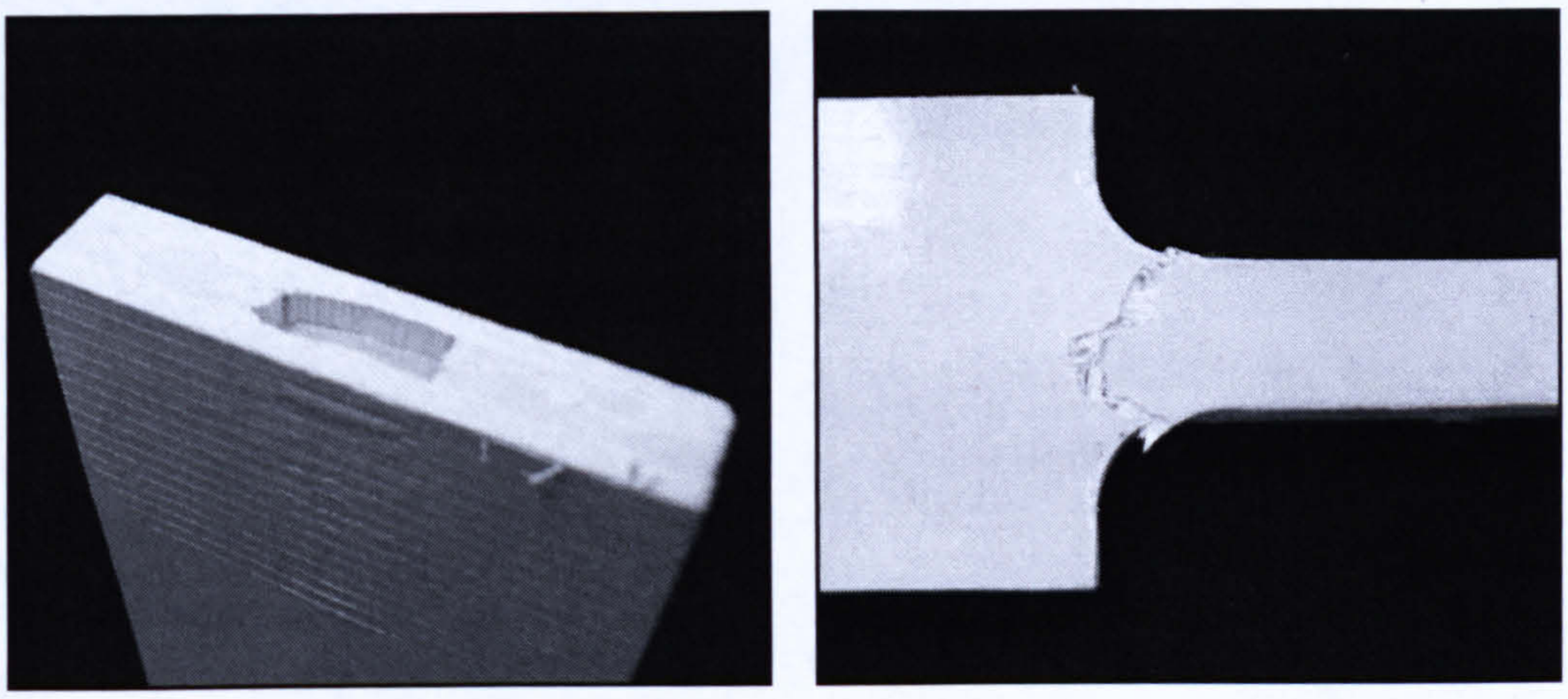

(i) (ii)

Figure 6.3. Close-up of a tensile test sample of the full section material, highlighting the core material pulling through the outer skins (i), and the outer skins failing (ii) leaving the inner core intact.

Unidirectional samples were also tested in flexure (E_1 and E_2), compression tests were carried out on the full section material only. The material was tested in this way for analysis purposes which is detailed in Chapter 7.

6.1.2. Tensile Strength

Tensile tests were carried out on both the unidirectional (core) material and the full thickness material at varying temperatures. Stress-strain curves of the tests were plotted.

Figure 6.4 shows the stress strain curves for the core material of a polyester pultrusion. The curves are in two distinct groups. The first set is the curves for the tests carried out at lower temperatures below the material's T_g (glass transition temperature). In this set, tensile failure occurred at higher stresses and strains. The second set is the tests which were carried out above the material's T_g. Tensile

strength for this group is much lower. This behaviour is as expected and is evident for all the tensile tests (see Figure 6.5, Figure 6.6, Figure 6.7).

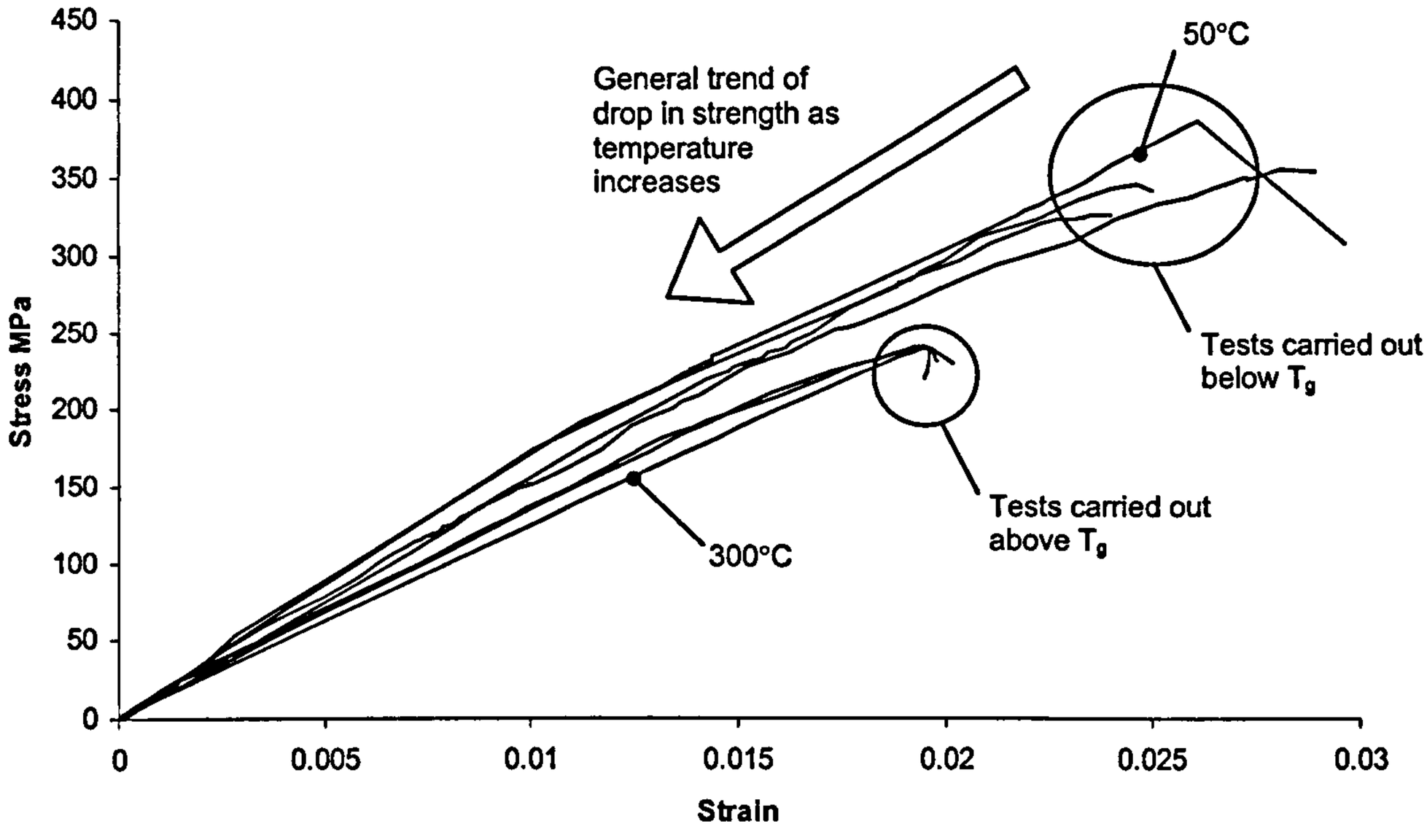

Figure 6.4. Stress-strain curves of unidirectional (core) polyester pultrusion undergoing tensile tests at varying temperatures. Note the two distinct groups of tests, those carried out below T_g and those above.

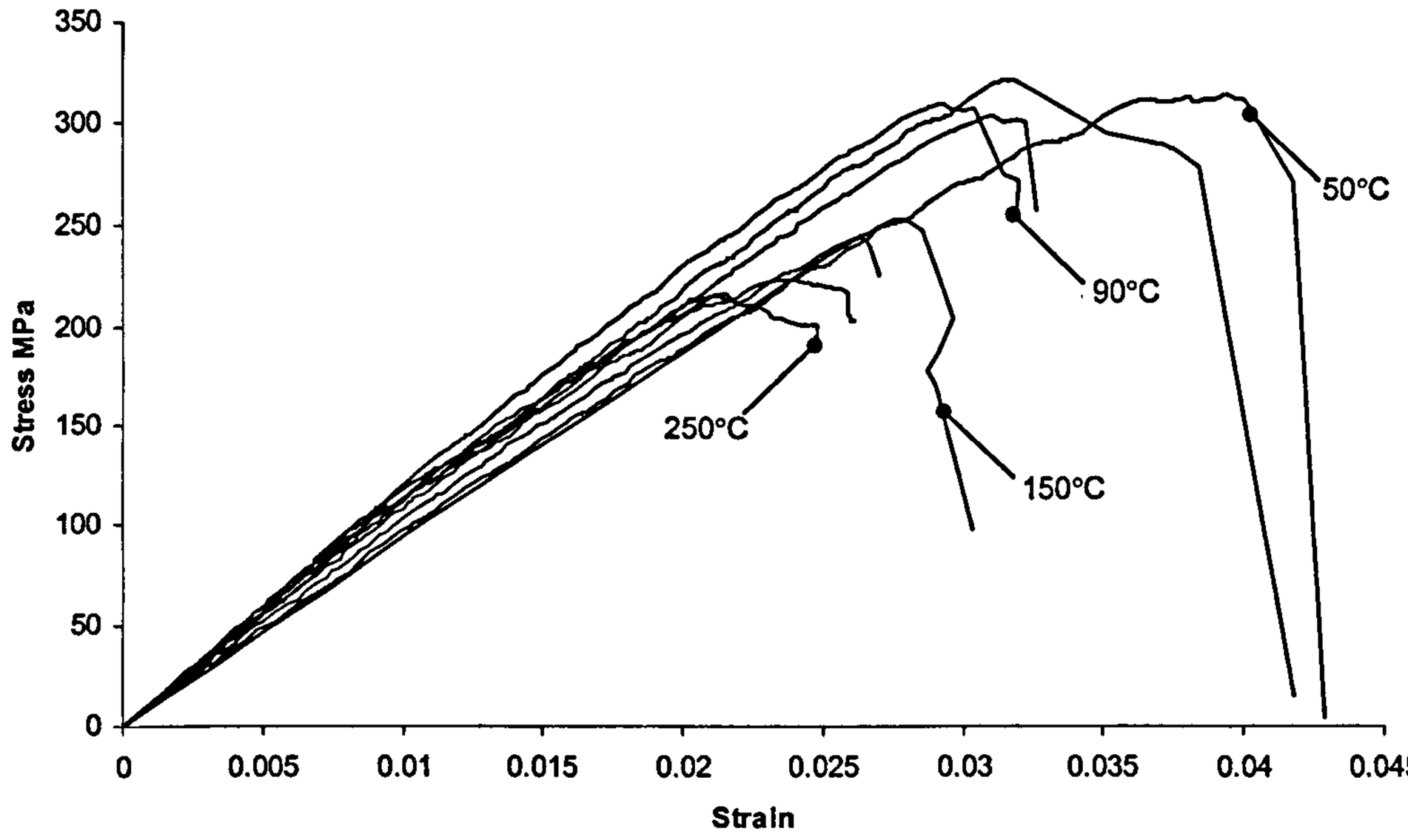

Figure 6.5. Stress-strain curves of the full section polyester pultrusion undergoing tensile tests at varying temperatures.

The drop in strength due to the material passing through it glass transition temperature (T_g) causing the resin to soften, was greater than anticipated. Consider Equation 6.2 which is based on the Rule of Mixtures Equation,

$$\sigma^* = \sigma_f^* V_f + \sigma_m^{'}(1 - V_f) \qquad (6.2)$$

where σ^* is the failure strength of the composite, σ_f^* is the failure strength of the fibres, $\sigma_m^{'}$ the stress in the matrix at the failure strain of the fibres, and V_f the fibre volume fraction. When the resin contribution to composite strength is considered a much lower drop should be expected.

This highlights that this is not the only process occurring. This phenomenon is still under discussion but is believed to be the 'composite action' effect on the material, whereby when a material is below its T_g all the reinforcement is subjected to the same strain levels. Once the matrix softens (when $T > T_g$) any waviness or misalignment in the fibres becomes apparent, causing fibres to fail at different strains, in this case reducing strength. This effect would be process dependent. For instance, pultruded composites would be affected less by this phenomenon than those that were laid up by hand. This is because any waviness causing this effect would be reduced as the material is pulled through the die. However, the fibres will still snag against each other and twist around each other causing this effect, particularly when you consider the large volume of fibres being pulled through the die at once.

At the higher temperatures; both the polyester and phenolic pultrusions maintain a high tensile strength. This is because tensile strength is ultimately dependent on fibre strength, which does not really deteriorate until 800°C.

At lower temperatures (below T_g) the phenolic material was has a higher tensile strength than the polyester material, and is therefore capable of reaching higher levels of strain, 5-6% compared to 3-4% strain for the polyester. This was true for both the unidirectional (core) material, and the full thickness pultrusion.

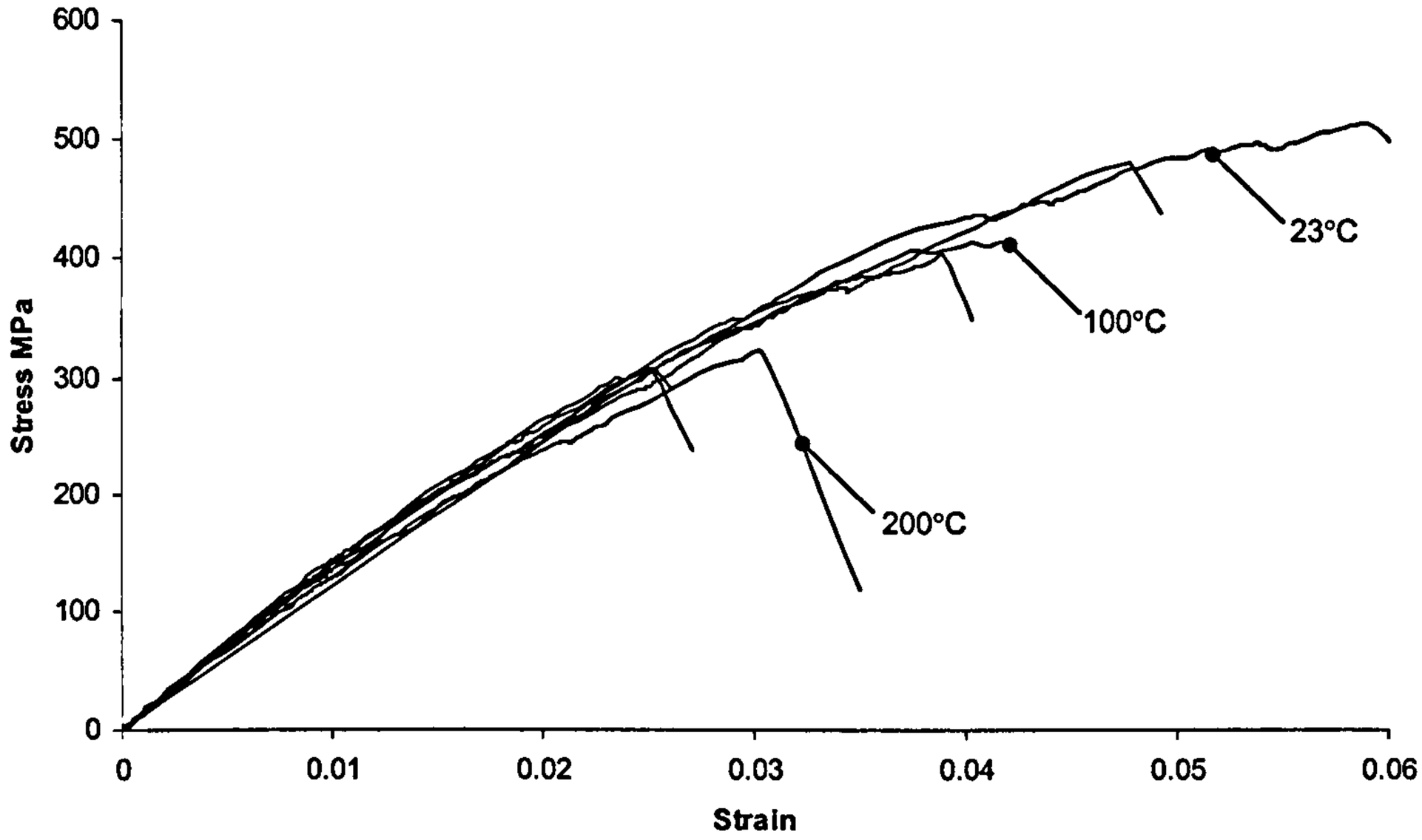

Figure 6.6. Stress-strain curves of unidirectional (core) phenolic pultrusion in tensile tests at different temperatures.

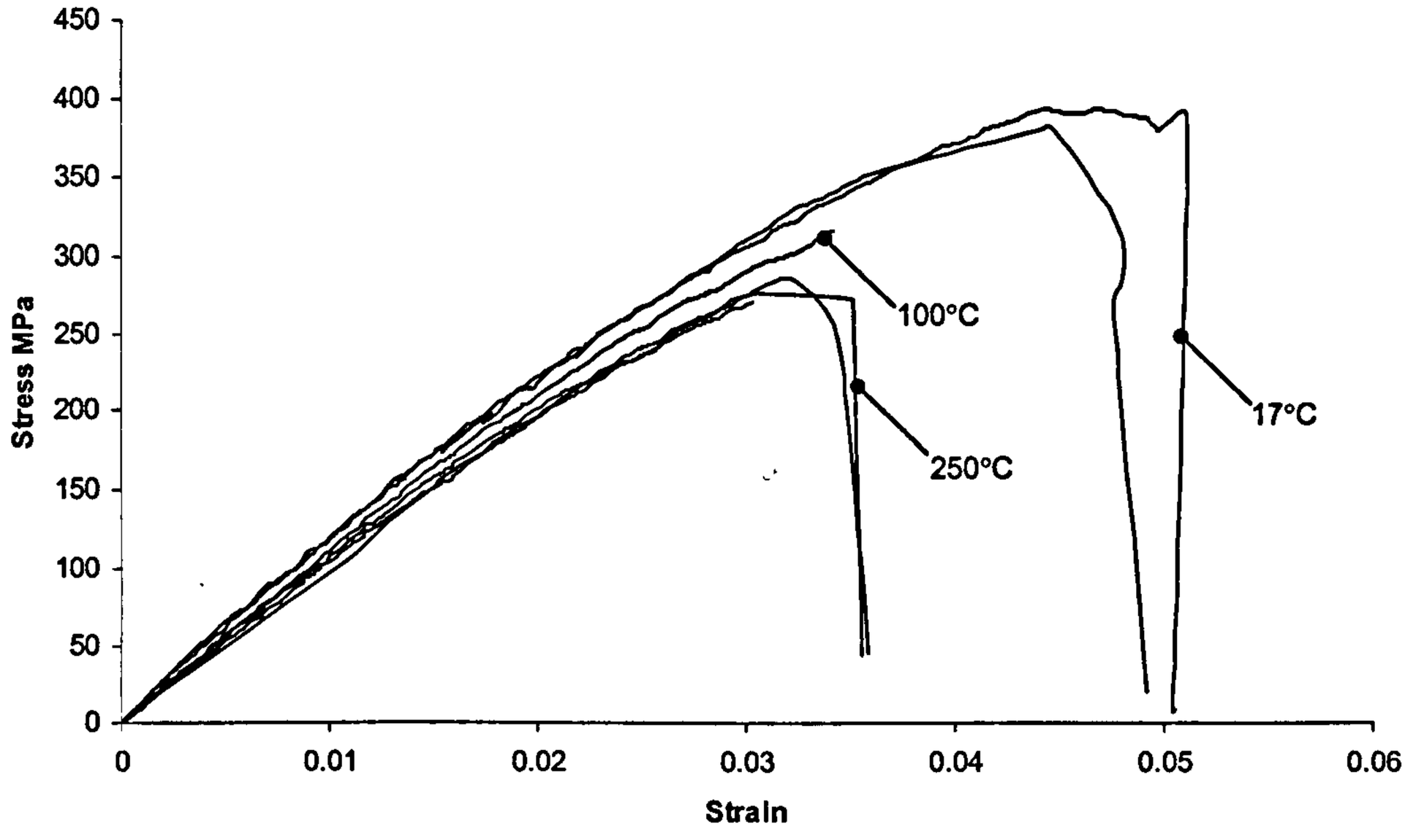

Figure 6.7. Stress-strain curves of the full section phenolic pultrusion undergoing tensile tests at varying temperatures.

6.1.3. Compressive Strength

Compression tests were carried out on full thickness pultrusions. Stress-strain curves of the tests were plotted (Figure 6.9 and Figure 6.10). Tests on the core material were not deemed necessary since the CSM/needle weave outer skins would provide negligible compressive strength.

The stress-strain curves follow the familiar saw-tooth profile associated with compression tests. The main feature is the level of compressive strength retained above T_g. This is noticeably lower than with the tensile results, highlighting the resin dependency of compressive strength.

The failure mechanism of compressive failure is very different to that of tensile. Failure involves the formation of a band of kinked material[82]. Failure is initiated in a region where the fibres are misaligned out of plane of the laminate. This region experiences high levels of shear loading between the fibres, eventually triggering failure by local shear deformation.

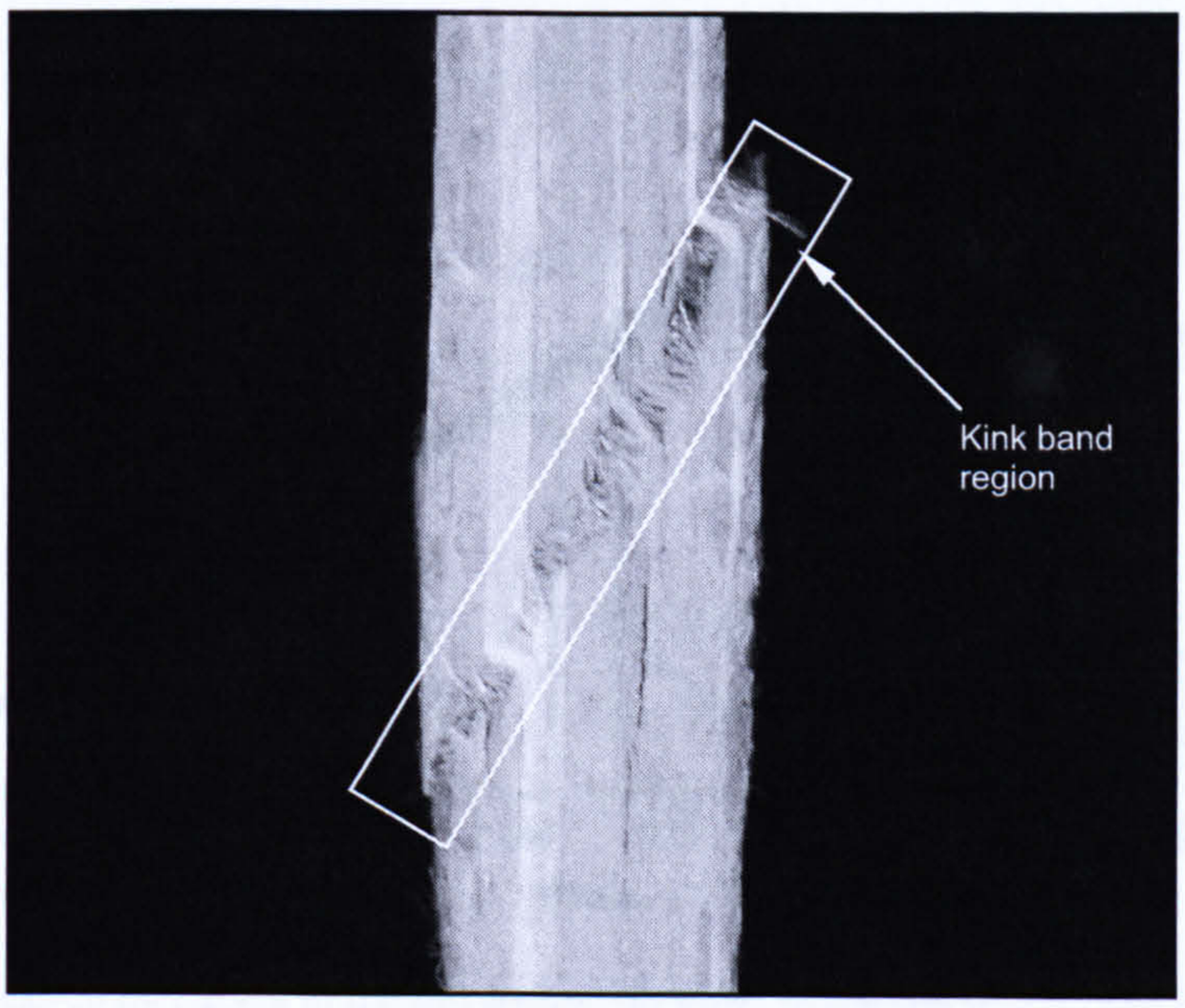

Figure 6.8. Close up of a compression sample of phenolic pultrusion, highlighting the band of kinked material.

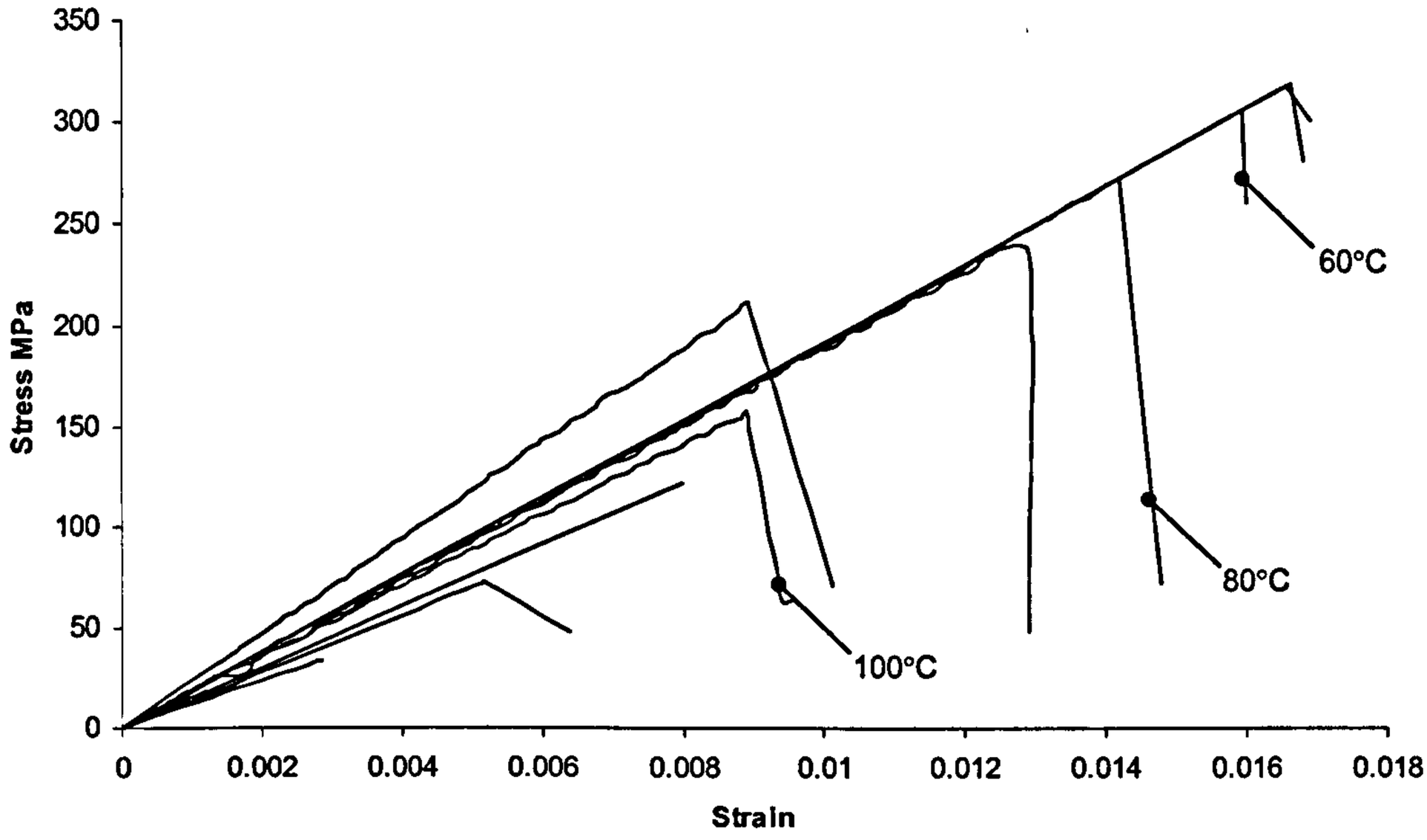

Figure 6.9. Stress-strain curves of the full section polyester pultrusion undergoing compression tests at varying temperatures.

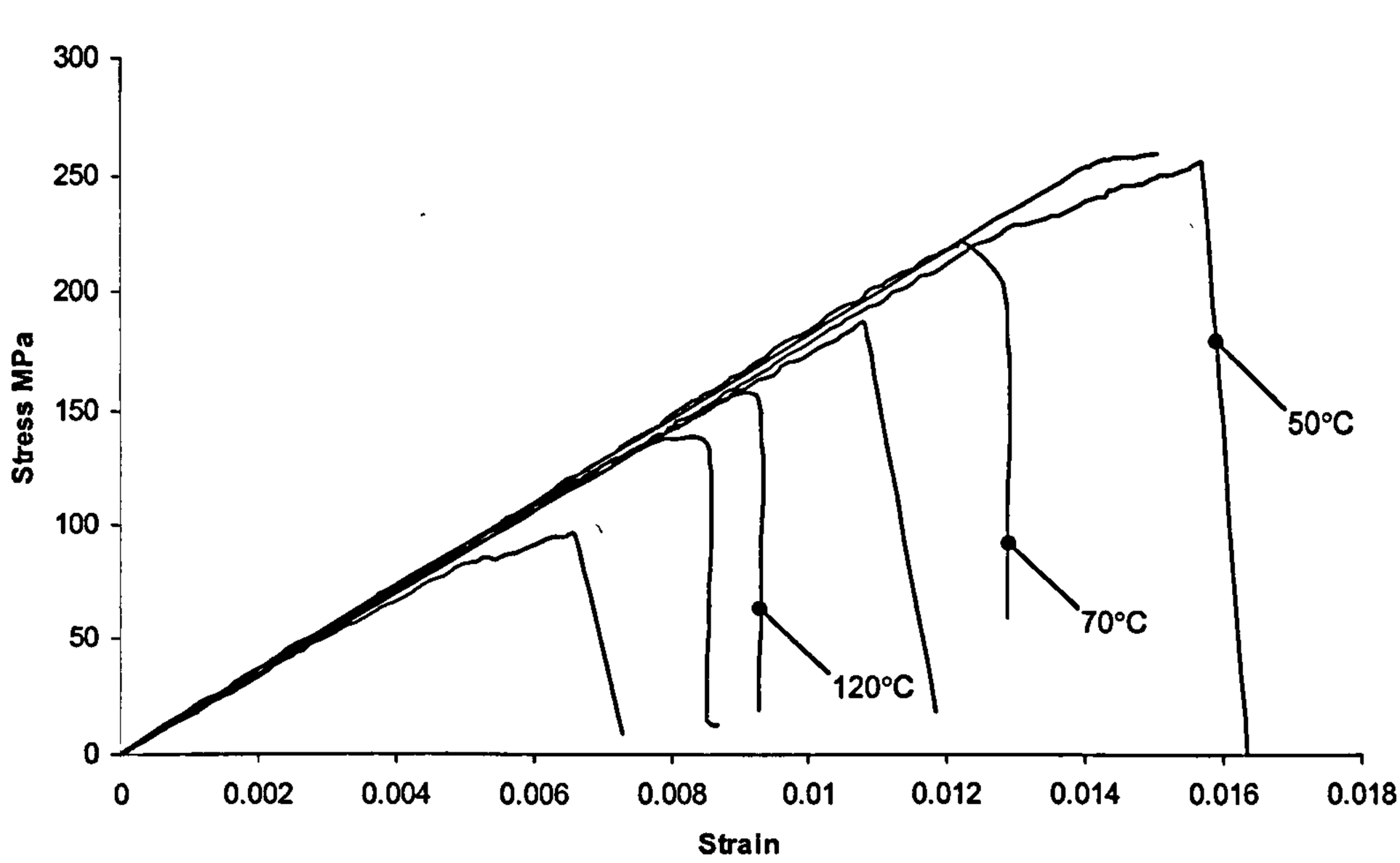

Figure 6.10. Stress-strain curves of the full section phenolic pultrusion undergoing compression tests at varying temperatures.

6.1.4. Longitudinal (E_1) and Transverse (E_2) Stiffness

Modulus tests were carried out on both the full thickness material and the unidirectional core in the longitudinal direction (E_1) and the core material in the transverse direction (E_2).

6.1.5. Mechanical Properties vs. Temperature

Throughout this section, curves have been fitted to the data points using the 4 parameter relationship (Equation 6.1), detailed at the beginning of this chapter.

Figure 6.11 shows the results of tensile measurements (σ_{T1}) of the polyester based material as a function of temperature. Figure 6.12 shows the results for the phenolic based material. Testing was carried out on both the full thickness of material (UD core sandwiched between CSM/needle weave skins), and the UD core itself. The material retained a large proportion of its strength at high temperature. This is due to the strength of the reinforcement, which in the case of E-glass retains a significant proportion of its strength up to at least 800°C.

The results for the full thickness material are not a true representation of the material tensile strength as a function of temperature. This is due to the skin material failing before the core material (Figure 6.3).

The results show a much higher tensile strength for the phenolic pultrusion when compared to the polyester pultrusion. If the fibre volume fractions of the materials (Table 4.2) are considered, one would expect the polyester material to outperform the phenolic material. However it is difficult to accurately predict the tensile strength of a fibre-reinforced material since you can never be sure if all the fibres are carrying any applied load. Fibres may follow a wavy or undulating path through the material, reducing their load-carrying ability. A possible reason why the phenolic material has a higher tensile strength in spite of its glass content becomes apparent when the manufacturing process is considered. The phenolic material is manufactured under a

higher resin injection pressure than the polyester. This may have the effect of reducing any waviness in fibre alignment, improving material strength.

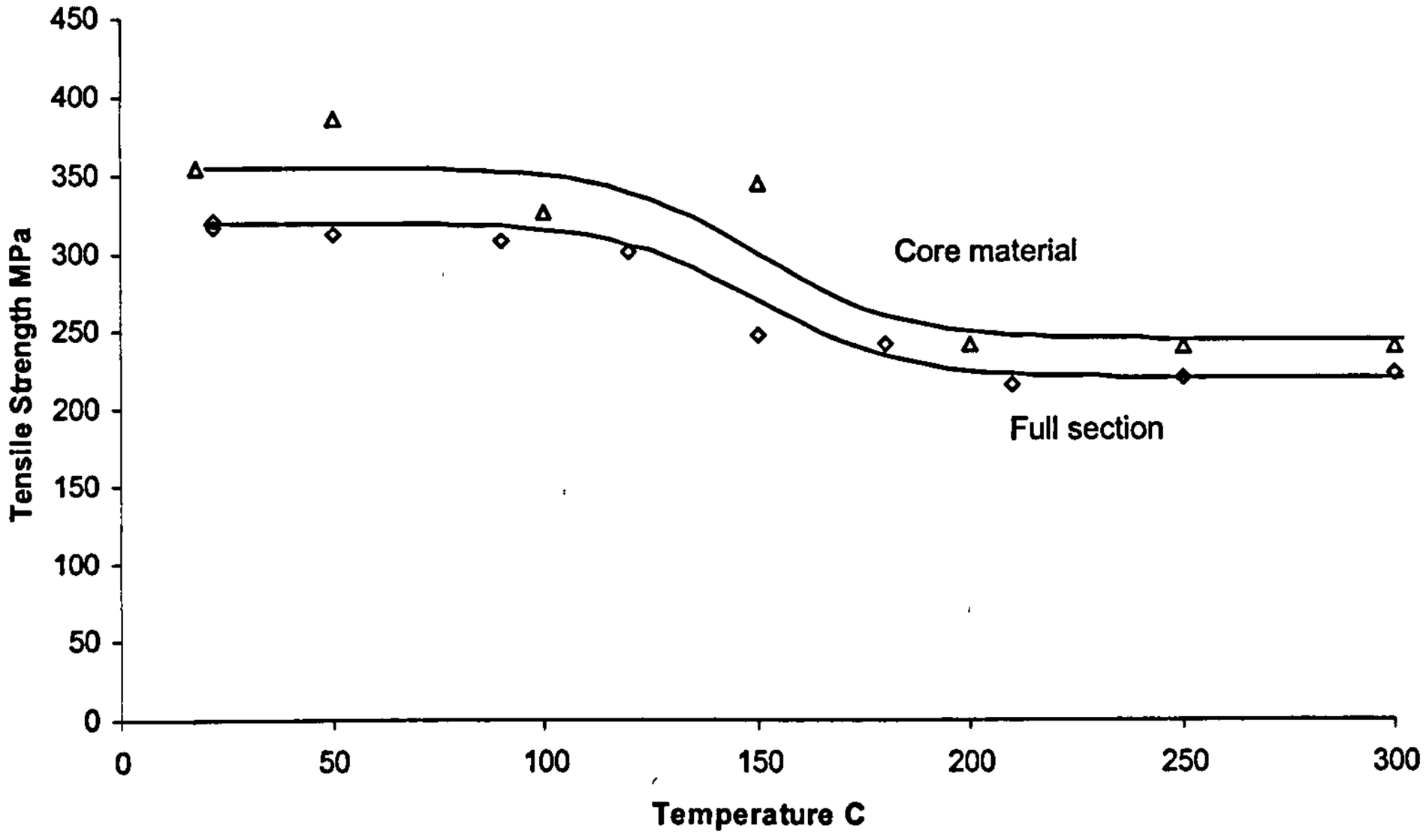

Figure 6.11. Tensile strength (σ_{T1}) vs. temperature of polyester pultrusion. Note both unidirectional (core) and the full section material were tested.

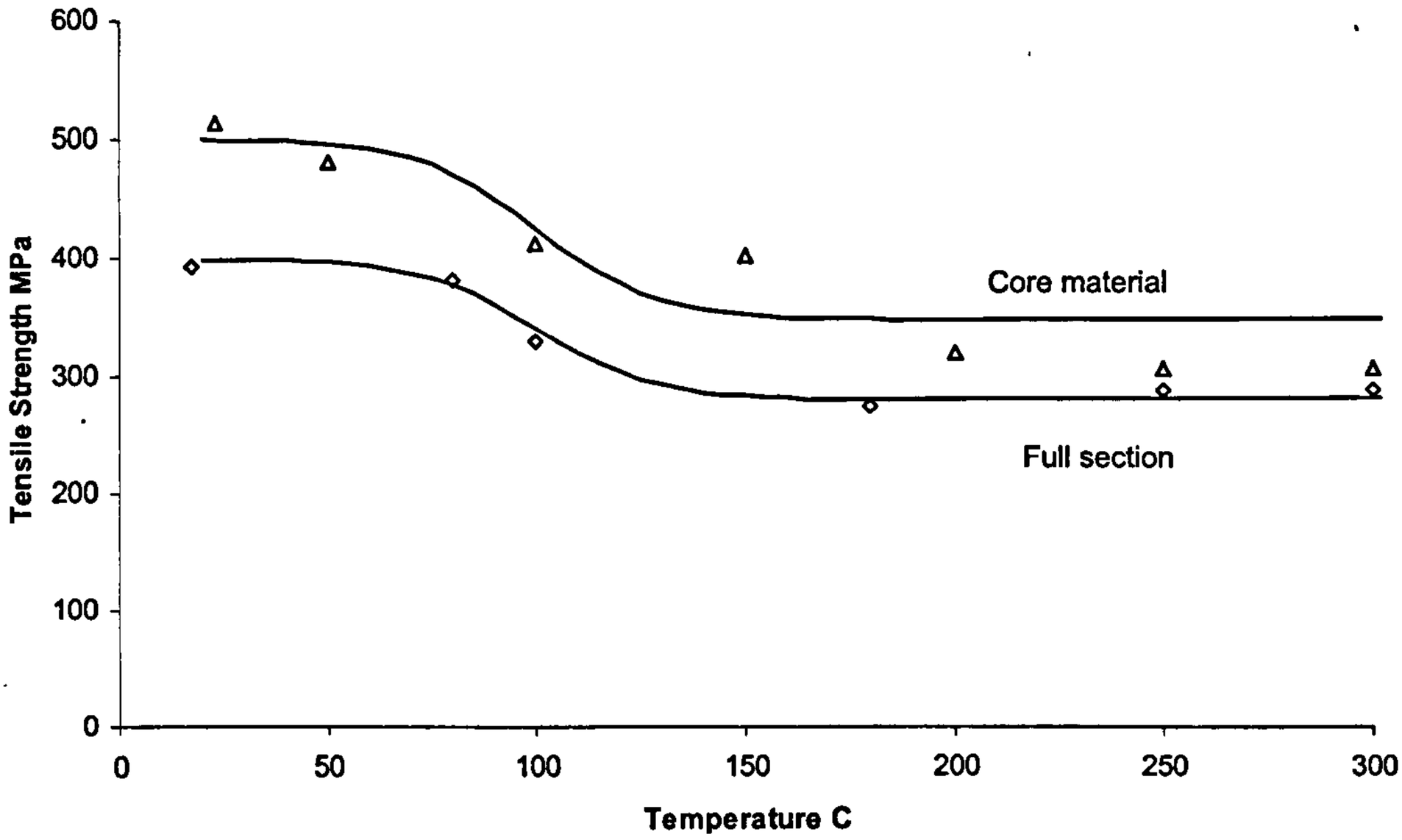

Figure 6.12. Tensile strength (σ_{T1}) vs. temperature of phenolic pultrusion. Note both unidirectional (core) and the full section material were tested.

Figure 6.13 and Figure 6.14 show the compressive strength (σ_{Cl}) of the polyester pultrusion and the phenolic pultrusion with respect to temperature respectively. The curves show a steep drop in compressive strength as temperature increases above the materials' T_g, stressing its dependency on the condition of the resin.

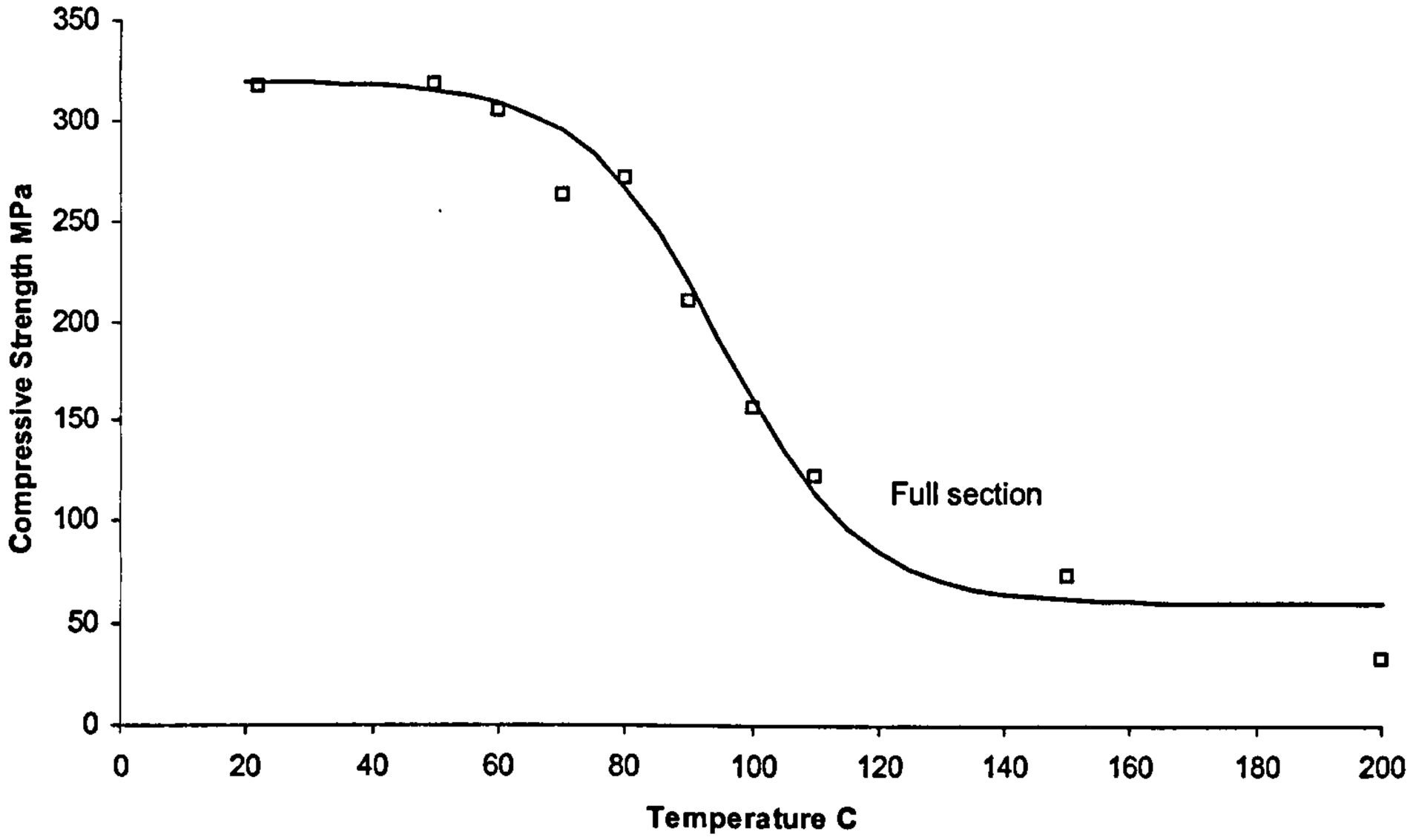

Figure 6.13. Compressive strength (σ_{Cl}) vs. temperature of polyester pultrusion. Note only the full section material was tested.

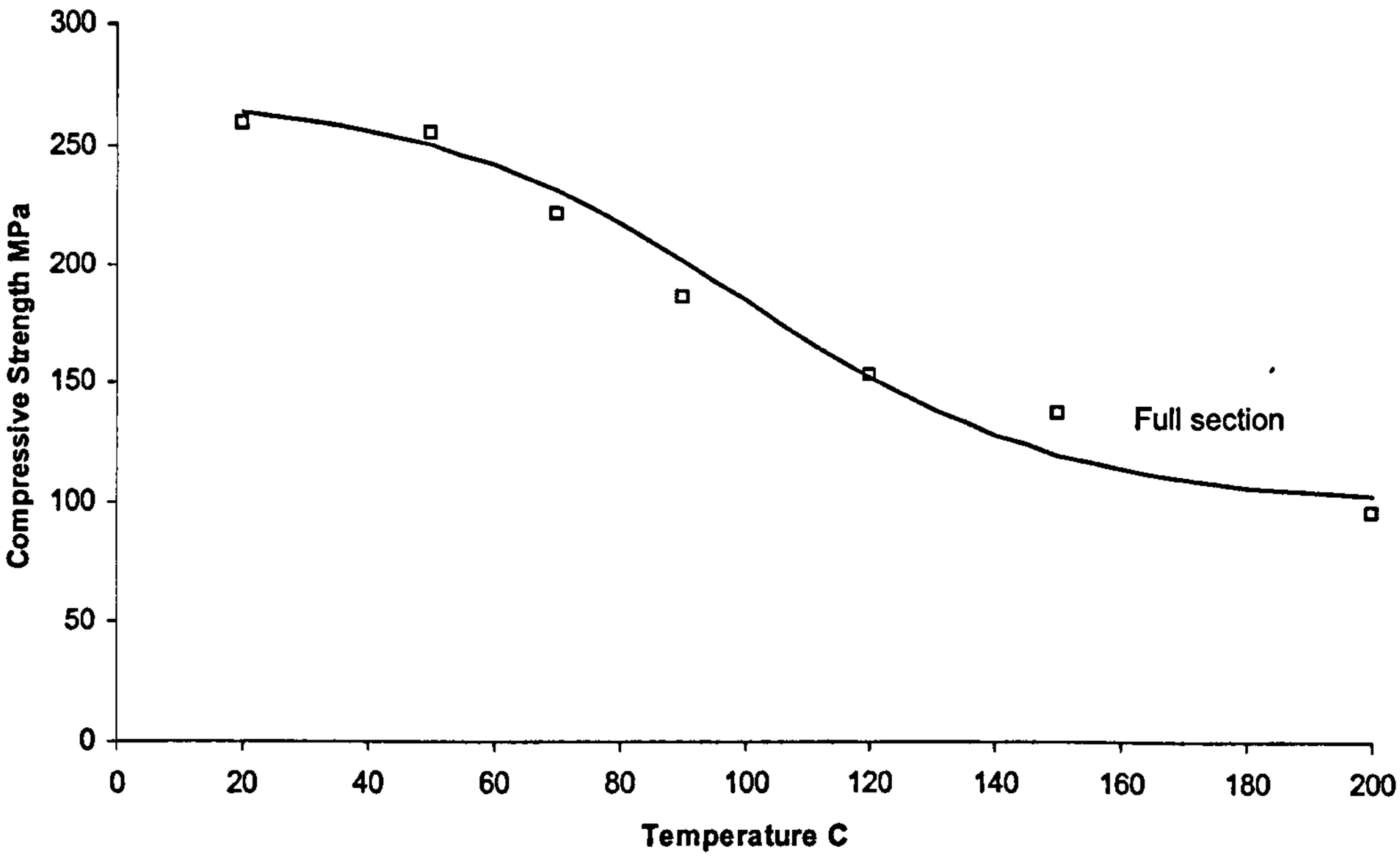

Figure 6.14. Compressive strength (σ_{Cl}) vs. temperature of phenolic pultrusion. Note only the full section material was tested.

The phenolic pultrusion has a considerably lower compressive strength than the polyester. This is caused by the much larger void content in the phenolic material, 24.8% (in the UD core) compared to 5.1% (UD core) for the polyester.

Figure 6.15 and Figure 6.16 illustrate the longitudinal stiffness (E_1) as a function of temperature for the polyester material and the phenolic material respectively. Data for both the unidirectional (core) and the full material are shown.

In the case of the polyester pultrusion the data show the familiar drop in magnitude as it passes through the T_g region. The phenolic material defies convention and does not demonstrate this behaviour.

Data points for both 1 second and 10 seconds have been shown. This is gives some indication of any creep that is taking place whilst the material is undergoing testing.

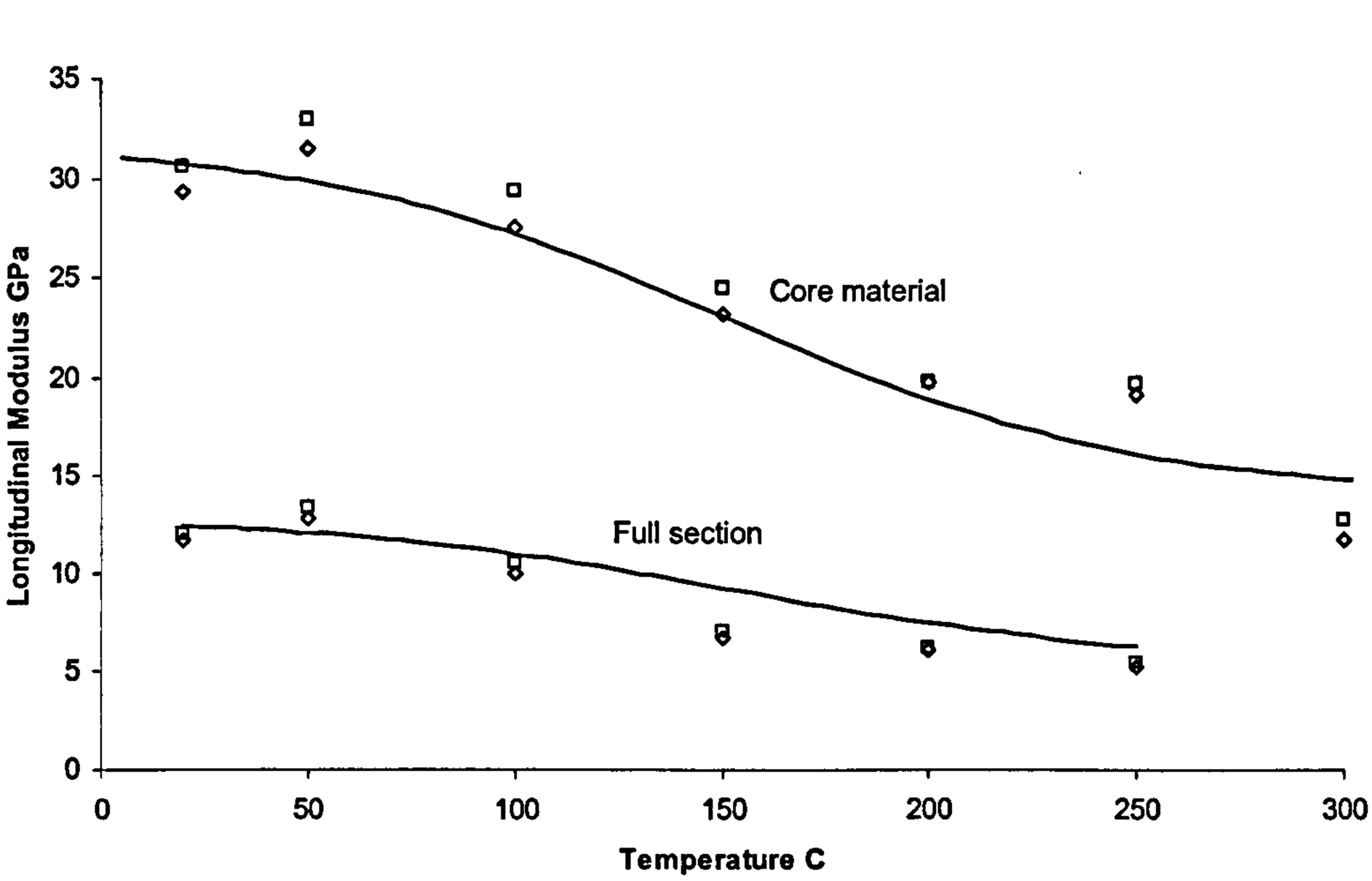

Figure 6.15. Longitudinal stiffness (E_1) vs. temperature of polyester pultrusion. Note both unidirectional (core) and the full section material were tested (□ denote stiffness at 1 second, ◇ at 10 seconds).

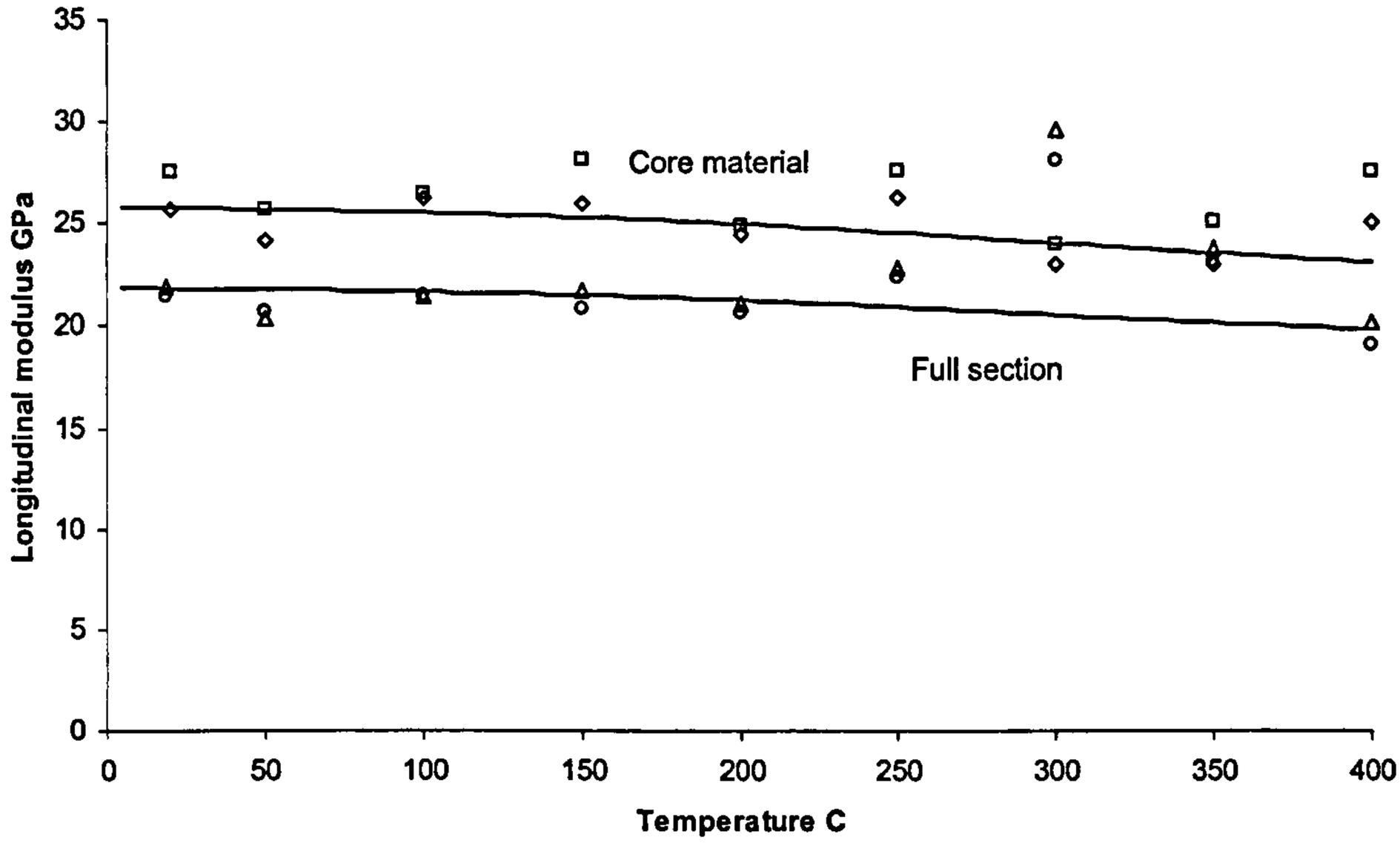

Figure 6.16. Longitudinal stiffness (E_1) vs. temperature of phenolic pultrusion. Note both unidirectional (core) and full thickness material were tested (□ denote stiffness at 1 second, ◇ 10 seconds for core material, △ denote 1 second and ○ 10 seconds for full section material).

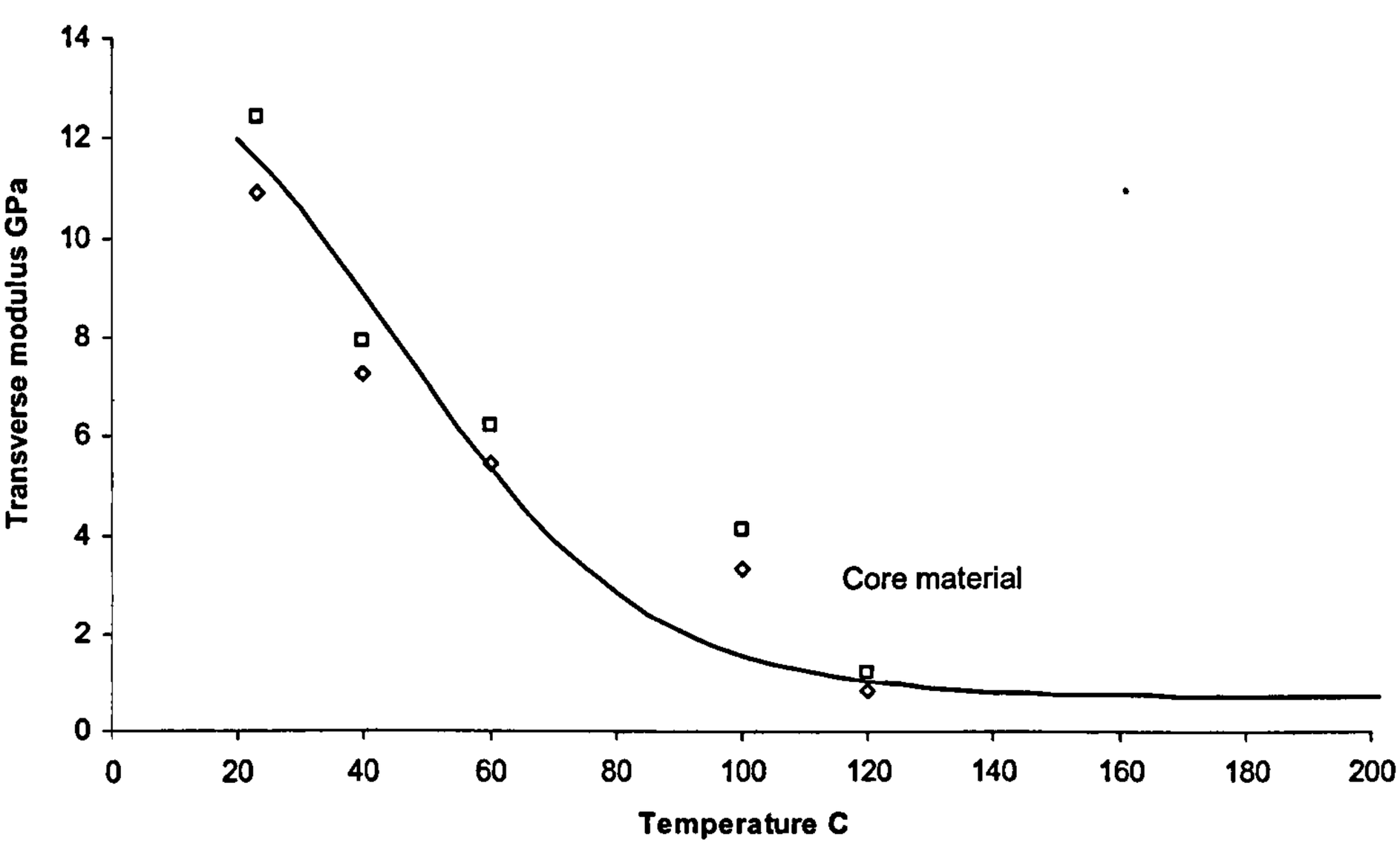

Figure 6.17. Transverse stiffness (E_2) vs. temperature of polyester pultrusion. Note only unidirectional (core) material was tested (□ denote stiffness at 1 second, ◇ 10 seconds).

Figure 6.17 and Figure 6.18 show the transverse stiffness (E_2) of the unidirectional (core) polyester material as a function of temperature and that of the phenolic respectively. Once again data for 1 second and 10 seconds is shown, and the drop in stiffness as the material passes through the T_g region is apparent in both materials.

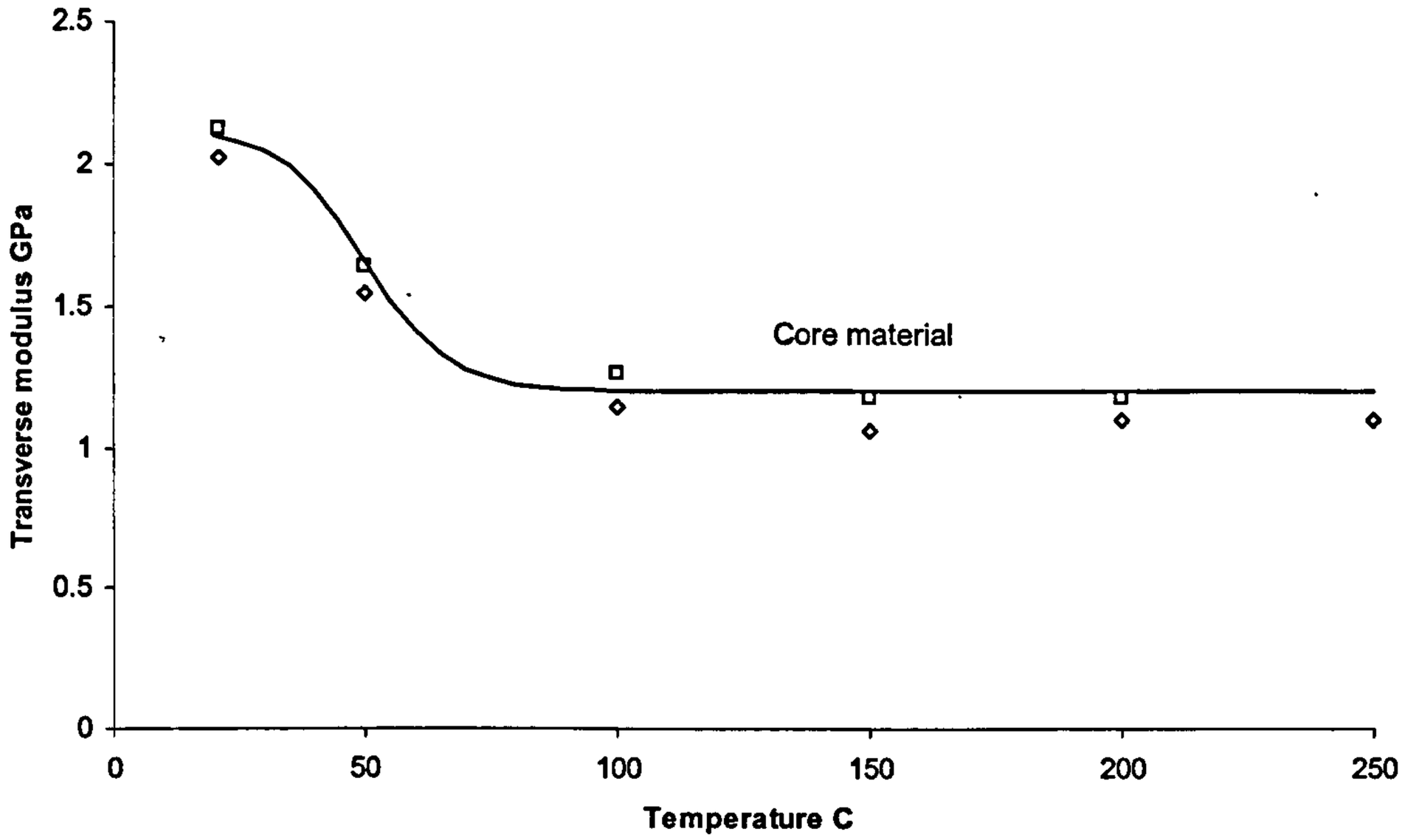

Figure 6.18. Transverse stiffness (E_2) vs. temperature of phenolic pultrusion. Note only unidirectional (core) material was tested (□ denote stiffness at 1 second, ◇ 10 seconds).

The parameters used to construct the curves using Equation 6.1 to describe all the mechanical properties as functions of temperature are listed in Table 6.1.

A value for shear modulus (G_{12}) at room temperature was established by carrying out a flexural stiffness test on a sample cut at a 45° angle from the longitudinal. The subsequent stiffness value was (E_{45}) was converted into a value for shear modulus through Equation 6.3, based on the compliance matrix,

$$G_{12} = \frac{E_{45}}{4} + \frac{E_2}{2\nu} - E_1 - E_2 \qquad (6.3)$$

where E_1, E_2 and ν are longitudinal stiffness, transverse stiffness, and poisons ration respectively. The resultant value for shear modulus (1.2 GPa) was low enough to assume that as the temperature rose it would drop rapidly, and higher temperature values would be next to zero.

Table 6.1. Table of parameters used to describe mechanical properties as a function of temperature (P_U, P_R, T_g and k are respectively, un-relaxed property value, relaxed property value, mechanical glass transition temperature and a constant describing the breadth of relaxation). Shear modulus has been omitted.

Material	**Polyester**				**Phenolic**			
Parameter	P_U	P_R	T_g	k	P_U	P_R	T_g	k
σ_{T1} (UD core)	354	242	150	0.03	500	347	100	0.035
σ_{T1} (Full material)	230	220	150	0.03	400	278	100	0.035
σ_{C1} (Full material)	320	60	95	0.045	270	100	100	0.02
E_1 (UD core)	32	14	150	0.01	26	22	300	0.005
E_1 (Full material)	13	6	100	0.025	22	19	300	0.05
E_2 (UD Core)	15.2	0.7	45	0.025	2.12	1.2	50	0.06

6.2. Fire Testing under Load

6.2.1. Tensile and Compressive Tests

Both tensile and compressive failure would occur with little warning. Once plies began to fail, complete failure occurred very soon after. The tensile strength curves both exhibit a high level of residual strength, due to glass retaining its strength at very high temperatures (Figure 6.19). The compressive stress rupture curves (Figure 6.20) show a more rapid decline in strength when compared to the tensile stress rupture curves. This underlines the fact that pultruded composites are particularly susceptible to compressive failure when subjected to fire.

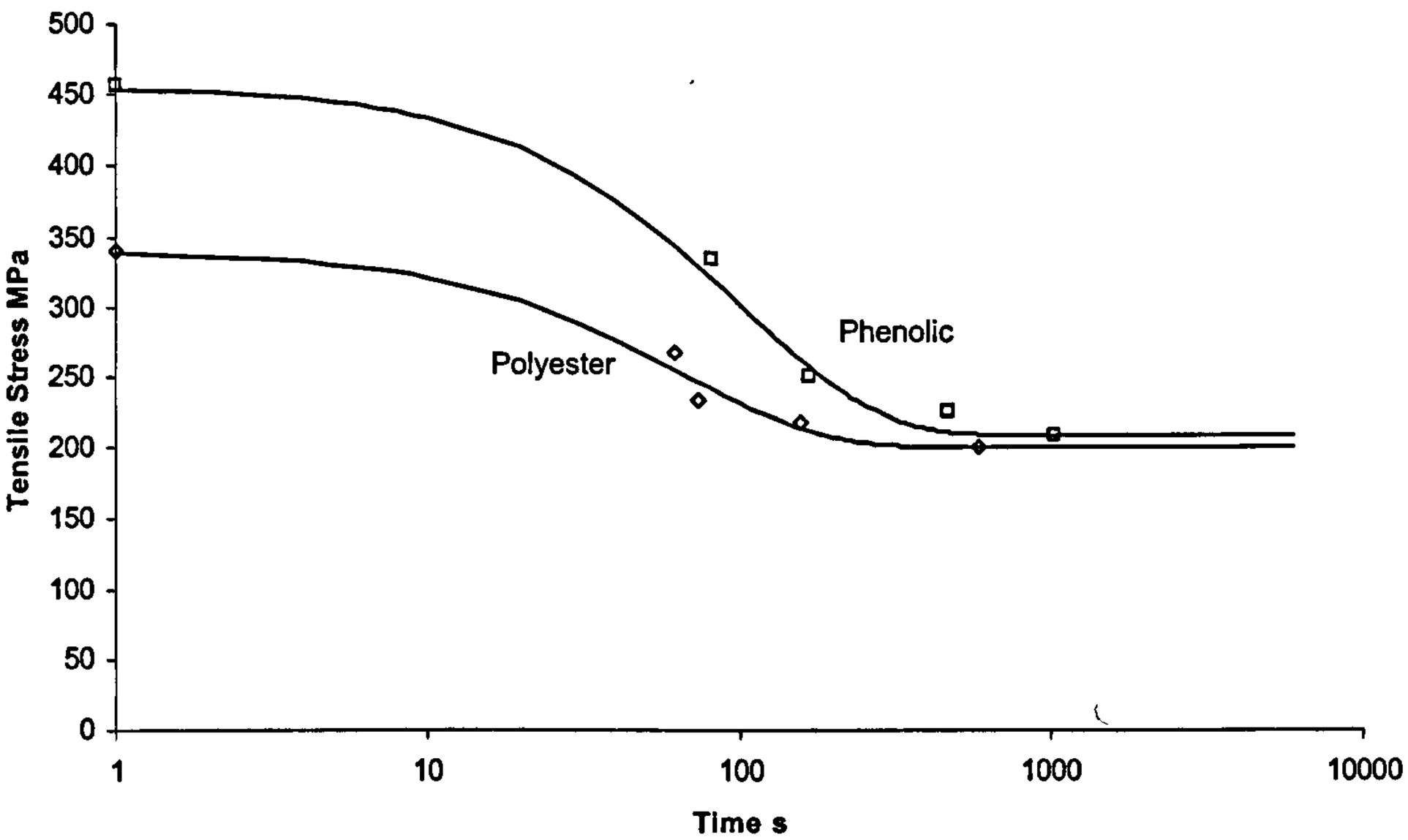

Figure 6.19. Tensile stress-rupture curve of both polyester ◇ and phenolic □ materials. Test samples were subjected to a heat flux of 50kWm^{-2}. Note the 1 second points represent the material ultimate tensile strength.

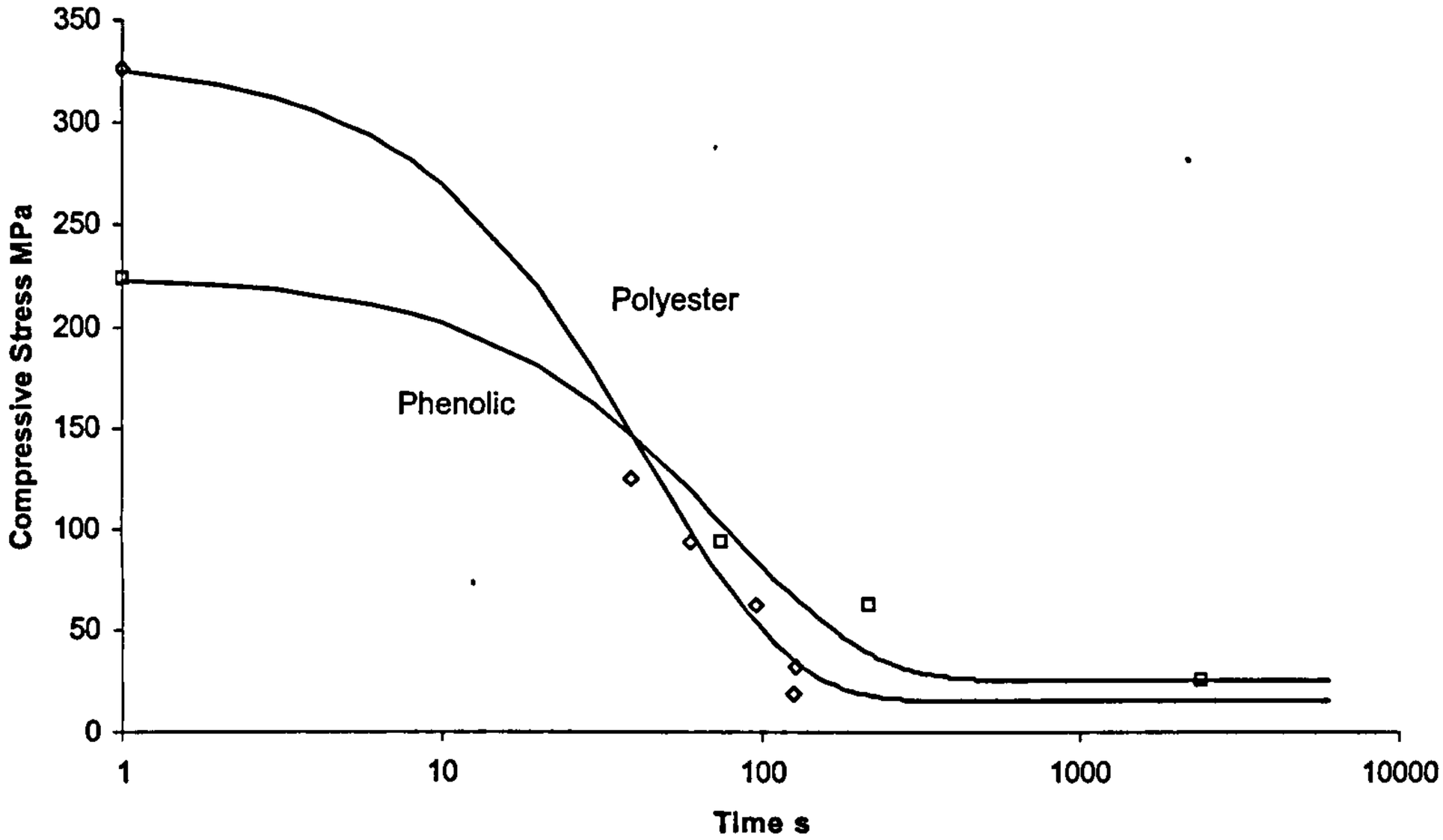

Figure 6.20. Compressive stress-rupture curve of both polyester □ and phenolic ◇ materials. Test samples were subjected to a heat flux of 50kWm^{-2}. Note the 1 second points represent the material ultimate compressive strength.

6.2.2. Pool Fire test under Load

The sections tested in the pool fire experiments all failed in a time period within the order of 100 seconds; with the exception of the 'I' beam (see Table 6.2). It is thought the rapid failure of the 'I' section was caused by the heat and flames being able to attack both sides, effectively removing the benefit of a cold face. The inside of the box sections acts as a cold face, noticeably extending their failure times (see Figure 6.21).

Table 6.2. Failure times for sections tested in a pool fire. Note the rapid failure of the 'I' section.

Beam description	Time to failure (secs)
60 x 60 x 5mm box (polyester)	42
100 x 100 x 6mm box (polyester)	83
100 x 100 x 8mm box (polyester)	88
120 x 60 x 6mm 'I' (polyester)	15

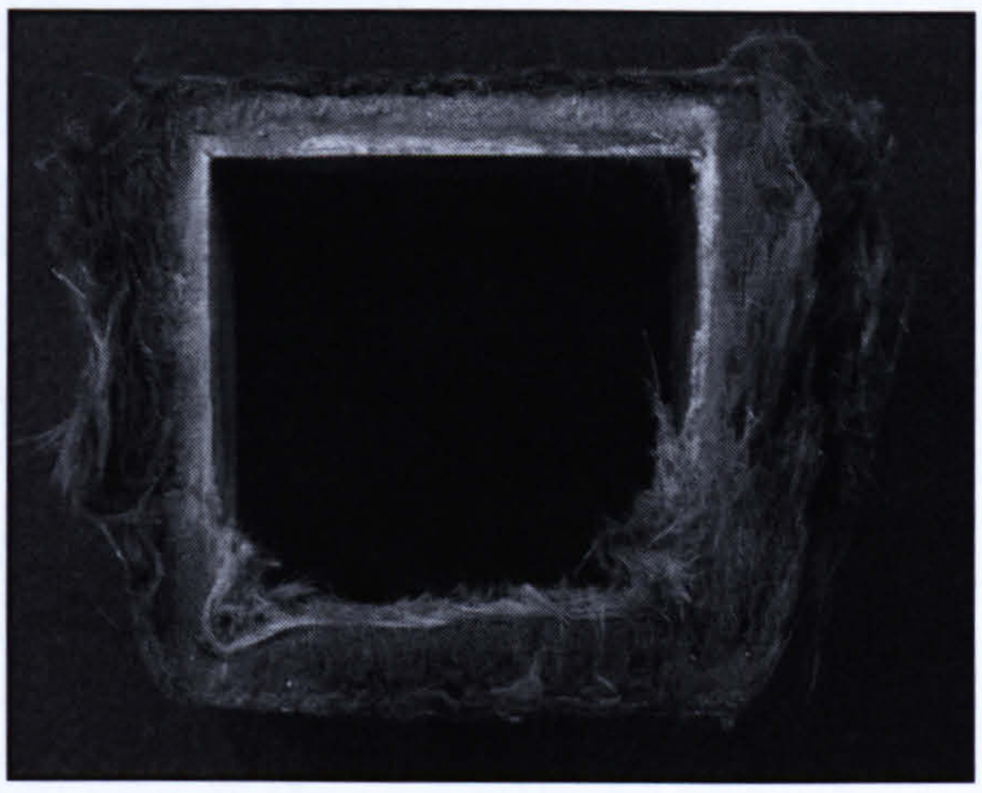

Figure 6.21. Section through a polyester box section showing the undamaged 'cold face' on the inside of the section.

In each case failure occurred suddenly and with little warning. Each section failed due to local buckling in the compressive skin (see Figure 6.22). The reason being that compressive stiffness is heavily dependent on resin depletion. The size of section had a limited effect on failure time with the larger 100 x 100mm box sections fairing better than the smaller 60 x 60mm section. This could perhaps be due to the heat taking longer to conduct through the larger sections, therefore taking longer to reach its T_g value, softening the material.

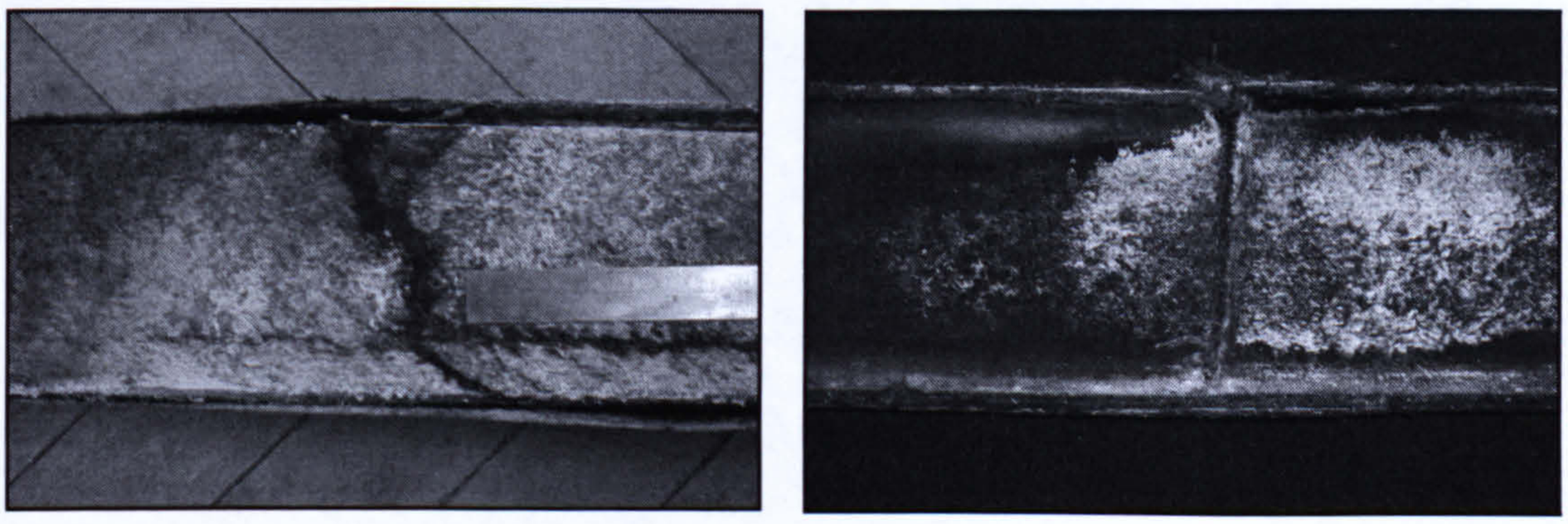

(i) **(ii)**

Figure 6.22. Local buckling in the compressive skin of a polyester box section (i), and a side view of a polyester 'I' section (ii), highlighting the failure point, initiated by local buckling of the top web.

6.2.3. Furnace test under Load

The sections tested in the furnace again all failed within a similar time period, in the order of 100 seconds. The phenolic sections lasted slightly longer (approximately 30 seconds) than the polyester sections (see Table 6.3). In each case failure was sudden and came with little warning, caused by local buckling in the compressive skin of the section. Once again this can be put down to the fact that stiffness in the compressive side of the beam is heavily dependent on the condition of the resin.

Table 6.3. Failure times for sections tested in a SOLAS fire curve furnace.

Beam description	Time to failure (secs)
60 x 60 x 5mm box (polyester)	124
60 x 60 x 5mm box (polyester)	120
60 x 60 x 5mm box (phenolic)	150
60 x 60 x 5mm box (phenolic)	152

The consistency of results highlights the consistency of the SOLAS furnace test.

6.2.4. Columns under compression

Compression tests were carried out on both polyester and phenolic columns. For both materials, the bare columns had dimensions of 60 x 60 x 5mm, and 90mm tall.

Figure 6.23 shows the effect various systems for improving fire performance on a polyester column. All the systems were tested at least once at a serviceable load, equivalent to 46 MPa.

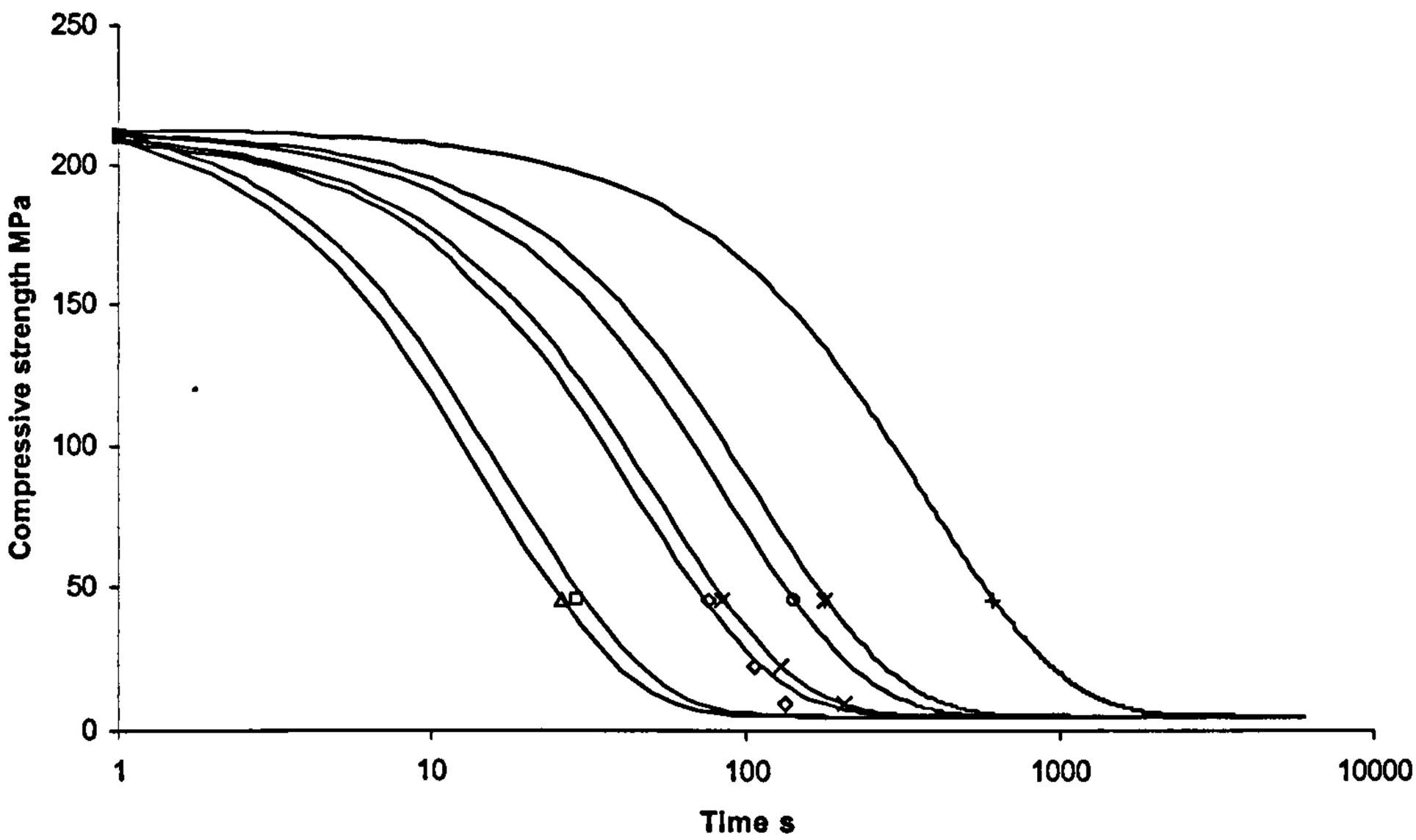

Figure 6.23. Results of compression tests on polyester box columns. From left to right: △ indicates Clariant coated column, □ bare column, ◇ Kerin coated column, × Geo-polymer coated column, ○ 'tinned' column∗ 'boxed column' with air insulator, + 'boxed column' with Kaowool insulator. Note that the 1 second point represents the ultimate compressive strength of the column.

It can be seen that of all the coated columns tested the 'tinned' column performed the best, extending failure time by approximately 110 seconds. Out of the 'boxed column's tested, the Kaowool insulated one performed the best, improving failure time by approximately 575 seconds, compared to the 128 seconds of the air insulated one.

The temperature profiles of the two 'boxed columns' tested are detailed in Figure 6.24 and Figure 6.25. It is seen that the temperature of the column increases far more rapidly in the air insulated case, than in the Kaowool insulated case.

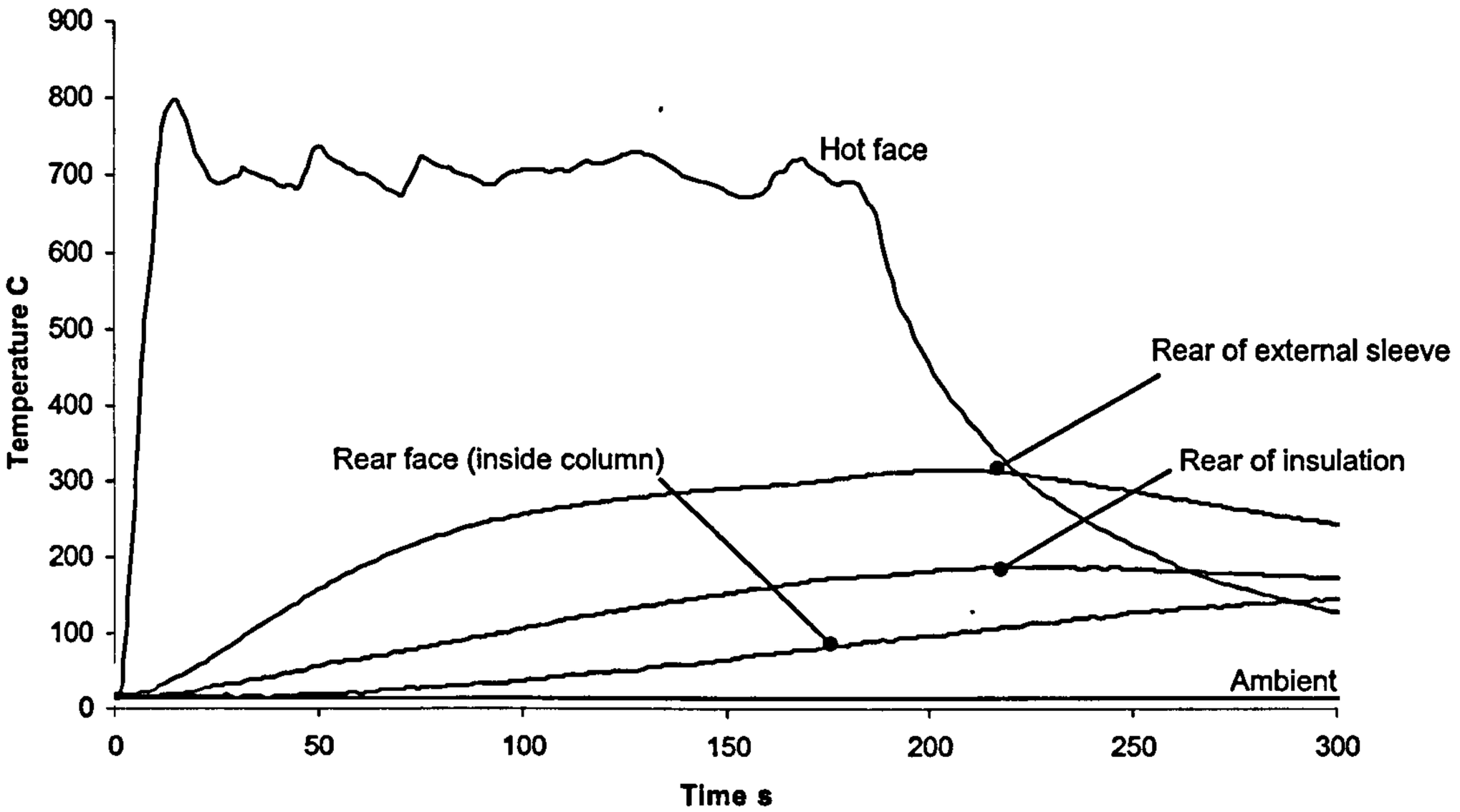

Figure 6.24. Temperature profiles through a 'boxed column' with air as the insulator.

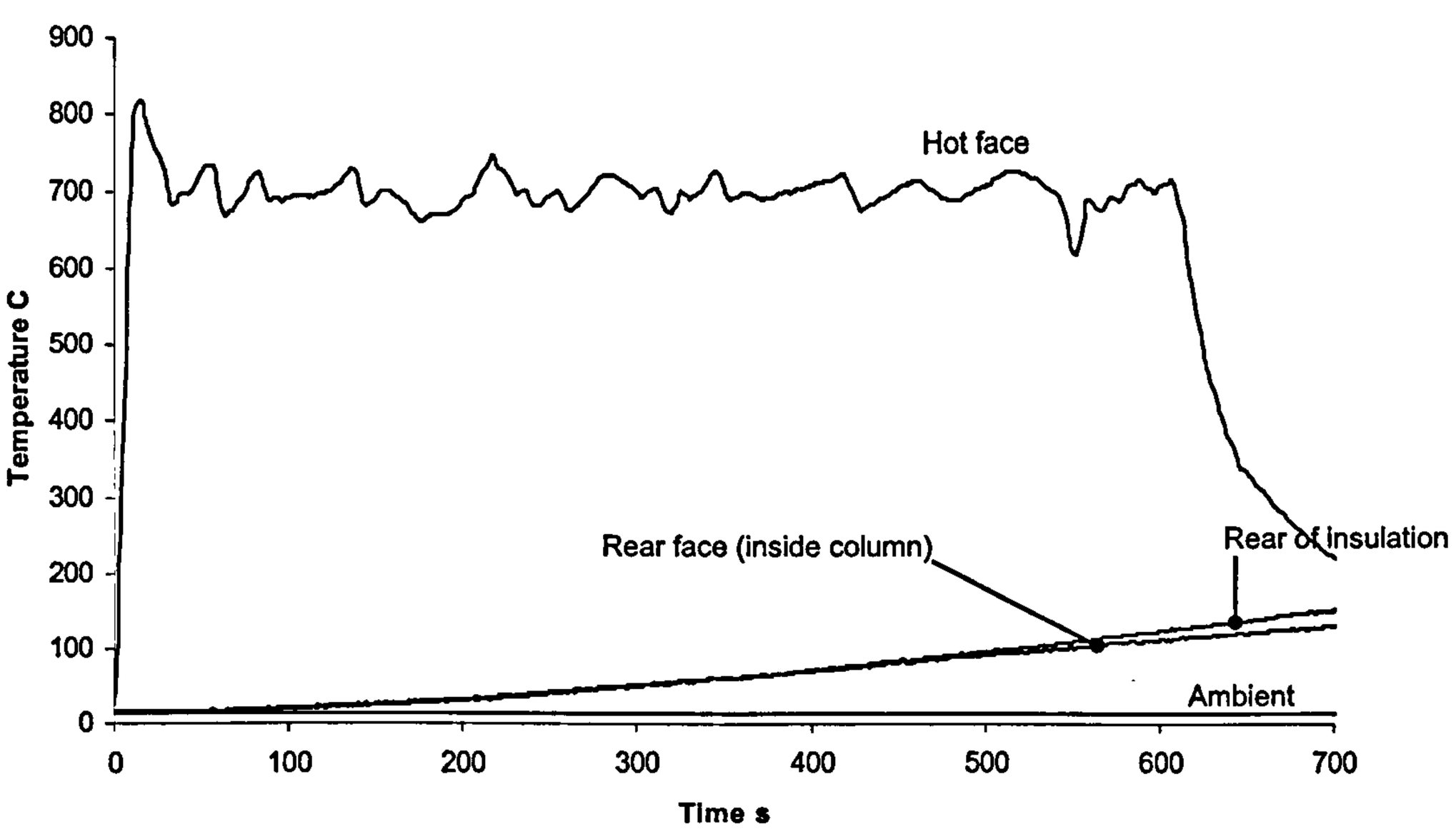

Figure 6.25. Temperature profile through a 'boxed column' with Kaowool as the insulator.

Figure 6.26 details the effect the 'tinned' system had on a phenolic column. Failure time was extended but not as significantly as with the polyester column. In this case it was only 23 seconds.

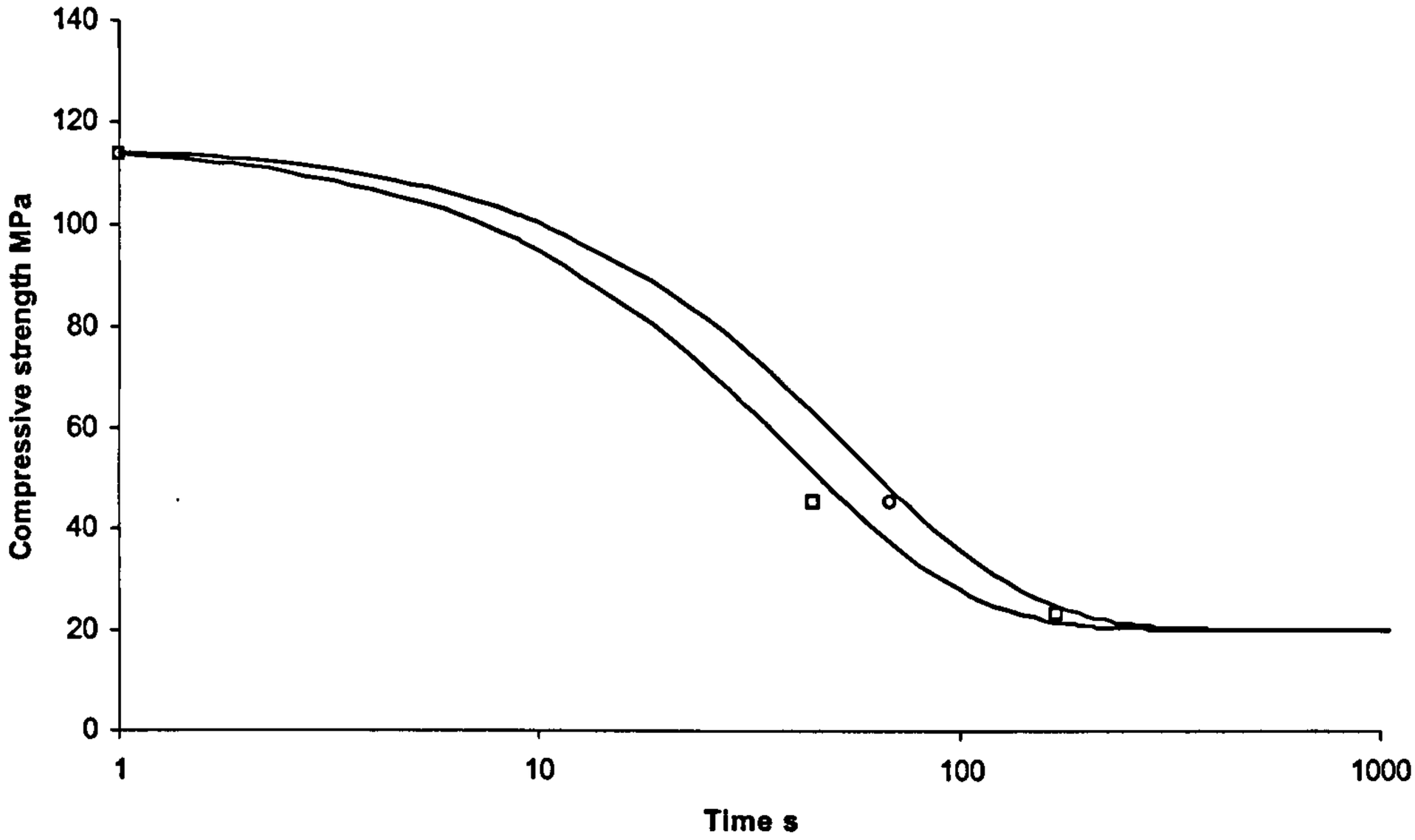

Figure 6.26. Results of compression tests on phenolic box columns. From left to right: □ indicate bare column, ○ 'tinned' column. Note that the 1 second point represents the ultimate compressive strength of the column.

6.3. Experimental reliability

This section discusses reliability issues relating to the range of experiments carried out in this thesis.

6.3.1. Mechanical properties at elevated temperatures

During this series of experiments, a great deal of care was taken to ensure that the material was at the stated temperature of the test. In each case (tensile, compressive, and flexure), the test utilised temperature controllers to maintain, and monitor the sample's temperature. During the tests it was ensured that the sample was fully saturated at the desired temperature by leaving it for a period of 20 to 30 minutes before any load was applied. Further to this, the flexure test rig also contained a 'dummy' sample, inside of which were thermocouples positioned at the mid point of its section (Figure 6.27) and at 3 points along its length.

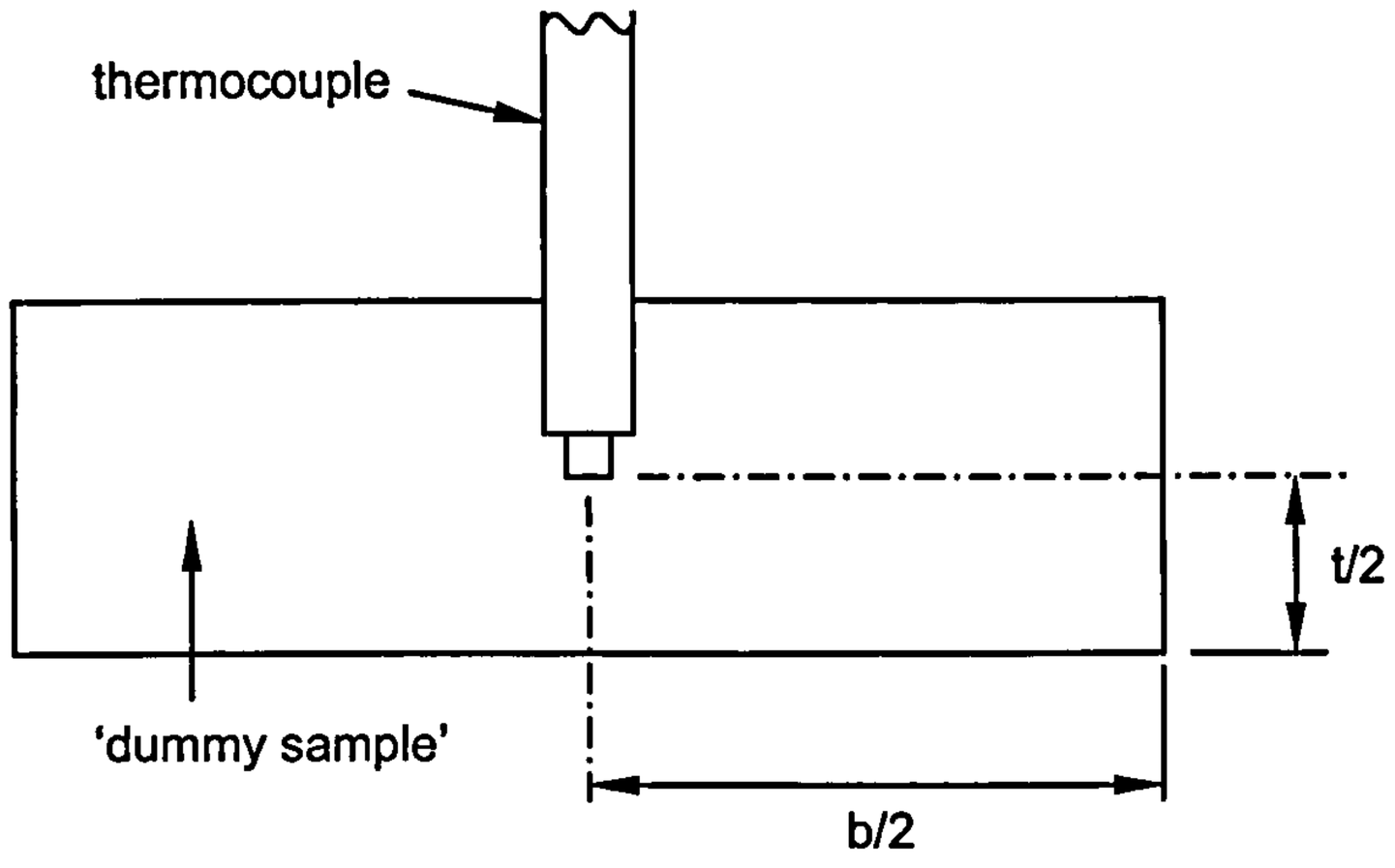

Figure 6.27. Sectional view through a 'dummy' flexural sample, indicating the position of the thermocouple tip in the sample mid-point.

All of the test rigs were well insulated during the heating and saturation periods. There was potential for the tensile and compressive tests to lose heat when the sample/rig came into contact with the test frame. Efforts were made to ensure that this period was as short as possible to reduce the heat sink effect. This involved ensuring that the test frame was set up and ready to go with only the cross head to be moved and load cell re-calibrated.

Overall, I feel that this series of experiments are very reliable and repeatable due to the use of temperature controlled heating systems, and sound experimental practice. The only major shortcoming of these experiments was that the temperature controllers were limited to 400°C. If higher rated temperature controllers had been available, a more marked decrease in mechanical properties of the phenolic material, in tension and flexure may have been observed.

The accuracy of some of the curves fitted to the results may be brought into question. The majority of the curves follow the experimental data well. Some of them however do not. In spite of this it was decided to continue with the hyperbolic tan function for reasons of simplicity. In any case the curves are there simply to provide

the failure model with a reasonably accurate trend describing how the mechanical properties decay at elevated temperatures.

6.3.2. Fire testing under load

Several problems exist with the experiments where the heat source is a propane burner.

The burner is calibrated using a pressure gauge. This pressure ties in with a local field temperature at the hot face of the sample. This in turn corresponds to a heat flux. During the mechanical testing with the burner, this pressure gauge facility was not available. This meant relying on the field temperature of the hot face as an indication of heat flux. Although in theory this would be sufficient, it is worth mentioning that this temperature is susceptible to the material flashing over. Careful monitoring of the material during testing is required, to ensure that the gas pressure is not reduced to compensate for the rise in field temperature due to flashover. This is to ensure that the sample is subjected to a consistent heat flux.

The test frame used in these experiments was an Avery 50 tonne Universal Testing Machine. This is a hydraulically operated machine, relying on an old fashioned analogue dial to indicate the load being applied. In spite of the errors associate with the machine's age (worn components, leaking hydraulics etc), the machine was always reliable and never broke down. Indeed, it's worth mentioning that the physical size of the machine prevented it overheating as a result of the flames from the propane burners.

Overall, largely due to the problems associated with controlling the propane burner, the results of these experiments can be only be regarded as indicative of a general trend.

6.3.3. Pool fire test under load

The pool fire tests can only be regarded as indicative tests. This is largely due to the unpredictable nature of the pool fire itself. Its temperature is extremely susceptible to thermal currents, and in this case, the elements too. The 'double flashover' effect of the fire also makes experiments difficult.

The rig itself also has errors associated with it. The load is applied with a hydraulic cylinder, operated with a manual hand-pump. The load is kept constant by monitoring the output form a load cell, and adjusting the pumping accordingly. This method is reasonably accurate but the time delays from the data acquisition system, not to mention the human factor, results in a constant load curve that looks a little shaky and noisy.

6.3.4. Furnace test under load

Similar to the pool-fire test, the furnace tests can only be regarded as indicative. Although the SOLAS furnace is more reliable and predictable than the pool fire, errors are present. Variations in furnace temperature will exist depending on things like whether or not the furnace has been used recently and the ambient room temperature. The test also assumes a constant temperature inside the furnace. This cannot be guaranteed.

The largest reliability issue exists with maintaining a constant load. In the case of the furnace test, hydraulics were deemed unnecessary, as the heat was wholly contained inside the furnace. This allowed the operator to stand next to the furnace to apply the load. This allowed a more simple method of applying a torque to a threaded bar to apply the load. This method did however introduce a more error into the experiment. This was due to the mechanical 'lag' in the system, something not experienced with hydraulics due to the incompressible nature of the hydraulic fluid. Further to this error was that associated with the feedback system as in the pool-fire test.

7. Modelling Behaviour under Load

A laminate analysis failure model was based on classical laminate theory [10, 83-85]. This is described in section 7.1 below. The model requires input from the thermal equation described in section 3.1, namely temperature evolution and residual resin content (RRC) through the thickness of the material. It also requires material mechanical properties as functions of temperature, detailed in chapter 6. The steps of the model are detailed in Figure 7.1.

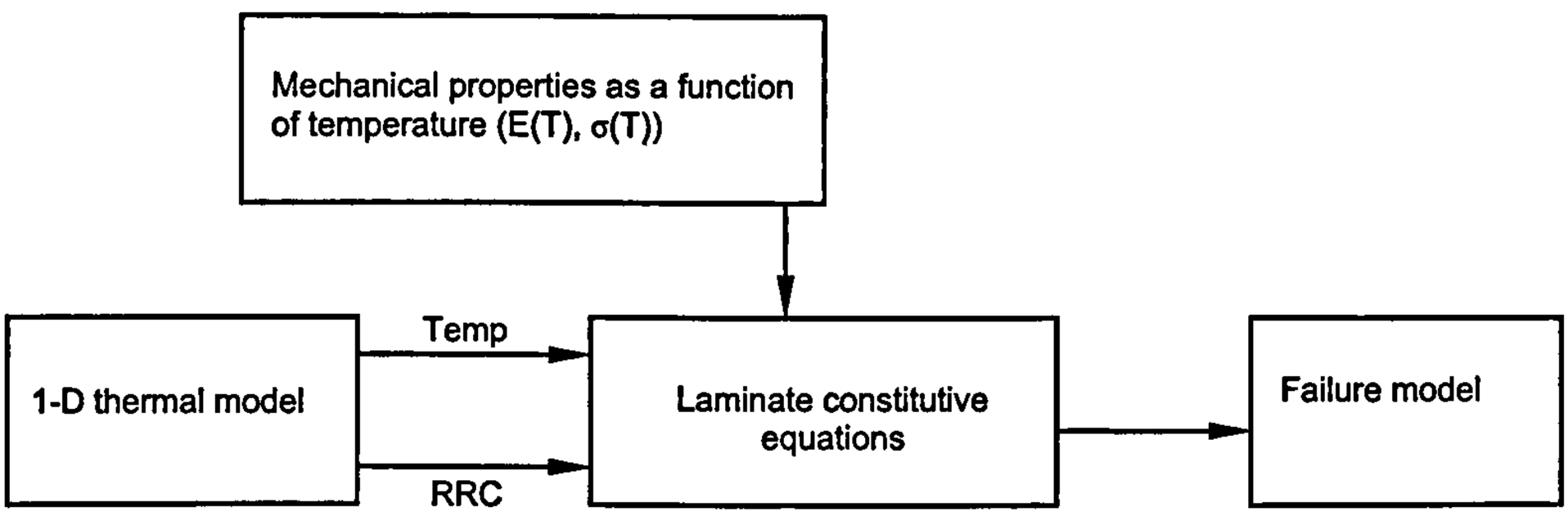

Figure 7.1. Flow chart describing the steps through modelling behaviour under load.

7.1. Laminate Constitutive Equations

Laminate theory [10, 83-85] is a commonly used tool in the composites industry to determine the strength and stiffness of a laminate. For the purpose of analysis, the pultruded material used in this thesis will be regarded as a laminate with a finite number of plys. Under isothermal conditions, applied forces and bending moments are related to the resultant mid-plane strains and curvatures by,

$$\begin{bmatrix} \tilde{N} \\ \tilde{M} \end{bmatrix} = \begin{bmatrix} \tilde{A} & \tilde{B} \\ \tilde{B} & \tilde{D} \end{bmatrix} \begin{bmatrix} \tilde{\varepsilon}_0 \\ \tilde{k} \end{bmatrix} \tag{7.1}$$

where, $\tilde{N}$ and $\tilde{M}$ are matrices of the normal loads and bending moments in the laminate:

$$\tilde{N} = \begin{bmatrix} N_x \\ N_y \\ N_{xy} \end{bmatrix} \quad \text{and} \quad \tilde{M} = \begin{bmatrix} M_x \\ M_y \\ M_{xy} \end{bmatrix} \tag{7.2}$$

and, $\tilde{\varepsilon}_0$ and $\tilde{k}$ are the mid-plane strains and curvatures:

$$\tilde{\varepsilon}_0 = \begin{bmatrix} \varepsilon_x \\ \varepsilon_y \\ \gamma_{xy} \end{bmatrix} \quad \text{and} \quad \tilde{k} = \begin{bmatrix} k_x \\ k_y \\ k_{xy} \end{bmatrix} \tag{7.3}$$

The $\tilde{A}$, $\tilde{B}$ and $\tilde{D}$ matrices are defined as,

$$\tilde{A} = \sum_{k=1}^{n} \int_{h_{k-1}}^{h_k} \tilde{\tilde{Q}} dz \qquad \tilde{B} = \sum_{k=1}^{n} \int_{h_{k-1}}^{h_k} \tilde{\tilde{Q}} z dz \qquad \tilde{D} = \sum_{k=1}^{n} \int_{h_{k-1}}^{h_k} \tilde{\tilde{Q}} z^2 dz \tag{7.4}$$

where $\tilde{Q}$ is the matrix of ply stiffness constants transformed to the co-ordinate system of the laminate:

$$\tilde{Q} = \begin{bmatrix} \tilde{Q}_{11} & \tilde{Q}_{12} & \tilde{Q}_{16} \\ \tilde{Q}_{12} & \tilde{Q}_{22} & \tilde{Q}_{26} \\ \tilde{Q}_{16} & \tilde{Q}_{26} & \tilde{Q}_{66} \end{bmatrix} \tag{7.5}$$

These constants vary from ply to ply according to the orientation within each layer. In this case they also vary in the z-direction due to the effects of temperature variation and resin content.

The boundary conditions of the problem are usually in the form of in-plane loads and moments, making the fully inverted version of equation (7.6) more preferable:

$$\begin{bmatrix} \tilde{\varepsilon}_0 \\ \tilde{k} \end{bmatrix} = \begin{bmatrix} \tilde{A}' & \tilde{B}' \\ \tilde{B}' & \tilde{D}' \end{bmatrix} \begin{bmatrix} \tilde{N} \\ \tilde{M} \end{bmatrix} \tag{7.6}$$

7.2. Input of Mechanical Properties vs. Temperature

As stated earlier, the mechanical properties as functions of time are a key input to the model. These are defined by equation 6.1 using parameters set out in Table 6.1. These values are inputted to the model through equation 7.7:

$$P(T) = [P_U + (P_U - P_R)(1 - \tanh(k(T - T_g)))]R^n \tag{7.7}$$

where R is resin content expressed as a decimal (100% being 1, i.e. virgin material, and 0.5 being 50%). For material loaded in tension, n.= 0, and for compression and flexure, $n = 1$. This was based upon the notion that compressive and flexural loading are heavily dependent upon resin condition, as opposed to tension, which is largely reliant upon fibre strength. The figures of 1 and 0 were decided upon based on previous work in this area[79, 86].

7.2.1. Mechanical Properties of CSM Skins

The material tested in this thesis has 3 distinct layers, CSM needle weave on the surfaces and unidirectional fibres in the central core (Figure 4.1 and Figure 6.2). This system caused problems whilst determining the materials' tensile strength as a function of temperature (see section 6.1.1).

This problem was overcome by treating the material as 3 separate layers, and determining mechanical properties as a function of temperature for each one. The data for the core material was determined experimentally using the methods set out in Chapter 4. This was not possible for the CSM material because the layers were

too thin to separate from the core material. The data for the CSM material was calculated by using combination of sandwich-beam theory and data from literature. These methods are detailed in Table 7.1. The data describing compressive strength as a function of temperature was determined entirely experimentally. In this case, splitting the material into its 3 layers was deemed unnecessary. This was due to the negligible effect the CSM needle weave layers would have on the materials' compressive strength.

Table 7.1. Methods used to determine mechanical properties as functions of temperature, for both UD core material and CSM needle weave outer layers. All experimental methods are described in Chapter 4.

Method adopted	**Property**
Experimental	$\sigma_{T\text{-}UD}$, σ_C, $E_{1\text{-}UD}$, $E_{2\text{-}UD}$
Sandwich-beam	E_{CSM}
Literature	$\sigma_{T\text{-}CSM}$

The sandwich-beam method considers the material as a typical sandwich beam and utilises the expression,

$$E_{Full} = E_{UD}\frac{t_1^3}{t_2^3} + E_{CSM}\left(\frac{t_2^3}{t_2^3} - \frac{t_1^3}{t_2^3}\right) \tag{7.8}$$

where E_{Full} is the flexural modulus of the full section of material, E_{UD} is the flexural modulus of the core material and E_{CSM} is the flexural modulus of the skin material. The thickness of the full section is t_2 and the thickness of the core material is t_1. This calculates the flexural modulus for the CSM skins from the flexural modulus of both the core material E_{UD}, and the full section, E_{Full} (both obtained experimentally). The resulting flexural modulus E_{CSM} is the same in both perpendicular and longitudinal directions. Equation 7.8 assumes a beam of constant width making E_{Full} a function of the relevant flexural moduli (E_{UD}, E_{CSM}) and ratio of the material thicknesses (t_1, t_2).

The tensile strength of the CSM material as a function of temperature was obtained through the literature. A tensile strength of 100 MPa [11, 87] was used as a room temperature tensile strength, degrading to a negligible strength of 1 MPa. The degradation in strength is governed by the same equation as all the other mechanical property data (Equation 6.1). The rate of degradation matches that of the core material i.e. the same values for k and T_g.

All of the mechanical properties for both the core material and skin material can be described with equation 6.1, and fitted using the four parameters P_U, P_R, T_g and k. A full set of these parameters used in the modelling is listed in Table 7.2.

Table 7.2. Parameters used to describe mechanical properties as a function of temperature for the laminate failure model. Parameters are listed for both the uni-directional and CSM material. Note that the parameters for compressive behaviour are the same for both the UD and skin material.

Material	**Polyester**				**Phenolic**			
Parameter	**P_U**	**P_R**	**T_g**	**k**	**P_U**	**P_R**	**T_g**	**k**
$\sigma_{T\text{-}UD}$	354	242	150	0.03	500	347	100	0.035
$\sigma_{T\text{-}CSM}$	100	1	150	0.03	100	1	150	0.03
$\sigma_{C\text{-}UD}$	320	60	95	0.045	270	100	100	0.02
$\sigma_{C\text{-}CSM}$	320	60	95	0.045	270	100	100	0.02
$E_{1\text{-}UD}$	32	14	150	0.01	26	22	300	0.005
$E_{1\text{-}CSM}$	6.5	3	0.015	160	20.5	18.7	230	0.008
$E_{2\text{-}UD}$	15.2	0.7	45	0.025	2.12	1.2	50	0.06
$E_{2\text{-}CSM}$	6.5	3	0.015	160	20.5	18.7	230	0.008

7.3. Results

7.3.1. A, B, D Matrix Evolution

Figure 7.2, Figure 7.3 and Figure 7.4 show the evolution of the ***A***, ***B***, ***D***, matrix components for an 8mm polyester pultrusion using the laminate failure model. Similarly Figure 7.6, Figure 7.7 and Figure 7.8 show this evolution for an 8mm phenolic pultrusion.

The ***A*** matrix components, relating to in-plane loads and deformations, decline over time reflecting the decline in overall mechanical properties. This decline is more marked in the polyester material when compared to that of the phenolic. This is due to phenolic composites retaining mechanical properties at high temperatures. The ***B*** matrix components describe the interaction between the in-plane loads and out-of-plane bending and twisting. This value is initially zero due to the symmetry of the material in the through-thickness direction. This rises to a peak as the CSM/needle weave skin is burnt away causing a symmetrical imbalance. The second, larger peak is caused by further asymmetry as the UD core material is degraded. Finally the ***D*** matrix components governing bending resistance decline with time. The influence of the progressive asymmetry can be seen with the shoulders in the curves. These coincide with the peaks in the ***B*** matrix curves.

Figure 7.5 and Figure 7.9 show the evolution of $\frac{1}{D'_{11}}$ for 8mm polyester and 8mm phenolic pultrusions respectively. This is equivalent to the material's 'flexural stiffness' (EI) [88]. Once again this declines over time reflecting the decline in overall mechanical properties. As with the ***D*** matrix components, a shoulder is visible on the curves, again reflecting the progressive asymmetry. As with the ***A*** matrix parameters this decline is far more significant in the polyester material, due to the phenolic material maintaining its mechanical properties at higher temperatures.

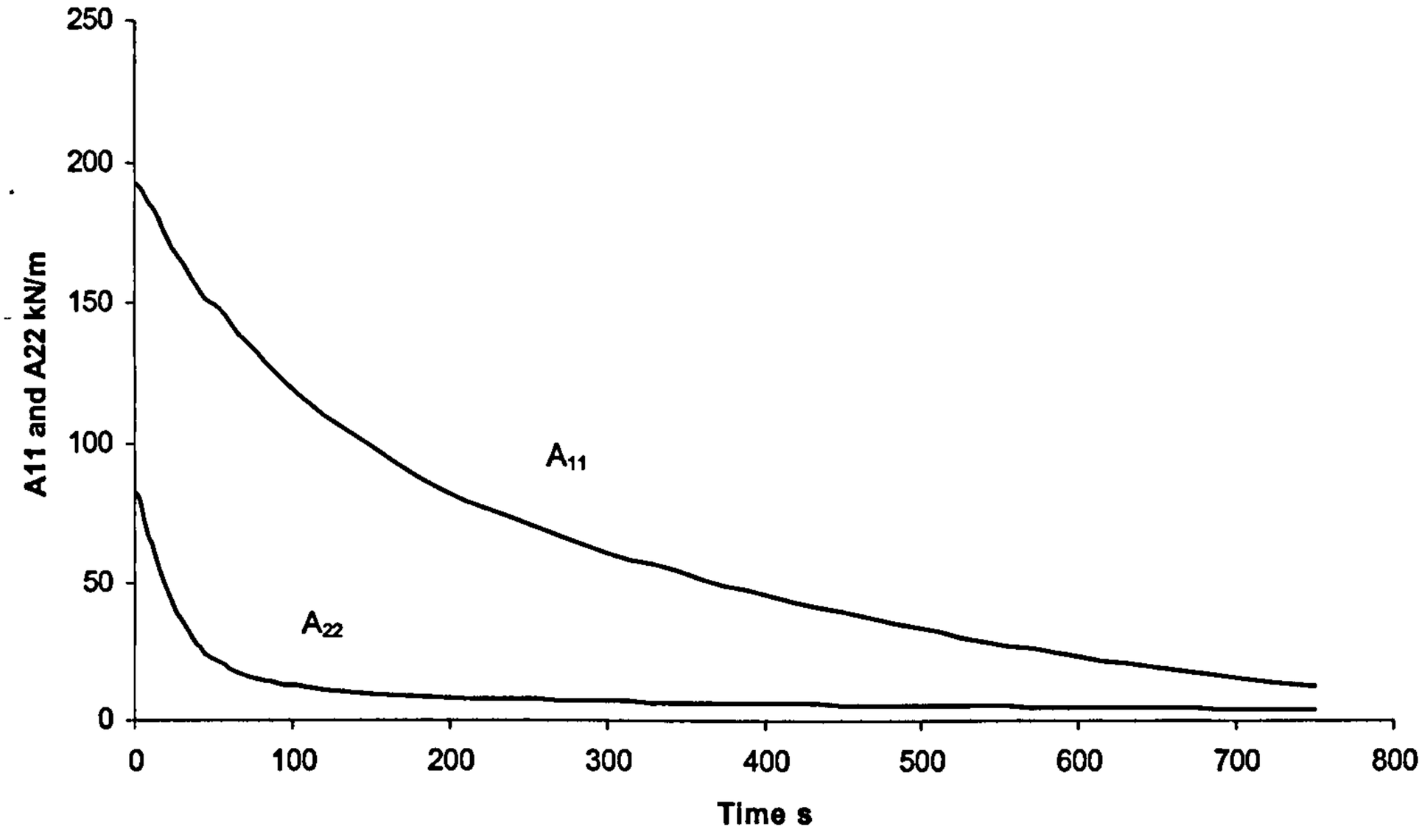

Figure 7.2. Evolution of the A component of the A, B, D matrix for an 8mm thick polyester pultrusion exposed to a one-sided heat flux of 50kWm^{-2}.

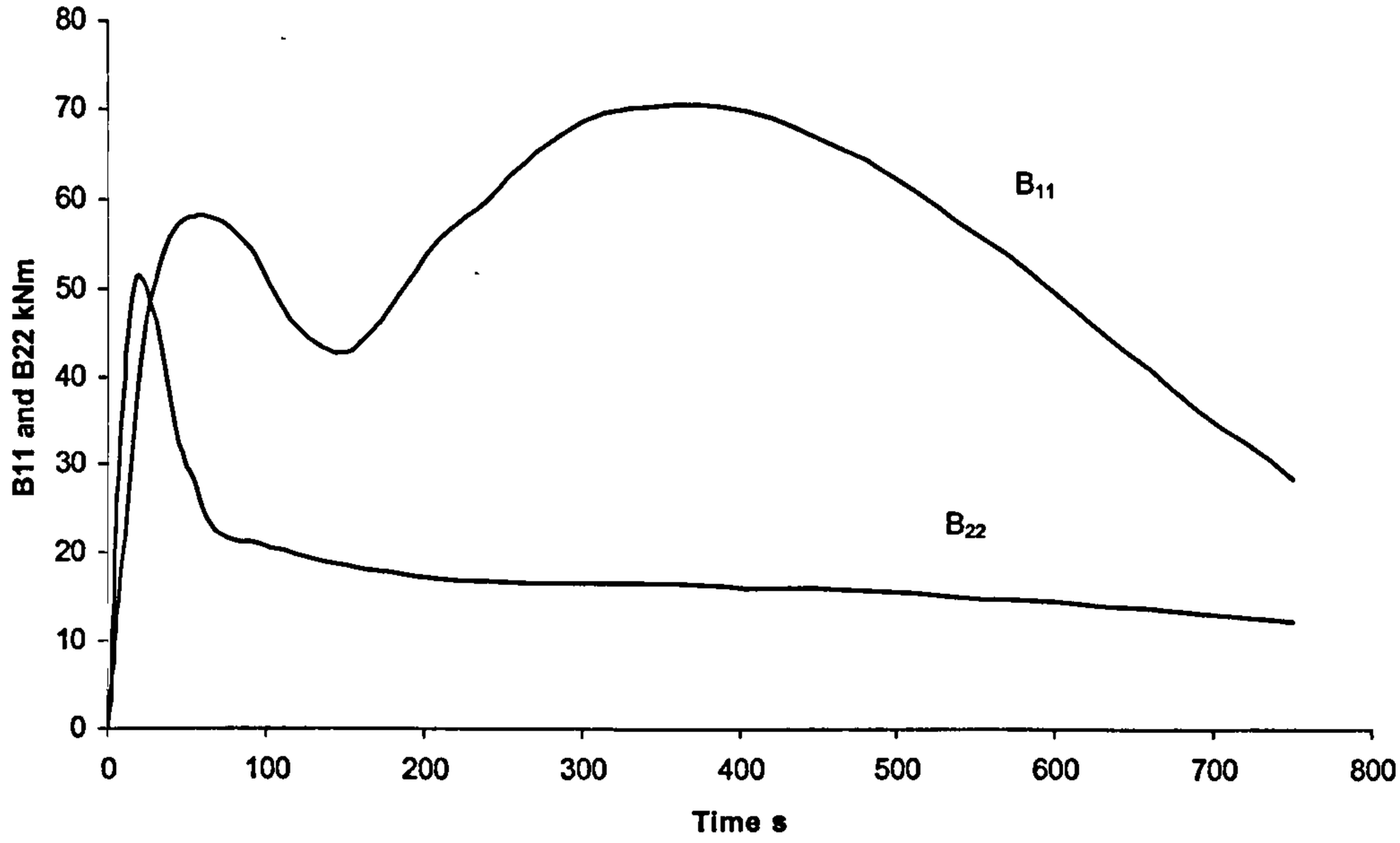

Figure 7.3. Evolution of the B component of the A, B, D matrix for am 8mm thick polyester pultrusion exposed to a one-sided heat flux of 50kWm^{-2}.

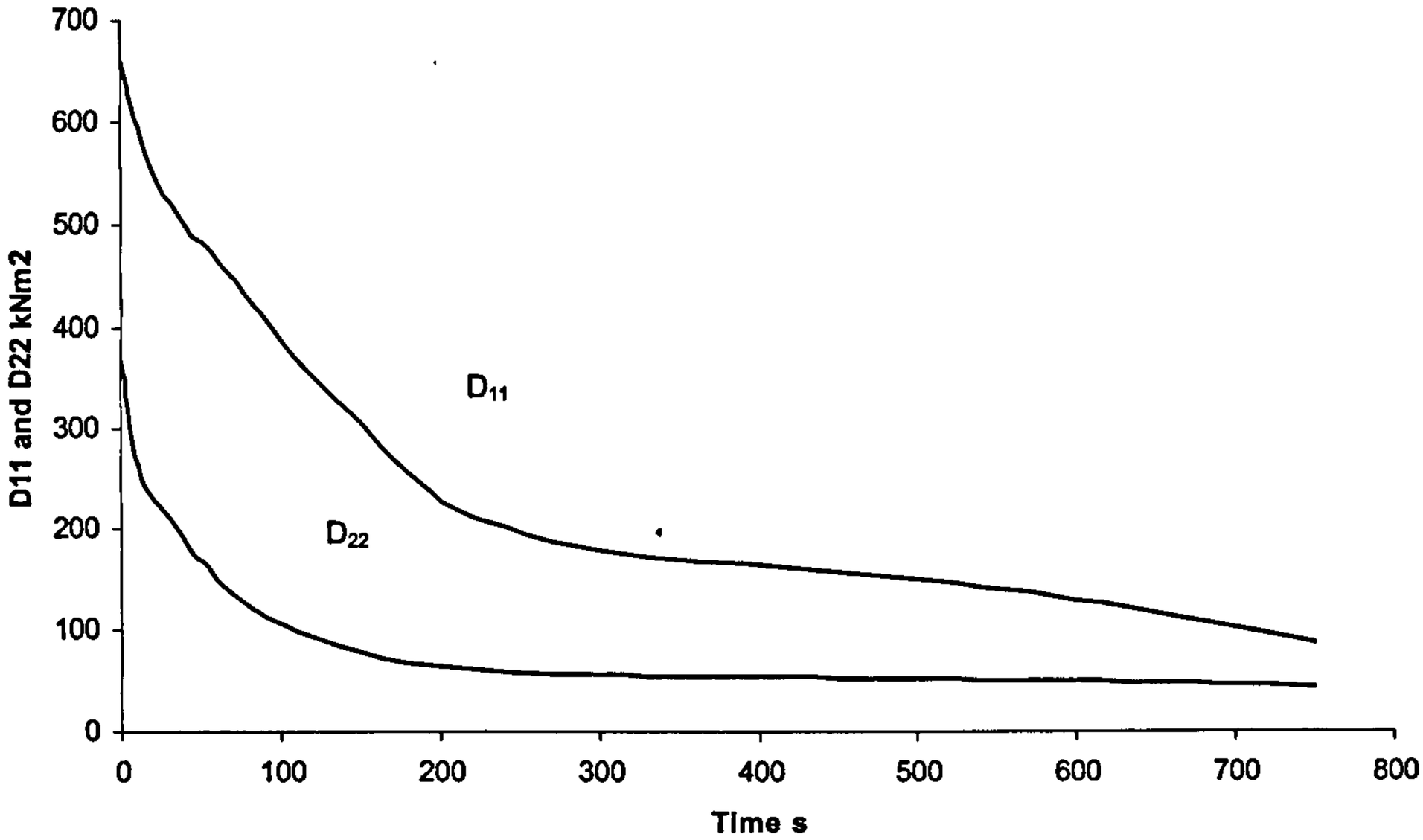

Figure 7.4. Evolution of the D component of the A, B, D matrix for an 8mm thick polyester pultrusion exposed to a one-sided heat flux of 50kWm^{-2}.

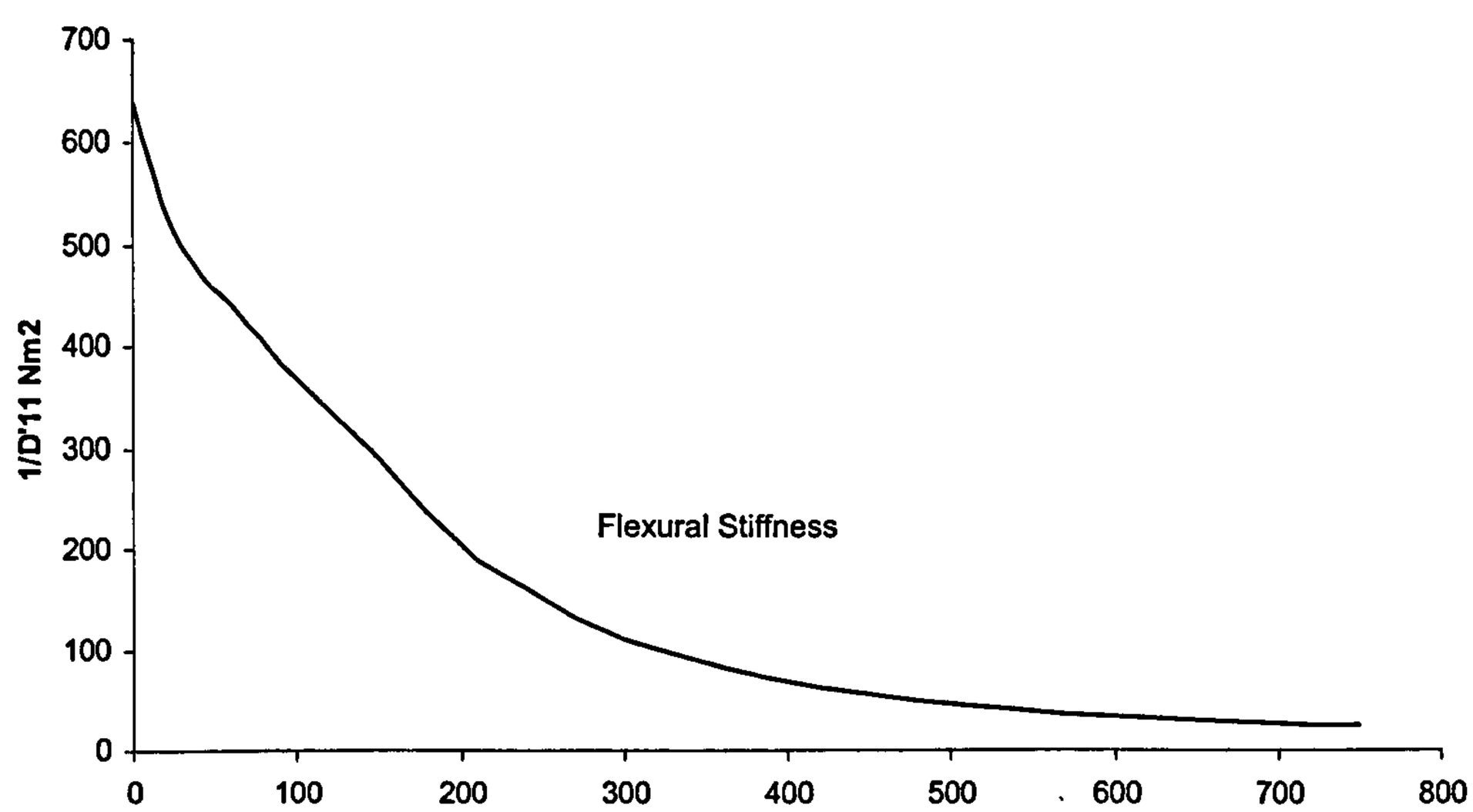

Figure 7.5. Evolution of flexural stiffness ($1/D'_{11}$) for an 8mm thick polyester pultrusion exposed to a one-sided heat flux of 50kWm^{-2}.

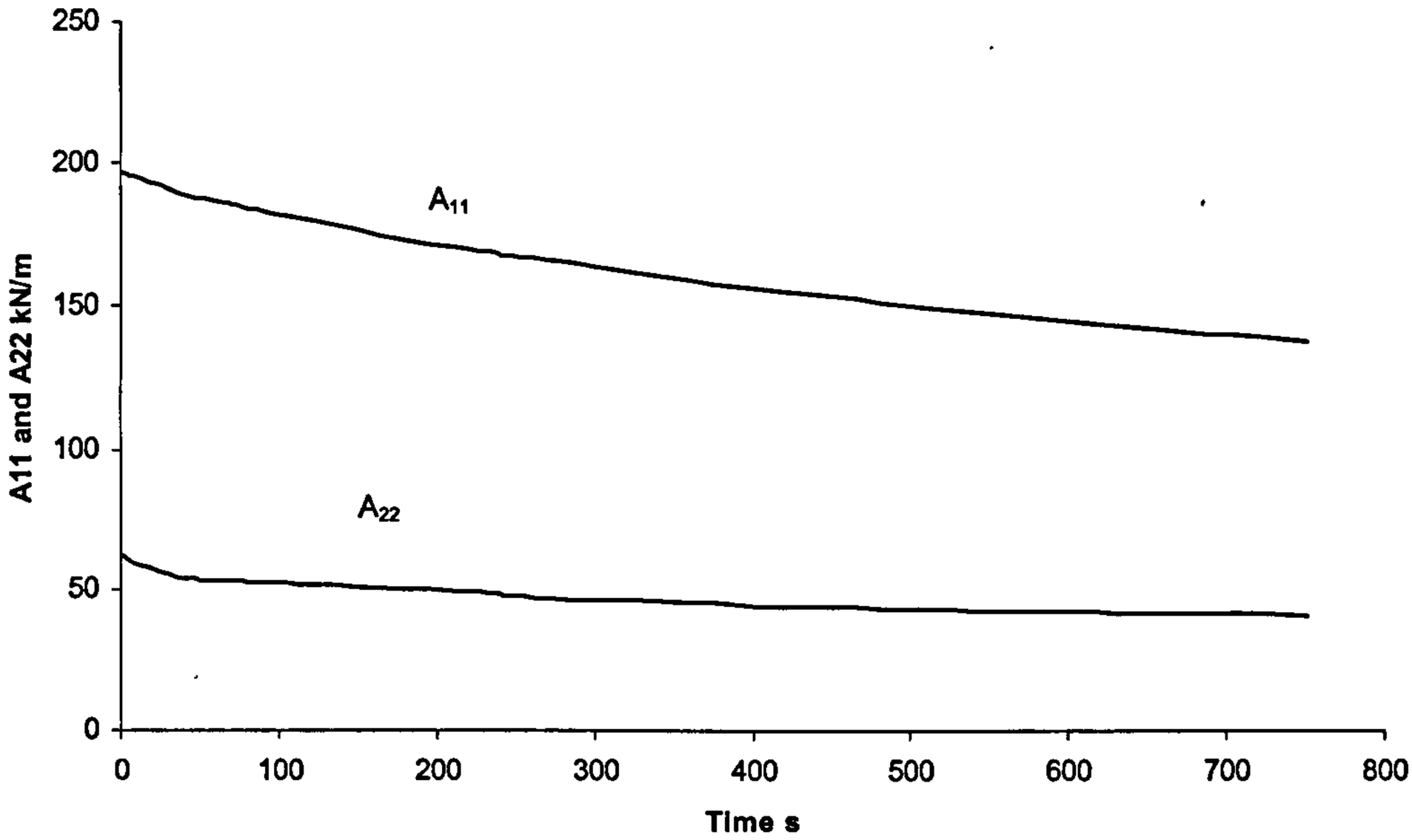

Figure 7.6. Evolution of the A component of the A, B, D matrix for an 8mm thick phenolic pultrusion exposed to a one-sided heat flux of 50kWm^{-2}.

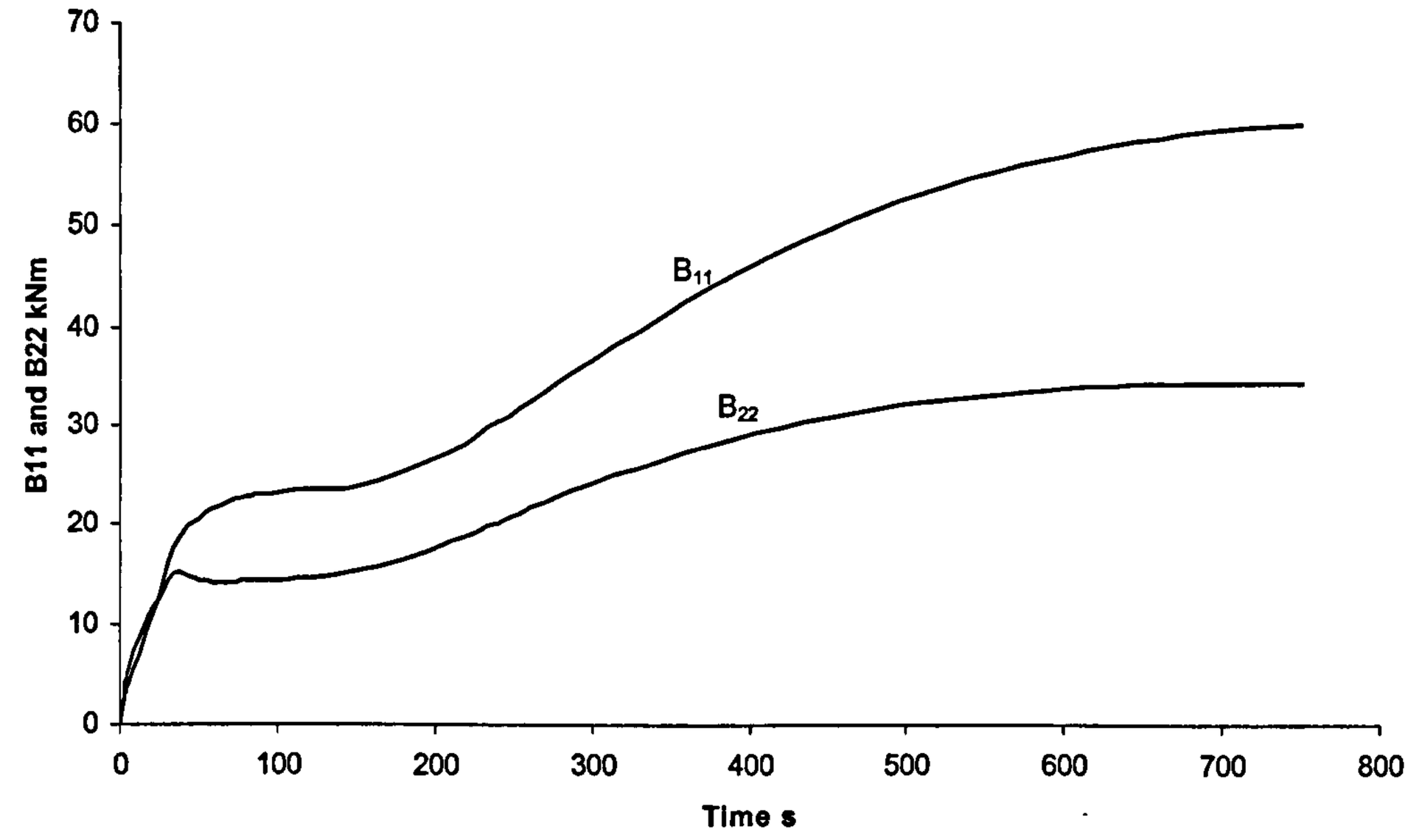

Figure 7.7. Evolution of the B component of the A, B, D matrix for an 8mm thick phenolic pultrusion exposed to a one-sided heat flux of 50kWm^{-2}.

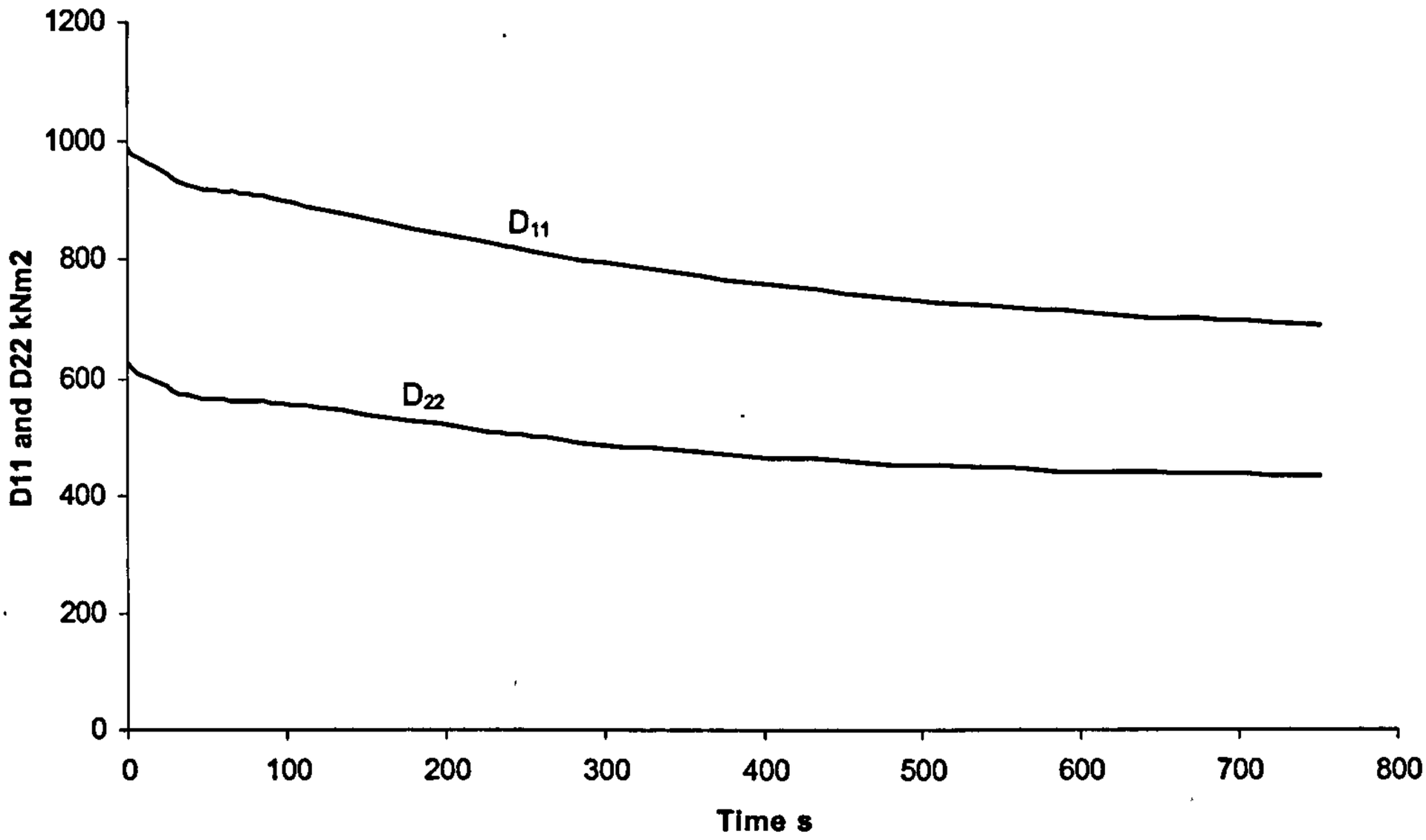

Figure 7.8. Evolution of the D component of the A, B, D matrix for an 8mm thick phenolic pultrusion exposed to a one-sided heat flux of 50kWm^{-2}.

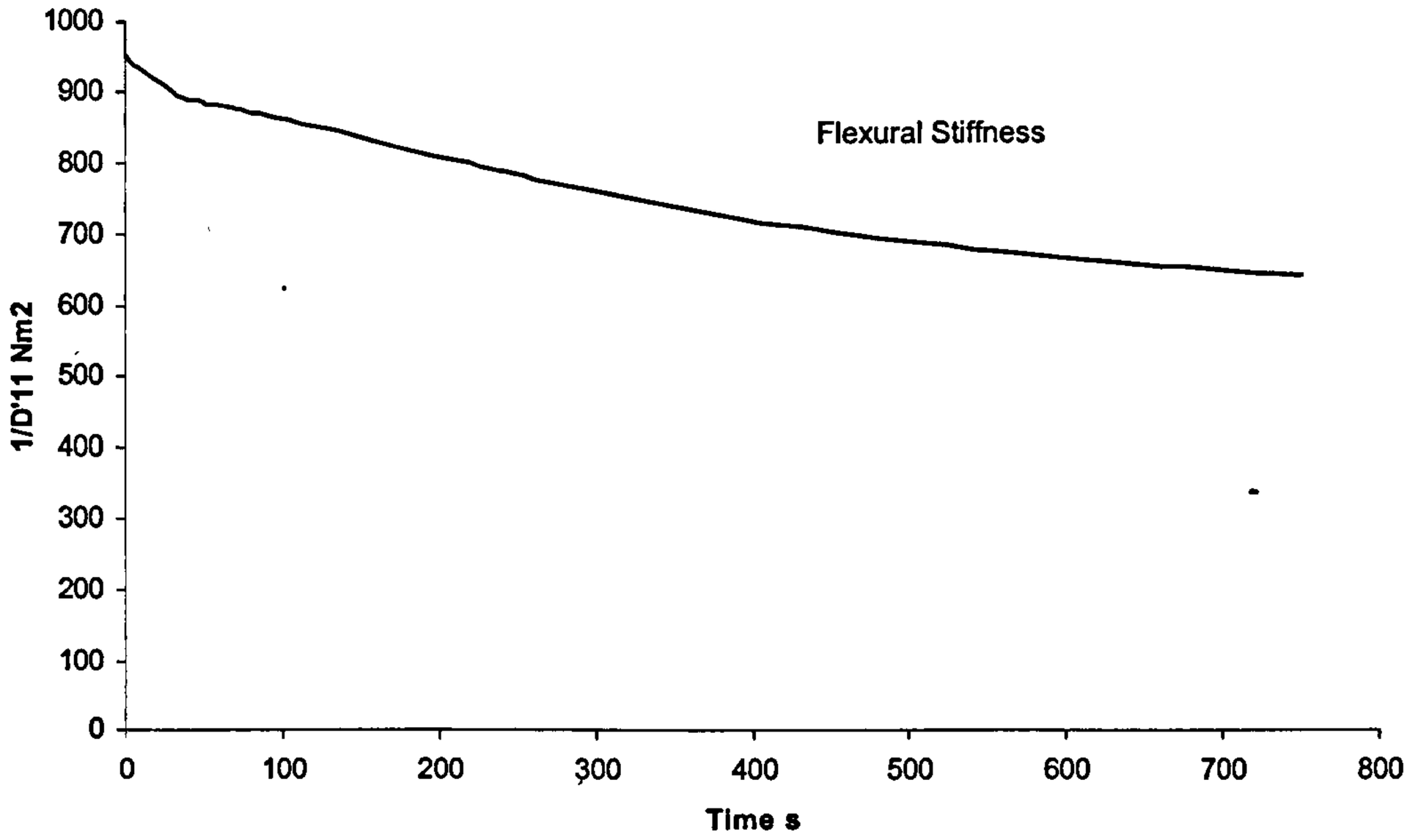

Figure 7.9. Evolution of flexural stiffness ($1/D'_{11}$) for an 8mm thick phenolic pultrusion exposed to a one-sided heat flux of 50kWm^{-2}.

All of the *A, B, D* matrix and flexural stiffness curves exhibit a general trend of decay as time and hence temperature progresses. This is true for both the polyester based pultrusion and the phenolic. This general decay is more marked in the polyester pultrusion than the phenolic. This corresponds with the results of the mechanical property experiments described in chapter 6. Bearing this in mind, it

might be worth considering running the model for a longer time period for the phenolic pultrusion. This would provide some indication of the time at which the phenolic material would begin to suffer significant decay in its mechanical properties. This would however require mechanical property data at higher temperatures.

7.3.2. Strengths Modelling

In order to model the strength of the material it was necessary to consider it as an 8mm thick laminate with 17 nodes, 1 node for each 0.5 mm in the through thickness direction. Strength was modelled by applying an increasing strain to the model. For each node, an applied stress was calculated from the applied strain and E_1 value as a function of temperature. If this applied stress exceeded the strength of the material (based on material strength as a function of temperature, $\sigma(T)$), then the material at that node was deemed to have failed, and have zero strength. If the applied stress did not exceed the strength of the material, then the stress at that node remained at the level of the applied stress (Figure 7.10). This process was repeated at each node. The stress in the material at any given strain was obtained by averaging the stress at each of the 17 nodes. The strength of the pultrusion as function of time was determined by taking the maximum stress value on the stress-strain curve for each time step (Figure 7.11).

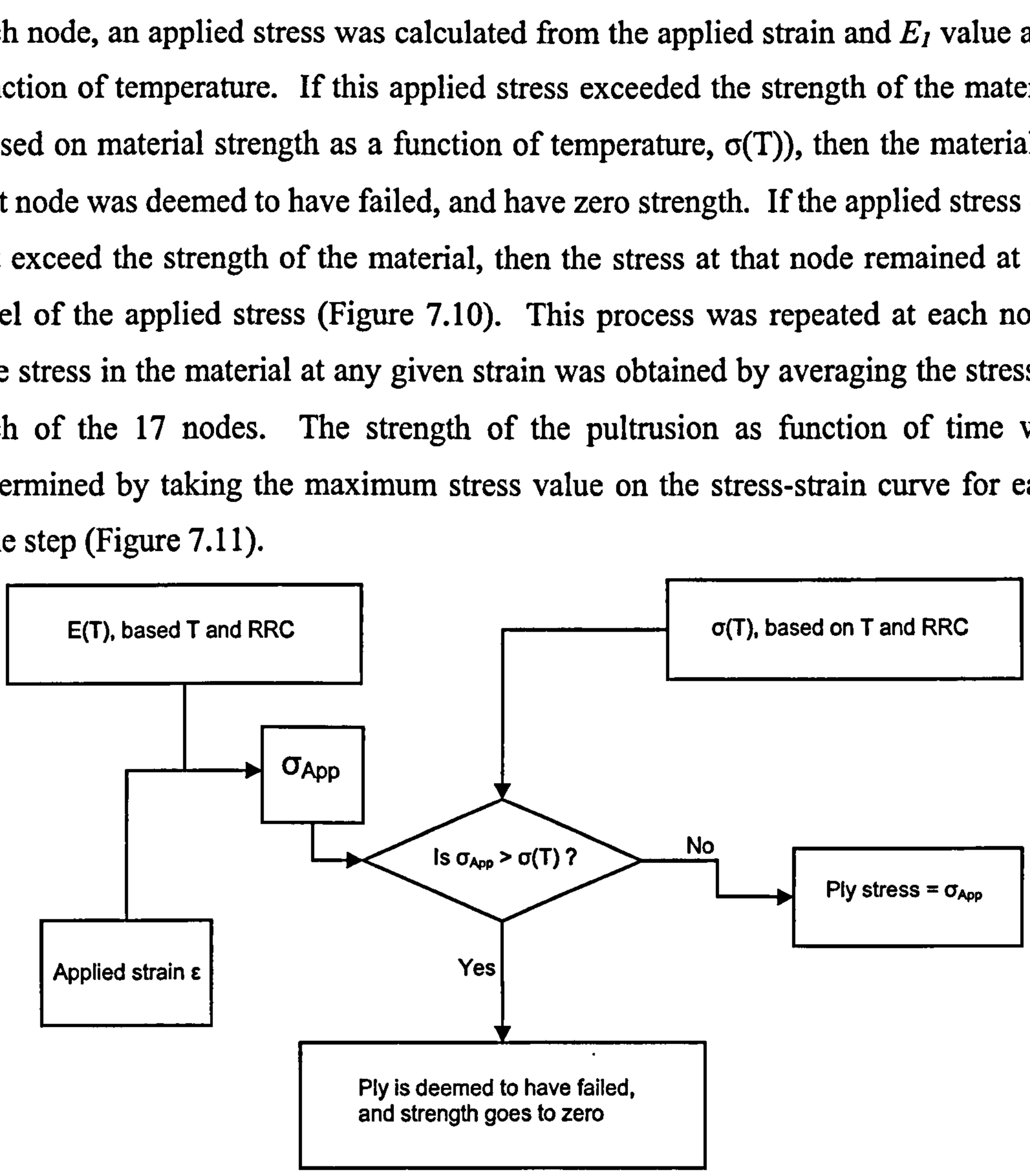

Figure 7.10. Algorithm describing the processes involved in modelling strength predictions. This method was adopted for both tensile and compressive strengths.

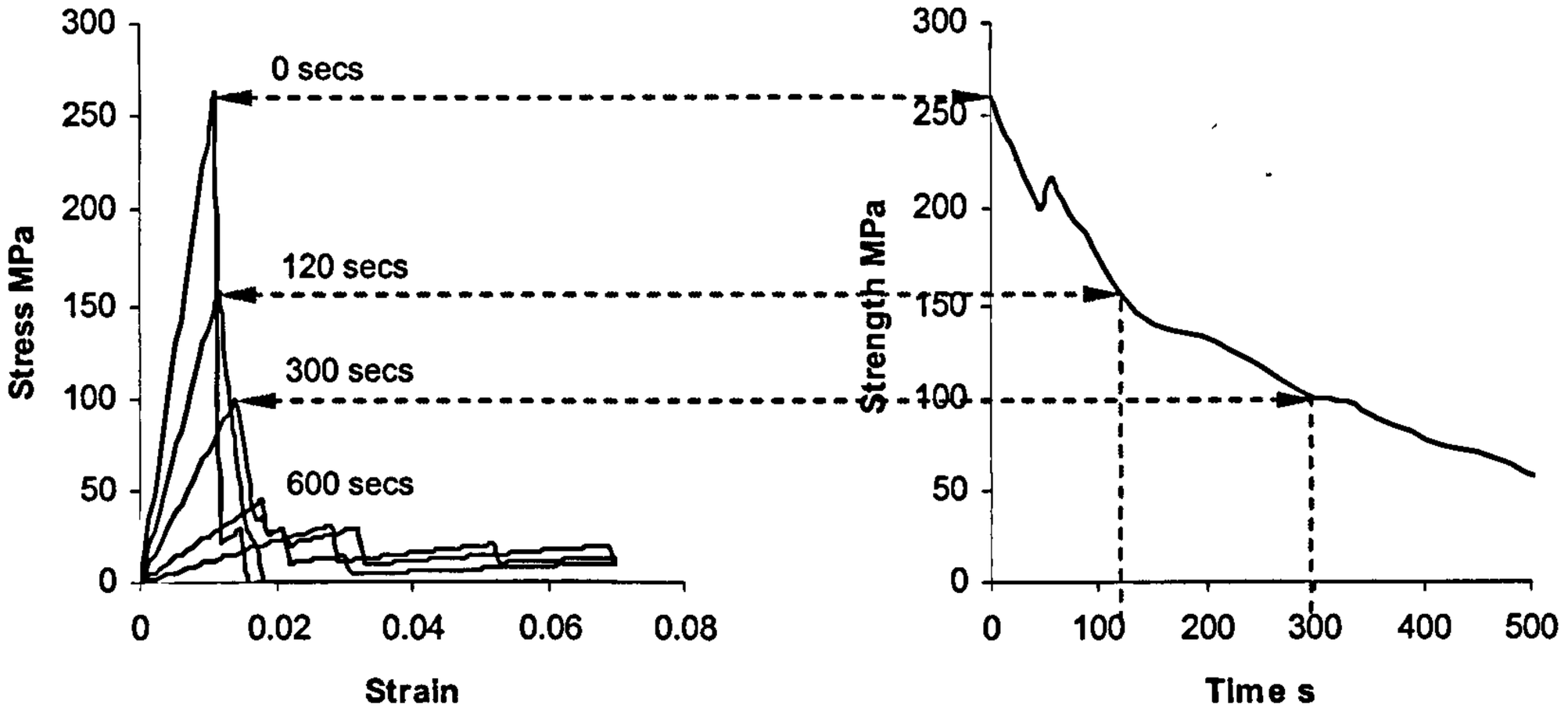

Figure 7.11. Stress-strain curves for a polyester pultrusion subject to 50kWm^{-2} heat flux (i). The maximum stress value on each curve for each time step is used to determine the strength of the pultrusion over time (ii).

By presuming that the material strength drops to zero when the applied stress exceeds its strength value, assumes that a saw-tooth stress-strain curve is followed. This is acceptable for compressive strength modelling as Figure 6.13 and Figure 6.14 show. For tensile strength modelling, this is not strictly true.

A second method was adopted which was based upon the actual stress-strain curve data from the tensile tests. The curves were modelled using the empirical equation,

$$\sigma = \sigma_{\max}\left[1 - e^{\frac{-E.\varepsilon}{\sigma_{\max}}}\right] \qquad (7.9)$$

where σ is the modelled stress in the material, σ_{max} an exaggerated strength value, E is the Young's Modulus and ε is an applied strain. A stress-strain curve is constructed over a range of applied strain. This curve is superimposed over each, real stress-strain curve by altering the values for E and σ_{max} (Figure 7.12). The result is a family of constructed stress-strain curves, matching the real stress-strain curves

for that material. This family of curves is used to model the stress at a particular node, at any given temperature. As soon the stress-strain curve reached the maximum material strength at that temperature, failure occurred.

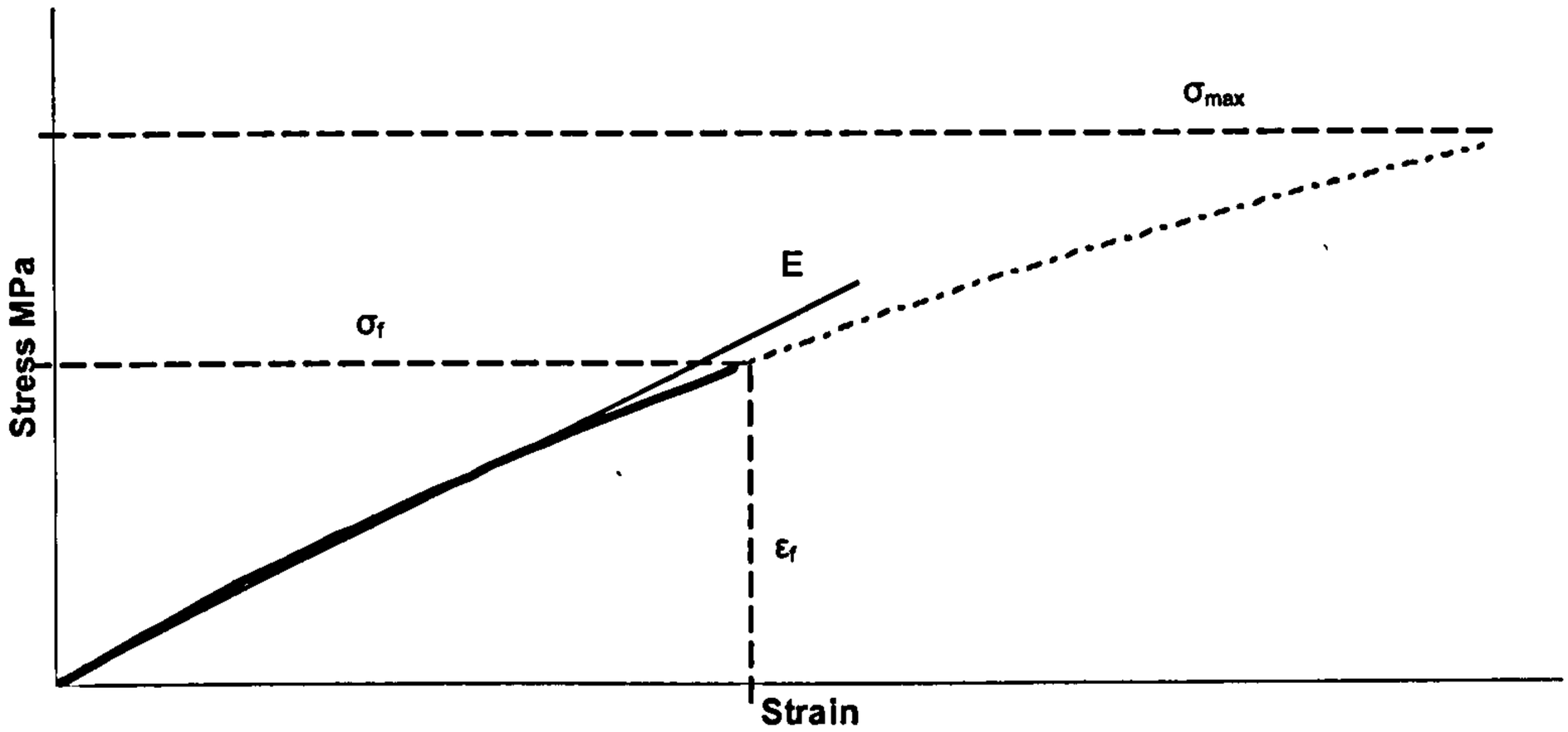

Figure 7.12. Empirical stress-strain curve governed by the parameters E and σ_{max}. σ_f represents failure strength and ε_f failure strain.

In this case it was assumed that the tensile test results for the full section material represented the true tensile failure of the material.

7.3.3. Tensile Strength Prediction

Figure 7.13 and Figure 7.14 show tensile strength as a function of time for a polyester pultrusion and phenolic pultrusion respectively. In both figures the two alternative methods for strength modelling have been shown.

The predictions for the polyester material reflect the downward trend of experimental points well. The 'saw-tooth' method (dotted line) for strength prediction underestimates the material strength. This is improved upon by the empirical method (solid line), which still underestimates it slightly. The reason for this may be because stress-strain curves of the full material section (all three layers) were used in the empirical analysis. These were combined with the tensile strength as a function of temperature data (Figure 6.11) for the full material section.

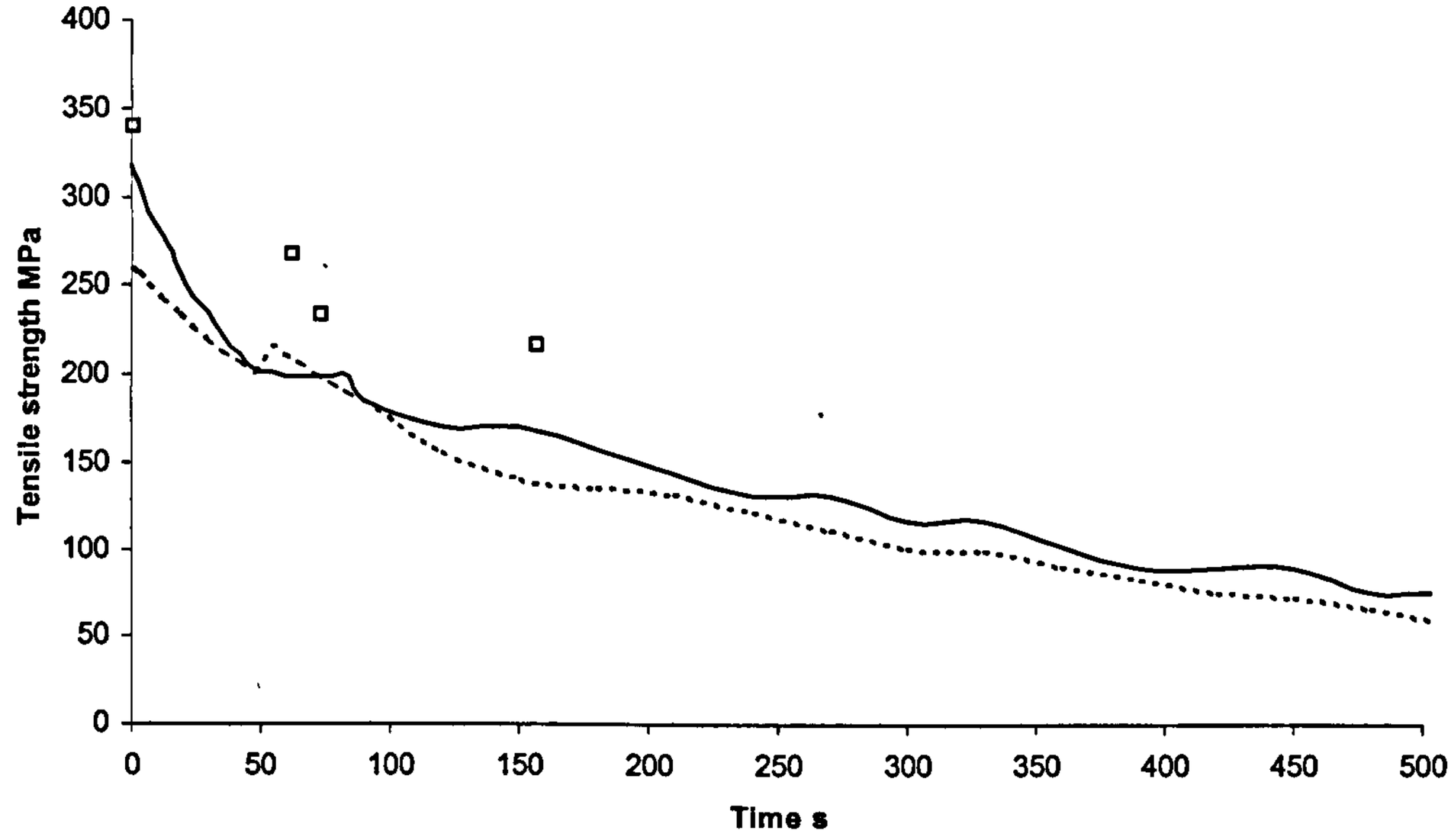

Figure 7.13. Model predictions for the relationship between time-to-failure and applied tensile stress along with experimental points for an 8mm thick polyester pultrusion, subjected to a one-sided heat flux of 50kWm^{-2}. Predictions are shown for both methods of strength modelling (Saw tooth method, dotted line, and empirical method, solid line).

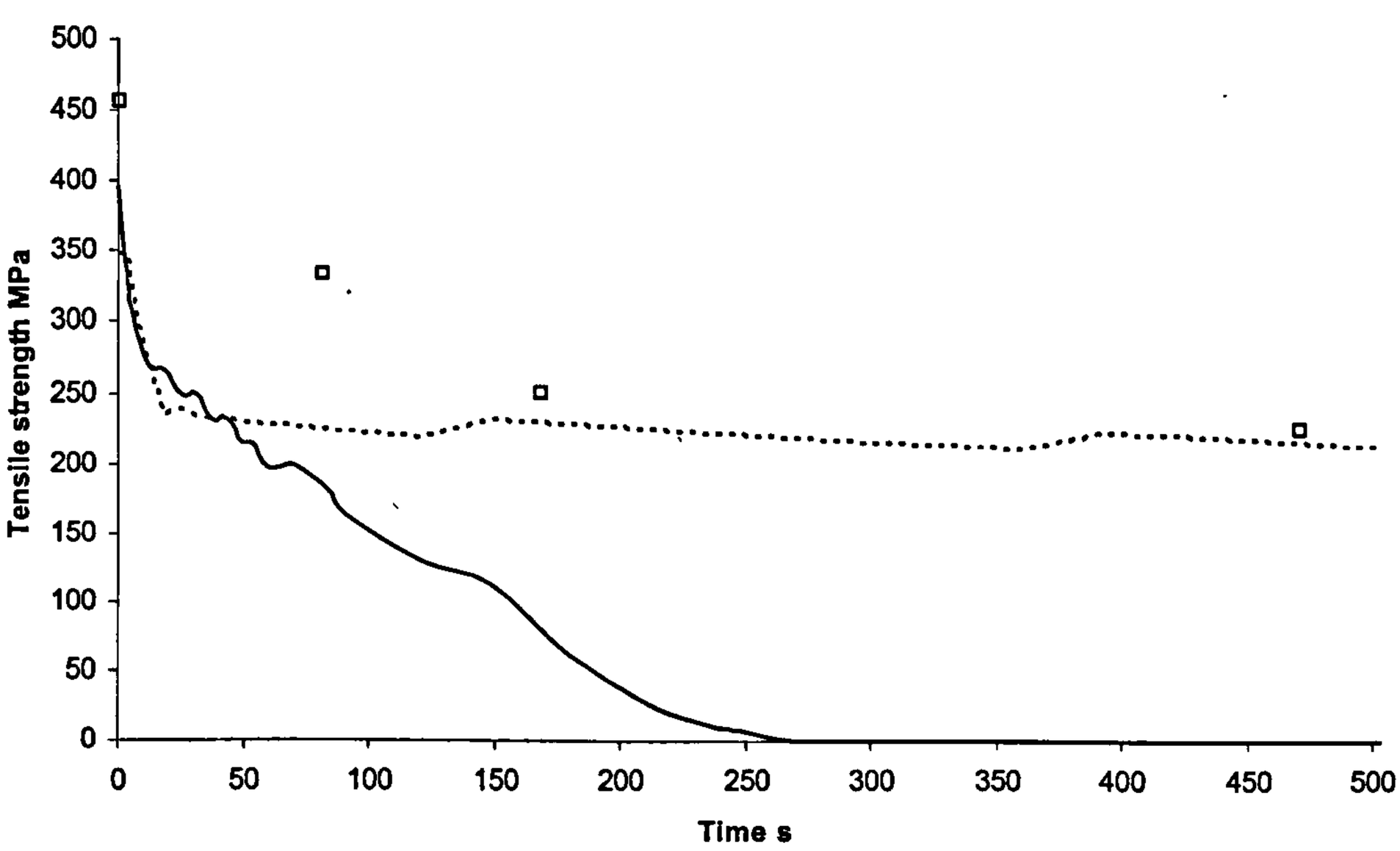

Figure 7.14. Model predictions for the relationship between time-to-failure and applied tensile stress along with experimental points for an 8mm thick phenolic pultrusion, subjected to a one-sided heat flux of 50kWm^{-2}. Predictions are shown for both methods of strength modelling (Saw tooth method, dotted line, and empirical method, solid line).

The predictions for the phenolic material reflect the downward trend of data. Once again the predictions underestimate the material strength. In this case the saw-tooth method provides a more accurate fit in the later stages of the fire.

More accurate fits could probably be achieved if real data for the tensile strength of the skins was available rather than relying on the literature. On a similar notion the stress-strain curves used for the empirical curve fitting did not provide a true representation of the tensile behaviour of the materials. During tensile testing, both the polyester and phenolic suffered form the uni-directional core pulling through the outer layers of CSM (Figure 6.3). Consequently the stiffness and strengths gained from the stress-strain curves maybe an underestimation of the true values.

The correlation between modelled and actual results for the phenolic material is weak. The modelled results underestimate the real data a great deal more than for the polyester material, suggesting that there is some other factor causing a greater underestimation than those already described. Perhaps a greater understanding of the physical changes that phenolic resin undergoes when subject to fire would go someway towards finding out what causes this underestimation. If mechanical property data in excess of 300°C was available this curve may have fitted better, since the model is reliant on this data.

7.3.4. Buckling and Compressive Strength Prediction

Figure 7.15 and Figure 7.16 show the evolution of compressive strength over time for an 8mm polyester pultrusion and 8mm phenolic pultrusion respectively. In each case the buckling response has been modelled too. The reason behind modelling both compressive and buckling failure is down to the fact that the samples tested could have failed compressively or through buckling, or indeed a combination of the two. The fundamental difference between the two is that compressive failure is governed solely by the compressive strength of the material. Buckling failure on the other hand is not only dependent on the material's compressive strength; it is also reliant on the material's geometry. The buckling response is particularly significant

when one considers that pultrusions are largely used as long slender beams, and hence more susceptible to buckling failure.

Compressive failure was modelled using the 'saw tooth' method (Figure 7.10). This method was chosen as if reflected the stress-strain curves. For both materials, the compressive strength degrades over time, reflecting the degradation in mechanical properties.

The buckling response was based on the equation,

$$\sigma_{buckling} = \frac{c}{tb^2}\sqrt{D_{11}D_{22}} \qquad (7.10)$$

where $\sigma_{buckling}$ is the buckling strength, t is the thickness of the test sample and b is the breadth. $\boldsymbol{D_{11}}$ and $\boldsymbol{D_{22}}$ are both components of the $\boldsymbol{D}$ portion of the $\boldsymbol{A}$, $\boldsymbol{B}$, $\boldsymbol{D}$ matrix. The constant c is associated with the edges constraints of the sample. This varies from 3.6 if the loaded sample is simply supported on all edges, to 7.5, if it is clamped at all edges [85] (see Figure 7.17).

The buckling curves in Figure 7.15 and Figure 7.16 have been constructed with the maximum value of 7.5 for the c constant. This figure provides the best fit for the data, and also corresponds with very snug fit of the buckling rig around the samples, corresponding to a fully clamped case. Further work needs to be carried out in this area to find an exact figure for c. This is detailed in Chapter 9.

The buckling response curves shown in Figure 7.15 and Figure 7.16 degrade over time reflecting the overall decline in mechanical properties. Both curves also contain a shoulder similar to those visible in the $\boldsymbol{D}$ matrix parameters. This is unsurprising when it is considered that the buckling response is a function of $\boldsymbol{D_{11}}$ and $\boldsymbol{D_{22}}$. However, in this case only one shoulder is apparent as opposed to two in the $\boldsymbol{D}$ matrix. This secondary shoulder has been reduced by the buckling strength equation 7.10.

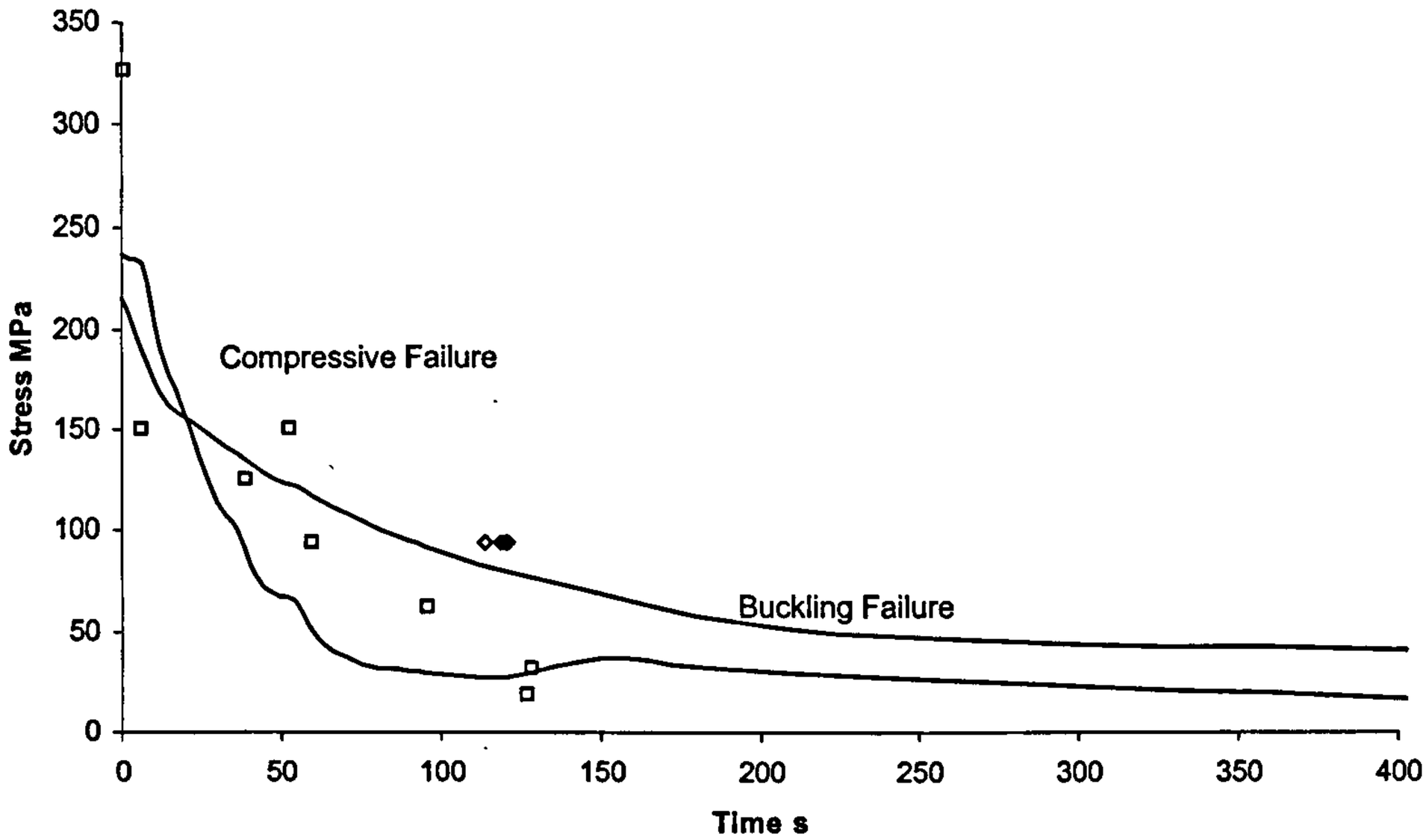

Figure 7.15. Model predictions for the relationship between time-to-failure and applied compressive stress for an 8mm thick polyester pultrusion, subjected to a one-sided heat flux of 50kWm^{-2}. Predictions are shown for both constrained buckling failure and compressive failure, along with experimental points. Results for both bare material □, and Clariant coated material ◇ are shown.

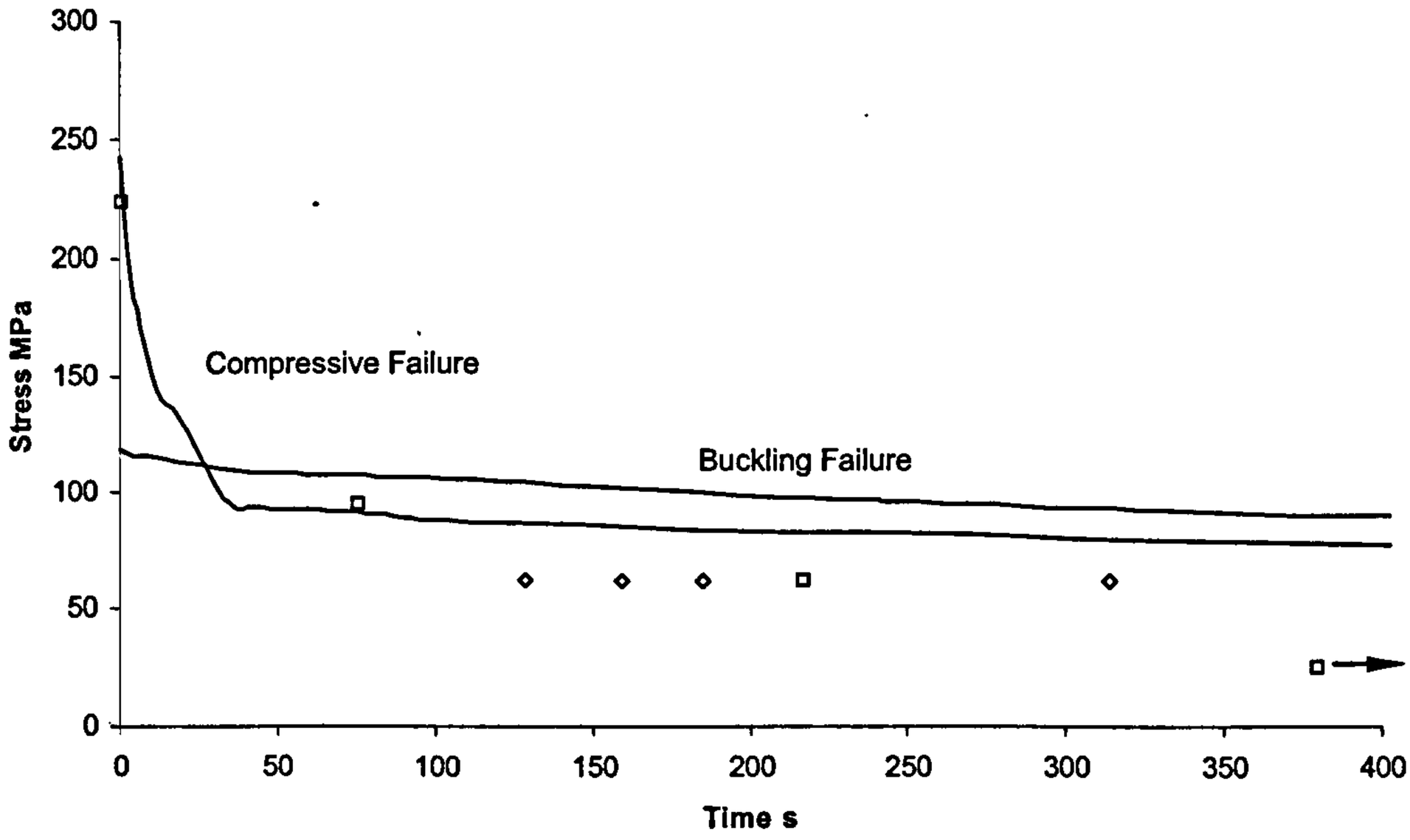

Figure 7.16. Model predictions for the relationship between time-to-failure and applied compressive stress for an 8mm thick phenolic pultrusion, subjected to a one-sided heat flux of 50kWm^{-2}. Predictions are shown for both constrained buckling failure and compressive failure, along with experimental points. Results for both bare material □, and Clariant coated material ◇ are shown.

Results for the intumescent coated material are also shown. The coated polyester material (Figure 7.15) lasted approximately 120 seconds, twice as long as the bare material at the equivalent stress. There was little difference between the different coatings. The results for the coated phenolic samples proved inconclusive. Three of the four coated samples tested failed before a bare sample tested at an equivalent stress. The single sample that improved on the bare sample's life-span was coated with 150phr Exolit AP740. This lasted 314 seconds compared to 217 seconds for the bare phenolic.

For both materials, the predictions for compressive and buckling failure accurately fit the experimental points.

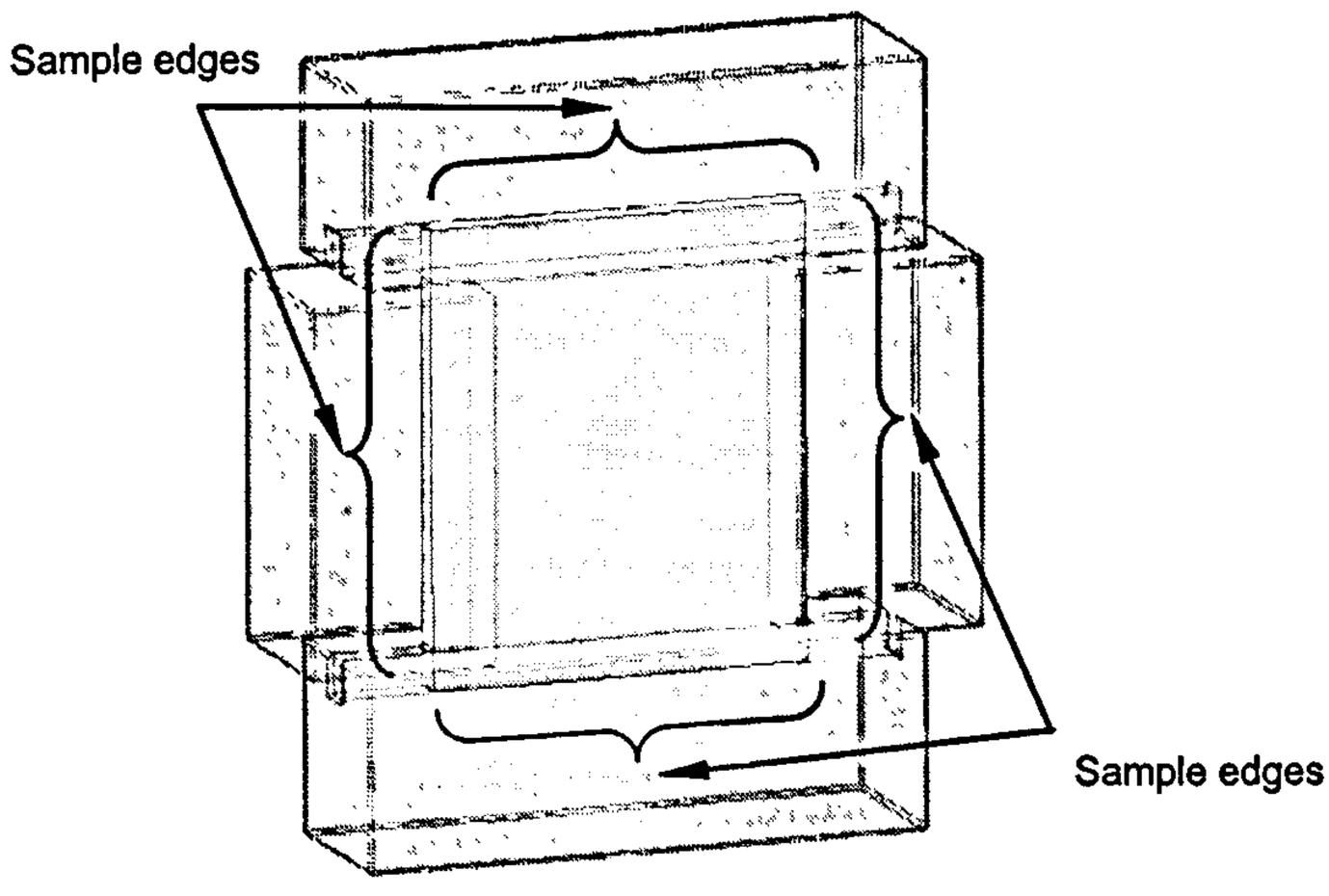

Figure 7.17. View of the constrained compression rig (detailed in Figure 5.11) highlighting the edges of the test sample. The way in which these edges are constrained, has a direct effect on the buckling response of the sample.

Overall, the modelled results reveal the dominant effect of exposing composites to fire whilst under load. Exposing a composite to the effects of fire alone will have little dramatic effect, as will applying a load to a composite. Combining the two however, results in catastrophic failure. This is reflected in the modelled results by their downward trend.

The results are limited by the experimental reliability of the fire under load tests. This is discussed in detail in section 6.3. Further limitations exist due to the underestimation of the tensile strength which is discussed earlier in this chapter. These limitations need to be considered before using this model as anything beyond a tool to determine a general trend. This position can be improved upon by obtaining real tensile data as a function of temperature of the CSM outer skins.

However the model's approach does provide an excellent foundation upon which to build a 3 layer failure model for marine composites. The 3 layers used in a typical marine composite ply usually have thicknesses in the magnitude of cm's, allowing mechanical property data at elevated temperatures for all of the separate layers to be obtained. This would overcome many of the problems encountered with this model.

8. Conclusions

8.1. Propane burner test

- The propane burner test, properly calibrated can provide a cheap and reliable method for fire resistance testing.

8.2. Thermal modelling

- The thermal model based on the simplified Henderson equation (equation 3.1) can accurately predict temperature evolution and residual resin content through a pultruded composite.

8.3. Mechanical properties as a function of temperature

- The equipment designed to carry out the series of mechanical property tests at different temperatures proved reliable. This is due to good experimental practice and well thermally insulated equipment.
- The empirical tanh relationship (equation 6.1) used to describe how the mechanical properties vary according to temperature proved reliable in most cases. It was noted however that in some cases the fit was perhaps not so good. It was decided to continue to use the tanh relationship in these cases for simplicity, besides the fit was reasonably accurate.
- Both materials experienced a higher loss in tensile strength than expected. This was due to the loss of 'composite action'.
- Higher rated temperature controllers should be used in future tests, capable of reaching temperatures in excess of 400°C.

8.4. Fire testing under Load

8.4.1. Tension

- Tensile failure would occur with little warning. Once plies began to fail, complete failure occurred very soon after.
- Both materials tested retained a high residual strength, due to the glass retaining its strength at high temperatures.

- Due to reliability issues with controlling the propane burner, these tests should only really be used to indicate a general trend.

8.4.2. Compression including intumescents

- Compressive failure would occur quickly and with little warning.
- The failure mechanism was a combination of compressive and buckling failure.
- Compressive strength declines more rapidly when compared to tensile strength, underlining the fact that pultruded composites are particularly susceptible to compressive failure when subjected to fire.
- Intumescent coatings extended the failure time for the polyester material, with little between any of the coatings tested. The results for the phenolic material proved inconclusive.
- Due to reliability issues with controlling the propane burner, these tests should only really be used to indicate a general trend.

8.4.3. Pool fire test

- Pultruded sections flexed to their design curvatures fail after a time in the order of 100 seconds.
- Failure always occurred on the compressive side and the mechanism was always local buckling. This is due to compressive stiffness being heavily reliant upon the condition of the matrix material.
- Box sections outperformed 'I' sections. This is because box sections effectively had a cold internal face. 'I' sections did not, as they were damaged on all sides by the fire.
- The pool fire proved difficult to predict and therefore lacked repeatability.

8.4.4. Furnace test

- The temperature controlled furnace was capable of matching the SOLAS fire curve.
- The test was very repeatable.
- Pultruded sections flexed to their design curvatures fail after a time in the order of 100 seconds.

- Once again, failure always occurred on the compressive side and the mechanism was always local buckling. This is due to compressive stiffness being heavily reliant upon the condition of the matrix material.
- Phenolic sections outperformed the polyester sections.
- The temperature inside the furnace cannot be guaranteed.

8.4.5. Columns including coatings

- The twin burner method adopted in the experiment provided an enveloping heat flux.
- In their bare state, the phenolic columns outperformed the polyester columns at a typical design stress.
- The 'boxed' columns performed best out of all the systems tested, although the silvered column results are also promising.
- Due to reliability issues with controlling the propane burner, these tests should only really be used to indicate a general trend.

8.5. Modelling

8.5.1. A, B, D Matrix Evolution

- The *A* matrix components, relating to in-plane loads and deformations, decline over time reflecting the decline in overall mechanical properties. This decline is more marked in the polyester material when compared to that of the phenolic.
- The ***B*** matrix components describe the interaction between the in-plane loads and out-of-plane bending and twisting. This value is initially zero due to the symmetry of the material in the through-thickness direction. This rises to a peak as the CSM/needle weave skin is burnt away causing a symmetrical imbalance. The second, larger peak is caused by further asymmetry as the UD core material is degraded.
- The ***D*** matrix components governing bending resistance decline with time. The influence of the progressive asymmetry can be seen with the shoulders in the curves. These coincide with the peaks in the ***B*** matrix curves.

- The model also shows the evolution of $\frac{1}{D'_{11}}$ which is equivalent to flexural stiffness.

8.5.2. Tensile Strength Prediction

- The model somewhat underestimates the tensile strength of both the polyester and phenolic pultrusions.
- In the case of the 'saw-tooth' modelling method, this may be caused by underestimating the strength of the skin material.
- In the case of the empirical modelling method, using the full section stress-strain curves may be the cause of this.
- It may be worth considering running the model for a longer length of time in the phenolic case to determine if and when the strength prediction tails off. However in order to do this, mechanical property data at higher temperatures would be required.

8.5.3. Compressive and Buckling Strength Prediction

- The model, after some initial underestimation, accurately predicts compressive failure for both polyester and phenolic pultrusion.
- Buckling response reflects the trend in experimental data, but is not fitted with an exact value for the constant *c*, governing the edge conditions.

Overall the 3 layer failure model provides an excellent basis on which to develop a failure model for 3 layer marine composite structures (sandwich panels).

9. Future Work

9.1. Thermally Induced Deformations

When a pultrusion or laminate is subject to a heat flux, distortions can occur in the absence of any externally applied force. The effect of theses thermally induced deformations can be accounted by modifying equation 7.1 to give,

$$\begin{bmatrix} \tilde{N} \\ \tilde{M} \end{bmatrix} = \begin{bmatrix} \tilde{A} & \tilde{B} \\ \tilde{B} & \tilde{D} \end{bmatrix} \begin{bmatrix} \tilde{\varepsilon}_0 - \tilde{\varepsilon}_0^T \\ \tilde{k} - \tilde{k}^T \end{bmatrix} \tag{9.1}$$

where, $\tilde{\varepsilon}_0^T$ and $\tilde{k}^T$ are the thermally induced strains and curvatures respectively, in the absence of any externally applied load. This would further improve the accuracy of the failure model.

9.2. Modelling of fire protective coatings

It would be possible to develop the thermal model to include the use of fire protective coatings. In order to do so it would be necessary to determine the thermal behaviour of such coatings. In particular, thermal conductivity, any radiative effects the material may have, and any volatile gases that may be emitted. This data will help to understand how a coating would affect temperature evolution in a pultrusion or laminate.

9.3. Sandwich panels

The three layer approach to analysing the pultruded material in this thesis could easily be used to model the structural integrity of sandwich panels in fire. Provided that data describing the mechanical properties of the constituent layers, as functions of temperature is obtainable, the model should work.

9.4. Buckling Response

In order to fully determine an accurate buckling response a new compression rig (Figure 5.3) would need to be designed. The new rig would need to be capable of accepting material of different thicknesses, thus allowing a relationship between *c* and *t* to be determined.

9.5. Structures

There is great potential for extending the model to consider full size structural elements such as the 'I' beams and box beams flexure tested in this thesis. In order to develop the model to consider large sections in flexure, several new inputs would be required.

Firstly, the model describing the resin degradation and temperature evolution would need to be adapted. This should take into account the effect of having a closed section like a box beam, or an open section like an 'I' beam. It was noted that box beams outperform 'I' beams in a pool fire due to the cold face on the inside of the box.

Secondly, the effect the fire has on the stiffness of the beam needs to be accounted for. Stiffness degrades as the material passes through the transition region. This degradation is more marked in compression than tension, due to compressive stiffness being heavily dependent upon resin condition (Figure 9.1). This problem is highlighted by the flexures tests carried out in this thesis, where every section tested, failed on the compressive side.

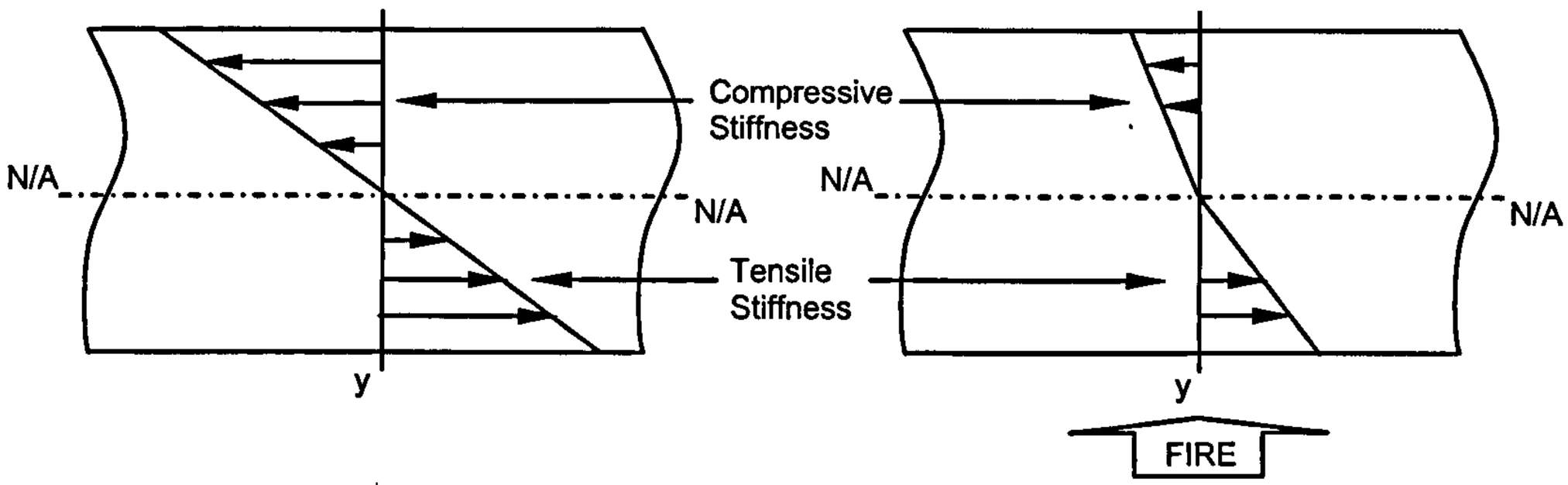

Figure 9.1. Comparison of compressive and tensile moduli of a pultruded composite section before (i) and durng a fire (ii), highlighting the rapid decline in compressive stiffness.

References

1. Anilturk, D. and Chan, W.S., *Structural stability of composite laminated column exposed to high temperature or fire.* Journal of Composite Materials, 2003. **37**(8): p. 687-700.
2. Dodds, N., Gibson, A.G., Dewhurst, D., and Davies, J.M., *Fire behaviour of composite laminates.* Composites: Part A, 2000. **31**(7): p. 689-702.
3. Gibson, A.G., Wright, P.N.H., Wu, Y.-S., and Evans, J.T., *Laminate theory analysis of composites under load in fire.* In press, 2006.
4. Looyeh, M.R.E., Bettess, P., and Gibson, A.G., *A one-dimensional finite element simulation for the fire-performance of GRP panels for offshore structures.* International Journal of Numerical Methods for Heat & Fluid Flow, 1997. 7(6): p. 609-625.
5. Lua, J. and O'Brien, J. *Fire simulation for woven fabric composites with temperature and mass dependent thermal mechanical properties.* in *Composites in Fire 3*. 2003. Newcastle upon Tyne, England.
6. Gibson, A.G., Wright, P.N.H., Wu, Y.-S., Mouritz, A.P., Mathys, Z., and Gardiner, C.P., *The integrity of polymer composites during and after fire.* Journal of Composite Materials, 2004. **38**(15): p. 1283-1308.
7. Henderson, J.B. and Wiecek, T.E., *A mathematical model to predict the thermal response of decomposing , expanding polymer laminates.* Journal of Composite Materials, 1987. **21**: p. 373-393.
8. Henderson, J.B., Wiebelt, J.A., and Tant, M.R., *A model for the thermal response of polymer composite materials with experimental verification.* Journal of Composite Materials, 1985. **19**: p. 579-595.
9. Gibson, A.G., Wright, P.N.H., Wu, Y.-S., Mouritz, A.P., Mathys, Z., and Gardiner, C.P., *Modelling residual mechanical properties of polymer composites after fire.* Plastics, Rubber and Composites, 2003. **32**(2): p. 81-90.
10. Eckold, G., *Design and Manufacture of Composite Structures*. 1994, Cambridge: Woodhead Publishing Ltd.
11. *Composite Materials in MaritimeStructures*. Cambridge Ocean Technology Series 4, ed. R.A. Shenoi and J.F. Wellicome. Vol. 1. Fundamental Aspects. 1993, Cambridge: Cambridge University Press.

12. *Image courtesy of www.ndt.net.*
13. *Image courtesy of www.jytt-intl.com.*
14. *Image courtesy of Fiberline Composites A/S.*
15. Babrauskas, V. and Peacock, R.D., *Heat release rate: The single most important variable in fire hazard.* Fire Safety Journal, 1992. **18**(3): p. 255-272.
16. Sorathia, U., Lyon, R.E., Ohlemiller, T., and Grenier, A., *A review of fire test methods and criteria for composites.* SAMPE Journal, 1997. **33**: p. 23-31.
17. Babrauskas, V. and Wickström, U. *The rational development of bench scale fire tests for full-scale fire prediction.* in *2nd International Fire Safety Science Symposium.* 1989.
18. Babrauskas, V., *Effective measurement techniques for heat, smoke and toxic fire gases.* Fire Safety Journal, 1991. **17**: p. 13-26.
19. Babrauskas, V. *Fire test methods for evaluation of fire retardant efficacy in polymeric materials.* in *Fire Retardancy of Polymeric Materials.* 2000. New York: Marcel Dekker, Inc.
20. *Image courtesy of www.pslc.ws.*
21. *Image courtesy of www.fire-testing.com.*
22. Babrauskas, V., *Fire test methods for evaluation of fire-retardant efficacy in polymeric materials*, in *Fire Retardancy of Polymeric Materials*, A.F. Grand and C.A. Wilkie, Editors. 2000, Marcel Dekker Inc.: New York. p. 81-113.
23. *Image courtesy of www.bolton.ac.uk.*
24. Greene, E., *Marine Composites, www.marinecomposites.com.*
25. *Image courtesy of www.mpa.uin-stuttgart.de.*
26. *Image courtesy of www.rockwool.com.*
27. *ISO 9705:1993 Fire tests on building materials and structures.*
28. *Image courtesy of www.armilcfs.com.*
29. Gibson, A.G., Wu, Y.-S., Naas, A.L., and McNaught, R.J. *A low cost burner technique for the development and modelling of laminates in fire.* in *Composites in Fire 3.* 2003. Newcastle upon Tyne, England.
30. Folkers, J. *Fire testing and performance of fiber glass pipe.* in *Composites in Fire.* 1999. Newcastle-upon-Tyne.

31. Hill, P.S. and White, G.C. *Fire testing and performance of composite materials*. in *Composites in Fire*. 1999. Newcastle-upon-Tyne.
32. *Image courtesy of www.spadeadam.biz.*
33. Gibson, A.G. *Basic mechanisms of fire damage in organic matrix composites.* in *Composites in Fire 3*. 2003. Newcastle upon Tyne, England.
34. Mouritz, A.P. and Mathys, Z., *Post-fire mechanical properties of marine polymer composites.* Composite Structures, 1999. **47**(1-4): p. 643-653.
35. Gibson, A.G., Wu, Y.-S., Chandler, H.W., Wilcox, J.A.D., and Bettess, P., *A model for the thermal performance of thick composite laminates in hydrocarbon fires.* Revue de l'Institut Français du Pétrole, 1995. **50**(1): p. 69-74 (special issue).
36. The Honourable Lord Cullen, *The Public Enquiry into the Piper Alpha Disaster*. 1990, HMSO: London.
37. Kalagiannakis, G., Hemelrijck, D.V., and Assche, G.V., *Measurements of of thermal properties of carbon/epoxy and glass/epoxy using modulated temperature differential scanning calorimetry.* Journal of Composite Materials, 2004(38): p. 163-174.
38. Tai, H., *Equivalent thermal conductivity of two- and three-dimensional orthogonally fiber-reinforced composites in one-dimensional heat flow.* Journal of Composites Technology & Research, 1996(18): p. 221-227.
39. Gowayed, Y., Hwang, J.-C., and Chapman, D., *Thermal conductivity of textile composites with arbitrary preform structures.* Journal of Composites Technology & Research, 1995(17): p. 56-62.
40. Havis, C., Peterson, G., and Fletcher, L., *Predicting the thermal conductivity and temperature distribution in aligned fibre composites.* Journal of Thermophysics, 1989(3): p. 416-422.
41. James, B., Wostenholm, G., Keen, G., and McIvor, S., *Prediction and measurement of the thermal conductivity of composite materials.* Journal of Physics D: Applied Physics, 1987: p. 261-268.
42. Fanucci, J.P., *Thermal response of radiantly heated kevlar and graphite/epoxy composites.* Journal of Composite Materials, 1987(21): p. 129-139.

43. Ott, H.-J., *Thermal conductivity of composite materials.* Plastics, Rubber Processing and Applications, 1981(1): p. 9-24.

44. Han, L. and Cosner, A., *Effective thermal conductivities of fibrous composites.* Journal of Heat Transfer, 1981(103): p. 387-392.

45. Progelhof, R.C., Throne, J.L., and Ruetsch, R.R., *Methods for predicting the thermal conductivity of composite systems: A review.* Polymer Engineering & Science, 1976. **16**(9).

46. Springer, G. and Tsai, S., *Thermal conductivity of unidirectional materials.* Journal of Composite Materials, 1967(1): p. 166-173.

47. Zalameda, J.N., *Measured through-the-thickness thermal diffusivity of carbon fiber reinforced composite materials.* Journal of Composites Technology & Research, 1995(21): p. 98-102.

48. Ladacki, M., *Silicon carbide in ablative chars.* Journal of the American Institute of Aeronautics and Astronautics, 1966(4): p. 1445-1447.

49. Dimitrienko, Y.I., *Thermomechanical behaviour of composite materials and structures under high temperatures: 2. Structures.* Composites, 1997(28A): p. 463-471.

50. Tant, M.R., Henderson, J.B., and Boyer, C.T., *Measurement and modelling of the thermochemical expansion of polymer composites.* Composites, 1985(16): p. 121-126.

51. Henderson, J.B. and Tant, M.R., *Measurement of thermal and chemical properties of a glass-filled polymer composite to high temperature.* High Temperatures-High Pressures, 1996(18): p. 17-28.

52. Henderson, J.B. and Doherty, M.P., *Measurement of selected properties of a glass-filled polymer composite to high temperature.* High Temperatures-High Pressures, 1987(19): p. 95-102.

53. Florio, J., Henderson, J.B., and Test, F.L., *Measurement of the thermochemical expansion of porous composite materials.* High Temperatures-High Pressures, 1989(21): p. 157-165.

54. Florio, J., Henderson, J.B., Test, F.L., and Hariharan, R., *A study of the effects of the assumption of local-thermal equilibrium on the overall thermally-induced response of a decomposition, glass-filled polymer composite.* International Journal of Heat & Mass Transfer, 1991(34): p. 135-147.

55. Sullivan, R.M., *A finite element method for thermochemically decomposing polymers*. 1990, The Pennsylvania State University.

56. Sullivan, R.M. and Salamon, N.J., *A finite element method for the thermochemical decomposition of polymeric materials - I. Theory.* International Journal of Engineering Science, 1992(30): p. 431-441.

57. Sullivan, R.M. and Salamon, N.J., *A finite element method for the thermochemical decomposition of polymeric materials - II. Carbon phenolic composites.* International Journal of Engineering Science, 1992(30): p. 939-951.

58. Sullivan, R.M., *A coupled solution method for the thermochemical response of decomposing expanding polymeric composites.* Journal of Composite Materials, 1993(27): p. 408-434.

59. Pering, G.A., Farrell, P.V., and Springer, G.S., *Degradation of tensile and shear properties of composites exposed to fire or high temperature.* Journal of Composite Materials, 1980(14): p. 54-66.

60. McManus, H.L. and Springer, G.S., *High temperature behaviour of thermochemical behaviour of carbon-phenolic and carbon-carbon composites, I. Analysis.* Journal of Composite Materials, 1992(26): p. 206-229.

61. McManus, H.L. and Springer, G.S., *High temperature behaviour of thermochemical behaviour of carbon-phenolic and carbon-carbon composites, II. Results.* Journal of Composite Materials, 1992(26): p. 230-255.

62. Dimitrienko, Y.I., *Thermomechanical behaviour of composite materials and structures under high temperatures: 1. Materials.* Composites, 1997(28A): p. 453-461.

63. Dimitrienko, Y.I., *Thermal stresses and heat-mass-transfer in ablating composite composite materials.* Journal of Heat and Mass Transfer, 1997(38): p. 139-146.

64. Mouritz, A.P., Gibson, A.G., Wu, Y.-S., Gardiner, C.P., and Mathys, Z., *Validation of the Gibson model for the fire reaction properties of fibre-polymer composites.* Fire and Materials, In press.

65. Chang, C.I., *Thermal effects on polymer composite structures.* Theoretical & Applied Fracture Mechanics, 1986(6): p. 113-120.

66. Kung, H.C., *A mathematical model of wood pyrolysis.* Combustion and Flame, 1972(18): p. 185-195.

67. Kansa, E.J., Perlee, H.E., and Chaiken, R.F., *Mathematical model of wood pyrolysis inlcuding internal forced convection.* Combustion and Flame, 1977. **29**: p. 311-324.

68. Looyeh, M.R.E. and Bettess, P., *A finite element model for the fire performance of GRP panels including variable thermal properties.* Finite Elements in Analysis & Design, 1998(30): p. 313-324.

69. Mouritz, A.P. and Mathys, Z., *Mechanical properties of fire-damaged glass-reinforced phenolic composites.* Fire and Materials, 2000. **34**: p. 67-75.

70. Mouritz, A.P. and Mathys, Z., *Post-fire mechanical properties of glass-reinforced polyester composites.* Composites Science and Technology, 2001. **61**(4): p. 475-490.

71. Bausano, J., Boyd, S., Lesko, J., and Case, S. *Composite life under sustained compression and one sided simulated fire exposure: characterisation and prediction.* in *Composites in Fire 3*. 2003. Newcastle upon Tyne, England.

72. Halverson, H., Bausano, J., Case, S., and Lesko, J. *Simulation of structural response of composite structures under fire exposure.* in *Composites in Fire 3*. 2003. Newcastle upon Tyne, England.

73. Mahieux, C.A. and Reifsnider, K.L., *Property modelling across transition temperatures in polymers: a robust stiffness–temperature model.* Polymer, 2001. **42**(7): p. 3281-3291.

74. Keller, T., Tracy, C., and Hugi, E., *Fire endurance of loaded and liquid-cooled GFRP slabs for construction.* Composites Part A, 2006. **37**(7): p. 1055-1067.

75. Massot, J.J. *Glass reinforced plastic heavy load flooring for offshore platforms.* in *Composite Materials in the Offshore Industry*. 1994. Institut Français du Pétrole, France.

76. Greene, E., *Fire performance of composite materials for naval applications.* 1993, Structural Composites Inc.: Melbourne, FL, USA.

77. Browne, T.N.A., *A Model for the Structural Integrity of Composite Laminates in Fire*, in *School of Mechanical & Systems Engineering*. PhD Thesis 2006, University of Newcastle-upon-Tyne: Newcastle-upon-Tyne.

78. *Fibre-reinforced plastic composites - Determination of flexural properties BS EN ISO 14125: 1998*. 2003.

79. Gardiner, C.P., Mathys, Z., and Mouritz, A.P., *Tensile and Compressive Properties of FRP Composites with Localised Fire Damage*. Applied Composite Materials, 2002. **9**(6): p. 353-367.

80. *Boeing Specification Support Standard, Advanced Composite Compression Tests BSS 7260*. 1986.

81. Kulcarni, A.P. and Gibson, R.F. *Non-destructive Characterisation of Effects of Temperature and Moisture on Elastic Moduli of Vinyl Ester Resin and E-glass Resin Composite*. in *American Society of Composites, 18th Annual Technical Conference*. 2003. Florida, USA.

82. Budiansky, B. and Fleck, N.A., *Compressive Failure of Fibre Composites*. Journal of Mech. Phys. Solids, 1993. **41**(1): p. 183-211.

83. Agarwal, B.D. and Broutman, L.J., *Analysis and performance of fiber composites*. 2nd ed. 1990, Chichester: John Wiley & Sons, Inc.

84. Hull, D., *An introduction to composite materials*. 1st ed. Cambridge Solid State Science Series. 1981, Cambridge: Cambridge University Press.

85. Young, W.C. and Budynas, R.G., *Roark's Formulas for Stress and Strain*. 7th ed. 2002, London: McGraw-Hill.

86. Couchman, L. and Mouritz, A.P., eds. *Modeling of Naval Composite Structures in Fire*. 2006, Cooperative Research Centre for Advacned Composite Structures on behalf of the United States Office of Naval Research.

87. Murphy, J., *Reinforced Plastics Handbook*. 1994, Oxford: Elsevier Advanced Technology.

88. Wang, J.S. and Chan, W.S., *Effects of defects on the buckling load of rodpack laminates*. Journal of the American Helicopter Society, 2000: p. 216-221.

Publications

A. G. Gibson, T. N. A. Browne, R. C. Easby, Y-S Wu, Z. Mathys, A. P. Mouritz
Laminate Theory Analysis of Composites under Load in Fire
Proc. of The 4th International Conference On Composite Materials For Offshore Operations. Houston TX, USA, October 2005.

T. N. A. Browne, R. C. Easby, A. Elmughrabi, A. G. Gibson, A. P. Mouritz
Composite Structures Under Load In Fire: Characterisation and Modeling
Proc. of DURACOSYS (Durability of Composite Systems). Virginia Tech, Blacksburg VA, USA, September 2006.

Appendix

Visual Basic Code

ABD Matrix calculation (Polyester)

```
Sub ABCDvsTime()


Rem Calculate matrix for all times
For j = 1 To 39


Dim Time(50)
Worksheets("Temp profile").Activate
Time(j) = ActiveSheet.Cells(j + 7, 1).Value

Worksheets("ABD Matrix").Activate
ActiveSheet.Cells(j + 24, 1).Value = Time(j)

Rem Calculate Q Matrix for each node

For i = 1 To 17
Rem Input temperature profiles
Dim tem(20)
Worksheets("Temp profile").Activate
tem(i) = ActiveSheet.Cells(j + 7, i + 1).Value

Rem Input rrc values
Dim rc(20)
Worksheets("RRC").Activate

rc(i) = ActiveSheet.Cells(j + 7, i + 1).Value

Rem Calculate E1,E2,G12,u21
Dim E1(20)
Dim E2(20)
Dim G12(20)
Dim u12(20)
Dim u21(20)
Dim cE1(20)
Dim cE2(20)
Dim cG12(20)
```

```
Dim TanhE1(20)
Dim TanhE2(20)
Dim TanhG12(20)
Dim TanhE1S(20)
Dim TanhE2S(20)
Dim TanhG12S(20)
Dim cE1s(20)
Dim cE2S(20)
Dim cG12S(20)
Worksheets("Model").Activate
Rem UD properties
TgE1 = ActiveSheet.Cells(4, 2)
TgE2 = ActiveSheet.Cells(5, 2)
TgG12 = ActiveSheet.Cells(6, 2)

kE1 = ActiveSheet.Cells(4, 3)
kE2 = ActiveSheet.Cells(5, 3)
kG12 = ActiveSheet.Cells(6, 3)

MuE1 = ActiveSheet.Cells(4, 4)
MuE2 = ActiveSheet.Cells(5, 4)
MuG12 = ActiveSheet.Cells(6, 4)

MrE1 = ActiveSheet.Cells(4, 5)
MrE2 = ActiveSheet.Cells(5, 5)
MrG12 = ActiveSheet.Cells(6, 5)

Rem CSM properties

TgE1S = ActiveSheet.Cells(11, 2)
TgE2S = ActiveSheet.Cells(12, 2)
TgG12S = ActiveSheet.Cells(13, 2)

kE1S = ActiveSheet.Cells(11, 3)
kE2S = ActiveSheet.Cells(12, 3)
kG12S = ActiveSheet.Cells(13, 3)

MuE1S = ActiveSheet.Cells(11, 4)
MuE2S = ActiveSheet.Cells(12, 4)
MuG12S = ActiveSheet.Cells(13, 4)

MrE1S = ActiveSheet.Cells(11, 5)
MrE2S = ActiveSheet.Cells(12, 5)
MrG12S = ActiveSheet.Cells(13, 5)

If i >= 4 And i <= 14 Then

cE1(i) = kE1 * (tem(i) - TgE1)
```

```
TanhE1(i) = (Exp(cE1(i)) - Exp(-cE1(i))) / (Exp(cE1(i)) + Exp(-cE1(i)))
E1(i) = (((1 - TanhE1(i)) * (MuE1 - MrE1)) / 2 + MrE1) * (rc(i) / 100) ^ 1

cE2(i) = kE2 * (tem(i) - TgE2)
TanhE2(i) = (Exp(cE2(i)) - Exp(-cE2(i))) / (Exp(cE2(i)) + Exp(-cE2(i)))
E2(i) = (((1 - TanhE2(i)) * (MuE2 - MrE2)) / 2 + MrE2) * (rc(i) / 100) ^ 1

cG12(i) = kG12 * (tem(i) - TgG12)
TanhG12(i) = (Exp(cG12(i)) - Exp(-cG12(i))) / (Exp(cG12(i)) + Exp(-cG12(i)))
G12(i) = (((1 - TanhG12(i)) * (MuG12 - MrG12)) / 2 + MrG12) * (rc(i) / 100) ^ 1

Else

cE1s(i) = kE1S * (tem(i) - TgE1S)
TanhE1S(i) = (Exp(cE1s(i)) - Exp(-cE1s(i))) / (Exp(cE1s(i)) + Exp(-cE1s(i)))
E1(i) = (((1 - TanhE1S(i)) * (MuE1S - MrE1S)) / 2 + MrE1S) * (rc(i) / 100) ^ 1

cE2S(i) = kE2S * (tem(i) - TgE2S)
TanhE2S(i) = (Exp(cE2S(i)) - Exp(-cE2S(i))) / (Exp(cE2S(i)) + Exp(-cE2S(i)))
E2(i) = (((1 - TanhE2S(i)) * (MuE2S - MrE2S)) / 2 + MrE2S) * (rc(i) / 100) ^ 1

cG12S(i) = kG12S * (tem(i) - TgG12S)
TanhG12S(i) = (Exp(cG12S(i)) - Exp(-cG12S(i))) / (Exp(cG12S(i)) + Exp(-
cG12S(i)))
G12(i) = (((1 - TanhG12S(i)) * (MuG12S - MrG12S)) / 2 + MrG12S) * (rc(i) / 100) ^
1

End If

u12(i) = ActiveSheet.Cells(3, 8).Value
u21(i) = u12(i) * E2(i) / E1(i)

Rem Calculate Q matrix
Dim Q11(20)
Dim Q12(20)
Dim Q22(20)
Dim Q66(20)

uxy = 1 - u12(i) * u21(i)
Q11(i) = E1(i) / uxy
Q12(i) = u12(i) * E2(i) / uxy
Q22(i) = E2(i) / uxy
Q13 = 0
Q21 = Q12
Q31 = 0
Q23 = 0
Q66(i) = G12(i)

Next i
```

```
Rem Calculating Ei
Dim thick(20)
Dim yi(20)

Dim Eyi(20)
Y = 0
Ey = 0
E = 0
bd3 = 0
EIO = 0
alpha = 0

For i = 1 To 17


Worksheets("Model").Activate
thick(i) = ActiveSheet.Cells(i + 19, 1).Value

Rem Printing
Worksheets("Sheet1").Activate
ActiveSheet.Cells(i + 2, 2).Value = thick(i) + 0.5
yi(i) = thick(i) + 0.5

Worksheets("Sheet1").Activate

ActiveSheet.Cells(i + 2, 4).Value = E1(i) * yi(i)
Eyi(i) = E1(i) * yi(i)
Ey = Ey + Eyi(i)
E = E + E1(i)

Next i
Y = Y + (Ey / E)
Worksheets("ABD Matrix").Activate
 ActiveSheet.Cells(j + 24, 2).Value = Y


Rem 2nd Loop
For i = 1 To 17
Worksheets("Model").Activate
thick(i) = ActiveSheet.Cells(i + 19, 1).Value

Rem Printing
Worksheets("Sheet1").Activate
ActiveSheet.Cells(i + 2, 2).Value = thick(i) + 0.5
yi(i) = thick(i) + 0.5
```

```
Worksheets("Sheet1").Activate
Rem ActiveSheet.Cells(i + 2, 3).Value = E1(i)


bd3 = bd3 + (E1(i) / 12)
ActiveSheet.Cells(19, 5).Value = Y
alpha = alpha + (E1(i) * (Y - yi(i)) ^ 2)
Next i
EIO = bd3 + alpha
Worksheets("ABD Matrix").Activate
ActiveSheet.Cells(j + 24, 3).Value = EIO

Rem Calculate ABD Matrix

A11 = (0.5 / 3) * ((Q11(1) + Q11(17)) + 4 * (Q11(2) + Q11(4) + Q11(6) + Q11(8) +
Q11(10) + Q11(12) + Q11(14) + Q11(16)) + 2 * (Q11(3) + Q11(5) + Q11(7) +
Q11(9) + Q11(11) + Q11(13) + Q11(15)))
A12 = (0.5 / 3) * ((Q12(1) + Q12(17)) + 4 * (Q12(2) + Q12(4) + Q12(6) + Q12(8) +
Q12(10) + Q12(12) + Q12(14) + Q12(16)) + 2 * (Q12(3) + Q12(5) + Q12(7) +
Q12(9) + Q12(11) + Q12(13) + Q12(15)))
A21 = (0.5 / 3) * ((Q12(1) + Q12(17)) + 4 * (Q12(2) + Q12(4) + Q12(6) + Q12(8) +
Q12(10) + Q12(12) + Q12(14) + Q12(16)) + 2 * (Q12(3) + Q12(5) + Q12(7) +
Q12(9) + Q12(11) + Q12(13) + Q12(15)))
A22 = (0.5 / 3) * ((Q22(1) + Q22(17)) + 4 * (Q22(2) + Q22(4) + Q22(6) + Q22(8) +
Q22(10) + Q22(12) + Q22(14) + Q22(16)) + 2 * (Q22(3) + Q22(5) + Q22(7) +
Q22(9) + Q22(11) + Q22(13) + Q22(15)))
A66 = (0.5 / 3) * ((Q66(1) + Q66(17)) + 4 * (Q66(2) + Q66(4) + Q66(6) + Q66(8) +
Q66(10) + Q66(12) + Q66(14) + Q66(16)) + 2 * (Q66(3) + Q66(5) + Q66(7) +
Q66(9) + Q66(11) + Q66(13) + Q66(15)))
A16 = 0
A61 = 0
A26 = 0
A62 = 0

B11 = (0.5 / 3) * (((Q11(1) * -4) + (Q11(17) * 4)) + 4 * ((Q11(2) * -3.5) + (Q11(4) *
-2.5) + (Q11(6) * -1.5) + (Q11(8) * -0.5) + (Q11(10) * 0.5) + (Q11(12) * 1.5) +
(Q11(14) * 2.5) + (Q11(16) * 3.5)) + 2 * ((Q11(3) * -3) + (Q11(5) * -2) + (Q11(7) *
-1) + (Q11(9) * 0) + (Q11(11) * 1) + (Q11(13) * 2) + (Q11(15) * 3)))
B12 = (0.5 / 3) * (((Q12(1) * -4) + (Q12(17) * 4)) + 4 * ((Q12(2) * -3.5) + (Q12(4) *
-2.5) + (Q12(6) * -1.5) + (Q12(8) * -0.5) + (Q12(10) * 0.5) + (Q12(12) * 1.5) +
(Q12(14) * 2.5) + (Q12(16) * 3.5)) + 2 * ((Q12(3) * -3) + (Q12(5) * -2) + (Q12(7) *
-1) + (Q12(9) * 0) + (Q12(11) * 1) + (Q12(13) * 2) + (Q12(15) * 3)))
B21 = (0.5 / 3) * (((Q12(1) * -4) + (Q12(17) * 4)) + 4 * ((Q12(2) * -3.5) + (Q12(4) *
-2.5) + (Q12(6) * -1.5) + (Q12(8) * -0.5) + (Q12(10) * 0.5) + (Q12(12) * 1.5) +
(Q12(14) * 2.5) + (Q12(16) * 3.5)) + 2 * ((Q12(3) * -3) + (Q12(5) * -2) + (Q12(7) *
-1) + (Q12(9) * 0) + (Q12(11) * 1) + (Q12(13) * 2) + (Q12(15) * 3)))
```

```
B22 = (0.5 / 3) * (((Q22(1) * -4) + (Q22(17) * 4)) + 4 * ((Q22(2) * -3.5) + (Q22(4) *
-2.5) + (Q22(6) * -1.5) + (Q22(8) * -0.5) + (Q22(10) * 0.5) + (Q22(12) * 1.5) +
(Q22(14) * 2.5) + (Q22(16) * 3.5)) + 2 * ((Q22(3) * -3) + (Q22(5) * -2) + (Q22(7) *
-1) + (Q22(9) * 0) + (Q22(11) * 1) + (Q22(13) * 2) + (Q22(15) * 3)))
B66 = (0.5 / 3) * (((Q66(1) * -4) + (Q66(17) * 4)) + 4 * ((Q66(2) * -3.5) + (Q66(4) *
-2.5) + (Q66(6) * -1.5) + (Q66(8) * -0.5) + (Q66(10) * 0.5) + (Q66(12) * 1.5) +
(Q66(14) * 2.5) + (Q66(16) * 3.5)) + 2 * ((Q66(3) * -3) + (Q66(5) * -2) + (Q66(7) *
-1) + (Q66(9) * 0) + (Q66(11) * 1) + (Q66(13) * 2) + (Q66(15) * 3)))
B16 = 0
B61 = 0
B26 = 0
B62 = 0

D11 = (0.5 / 3) * (((Q11(1) * 16) + (Q11(17) * 16)) + 4 * ((Q11(2) * 12.25) +
(Q11(4) * 6.25) + (Q11(6) * 2.25) + (Q11(8) * 0.25) + (Q11(10) * 0.25) + (Q11(12)
* 2.25) + (Q11(14) * 6.25) + (Q11(16) * 12.25)) + 2 * ((Q11(3) * 9) + (Q11(5) * 4)
+ (Q11(7) * 1) + (Q11(9) * 0) + (Q11(11) * 1) + (Q11(13) * 4) + (Q11(15) * 9)))
D12 = (0.5 / 3) * (((Q12(1) * 16) + (Q12(17) * 16)) + 4 * ((Q12(2) * 12.25) +
(Q12(4) * 6.25) + (Q12(6) * 2.25) + (Q12(8) * 0.25) + (Q12(10) * 0.25) + (Q12(12)
* 2.25) + (Q12(14) * 6.25) + (Q12(16) * 12.25)) + 2 * ((Q12(3) * 9) + (Q12(5) * 4)
+ (Q12(7) * 1) + (Q12(9) * 0) + (Q12(11) * 1) + (Q12(13) * 4) + (Q12(15) * 9)))
D21 = (0.5 / 3) * (((Q12(1) * 16) + (Q12(17) * 16)) + 4 * ((Q12(2) * 12.25) +
(Q12(4) * 6.25) + (Q12(6) * 2.25) + (Q12(8) * 0.25) + (Q12(10) * 0.25) + (Q12(12)
* 2.25) + (Q12(14) * 6.25) + (Q12(16) * 12.25)) + 2 * ((Q12(3) * 9) + (Q12(5) * 4)
+ (Q12(7) * 1) + (Q12(9) * 0) + (Q12(11) * 1) + (Q12(13) * 4) + (Q12(15) * 9)))
D22 = (0.5 / 3) * (((Q22(1) * 16) + (Q22(17) * 16)) + 4 * ((Q22(2) * 12.25) +
(Q22(4) * 6.25) + (Q22(6) * 2.25) + (Q22(8) * 0.25) + (Q22(10) * 0.25) + (Q22(12)
* 2.25) + (Q22(14) * 6.25) + (Q22(16) * 12.25)) + 2 * ((Q22(3) * 9) + (Q22(5) * 4)
+ (Q22(7) * 1) + (Q22(9) * 0) + (Q22(11) * 1) + (Q22(13) * 4) + (Q22(15) * 9)))
D66 = (0.5 / 3) * (((Q66(1) * 16) + (Q66(17) * 16)) + 4 * ((Q66(2) * 12.25) +
(Q66(4) * 6.25) + (Q66(6) * 2.25) + (Q66(8) * 0.25) + (Q66(10) * 0.25) + (Q66(12)
* 2.25) + (Q66(14) * 6.25) + (Q66(16) * 12.25)) + 2 * ((Q66(3) * 9) + (Q66(5) * 4)
+ (Q66(7) * 1) + (Q66(9) * 0) + (Q66(11) * 1) + (Q66(13) * 4) + (Q66(15) * 9)))
D16 = 0
D61 = 0
D26 = 0
D62 = 0

Worksheets("Model").Activate

ActiveSheet.Cells(43, 2).Value = A11
ActiveSheet.Cells(44, 2).Value = A12
ActiveSheet.Cells(43, 3).Value = A21
ActiveSheet.Cells(44, 3).Value = A22
ActiveSheet.Cells(45, 3).Value = A26
ActiveSheet.Cells(44, 4).Value = A62
ActiveSheet.Cells(45, 2).Value = A16
ActiveSheet.Cells(43, 4).Value = A61
ActiveSheet.Cells(45, 4).Value = A66
```

```
ActiveSheet.Cells(43, 6).Value = B11
ActiveSheet.Cells(44, 6).Value = B12
ActiveSheet.Cells(43, 7).Value = B21
ActiveSheet.Cells(44, 7).Value = B22
ActiveSheet.Cells(45, 7).Value = B26
ActiveSheet.Cells(44, 8).Value = B62
ActiveSheet.Cells(45, 6).Value = B16
ActiveSheet.Cells(43, 8).Value = B61
ActiveSheet.Cells(45, 8).Value = B66

ActiveSheet.Cells(48, 2).Value = B11
ActiveSheet.Cells(49, 2).Value = B12
ActiveSheet.Cells(48, 3).Value = B21
ActiveSheet.Cells(49, 3).Value = B22
ActiveSheet.Cells(50, 3).Value = B26
ActiveSheet.Cells(49, 4).Value = B62
ActiveSheet.Cells(50, 2).Value = B16
ActiveSheet.Cells(48, 4).Value = B61
ActiveSheet.Cells(50, 4).Value = B66

ActiveSheet.Cells(48, 6).Value = D11
ActiveSheet.Cells(49, 6).Value = D12
ActiveSheet.Cells(48, 7).Value = D21
ActiveSheet.Cells(49, 7).Value = D22
ActiveSheet.Cells(50, 7).Value = D26
ActiveSheet.Cells(49, 8).Value = D62
ActiveSheet.Cells(50, 6).Value = D16
ActiveSheet.Cells(48, 8).Value = D61
ActiveSheet.Cells(50, 8).Value = D66

Rem Inputing Inverted ABD matrix into ABD Matrix worksheet
Dim A1dash(20)
Dim A2dash(20)
Dim A6dash(20)

Dim B1dash(20)
Dim B2dash(20)
Dim B6dash(20)

Dim C1dash(20)
Dim C2dash(20)
Dim C6dash(20)

Dim D1dash(20)
Dim D2dash(20)
Dim D6dash(20)

For i = 1 To 3
```

```
Worksheets("Model").Activate

A1dash(i) = ActiveSheet.Cells(54, i + 1).Value
A2dash(i) = ActiveSheet.Cells(55, i + 1).Value
A6dash(i) = ActiveSheet.Cells(56, i + 1).Value

B1dash(i) = ActiveSheet.Cells(54, i + 5).Value
B2dash(i) = ActiveSheet.Cells(55, i + 5).Value
B6dash(i) = ActiveSheet.Cells(56, i + 5).Value

C1dash(i) = ActiveSheet.Cells(59, i + 1).Value
C2dash(i) = ActiveSheet.Cells(60, i + 1).Value
C6dash(i) = ActiveSheet.Cells(61, i + 1).Value

D1dash(i) = ActiveSheet.Cells(59, i + 5).Value
D2dash(i) = ActiveSheet.Cells(60, i + 5).Value
D6dash(i) = ActiveSheet.Cells(61, i + 5).Value

Worksheets("ABD Matrix").Activate

ActiveSheet.Cells(j + 24, i + 3).Value = A1dash(i)
ActiveSheet.Cells(j + 24, i + 6).Value = A2dash(i)
ActiveSheet.Cells(j + 24, i + 9).Value = A6dash(i)

ActiveSheet.Cells(j + 24, i + 12).Value = B1dash(i)
ActiveSheet.Cells(j + 24, i + 15).Value = B2dash(i)
ActiveSheet.Cells(j + 24, i + 18).Value = B6dash(i)

ActiveSheet.Cells(j + 24, i + 21).Value = C1dash(i)
ActiveSheet.Cells(j + 24, i + 24).Value = C2dash(i)
ActiveSheet.Cells(j + 24, i + 27).Value = C6dash(i)

ActiveSheet.Cells(j + 24, i + 30).Value = D1dash(i)
ActiveSheet.Cells(j + 24, i + 33).Value = D2dash(i)
ActiveSheet.Cells(j + 24, i + 36).Value = D6dash(i)

Next i

ActiveSheet.Cells(j + 24, 43).Value = D11
ActiveSheet.Cells(j + 24, 44).Value = D22

ActiveSheet.Cells(j + 24, 53).Value = A11
ActiveSheet.Cells(j + 24, 54).Value = A12
ActiveSheet.Cells(j + 24, 55).Value = A21
ActiveSheet.Cells(j + 24, 56).Value = A22
ActiveSheet.Cells(j + 24, 57).Value = A26
ActiveSheet.Cells(j + 24, 58).Value = A62
ActiveSheet.Cells(j + 24, 59).Value = A16
```

```
ActiveSheet.Cells(j + 24, 60).Value = A61
ActiveSheet.Cells(j + 24, 61).Value = A66

ActiveSheet.Cells(j + 24, 62).Value = B11
ActiveSheet.Cells(j + 24, 63).Value = B12
ActiveSheet.Cells(j + 24, 64).Value = B21
ActiveSheet.Cells(j + 24, 65).Value = B22
ActiveSheet.Cells(j + 24, 66).Value = B26
ActiveSheet.Cells(j + 24, 67).Value = B62
ActiveSheet.Cells(j + 24, 68).Value = B16
ActiveSheet.Cells(j + 24, 69).Value = B61
ActiveSheet.Cells(j + 24, 70).Value = B66

ActiveSheet.Cells(j + 24, 71).Value = D12
ActiveSheet.Cells(j + 24, 72).Value = D21
ActiveSheet.Cells(j + 24, 73).Value = D26
ActiveSheet.Cells(j + 24, 74).Value = D62
ActiveSheet.Cells(j + 24, 75).Value = D16
ActiveSheet.Cells(j + 24, 76).Value = D61
ActiveSheet.Cells(j + 24, 77).Value = D66

Next j

End Sub
```

Tensile and Compressive strengths as functions of time (Polyester)

```
Sub StrengthsVsTime()

Rem  Carry out strength calculations for all time intervals
For j = 1 To 39
Dim Time(50)

Worksheets("Temp Profile").Activate
Time(j) = ActiveSheet.Cells(j + 7, 1).Value

Worksheets("Strengths vs Time").Activate
ActiveSheet.Cells(j + 30, 4).Value = Time(j)
ActiveSheet.Cells(j + 77, 4).Value = Time(j)

Rem Calculate E1 per node
For i = 1 To 17

Rem input temperature values
Dim tem(20)

Worksheets("Temp profile").Activate
tem(i) = ActiveSheet.Cells(j + 7, i + 1).Value

Rem input RRC values
Dim rc(20)


Worksheets("RRC").Activate
rc(i) = ActiveSheet.Cells(j + 7, i + 1).Value


Rem calculate E1
Dim E1(20)
Dim cE1(20)
Dim TanhE1(20)
Dim cE1s(20)
Dim TanhE1S(20)

Worksheets("Model").Activate
Rem UD paramters
TgE1 = ActiveSheet.Cells(4, 2)
kE1 = ActiveSheet.Cells(4, 3)
MuE1 = ActiveSheet.Cells(4, 4)
MrE1 = ActiveSheet.Cells(4, 5)
Rem CSM NEedle weave paramters
TgE1S = ActiveSheet.Cells(11, 2)
```

```
kE1S = ActiveSheet.Cells(11, 3)
MuE1S = ActiveSheet.Cells(11, 4)
MrE1S = ActiveSheet.Cells(11, 5)

If i >= 4 And i <= 14 Then

cE1(i) = kE1 * (tem(i) - TgE1)
TanhE1(i) = (Exp(cE1(i)) - Exp(-cE1(i))) / (Exp(cE1(i)) + Exp(-cE1(i)))
E1(i) = (((1 - TanhE1(i)) * (MuE1 - MrE1)) / 2 + MrE1) * (rc(i) / 100) ^ 1
Else:

cE1s(i) = kE1S * (tem(i) - TgE1S)
TanhE1S(i) = (Exp(cE1s(i)) - Exp(-cE1s(i))) / (Exp(cE1s(i)) + Exp(-cE1s(i)))
E1(i) = (((1 - TanhE1S(i)) * (MuE1S - MrE1S)) / 2 + MrE1S) * (rc(i) / 100) ^ 1
End If
Rem Lamina node strength
Dim sT(20)
Dim sC(20)

Rem UD properties

TgsT = ActiveSheet.Cells(7, 2)
TgsC = ActiveSheet.Cells(8, 2)
ksT = ActiveSheet.Cells(7, 3)
ksC = ActiveSheet.Cells(8, 3)
MusT = ActiveSheet.Cells(7, 4)
MusC = ActiveSheet.Cells(8, 4)
MrsT = ActiveSheet.Cells(7, 5)
MrsC = ActiveSheet.Cells(8, 5)

Rem CSM properties

TgsTS = ActiveSheet.Cells(14, 2)
TgsCS = ActiveSheet.Cells(15, 2)
ksTS = ActiveSheet.Cells(14, 3)
ksCS = ActiveSheet.Cells(15, 3)
MusTS = ActiveSheet.Cells(14, 4)
MusCS = ActiveSheet.Cells(15, 4)
MrsTS = ActiveSheet.Cells(14, 5)
MrsCS = ActiveSheet.Cells(15, 5)

If i >= 4 And i <= 14 Then

csT = ksT * (tem(i) - TgsT)
TanhsT = (Exp(csT) - Exp(-csT)) / (Exp(csT) + Exp(-csT))
sT(i) = (((1 - TanhsT) * (MusT - MrsT)) / 2 + MrsT) * (rc(i) / 100) ^ 0

csC = ksC * (tem(i) - TgsC)
```

```
TanhsC = (Exp(csC) - Exp(-csC)) / (Exp(csC) + Exp(-csC))
sC(i) = (((1 - TanhsC) * (MusC - MrsC)) / 2 + MrsC) * (rc(i) / 100) ^ 0

Else:

csTS = ksTS * (tem(i) - TgsTS)
TanhsTS = (Exp(csTS) - Exp(-csTS)) / (Exp(csTS) + Exp(-csTS))
sT(i) = (((1 - TanhsTS) * (MusTS - MrsTS)) / 2 + MrsTS) * (rc(i) / 100) ^ 1

csCS = ksCS * (tem(i) - TgsCS)
TanhsCS = (Exp(csCS) - Exp(-csCS)) / (Exp(csCS) + Exp(-csCS))
sC(i) = (((1 - TanhsCS) * (MusCS - MrsCS)) / 2 + MrsCS) * (rc(i) / 100) ^ 1
End If
Next i

Rem Stress at a point (tensile and compressive loading)

Dim TStress(20)
Dim TStren(80)
Dim CStress(20)
Dim CStren(80)

For k = 0 To 70
For i = 1 To 17
strain = k / 1000


TStress(i) = strain * E1(i) * 1000
CStress(i) = strain * E1(i) * 1000

If TStress(i) >= sT(i) Then TStress(i) = 0
If CStress(i) >= sC(i) Then CStress(i) = 0
Next i

TStren(k) = (0.5 / 3 * ((TStress(1) + TStress(17)) + 4 * (TStress(2) + TStress(4) +
TStress(6) + TStress(8) + TStress(10) + TStress(12) + TStress(14) + TStress(16)) + 2
* (TStress(3) + TStress(5) + TStress(7) + TStress(9) + TStress(11) + TStress(13) +
TStress(15)))) / 8
CStren(k) = (0.5 / 3 * ((CStress(1) + CStress(17)) + 4 * (CStress(2) + CStress(4) +
CStress(6) + CStress(8) + CStress(10) + CStress(12) + CStress(14) + CStress(16)) +
2 * (CStress(3) + CStress(5) + CStress(7) + CStress(9) + CStress(11) + CStress(13)
+ CStress(15)))) / 8

Worksheets("Strengths vs Time").Activate
ActiveSheet.Cells(j + 30, k + 5).Value = TStren(k)
ActiveSheet.Cells(j + 77, k + 5).Value = CStren(k)

Next k
Next j
```

```
End Sub
```

Stress strain curve modelling (Polyester)

```
Sub StressStrainCurves()


For j = 1 To 39

Dim Time(50)
Dim tem(20)
Dim TStress(20)
Dim sT(20)
Dim TStren(200)

Worksheets("Temp profile").Activate
Time(j) = ActiveSheet.Cells(j + 7, 1).Value

Worksheets("Output").Activate
ActiveSheet.Cells(j + 7, 1).Value = Time(j)


For k = 0 To 70

For i = 1 To 17

Worksheets("Temp Profile").Activate
tem(i) = ActiveSheet.Cells(j + 7, i + 1).Value


If 0 < tem(i) <= 33.5 Then E = 12          'Alter values here
If 0 < tem(i) <= 33.5 Then sig = 1250       'Alter values here

If 33.5 < tem(i) <= 70 Then E = 10.2        'Alter values here
If 33.5 < tem(i) <= 70 Then sig = 1200      'Alter values here

If 70 < tem(i) <= 105 Then E = 12.7         'Alter values here
If 70 < tem(i) <= 105 Then sig = 1100       'Alter values here

If 105 < tem(i) <= 135 Then E = 11.5        'Alter values here
If 105 < tem(i) <= 135 Then sig = 1250      'Alter values here

If 135 < tem(i) <= 180 Then E = 11.35       'Alter values here
If 135 < tem(i) <= 180 Then sig = 750       'Alter values here

If 180 < tem(i) <= 230 Then E = 13          'Alter values here
If 180 < tem(i) <= 230 Then sig = 575       'Alter values here
```

```
If 230 < tem(i) <= 275 Then E = 12.8        'Alter values here
If 230 < tem(i) <= 275 Then sig = 615       'Alter values here

If 275 < tem(i) <= 300 Then E = 12.5        'Alter values here
If 275 < tem(i) <= 300 Then sig = 575       'Alter values here

If 300 < tem(i) Then E = 1000000
If 300 < tem(i) Then sig = 1000000
strain = k / 1000

TStress(i) = sig * (1 - Exp((-(1000 * E) * strain) / sig))

TgsT = 195    'Alter values here
ksT = 0.03  'Alter values here
MusT = 320   'Alter values here
MrsT = 220    'Alter values here


csT = ksT * (tem(i) - TgsT)
TanhsT = (Exp(csT) - Exp(-csT)) / (Exp(csT) + Exp(-csT))
sT(i) = (((1 - TanhsT) * (MusT - MrsT)) / 2 + MrsT)

If TStress(i) >= sT(i) Then TStress(i) = 0

Next i

'Trapezium rule

TStren(k) = ((0.5 / 2) * ((TStress(1) + TStress(17)) + 2 * (TStress(2) + TStress(3) +
TStress(4) + TStress(5) + TStress(6) + TStress(7) + TStress(8) + TStress(9) +
TStress(10) + TStress(11) + TStress(12) + TStress(13) + TStress(14) + TStress(15) +
TStress(16)))) / 8


Worksheets("Output").Activate
ActiveSheet.Cells(j + 7, k + 2).Value = TStren(k)

Next k

Next j



End Sub
```

ABD Matrix calculation (Phenolic)

```
Sub ABCDvsTime()

Rem Calculate matrix for all times
For j = 1 To 39


Dim Time(50)
Worksheets("Temp profile").Activate
Time(j) = ActiveSheet.Cells(j + 7, 1).Value

Worksheets("ABD Matrix").Activate
ActiveSheet.Cells(j + 24, 1).Value = Time(j)

Rem Calculate Q Matrix for each node

For i = 1 To 17
Rem Input temperature profiles
Dim tem(20)
Worksheets("Temp profile").Activate
tem(i) = ActiveSheet.Cells(j + 7, i + 1).Value

Rem Input rrc values
Dim rc(20)
Worksheets("RRC").Activate

rc(i) = ActiveSheet.Cells(j + 7, i + 1).Value

Rem Calculate E1,E2,G12,u21
Dim E1(20)
Dim E2(20)
Dim G12(20)
Dim u12(20)
Dim u21(20)
Dim cE1(20)
Dim cE2(20)
Dim cG12(20)
Dim TanhE1(20)
Dim TanhE2(20)
Dim TanhG12(20)
Dim TanhE1S(20)
Dim TanhE2S(20)
Dim TanhG12S(20)
```

```
Dim cE1s(20)
Dim cE2S(20)
Dim cG12S(20)

Worksheets("Model").Activate
Rem UD properties
TgE1 = ActiveSheet.Cells(4, 2)
TgE2 = ActiveSheet.Cells(5, 2)
TgG12 = ActiveSheet.Cells(6, 2)

kE1 = ActiveSheet.Cells(4, 3)
kE2 = ActiveSheet.Cells(5, 3)
kG12 = ActiveSheet.Cells(6, 3)

MuE1 = ActiveSheet.Cells(4, 4)
MuE2 = ActiveSheet.Cells(5, 4)
MuG12 = ActiveSheet.Cells(6, 4)

MrE1 = ActiveSheet.Cells(4, 5)
MrE2 = ActiveSheet.Cells(5, 5)
MrG12 = ActiveSheet.Cells(6, 5)

Rem CSM properties

TgE1S = ActiveSheet.Cells(11, 2)
TgE2S = ActiveSheet.Cells(12, 2)
TgG12S = ActiveSheet.Cells(13, 2)

kE1S = ActiveSheet.Cells(11, 3)
kE2S = ActiveSheet.Cells(12, 3)
kG12S = ActiveSheet.Cells(13, 3)

MuE1S = ActiveSheet.Cells(11, 4)
MuE2S = ActiveSheet.Cells(12, 4)
MuG12S = ActiveSheet.Cells(13, 4)

MrE1S = ActiveSheet.Cells(11, 5)
MrE2S = ActiveSheet.Cells(12, 5)
MrG12S = ActiveSheet.Cells(13, 5)

If i >= 4 And i <= 14 Then

cE1(i) = kE1 * (tem(i) - TgE1)
TanhE1(i) = (Exp(cE1(i)) - Exp(-cE1(i))) / (Exp(cE1(i)) + Exp(-cE1(i)))
E1(i) = (((1 - TanhE1(i)) * (MuE1 - MrE1)) / 2 + MrE1) * (rc(i) / 100) ^ 1

cE2(i) = kE2 * (tem(i) - TgE2)
TanhE2(i) = (Exp(cE2(i)) - Exp(-cE2(i))) / (Exp(cE2(i)) + Exp(-cE2(i)))
E2(i) = (((1 - TanhE2(i)) * (MuE2 - MrE2)) / 2 + MrE2) * (rc(i) / 100) ^ 1
```

```
cG12(i) = kG12 * (tem(i) - TgG12)
TanhG12(i) = (Exp(cG12(i)) - Exp(-cG12(i))) / (Exp(cG12(i)) + Exp(-cG12(i)))
G12(i) = (((1 - TanhG12(i)) * (MuG12 - MrG12)) / 2 + MrG12) * (rc(i) / 100) ^ 1

Else

cE1s(i) = kE1S * (tem(i) - TgE1S)
TanhE1S(i) = (Exp(cE1s(i)) - Exp(-cE1s(i))) / (Exp(cE1s(i)) + Exp(-cE1s(i)))
E1(i) = (((1 - TanhE1S(i)) * (MuE1S - MrE1S)) / 2 + MrE1S) * (rc(i) / 100) ^ 1

cE2S(i) = kE2S * (tem(i) - TgE2S)
TanhE2S(i) = (Exp(cE2S(i)) - Exp(-cE2S(i))) / (Exp(cE2S(i)) + Exp(-cE2S(i)))
E2(i) = (((1 - TanhE2S(i)) * (MuE2S - MrE2S)) / 2 + MrE2S) * (rc(i) / 100) ^ 1

cG12S(i) = kG12S * (tem(i) - TgG12S)
TanhG12S(i) = (Exp(cG12S(i)) - Exp(-cG12S(i))) / (Exp(cG12S(i)) + Exp(-
cG12S(i)))
G12(i) = (((1 - TanhG12S(i)) * (MuG12S - MrG12S)) / 2 + MrG12S) * (rc(i) / 100) ^
1

End If

u12(i) = ActiveSheet.Cells(3, 8).Value
u21(i) = u12(i) * E2(i) / E1(i)

Rem Calculate Q matrix
Dim Q11(20)
Dim Q12(20)
Dim Q22(20)
Dim Q66(20)

uxy = 1 - u12(i) * u21(i)
Q11(i) = E1(i) / uxy
Q12(i) = u12(i) * E2(i) / uxy
Q22(i) = E2(i) / uxy
Q13 = 0
Q21 = Q12
Q31 = 0
Q23 = 0
Q66(i) = G12(i)

Next i


Rem Calculating Ei
Dim thick(20)
Dim yi(20)
```

```
Dim Eyi(20)
Y = 0
Ey = 0
E = 0
bd3 = 0
EIO = 0
alpha = 0

For i = 1 To 17

Worksheets("Model").Activate
thick(i) = ActiveSheet.Cells(i + 19, 1).Value

Rem Printing
Worksheets("Sheet1").Activate
ActiveSheet.Cells(i + 2, 2).Value = thick(i) + 0.5
yi(i) = thick(i) + 0.5

Worksheets("Sheet1").Activate

ActiveSheet.Cells(i + 2, 4).Value = E1(i) * yi(i)
Eyi(i) = E1(i) * yi(i)
Ey = Ey + Eyi(i)
E = E + E1(i)

Next i
Y = Y + (Ey / E)
Worksheets("ABD Matrix").Activate
 ActiveSheet.Cells(j + 24, 2).Value = Y


Rem 2nd Loop

For i = 1 To 17
Worksheets("Model").Activate
thick(i) = ActiveSheet.Cells(i + 19, 1).Value

Rem Printing
Worksheets("Sheet1").Activate
ActiveSheet.Cells(i + 2, 2).Value = thick(i) + 0.5
yi(i) = thick(i) + 0.5


Worksheets("Sheet1").Activate
Rem ActiveSheet.Cells(i + 2, 3).Value = E1(i)
```

```
bd3 = bd3 + (E1(i) / 12)
ActiveSheet.Cells(19, 5).Value = Y
alpha = alpha + (E1(i) * (Y - yi(i)) ^ 2)

Next i
EIO = bd3 + alpha
Worksheets("ABD Matrix").Activate
ActiveSheet.Cells(j + 24, 3).Value = EIO

Rem Calculate ABD Matrix

A11 = (0.5 / 3) * ((Q11(1) + Q11(17)) + 4 * (Q11(2) + Q11(4) + Q11(6) + Q11(8) +
Q11(10) + Q11(12) + Q11(14) + Q11(16)) + 2 * (Q11(3) + Q11(5) + Q11(7) +
Q11(9) + Q11(11) + Q11(13) + Q11(15)))
A12 = (0.5 / 3) * ((Q12(1) + Q12(17)) + 4 * (Q12(2) + Q12(4) + Q12(6) + Q12(8) +
Q12(10) + Q12(12) + Q12(14) + Q12(16)) + 2 * (Q12(3) + Q12(5) + Q12(7) +
Q12(9) + Q12(11) + Q12(13) + Q12(15)))
A21 = (0.5 / 3) * ((Q12(1) + Q12(17)) + 4 * (Q12(2) + Q12(4) + Q12(6) + Q12(8) +
Q12(10) + Q12(12) + Q12(14) + Q12(16)) + 2 * (Q12(3) + Q12(5) + Q12(7) +
Q12(9) + Q12(11) + Q12(13) + Q12(15)))
A22 = (0.5 / 3) * ((Q22(1) + Q22(17)) + 4 * (Q22(2) + Q22(4) + Q22(6) + Q22(8) +
Q22(10) + Q22(12) + Q22(14) + Q22(16)) + 2 * (Q22(3) + Q22(5) + Q22(7) +
Q22(9) + Q22(11) + Q22(13) + Q22(15)))
A66 = (0.5 / 3) * ((Q66(1) + Q66(17)) + 4 * (Q66(2) + Q66(4) + Q66(6) + Q66(8) +
Q66(10) + Q66(12) + Q66(14) + Q66(16)) + 2 * (Q66(3) + Q66(5) + Q66(7) +
Q66(9) + Q66(11) + Q66(13) + Q66(15)))
A16 = 0
A61 = 0
A26 = 0
A62 = 0

B11 = (0.5 / 3) * (((Q11(1) * -4) + (Q11(17) * 4)) + 4 * ((Q11(2) * -3.5) + (Q11(4) *
-2.5) + (Q11(6) * -1.5) + (Q11(8) * -0.5) + (Q11(10) * 0.5) + (Q11(12) * 1.5) +
(Q11(14) * 2.5) + (Q11(16) * 3.5)) + 2 * ((Q11(3) * -3) + (Q11(5) * -2) + (Q11(7) *
-1) + (Q11(9) * 0) + (Q11(11) * 1) + (Q11(13) * 2) + (Q11(15) * 3)))
B12 = (0.5 / 3) * (((Q12(1) * -4) + (Q12(17) * 4)) + 4 * ((Q12(2) * -3.5) + (Q12(4) *
-2.5) + (Q12(6) * -1.5) + (Q12(8) * -0.5) + (Q12(10) * 0.5) + (Q12(12) * 1.5) +
(Q12(14) * 2.5) + (Q12(16) * 3.5)) + 2 * ((Q12(3) * -3) + (Q12(5) * -2) + (Q12(7) *
-1) + (Q12(9) * 0) + (Q12(11) * 1) + (Q12(13) * 2) + (Q12(15) * 3)))
B21 = (0.5 / 3) * (((Q12(1) * -4) + (Q12(17) * 4)) + 4 * ((Q12(2) * -3.5) + (Q12(4) *
-2.5) + (Q12(6) * -1.5) + (Q12(8) * -0.5) + (Q12(10) * 0.5) + (Q12(12) * 1.5) +
(Q12(14) * 2.5) + (Q12(16) * 3.5)) + 2 * ((Q12(3) * -3) + (Q12(5) * -2) + (Q12(7) *
-1) + (Q12(9) * 0) + (Q12(11) * 1) + (Q12(13) * 2) + (Q12(15) * 3)))
B22 = (0.5 / 3) * (((Q22(1) * -4) + (Q22(17) * 4)) + 4 * ((Q22(2) * -3.5) + (Q22(4) *
-2.5) + (Q22(6) * -1.5) + (Q22(8) * -0.5) + (Q22(10) * 0.5) + (Q22(12) * 1.5) +
(Q22(14) * 2.5) + (Q22(16) * 3.5)) + 2 * ((Q22(3) * -3) + (Q22(5) * -2) + (Q22(7) *
-1) + (Q22(9) * 0) + (Q22(11) * 1) + (Q22(13) * 2) + (Q22(15) * 3)))
B66 = (0.5 / 3) * (((Q66(1) * -4) + (Q66(17) * 4)) + 4 * ((Q66(2) * -3.5) + (Q66(4) *
-2.5) + (Q66(6) * -1.5) + (Q66(8) * -0.5) + (Q66(10) * 0.5) + (Q66(12) * 1.5) +
```

```
(Q66(14) * 2.5) + (Q66(16) * 3.5)) + 2 * ((Q66(3) * -3) + (Q66(5) * -2) + (Q66(7) *
-1) + (Q66(9) * 0) + (Q66(11) * 1) + (Q66(13) * 2) + (Q66(15) * 3)))
B16 = 0
B61 = 0
B26 = 0
B62 = 0

D11 = (0.5 / 3) * (((Q11(1) * 16) + (Q11(17) * 16)) + 4 * ((Q11(2) * 12.25) +
(Q11(4) * 6.25) + (Q11(6) * 2.25) + (Q11(8) * 0.25) + (Q11(10) * 0.25) + (Q11(12)
* 2.25) + (Q11(14) * 6.25) + (Q11(16) * 12.25)) + 2 * ((Q11(3) * 9) + (Q11(5) * 4)
+ (Q11(7) * 1) + (Q11(9) * 0) + (Q11(11) * 1) + (Q11(13) * 4) + (Q11(15) * 9)))
D12 = (0.5 / 3) * (((Q12(1) * 16) + (Q12(17) * 16)) + 4 * ((Q12(2) * 12.25) +
(Q12(4) * 6.25) + (Q12(6) * 2.25) + (Q12(8) * 0.25) + (Q12(10) * 0.25) + (Q12(12)
* 2.25) + (Q12(14) * 6.25) + (Q12(16) * 12.25)) + 2 * ((Q12(3) * 9) + (Q12(5) * 4)
+ (Q12(7) * 1) + (Q12(9) * 0) + (Q12(11) * 1) + (Q12(13) * 4) + (Q12(15) * 9)))
D21 = (0.5 / 3) * (((Q12(1) * 16) + (Q12(17) * 16)) + 4 * ((Q12(2) * 12.25) +
(Q12(4) * 6.25) + (Q12(6) * 2.25) + (Q12(8) * 0.25) + (Q12(10) * 0.25) + (Q12(12)
* 2.25) + (Q12(14) * 6.25) + (Q12(16) * 12.25)) + 2 * ((Q12(3) * 9) + (Q12(5) * 4)
+ (Q12(7) * 1) + (Q12(9) * 0) + (Q12(11) * 1) + (Q12(13) * 4) + (Q12(15) * 9)))
D22 = (0.5 / 3) * (((Q22(1) * 16) + (Q22(17) * 16)) + 4 * ((Q22(2) * 12.25) +
(Q22(4) * 6.25) + (Q22(6) * 2.25) + (Q22(8) * 0.25) + (Q22(10) * 0.25) + (Q22(12)
* 2.25) + (Q22(14) * 6.25) + (Q22(16) * 12.25)) + 2 * ((Q22(3) * 9) + (Q22(5) * 4)
+ (Q22(7) * 1) + (Q22(9) * 0) + (Q22(11) * 1) + (Q22(13) * 4) + (Q22(15) * 9)))
D66 = (0.5 / 3) * (((Q66(1) * 16) + (Q66(17) * 16)) + 4 * ((Q66(2) * 12.25) +
(Q66(4) * 6.25) + (Q66(6) * 2.25) + (Q66(8) * 0.25) + (Q66(10) * 0.25) + (Q66(12)
* 2.25) + (Q66(14) * 6.25) + (Q66(16) * 12.25)) + 2 * ((Q66(3) * 9) + (Q66(5) * 4)
+ (Q66(7) * 1) + (Q66(9) * 0) + (Q66(11) * 1) + (Q66(13) * 4) + (Q66(15) * 9)))
D16 = 0
D61 = 0
D26 = 0
D62 = 0

Worksheets("Model").Activate

ActiveSheet.Cells(43, 2).Value = A11
ActiveSheet.Cells(44, 2).Value = A12
ActiveSheet.Cells(43, 3).Value = A21
ActiveSheet.Cells(44, 3).Value = A22
ActiveSheet.Cells(45, 3).Value = A26
ActiveSheet.Cells(44, 4).Value = A62
ActiveSheet.Cells(45, 2).Value = A16
ActiveSheet.Cells(43, 4).Value = A61
ActiveSheet.Cells(45, 4).Value = A66

ActiveSheet.Cells(43, 6).Value = B11
ActiveSheet.Cells(44, 6).Value = B12
ActiveSheet.Cells(43, 7).Value = B21
ActiveSheet.Cells(44, 7).Value = B22
ActiveSheet.Cells(45, 7).Value = B26
```

```
ActiveSheet.Cells(44, 8).Value = B62
ActiveSheet.Cells(45, 6).Value = B16
ActiveSheet.Cells(43, 8).Value = B61
ActiveSheet.Cells(45, 8).Value = B66

ActiveSheet.Cells(48, 2).Value = B11
ActiveSheet.Cells(49, 2).Value = B12
ActiveSheet.Cells(48, 3).Value = B21
ActiveSheet.Cells(49, 3).Value = B22
ActiveSheet.Cells(50, 3).Value = B26
ActiveSheet.Cells(49, 4).Value = B62
ActiveSheet.Cells(50, 2).Value = B16
ActiveSheet.Cells(48, 4).Value = B61
ActiveSheet.Cells(50, 4).Value = B66

ActiveSheet.Cells(48, 6).Value = D11
ActiveSheet.Cells(49, 6).Value = D12
ActiveSheet.Cells(48, 7).Value = D21
ActiveSheet.Cells(49, 7).Value = D22
ActiveSheet.Cells(50, 7).Value = D26
ActiveSheet.Cells(49, 8).Value = D62
ActiveSheet.Cells(50, 6).Value = D16
ActiveSheet.Cells(48, 8).Value = D61
ActiveSheet.Cells(50, 8).Value = D66

Rem Inputing Inverted ABD matrix into ABD Matrix worksheet
Dim A1dash(20)
Dim A2dash(20)
Dim A6dash(20)

Dim B1dash(20)
Dim B2dash(20)
Dim B6dash(20)

Dim C1dash(20)
Dim C2dash(20)
Dim C6dash(20)

Dim D1dash(20)
Dim D2dash(20)
Dim D6dash(20)

For i = 1 To 3

Worksheets("Model").Activate

A1dash(i) = ActiveSheet.Cells(54, i + 1).Value
A2dash(i) = ActiveSheet.Cells(55, i + 1).Value
A6dash(i) = ActiveSheet.Cells(56, i + 1).Value
```

```
B1dash(i) = ActiveSheet.Cells(54, i + 5).Value
B2dash(i) = ActiveSheet.Cells(55, i + 5).Value
B6dash(i) = ActiveSheet.Cells(56, i + 5).Value

C1dash(i) = ActiveSheet.Cells(59, i + 1).Value
C2dash(i) = ActiveSheet.Cells(60, i + 1).Value
C6dash(i) = ActiveSheet.Cells(61, i + 1).Value

D1dash(i) = ActiveSheet.Cells(59, i + 5).Value
D2dash(i) = ActiveSheet.Cells(60, i + 5).Value
D6dash(i) = ActiveSheet.Cells(61, i + 5).Value

Worksheets("ABD Matrix").Activate

ActiveSheet.Cells(j + 24, i + 3).Value = A1dash(i)
ActiveSheet.Cells(j + 24, i + 6).Value = A2dash(i)
ActiveSheet.Cells(j + 24, i + 9).Value = A6dash(i)

ActiveSheet.Cells(j + 24, i + 12).Value = B1dash(i)
ActiveSheet.Cells(j + 24, i + 15).Value = B2dash(i)
ActiveSheet.Cells(j + 24, i + 18).Value = B6dash(i)

ActiveSheet.Cells(j + 24, i + 21).Value = C1dash(i)
ActiveSheet.Cells(j + 24, i + 24).Value = C2dash(i)
ActiveSheet.Cells(j + 24, i + 27).Value = C6dash(i)

ActiveSheet.Cells(j + 24, i + 30).Value = D1dash(i)
ActiveSheet.Cells(j + 24, i + 33).Value = D2dash(i)
ActiveSheet.Cells(j + 24, i + 36).Value = D6dash(i)

Next i

ActiveSheet.Cells(j + 24, 43).Value = D11
ActiveSheet.Cells(j + 24, 44).Value = D22

ActiveSheet.Cells(j + 24, 53).Value = A11
ActiveSheet.Cells(j + 24, 54).Value = A12
ActiveSheet.Cells(j + 24, 55).Value = A21
ActiveSheet.Cells(j + 24, 56).Value = A22
ActiveSheet.Cells(j + 24, 57).Value = A26
ActiveSheet.Cells(j + 24, 58).Value = A62
ActiveSheet.Cells(j + 24, 59).Value = A16
ActiveSheet.Cells(j + 24, 60).Value = A61
ActiveSheet.Cells(j + 24, 61).Value = A66

ActiveSheet.Cells(j + 24, 62).Value = B11
ActiveSheet.Cells(j + 24, 63).Value = B12
ActiveSheet.Cells(j + 24, 64).Value = B21
```

```
ActiveSheet.Cells(j + 24, 65).Value = B22
ActiveSheet.Cells(j + 24, 66).Value = B26
ActiveSheet.Cells(j + 24, 67).Value = B62
ActiveSheet.Cells(j + 24, 68).Value = B16
ActiveSheet.Cells(j + 24, 69).Value = B61
ActiveSheet.Cells(j + 24, 70).Value = B66

ActiveSheet.Cells(j + 24, 71).Value = D12
ActiveSheet.Cells(j + 24, 72).Value = D21
ActiveSheet.Cells(j + 24, 73).Value = D26
ActiveSheet.Cells(j + 24, 74).Value = D62
ActiveSheet.Cells(j + 24, 75).Value = D16
ActiveSheet.Cells(j + 24, 76).Value = D61
ActiveSheet.Cells(j + 24, 77).Value = D66

Next j

End Sub
```

Tensile and Compressive strengths as functions of time (Phenolic)

```
Sub StrengthsVsTime()

Rem  Carry out strength calculations for all time intervals
For j = 1 To 39
Dim Time(50)

Worksheets("Temp Profile").Activate
Time(j) = ActiveSheet.Cells(j + 7, 1).Value

Worksheets("Strengths vs Time").Activate
ActiveSheet.Cells(j + 30, 4).Value = Time(j)
ActiveSheet.Cells(j + 77, 4).Value = Time(j)

Rem Calculate E1 per node
For i = 1 To 17

Rem input temperature values
Dim tem(20)

Worksheets("Temp profile").Activate
tem(i) = ActiveSheet.Cells(j + 7, i + 1).Value

Rem input RRC values
Dim rc(20)


Worksheets("RRC").Activate
rc(i) = ActiveSheet.Cells(j + 7, i + 1).Value


Rem calculate E1
Dim E1(20)
Dim cE1(20)
Dim TanhE1(20)
Dim cE1s(20)
Dim TanhE1S(20)

Worksheets("Model").Activate
Rem UD paramters
TgE1 = ActiveSheet.Cells(4, 2)
kE1 = ActiveSheet.Cells(4, 3)
MuE1 = ActiveSheet.Cells(4, 4)
MrE1 = ActiveSheet.Cells(4, 5)
Rem CSM NEedle weave paramters
TgE1S = ActiveSheet.Cells(11, 2)
```

```
kE1S = ActiveSheet.Cells(11, 3)
MuE1S = ActiveSheet.Cells(11, 4)
MrE1S = ActiveSheet.Cells(11, 5)

If i >= 4 And i <= 14 Then

cE1(i) = kE1 * (tem(i) - TgE1)
TanhE1(i) = (Exp(cE1(i)) - Exp(-cE1(i))) / (Exp(cE1(i)) + Exp(-cE1(i)))
E1(i) = (((1 - TanhE1(i)) * (MuE1 - MrE1)) / 2 + MrE1) * (rc(i) / 100) ^ 1
Else:

cE1s(i) = kE1S * (tem(i) - TgE1S)
TanhE1S(i) = (Exp(cE1s(i)) - Exp(-cE1s(i))) / (Exp(cE1s(i)) + Exp(-cE1s(i)))
E1(i) = (((1 - TanhE1S(i)) * (MuE1S - MrE1S)) / 2 + MrE1S) * (rc(i) / 100) ^ 1
End If
Rem Lamina node strength
Dim sT(20)
Dim sC(20)

Rem UD properties

TgsT = ActiveSheet.Cells(7, 2)
TgsC = ActiveSheet.Cells(8, 2)
ksT = ActiveSheet.Cells(7, 3)
ksC = ActiveSheet.Cells(8, 3)
MusT = ActiveSheet.Cells(7, 4)
MusC = ActiveSheet.Cells(8, 4)
MrsT = ActiveSheet.Cells(7, 5)
MrsC = ActiveSheet.Cells(8, 5)

Rem CSM properties

TgsTS = ActiveSheet.Cells(14, 2)
TgsCS = ActiveSheet.Cells(15, 2)
ksTS = ActiveSheet.Cells(14, 3)
ksCS = ActiveSheet.Cells(15, 3)
MusTS = ActiveSheet.Cells(14, 4)
MusCS = ActiveSheet.Cells(15, 4)
MrsTS = ActiveSheet.Cells(14, 5)
MrsCS = ActiveSheet.Cells(15, 5)

If i >= 4 And i <= 14 Then

csT = ksT * (tem(i) - TgsT)
TanhsT = (Exp(csT) - Exp(-csT)) / (Exp(csT) + Exp(-csT))
sT(i) = (((1 - TanhsT) * (MusT - MrsT)) / 2 + MrsT) * (rc(i) / 100) ^ 0

csC = ksC * (tem(i) - TgsC)
```

```
TanhsC = (Exp(csC) - Exp(-csC)) / (Exp(csC) + Exp(-csC))
sC(i) = (((1 - TanhsC) * (MusC - MrsC)) / 2 + MrsC) * (rc(i) / 100) ^ 0

Else:

csTS = ksTS * (tem(i) - TgsTS)
TanhsTS = (Exp(csTS) - Exp(-csTS)) / (Exp(csTS) + Exp(-csTS))
sT(i) = (((1 - TanhsTS) * (MusTS - MrsTS)) / 2 + MrsTS) * (rc(i) / 100) ^ 1

csCS = ksCS * (tem(i) - TgsCS)
TanhsCS = (Exp(csCS) - Exp(-csCS)) / (Exp(csCS) + Exp(-csCS))
sC(i) = (((1 - TanhsCS) * (MusCS - MrsCS)) / 2 + MrsCS) * (rc(i) / 100) ^ 1
End If
Next i

Rem Stress at a point (tensile and compressive loading)

Dim TStress(20)
Dim TStren(80)
Dim CStress(20)
Dim CStren(80)

For k = 0 To 70
For i = 1 To 17
strain = k / 1000


TStress(i) = strain * E1(i) * 1000
CStress(i) = strain * E1(i) * 1000

If TStress(i) >= sT(i) Then TStress(i) = 0
If CStress(i) >= sC(i) Then CStress(i) = 0
Next i

TStren(k) = (0.5 / 3 * ((TStress(1) + TStress(17)) + 4 * (TStress(2) + TStress(4) +
TStress(6) + TStress(8) + TStress(10) + TStress(12) + TStress(14) + TStress(16)) + 2
* (TStress(3) + TStress(5) + TStress(7) + TStress(9) + TStress(11) + TStress(13) +
TStress(15)))) / 8
CStren(k) = (0.5 / 3 * ((CStress(1) + CStress(17)) + 4 * (CStress(2) + CStress(4) +
CStress(6) + CStress(8) + CStress(10) + CStress(12) + CStress(14) + CStress(16)) +
2 * (CStress(3) + CStress(5) + CStress(7) + CStress(9) + CStress(11) + CStress(13)
+ CStress(15)))) / 8

Worksheets("Strengths vs Time").Activate
ActiveSheet.Cells(j + 30, k + 5).Value = TStren(k)
ActiveSheet.Cells(j + 77, k + 5).Value = CStren(k)

Next k
Next j
```

```
End Sub
```

Stress strain curve modelling (Phenolic)

```
Sub StressStrainCurves()

For j = 1 To 39

Dim Time(50)
Dim tem(20)
Dim TStress(20)
Dim sT(20)
Dim TStren(200)

Worksheets("Temp profile").Activate
Time(j) = ActiveSheet.Cells(j + 7, 1).Value

Worksheets("Output").Activate
ActiveSheet.Cells(j + 7, 1).Value = Time(j)


For k = 0 To 70

For i = 1 To 17

Worksheets("Temp Profile").Activate
tem(i) = ActiveSheet.Cells(j + 7, i + 1).Value


If 0 < tem(i) <= 48.5 Then E = 13.25          'Alter values here
If 0 < tem(i) <= 48.5 Then sig = 700         'Alter values here

If 48.5 < tem(i) <= 90 Then E = 12.9          'Alter values here
If 48.5 < tem(i) <= 90 Then sig = 800        'Alter values here

If 90 < tem(i) <= 140 Then E = 12.1           'Alter values here
If 90 < tem(i) <= 140 Then sig = 790       'Alter values here

If 140 < tem(i) <= 215 Then E = 11.3          'Alter values here
If 140 < tem(i) <= 215 Then sig = 780       'Alter values here

If 215 < tem(i) <= 275 Then E = 11.5          'Alter values here
If 215 < tem(i) <= 275 Then sig = 800       'Alter values here

If 275 < tem(i) <= 300 Then E = 10.8          'Alter values here
If 275 < tem(i) <= 300 Then sig = 1150        'Alter values here
```

```
If 300 < tem(i) Then E = 1000000
If 300 < tem(i) Then sig = 1000000


strain = k / 1000

TStress(i) = sig * (1 - Exp((-(1000 * E) * strain) / sig))

TgsT = 100    'Alter values here
ksT = 0.035  'Alter values here
MusT = 400   'Alter values here 500
MrsT = 278    'Alter values here 347


csT = ksT * (tem(i) - TgsT)
TanhsT = (Exp(csT) - Exp(-csT)) / (Exp(csT) + Exp(-csT))
sT(i) = (((1 - TanhsT) * (MusT - MrsT)) / 2 + MrsT)


If TStress(i) >= sT(i) Then TStress(i) = 0

Next i

'Trapezium rule

TStren(k) = ((0.5 / 2) * ((TStress(1) + TStress(17)) + 2 * (TStress(2) + TStress(3) +
TStress(4) + TStress(5) + TStress(6) + TStress(7) + TStress(8) + TStress(9) +
TStress(10) + TStress(11) + TStress(12) + TStress(13) + TStress(14) + TStress(15) +
TStress(16)))) / 8


Worksheets("Output").Activate
ActiveSheet.Cells(j + 7, k + 2).Value = TStren(k)

Next k

Next j


End Sub
```

Thermal Model Outputs

Table A. Typical temperature evolution output file for an 8mm polyester pultrusion. The table from left to right reads; Time is seconds, temperature (Tfur) in °C, followed by the temperatures in °C at nodes, 1, 3, 5, 40, 47, 49 and 51.

time	Tfur	ND1	ND2	ND3	ND4	ND5	ND6	ND7
		1	3	5	40	47	49	51
0	0	17	17	17	17	17	17	17
3.11	708.5	209.8	105	46.7	17	17	17	17
6.23	708.5	265.6	160.6	86.7	17	17	17	17
9.34	708.5	303.4	200.2	120.5	17.1	17	17	17
12.46	708.5	332.4	231.2	149.1	17.4	17.1	17	17
15.57	708.5	355.9	256.8	173.8	18.3	17.3	17.2	17.1
18.69	708.5	375.5	278.5	195.5	19.7	17.9	17.5	17.4
21.8	708.5	392.2	297.3	214.7	21.8	18.9	18.2	18
24.92	708.5	406.5	313.6	231.9	24.6	20.4	19.2	19
28.03	708.5	418.5	327.7	247.2	27.9	22.4	20.8	20.4
31.15	708.5	428.4	339.6	260.8	31.7	25	22.9	22.4
34.26	708.5	436.4	349.6	272.8	36	28	25.4	24.8
37.37	708.5	442.8	357.8	283.2	40.7	31.5	28.5	27.7
40.49	708.5	447.9	364.6	292.3	45.8	35.4	31.9	31
43.6	708.5	452	370.1	300.1	51.1	39.7	35.8	34.7
46.72	708.5	455.3	374.8	307	56.6	44.4	40	38.8
49.83	708.5	458.1	378.8	313	62.4	49.3	44.6	43.1
52.95	708.5	460.6	382.2	318.3	68.2	54.4	49.4	47.8
56.06	708.5	462.8	385.2	323.1	74.2	59.7	54.4	52.6
59.18	708.5	464.8	388	327.4	80.2	65.2	59.6	57.5
62.29	708.5	466.6	390.4	331.4	86.2	70.8	64.9	62.6
65.41	708.5	468.3	392.8	335	92.2	76.4	70.2	67.8
68.52	708.5	470	394.9	338.4	98.1	82.1	75.7	73
71.63	708.5	471.7	397	341.5	104.1	87.7	81.1	78.2
74.75	708.5	473.3	398.9	344.5	109.9	93.3	86.5	83.4
77.86	708.5	474.9	400.9	347.3	115.7	98.9	91.9	88.6
80.98	708.5	476.5	402.7	350	121.4	104.5	97.3	93.7
84.09	708.5	478.1	404.5	352.6	127	109.9	102.5	98.8
87.21	708.5	479.7	406.3	355.1	132.4	115.3	107.8	103.7
90.32	708.5	481.4	408.1	357.5	137.8	120.6	112.9	108.6
93.44	708.5	483.1	409.9	359.9	143.1	125.8	117.9	113.4
96.55	708.5	484.8	411.8	362.2	148.2	130.9	122.8	118.1
99.67	708.5	486.6	413.6	364.4	153.3	135.8	127.6	122.6
102.78	708.5	488.5	415.4	366.6	158.2	140.7	132.3	127.1
105.89	708.5	490.4	417.3	368.7	163	145.4	136.9	131.4
109.01	708.5	492.3	419.2	370.9	167.7	150.1	141.3	135.6
112.12	708.5	494.4	421.1	372.9	172.2	154.6	145.7	139.7
115.24	708.5	496.5	423.1	375	176.7	159	149.9	143.7
118.35	708.5	498.6	425.1	377.1	181	163.2	154	147.6
121.47	708.5	500.8	427.2	379.1	185.3	167.4	158	151.4
124.58	708.5	503	429.3	381.1	189.4	171.5	161.9	155
127.7	708.5	505.2	431.4	383.1	193.4	175.4	165.7	158.6

130.81	708.5	507.5	433.5	385	197.3	179.2	169.4	162
133.93	708.5	509.7	435.7	386.9	201.1	183	172.9	165.3
137.04	708.5	511.8	437.8	388.8	204.8	186.6	176.4	168.6
140.15	708.5	513.9	439.9	390.6	208.4	190.1	179.8	171.7
143.27	708.5	516	442	392.4	211.9	193.6	183	174.8
146.38	708.5	517.9	444.1	394.2	215.3	196.9	186.2	177.7
149.5	708.5	519.8	446.2	395.9	218.6	200.1	189.3	180.6
152.61	708.5	521.7	448.3	397.6	221.8	203.3	192.3	183.3
155.73	708.5	523.5	450.4	399.3	224.9	206.3	195.2	186
158.84	708.5	525.3	452.5	401	228	209.3	198	188.6
161.96	708.5	527.1	454.7	402.7	230.9	212.1	200.7	191.1
165.07	708.5	528.9	456.9	404.3	233.8	214.9	203.4	193.8
168.19	708.5	530.7	459.1	406	236.6	217.7	206.1	196.4
171.3	708.5	532.5	461.4	407.7	239.3	220.4	208.7	198.8
174.41	708.5	534.4	463.6	409.3	241.9	223	211.2	201.1
177.53	708.5	536.2	465.9	411	244.5	225.5	213.6	203.3
180.64	708.5	538.1	468.2	412.7	247	228	215.9	205.4
183.76	708.5	539.9	470.5	414.4	249.4	230.3	218.2	207.5
186.87	708.5	541.7	472.7	416.1	251.8	232.6	220.3	209.5
189.99	708.5	543.5	474.9	417.8	254	234.8	222.4	211.4
193.1	708.5	545.2	477	419.5	256.2	237	224.4	213.3
196.22	708.5	546.9	479.1	421.2	258.4	239.1	226.4	215.1
199.33	708.5	548.5	481.1	422.9	260.4	241.1	228.3	216.8
202.45	708.5	550.1	483.1	424.5	262.4	243	230.1	218.5
205.56	708.5	551.7	485	426.2	264.3	244.9	231.9	220.1
208.67	708.5	553.2	486.9	427.9	266.2	246.7	233.6	221.7
211.79	708.5	554.7	488.8	429.6	268	248.4	235.3	223.2
214.9	708.5	556.2	490.7	431.3	269.8	250.1	236.8	224.6
218.02	708.5	557.7	492.6	433	271.5	251.8	238.4	226.1
221.13	708.5	559.2	494.4	434.7	273.1	253.4	239.9	227.4
224.25	708.5	560.7	496.3	436.5	274.7	254.9	241.3	228.7
227.36	708.5	562.1	498.1	438.2	276.2	256.4	242.7	230
230.48	708.5	563.5	499.8	439.9	277.7	257.8	244.1	231.2
233.59	708.5	564.9	501.6	441.6	279.1	259.2	245.3	232.4
236.71	708.5	566.2	503.2	443.2	280.5	260.5	246.6	233.5
239.82	708.5	567.5	504.8	444.9	281.8	261.8	247.8	234.6
242.93	708.5	568.7	506.3	446.5	283.1	263	249	235.7
246.05	708.5	569.8	507.8	448.1	284.3	264.2	250.1	236.7
249.16	708.5	570.9	509.2	449.6	285.5	265.4	251.2	237.7
252.28	708.5	572	510.5	451.1	286.7	266.5	252.2	238.6
255.39	708.5	573.1	511.8	452.6	287.8	267.6	253.2	239.6
258.51	708.5	574.1	513.1	454.1	288.9	268.6	254.2	240.4
261.62	708.5	575.1	514.3	455.6	289.9	269.6	255.1	241.3
264.74	708.5	576	515.6	457	290.9	270.6	256	242.1
267.85	708.5	577	516.8	458.5	291.9	271.5	256.9	242.9
270.97	708.5	578	518	460	292.8	272.4	257.8	243.7
274.08	708.5	578.9	519.2	461.4	293.7	273.3	258.6	244.4
277.19	708.5	579.9	520.5	462.9	294.6	274.1	259.4	245.1
280.31	708.5	580.8	521.7	464.3	295.4	274.9	260.1	245.8
283.42	708.5	581.8	522.9	465.7	296.3	275.7	260.8	246.5
286.54	708.5	582.7	524	467.2	297.1	276.5	261.6	247.1
289.65	708.5	583.6	525.2	468.6	297.8	277.2	262.2	247.7
292.77	708.5	584.6	526.4	470	298.6	277.9	262.9	248.3

295.88	708.5	585.5	527.5	471.3	299.3	278.6	263.5	248.9
299	708.5	586.4	528.7	472.7	300	279.3	264.2	249.5
302.11	708.5	587.2	529.8	474.1	300.7	279.9	264.8	250
305.23	708.5	588.1	530.9	475.4	301.4	280.6	265.4	250.6
308.34	708.5	589	532	476.7	302	281.2	265.9	251.1
311.45	708.5	589.8	533.1	478	302.6	281.8	266.5	251.6
314.57	708.5	590.7	534.1	479.3	303.3	282.4	267	252
317.68	708.5	591.5	535.2	480.5	303.9	282.9	267.5	252.5
320.8	708.5	592.3	536.2	481.8	304.4	283.5	268	253
323.91	708.5	593.1	537.2	483	305	284	268.5	253.4
327.03	708.5	593.9	538.2	484.2	305.6	284.5	269	253.8
330.14	708.5	594.6	539.2	485.4	306.1	285	269.5	254.3
333.26	708.5	595.4	540.2	486.5	306.7	285.5	269.9	254.7
336.37	708.5	596.2	541.2	487.7	307.2	286	270.4	255.1
339.49	708.5	596.9	542.1	488.8	307.7	286.5	270.8	255.5
342.6	708.5	597.6	543	490	308.2	287	271.3	255.9
345.71	708.5	598.3	544	491.1	308.7	287.4	271.7	256.3
348.83	708.5	599.1	544.9	492.2	309.2	287.9	272.1	256.6
351.94	708.5	599.8	545.8	493.2	309.7	288.3	272.5	257
355.06	708.5	600.4	546.7	494.3	310.2	288.8	272.9	257.4
358.17	708.5	601.1	547.5	495.4	310.6	289.2	273.3	257.7
361.29	708.5	601.8	548.4	496.4	311.1	289.6	273.7	258.1
364.4	708.5	602.5	549.2	497.4	311.6	290	274.1	258.4
367.52	708.5	603.1	550.1	498.5	312	290.5	274.5	258.7
370.63	708.5	603.8	550.9	499.5	312.5	290.9	274.8	259.1
373.75	708.5	604.4	551.7	500.4	312.9	291.3	275.2	259.4
376.86	708.5	605	552.6	501.4	313.3	291.6	275.5	259.7
379.97	708.5	605.7	553.4	502.4	313.8	292	275.9	260
383.09	708.5	606.3	554.1	503.3	314.2	292.4	276.2	260.3
386.2	708.5	606.9	554.9	504.3	314.6	292.8	276.6	260.6
389.32	708.5	607.5	555.7	505.2	315	293.2	276.9	260.9
392.43	708.5	608.1	556.5	506.1	315.4	293.5	277.3	261.2
395.55	708.5	608.7	557.2	507	315.8	293.9	277.6	261.5
398.66	708.5	609.2	558	507.9	316.2	294.3	277.9	261.8
401.78	708.5	609.8	558.7	508.8	316.6	294.6	278.3	262.1
404.89	708.5	610.4	559.4	509.7	317	295	278.6	262.4
408.01	708.5	610.9	560.1	510.6	317.4	295.3	278.9	262.7
411.12	708.5	611.5	560.8	511.4	317.8	295.7	279.2	263
414.23	708.5	612	561.5	512.3	318.2	296	279.5	263.3
417.35	708.5	612.5	562.2	513.1	318.6	296.4	279.8	263.6
420.46	708.5	613.1	562.9	514	319	296.7	280.2	263.8
423.58	708.5	613.6	563.6	514.8	319.4	297.1	280.5	264.1
426.69	708.5	614.1	564.3	515.6	319.7	297.4	280.8	264.4
429.81	708.5	614.6	564.9	516.4	320.1	297.7	281.1	264.7
432.92	708.5	615.1	565.6	517.2	320.5	298.1	281.4	264.9
436.04	708.5	615.6	566.2	518	320.9	298.4	281.7	265.2
439.15	708.5	616.1	566.9	518.7	321.2	298.7	282	265.5
442.27	708.5	616.6	567.5	519.5	321.6	299.1	282.3	265.7
445.38	708.5	617.1	568.1	520.3	322	299.4	282.6	266
448.49	708.5	617.6	568.7	521	322.4	299.7	282.9	266.3
451.61	708.5	618	569.3	521.7	322.7	300	283.1	266.5
454.72	708.5	618.5	569.9	522.5	323.1	300.4	283.4	266.8
457.84	708.5	618.9	570.5	523.2	323.4	300.7	283.7	267

460.95	708.5	619.4	571.1	523.9	323.8	301	284	267.3
464.07	708.5	619.8	571.7	524.6	324.2	301.3	284.3	267.5
467.18	708.5	620.3	572.3	525.3	324.5	301.6	284.6	267.8
470.3	708.5	620.7	572.9	526	324.9	301.9	284.9	268
473.41	708.5	621.2	573.4	526.7	325.2	302.2	285.1	268.3
476.53	708.5	621.6	574	527.4	325.6	302.6	285.4	268.5
479.64	708.5	622	574.5	528.1	325.9	302.9	285.7	268.8
482.75	708.5	622.4	575.1	528.7	326.3	303.2	286	269
485.87	708.5	622.9	575.6	529.4	326.6	303.5	286.3	269.3
488.98	708.5	623.3	576.2	530	327	303.8	286.5	269.5
492.1	708.5	623.7	576.7	530.7	327.3	304.1	286.8	269.8
495.21	708.5	624.1	577.2	531.3	327.7	304.4	287.1	270
498.33	708.5	624.5	577.7	532	328	304.7	287.3	270.2
501.44	708.5	624.9	578.3	532.6	328.3	305	287.6	270.5
504.56	708.5	625.3	578.8	533.2	328.7	305.3	287.9	270.7
507.67	708.5	625.6	579.3	533.8	329	305.6	288.2	271
510.79	708.5	626	579.8	534.4	329.4	305.9	288.4	271.2
513.9	708.5	626.4	580.3	535	329.7	306.2	288.7	271.4
517.01	708.5	626.8	580.7	535.6	330	306.5	289	271.7
520.13	708.5	627.1	581.2	536.2	330.4	306.8	289.2	271.9
523.24	708.5	627.5	581.7	536.8	330.7	307.1	289.5	272.1
526.36	708.5	627.9	582.2	537.4	331	307.4	289.7	272.4
529.47	708.5	628.2	582.7	538	331.4	307.6	290	272.6
532.59	708.5	628.6	583.1	538.5	331.7	307.9	290.3	272.8
535.7	708.5	628.9	583.6	539.1	332	308.2	290.5	273.1
538.82	708.5	629.3	584	539.6	332.4	308.5	290.8	273.3
541.93	708.5	629.6	584.5	540.2	332.7	308.8	291	273.5
545.05	708.5	630	584.9	540.7	333	309.1	291.3	273.7
548.16	708.5	630.3	585.4	541.3	333.3	309.4	291.5	274
551.27	708.5	630.6	585.8	541.8	333.7	309.6	291.8	274.2
554.39	708.5	631	586.2	542.3	334	309.9	292.1	274.4
557.5	708.5	631.3	586.7	542.9	334.3	310.2	292.3	274.6
560.62	708.5	631.6	587.1	543.4	334.6	310.5	292.6	274.9
563.73	708.5	632	587.5	543.9	335	310.8	292.8	275.1
566.85	708.5	632.3	587.9	544.4	335.3	311.1	293.1	275.3
569.96	708.5	632.6	588.4	544.9	335.6	311.3	293.3	275.5
573.08	708.5	632.9	588.8	545.4	335.9	311.6	293.6	275.8
576.19	708.5	633.2	589.2	545.9	336.2	311.9	293.8	276
579.31	708.5	633.5	589.6	546.4	336.6	312.2	294.1	276.2
582.42	708.5	633.8	590	546.9	336.9	312.4	294.3	276.4
585.53	708.5	634.1	590.4	547.4	337.2	312.7	294.6	276.6
588.65	708.5	634.4	590.8	547.9	337.5	313	294.8	276.9
591.76	708.5	634.7	591.2	548.4	337.8	313.3	295	277.1
594.88	708.5	635	591.5	548.8	338.1	313.5	295.3	277.3
597.99	708.5	635.3	591.9	549.3	338.5	313.8	295.5	277.5
601.11	708.5	635.6	592.3	549.8	338.8	314.1	295.8	277.7
604.22	708.5	635.9	592.7	550.2	339.1	314.3	296	277.9
607.34	708.5	636.2	593	550.7	339.4	314.6	296.3	278.2
610.45	708.5	636.4	593.4	551.1	339.7	314.9	296.5	278.4
613.57	708.5	636.7	593.8	551.6	340	315.2	296.7	278.6
616.68	708.5	637	594.1	552	340.3	315.4	297	278.8
619.79	708.5	637.3	594.5	552.5	340.6	315.7	297.2	279
622.91	708.5	637.5	594.9	552.9	340.9	315.9	297.4	279.2

626.02	708.5	637.8	595.2	553.3	341.2	316.2	297.7	279.4
629.14	708.5	638.1	595.6	553.8	341.5	316.5	297.9	279.6
632.25	708.5	638.3	595.9	554.2	341.8	316.7	298.1	279.8
635.37	708.5	638.6	596.2	554.6	342.2	317	298.4	280
638.48	708.5	638.8	596.6	555	342.5	317.3	298.6	280.2
641.6	708.5	639.1	596.9	555.4	342.8	317.5	298.8	280.4
644.71	708.5	639.3	597.3	555.8	343.1	317.8	299.1	280.6
647.83	708.5	639.6	597.6	556.2	343.4	318	299.3	280.9
650.94	708.5	639.8	597.9	556.7	343.7	318.3	299.5	281.1
654.05	708.5	640.1	598.2	557.1	344	318.6	299.8	281.3
657.17	708.5	640.3	598.6	557.4	344.3	318.8	300	281.5
660.28	708.5	640.6	598.9	557.8	344.6	319.1	300.2	281.7
663.4	708.5	640.8	599.2	558.2	344.9	319.3	300.5	281.9
666.51	708.5	641.1	599.5	558.6	345.2	319.6	300.7	282.1
669.63	708.5	641.3	599.8	559	345.5	319.8	300.9	282.3
672.74	708.5	641.5	600.1	559.4	345.8	320.1	301.1	282.5
675.86	708.5	641.8	600.4	559.8	346	320.3	301.4	282.7
678.97	708.5	642	600.8	560.1	346.3	320.6	301.6	282.9
682.09	708.5	642.2	601.1	560.5	346.6	320.8	301.8	283.1
685.2	708.5	642.5	601.4	560.9	346.9	321.1	302	283.3
688.31	708.5	642.7	601.7	561.2	347.2	321.3	302.3	283.4
691.43	708.5	642.9	602	561.6	347.5	321.6	302.5	283.6
694.54	708.5	643.1	602.2	562	347.8	321.8	302.7	283.8
697.66	708.5	643.3	602.5	562.3	348.1	322.1	302.9	284
700.77	708.5	643.6	602.8	562.7	348.4	322.3	303.1	284.2
703.89	708.5	643.8	603.1	563	348.7	322.6	303.4	284.4
707	708.5	644	603.4	563.4	349	322.8	303.6	284.6
710.12	708.5	644.2	603.7	563.7	349.2	323.1	303.8	284.8
713.23	708.5	644.4	604	564.1	349.5	323.3	304	285
716.35	708.5	644.6	604.2	564.4	349.8	323.5	304.2	285.2
719.46	708.5	644.8	604.5	564.8	350.1	323.8	304.4	285.4
722.57	708.5	645	604.8	565.1	350.4	324	304.6	285.6
725.69	708.5	645.2	605	565.4	350.7	324.3	304.9	285.7
728.8	708.5	645.4	605.3	565.8	351	324.5	305.1	285.9
731.92	708.5	645.6	605.6	566.1	351.2	324.7	305.3	286.1
735.03	708.5	645.8	605.9	566.4	351.5	325	305.5	286.3
738.15	708.5	646	606.1	566.7	351.8	325.2	305.7	286.5
741.26	708.5	646.2	606.4	567.1	352.1	325.5	305.9	286.7
744.38	708.5	646.4	606.6	567.4	352.4	325.7	306.1	286.9
747.49	708.5	646.6	606.9	567.7	352.6	325.9	306.4	287.1
750.61	708.5	646.8	607.1	568	352.9	326.2	306.6	287.2
753.72	708.5	647	607.4	568.3	353.2	326.4	306.8	287.4
756.83	708.5	647.2	607.6	568.6	353.5	326.6	307	287.6
759.95	708.5	647.4	607.9	568.9	353.8	326.9	307.2	287.8
763.06	708.5	647.6	608.1	569.2	354	327.1	307.4	288
766.18	708.5	647.8	608.4	569.5	354.3	327.3	307.6	288.2
769.29	708.5	647.9	608.6	569.8	354.6	327.6	307.8	288.3
772.41	708.5	648.1	608.9	570.1	354.9	327.8	308	288.5
775.52	708.5	648.3	609.1	570.4	355.1	328	308.2	288.7
778.64	708.5	648.5	609.3	570.7	355.4	328.3	308.4	288.9

Table B. Typical residual resin content output file for an 8mm polyester pultrusion. The table from left to right reads; Time is seconds, followed by the residual resin content in % at nodes 1, 3, 5, 40, 47, 49 and 51.

(s)	RRC at ND= 1	ND= 3	ND= 5	ND=40	ND=47	ND=49	ND=51
0	100	100	100	100	100	100	100
3.1	100	100	100	100	100	100	100
6.2	100	100	100	100	100	100	100
9.3	100	100	100	100	100	100	100
12.5	99.999	100	100	100	100	100	100
15.6	99.992	100	100	100	100	100	100
18.7	99.966	99.999	100	100	100	100	100
21.8	99.89	99.993	100	100	100	100	100
24.9	99.709	99.979	100	100	100	100	100
28	99.347	99.943	100	100	100	100	100
31.1	98.712	99.871	100	100	100	100	100
34.3	97.727	99.743	100	100	100	100	100
37.4	96.344	99.538	99.996	100	100	100	100
40.5	94.557	99.243	99.992	100	100	100	100
43.6	92.386	98.844	99.983	100	100	100	100
46.7	89.871	98.338	99.971	100	100	100	100
49.8	87.056	97.72	99.952	100	100	100	100
52.9	83.986	96.991	99.926	100	100	100	100
56.1	80.703	96.151	99.892	100	100	100	100
59.2	77.245	95.2	99.847	100	100	100	100
62.3	73.647	94.141	99.792	100	100	100	100
65.4	69.941	92.974	99.723	100	100	100	100
68.5	66.153	91.701	99.64	100	100	100	100
71.6	62.311	90.322	99.541	100	100	100	100
74.7	58.438	88.839	99.425	100	100	100	100
77.9	54.557	87.251	99.291	100	100	100	100
81	50.69	85.558	99.135	100	100	100	100
84.1	46.857	83.762	98.958	100	100	100	100
87.2	43.077	81.861	98.756	100	100	100	100
90.3	39.371	79.855	98.528	100	100	100	100
93.4	35.758	77.743	98.272	100	100	100	100
96.6	32.256	75.527	97.985	100	100	100	100
99.7	28.884	73.205	97.666	100	100	100	100
102.8	25.661	70.777	97.311	100	100	100	100
105.9	22.606	68.244	96.917	100	100	100	100
109	19.735	65.608	96.483	100	100	100	100
112.1	17.064	62.869	96.004	100	100	100	100
115.2	14.611	60.031	95.478	100	100	100	100
118.4	12.386	57.099	94.902	100	100	100	100
121.5	10.4	54.079	94.271	100	100	100	100
124.6	8.659	50.981	93.582	100	100	100	100

127.7	7.163	47.817	92.833	100	100	100	100
130.8	5.908	44.602	92.019	100	100	100	100
133.9	4.882	41.357	91.137	100	100	100	100
137	4.067	38.104	90.185	100	100	100	100
140.2	3.44	34.869	89.16	100	100	100	100
143.3	2.972	31.681	88.06	100	100	100	100
146.4	2.636	28.568	86.883	100	100	100	100
149.5	2.402	25.559	85.628	100	100	100	100
152.6	2.246	22.681	84.294	100	100	100	100
155.7	2.145	19.956	82.879	100	100	100	100
158.8	2.082	17.406	81.383	100	100	100	100
162	2.045	15.049	79.804	100	100	100	100
165.1	2.023	12.896	78.141	100	100	100	100
168.2	2.012	10.957	76.392	100	100	100	100
171.3	2.006	9.239	74.557	100	100	100	100
174.4	2.002	7.742	72.634	100	100	100	100
177.5	2.001	6.463	70.623	100	100	100	100
180.6	2	5.393	68.526	100	100	100	100
183.8	2	4.519	66.343	100	100	100	100
186.9	2	3.824	64.077	100	100	100	100
190	2	3.285	61.732	100	100	100	100
193.1	2	2.881	59.314	100	100	100	100
196.2	2	2.586	56.829	100	100	100	100
199.3	2	2.379	54.284	100	100	100	100
202.4	2	2.237	51.689	100	100	100	100
205.6	2	2.143	49.051	100	100	100	100
208.7	2	2.084	46.38	100	100	100	100
211.8	2	2.047	43.687	100	100	100	100
214.9	2	2.026	40.983	100	100	100	100
218	2	2.013	38.281	100	100	100	100
221.1	2	2.007	35.592	99.996	100	100	100
224.2	2	2.003	32.933	99.993	100	100	100
227.4	2	2.001	30.317	99.99	100	100	100
230.5	2	2.001	27.763	99.987	100	100	100
233.6	2	2	25.286	99.984	100	100	100
236.7	2	2	22.903	99.98	100	100	100
239.8	2	2	20.63	99.977	100	100	100
242.9	2	2	18.48	99.974	100	100	100
246	2	2	16.466	99.971	99.998	100	100
249.2	2	2	14.597	99.967	99.996	100	100
252.3	2	2	12.878	99.964	99.994	100	100
255.4	2	2	11.312	99.961	99.993	100	100
258.5	2	2	9.899	99.955	99.991	100	100
261.6	2	2	8.638	99.949	99.989	100	100
264.7	2	2	7.523	99.942	99.987	100	100
267.9	2	2	6.548	99.936	99.985	100	100
271	2	2	5.704	99.93	99.983	100	100
274.1	2	2	4.983	99.923	99.982	100	100
277.2	2	2	4.373	99.917	99.98	100	100

280.3	2	2	3.865	99.91	99.978	100	100
283.4	2	2	3.446	99.904	99.976	100	100
286.5	2	2	3.106	99.894	99.974	100	100
289.7	2	2	2.834	99.884	99.973	100	100
292.8	2	2	2.62	99.875	99.971	100	100
295.9	2	2	2.454	99.865	99.969	99.998	100
299	2	2	2.327	99.855	99.967	99.996	100
302.1	2	2	2.232	99.846	99.963	99.994	100
305.2	2	2	2.161	99.836	99.959	99.993	100
308.3	2	2	2.11	99.825	99.956	99.991	100
311.5	2	2	2.074	99.812	99.952	99.989	100
314.6	2	2	2.049	99.799	99.949	99.987	100
317.7	2	2	2.032	99.786	99.945	99.985	100
320.8	2	2	2.02	99.774	99.941	99.984	100
323.9	2	2	2.013	99.761	99.938	99.982	100
327	2	2	2.008	99.748	99.934	99.98	100
330.1	2	2	2.005	99.734	99.931	99.978	100
333.3	2	2	2.003	99.718	99.927	99.976	100
336.4	2	2	2.002	99.701	99.923	99.975	100
339.5	2	2	2.001	99.685	99.92	99.973	100
342.6	2	2	2	99.669	99.916	99.971	100
345.7	2	2	2	99.653	99.911	99.969	100
348.8	2	2	2	99.637	99.905	99.967	100
351.9	2	2	2	99.618	99.9	99.966	100
355.1	2	2	2	99.599	99.895	99.964	100
358.2	2	2	2	99.58	99.889	99.962	100
361.3	2	2	2	99.561	99.884	99.96	100
364.4	2	2	2	99.541	99.878	99.958	100
367.5	2	2	2	99.522	99.873	99.956	100
370.6	2	2	2	99.501	99.867	99.955	100
373.7	2	2	2	99.478	99.862	99.953	100
376.9	2	2	2	99.456	99.857	99.951	100
380	2	2	2	99.433	99.851	99.949	100
383.1	2	2	2	99.411	99.845	99.947	100
386.2	2	2	2	99.388	99.838	99.946	100
389.3	2	2	2	99.363	99.831	99.944	100
392.4	2	2	2	99.337	99.824	99.942	100
395.5	2	2	2	99.312	99.817	99.94	100
398.7	2	2	2	99.286	99.809	99.938	100
401.8	2	2	2	99.26	99.802	99.937	100
404.9	2	2	2	99.233	99.795	99.935	100
408	2	2	2	99.204	99.788	99.933	100
411.1	2	2	2	99.175	99.78	99.931	99.999
414.2	2	2	2	99.146	99.773	99.927	99.997
417.3	2	2	2	99.117	99.766	99.923	99.996
420.5	2	2	2	99.087	99.757	99.92	99.994
423.6	2	2	2	99.055	99.748	99.916	99.992
426.7	2	2	2	99.023	99.739	99.913	99.99
429.8	2	2	2	98.99	99.73	99.909	99.988

432.9	2	2	2	98.958	99.721	99.905	99.986
436	2	2	2	98.924	99.712	99.902	99.985
439.2	2	2	2	98.888	99.703	99.898	99.983
442.3	2	2	2	98.853	99.694	99.894	99.981
445.4	2	2	2	98.818	99.685	99.891	99.979
448.5	2	2	2	98.781	99.676	99.887	99.977
451.6	2	2	2	98.743	99.665	99.884	99.976
454.7	2	2	2	98.704	99.654	99.88	99.974
457.8	2	2	2	98.666	99.643	99.876	99.972
461	2	2	2	98.627	99.632	99.873	99.97
464.1	2	2	2	98.585	99.621	99.869	99.968
467.2	2	2	2	98.543	99.611	99.866	99.967
470.3	2	2	2	98.501	99.6	99.862	99.965
473.4	2	2	2	98.459	99.589	99.858	99.963
476.5	2	2	2	98.414	99.577	99.855	99.961
479.6	2	2	2	98.369	99.565	99.851	99.959
482.8	2	2	2	98.324	99.552	99.847	99.958
485.9	2	2	2	98.277	99.54	99.844	99.956
489	2	2	2	98.229	99.527	99.84	99.954
492.1	2	2	2	98.181	99.514	99.837	99.952
495.2	2	2	2	98.133	99.502	99.833	99.95
498.3	2	2	2	98.082	99.489	99.827	99.949
501.4	2	2	2	98.031	99.475	99.822	99.947
504.6	2	2	2	97.979	99.461	99.816	99.945
507.7	2	2	2	97.926	99.447	99.811	99.943
510.8	2	2	2	97.872	99.432	99.806	99.941
513.9	2	2	2	97.817	99.418	99.8	99.939
517	2	2	2	97.761	99.403	99.795	99.938
520.1	2	2	2	97.704	99.389	99.789	99.936
523.2	2	2	2	97.646	99.374	99.784	99.934
526.4	2	2	2	97.588	99.358	99.778	99.932
529.5	2	2	2	97.527	99.341	99.773	99.93
532.6	2	2	2	97.466	99.325	99.768	99.929
535.7	2	2	2	97.404	99.309	99.762	99.927
538.8	2	2	2	97.34	99.292	99.757	99.925
541.9	2	2	2	97.276	99.276	99.751	99.923
545	2	2	2	97.211	99.259	99.746	99.921
548.2	2	2	2	97.143	99.24	99.741	99.92
551.3	2	2	2	97.076	99.222	99.735	99.918
554.4	2	2	2	97.007	99.204	99.73	99.916
557.5	2	2	2	96.937	99.186	99.724	99.914
560.6	2	2	2	96.866	99.168	99.717	99.912
563.7	2	2	2	96.793	99.149	99.71	99.911
566.8	2	2	2	96.719	99.129	99.703	99.909
570	2	2	2	96.645	99.109	99.696	99.907
573.1	2	2	2	96.568	99.089	99.689	99.905
576.2	2	2	2	96.491	99.069	99.681	99.903
579.3	2	2	2	96.412	99.05	99.674	99.902
582.4	2	2	2	96.332	99.028	99.667	99.9

585.5	2	2	2	96.251	99.006	99.66	99.898
588.6	2	2	2	96.168	98.984	99.652	99.896
591.8	2	2	2	96.084	98.963	99.645	99.894
594.9	2	2	2	95.998	98.941	99.638	99.893
598	2	2	2	95.912	98.918	99.631	99.891
601.1	2	2	2	95.824	98.895	99.623	99.889
604.2	2	2	2	95.734	98.871	99.616	99.887
607.3	2	2	2	95.643	98.848	99.609	99.885
610.5	2	2	2	95.55	98.824	99.601	99.883
613.6	2	2	2	95.457	98.799	99.592	99.882
616.7	2	2	2	95.361	98.774	99.583	99.88
619.8	2	2	2	95.265	98.749	99.574	99.878
622.9	2	2	2	95.166	98.723	99.565	99.876
626	2	2	2	95.067	98.698	99.556	99.872
629.1	2	2	2	94.965	98.671	99.547	99.868
632.3	2	2	2	94.863	98.644	99.538	99.865
635.4	2	2	2	94.758	98.617	99.529	99.861
638.5	2	2	2	94.653	98.59	99.52	99.858
641.6	2	2	2	94.545	98.562	99.511	99.854
644.7	2	2	2	94.436	98.533	99.502	99.85
647.8	2	2	2	94.325	98.504	99.493	99.847
650.9	2	2	2	94.213	98.475	99.484	99.843
654.1	2	2	2	94.099	98.446	99.474	99.839
657.2	2	2	2	93.983	98.415	99.464	99.836
660.3	2	2	2	93.866	98.385	99.453	99.832
663.4	2	2	2	93.747	98.354	99.442	99.829
666.5	2	2	2	93.626	98.323	99.431	99.825
669.6	2	2	2	93.504	98.291	99.42	99.821
672.7	2	2	2	93.379	98.258	99.409	99.818
675.9	2	2	2	93.254	98.225	99.399	99.814
679	2	2	2	93.125	98.193	99.388	99.811
682.1	2	2	2	92.996	98.159	99.377	99.807
685.2	2	2	2	92.865	98.124	99.366	99.803
688.3	2	2	2	92.732	98.09	99.355	99.8
691.4	2	2	2	92.596	98.055	99.344	99.796
694.5	2	2	2	92.46	98.019	99.332	99.792
697.7	2	2	2	92.321	97.983	99.319	99.789
700.8	2	2	2	92.18	97.947	99.307	99.785
703.9	2	2	2	92.038	97.91	99.294	99.782
707	2	2	2	91.893	97.872	99.281	99.778
710.1	2	2	2	91.747	97.834	99.269	99.774
713.2	2	2	2	91.599	97.796	99.256	99.771
716.3	2	2	2	91.448	97.756	99.243	99.767
719.5	2	2	2	91.296	97.716	99.231	99.764
722.6	2	2	2	91.142	97.677	99.218	99.76
725.7	2	2	2	90.986	97.636	99.205	99.756
728.8	2	2	2	90.828	97.594	99.191	99.753
731.9	2	2	2	90.667	97.553	99.177	99.749
735	2	2	2	90.505	97.511	99.162	99.745

738.1	2	2	2	90.341	97.467	99.148	99.742
741.3	2	2	2	90.174	97.424	99.133	99.738
744.4	2	2	2	90.006	97.381	99.119	99.735
747.5	2	2	2	89.835	97.336	99.105	99.731
750.6	2	2	2	89.662	97.291	99.09	99.725
753.7	2	2	2	89.487	97.245	99.076	99.72
756.8	2	2	2	89.31	97.199	99.061	99.715
759.9	2	2	2	89.131	97.152	99.045	99.709
763.1	2	2	2	88.95	97.105	99.029	99.704
766.2	2	2	2	88.766	97.057	99.013	99.698
769.3	2	2	2	88.58	97.008	98.997	99.693
772.4	2	2	2	88.392	96.959	98.98	99.687
775.5	2	2	2	88.202	96.909	98.964	99.682
778.6	2	2	2	88.01	96.858	98.948	99.677

Engineering Drawings

D
C
B
A
1
2
3
4
5
6
Designed by
Rob Easby
Checked by
Approved by - date
Date
01/08/2008
Material supplied
Comp PE
Edition
Compression sample
(polyester 10mm)
Quantity as specified
150.00
30.00
10.00

D
C
B
A
1
2
3
4
5
6
Designed by
Rob Easby
Checked by
Approved by - date
Date
01/09/2006
Material supplied
Comp Ph
Compression sample
(phenolic 8mm)
Quantity as specified
150.00
30.00
8.00

D
C
B
A
1
2
3
4
5
6
118,00
100,00
8,00
Designed by
Rob Easby
Checked by
Approved by - date
Constrained compression sample
Quantity as specified
Material supplied
Boeing
Sheet
1 / 1

Ø9,50 THRU
Ø10,00 THRU
50,00
20,00
60,00
70,00
15,00
100,00
6,50
30,00
100,00
30,00
Designed by
Rob Easby
Checked by
Approved by
Date
01/09/2006
Material: Aluminium
Tensile heating block
Tensile heating block
Quantity 2

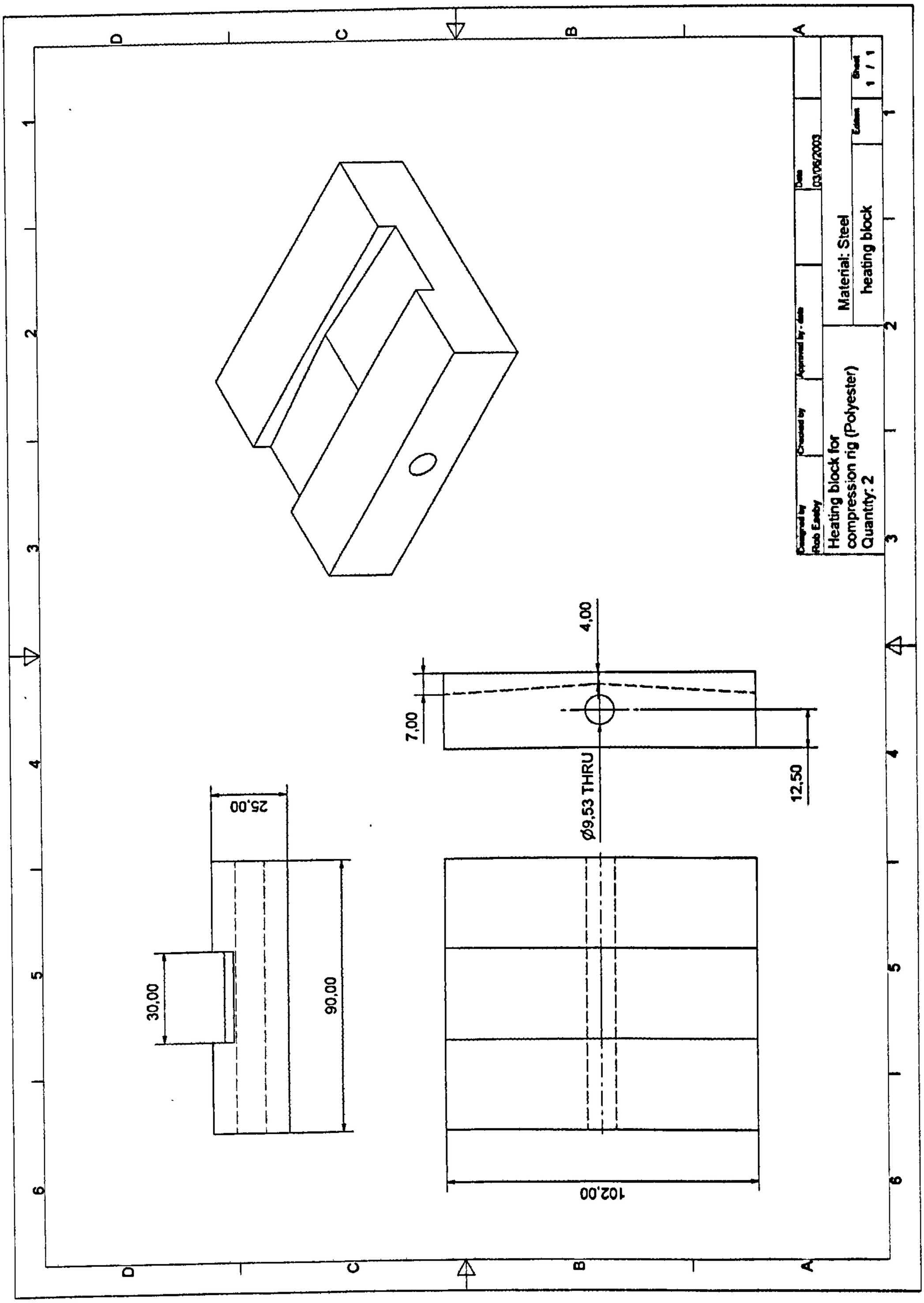
Designed by
Rob Easby
Checked by
Approved by - date
Date
03/06/2003
Heating block for
compression rig (Polyester)
Quantity: 2
Material: Steel
heating block
4,00
7,00
Ø9,53 THRU
12,50
25,00
30,00
90,00
102,00

6,50
90,00
30,00
102,00
Designed by Rob Easby
Checked by
Approved by - date
Date 05/09/2003
Material: Steel
Heating block for compression rig (phenolic)
Quantity: 2
heating block
Edition 1
3,37°
12,50
Ø9,53 THRU
3,50
25,00

45,00
30,00
15,00
Ø10,00 THRU
91,00
45,00
52,00
50,00
10,00
51,00
10,00
10,00
20,00
Designed by
Rob Easby
Checked by
Approved by - date
Date
06/09/2006
Material: Steel
End block 1.3
Compression rig
End block
Quantity 4

Designed by
Rob Easby
Checked by
Approved by - date
Date
06/08/2003
Material: Steel
End plate for
Phenolic compression rig
Quantity 4
end plate
15,00
15,00
27,00
52,00
5,00
51,00
10,00
91,00
8,00
25,00

10.00
49.00
95.00
1.00
8.00
50.00
1.00
Material: Steel
Boeing block top&bot
Constrained comp ng
Top/bottom
Quantity 2
Designed by
Rob Easby
Checked by
Approved by - date
Date
06/09/2006
Sheet
1 / 1

D
C
B
A
1
2
3
4
5
6
10,00
150,00
50,00
1,00
1,00
8,00
50,00
Designed by
Rob Easby
Checked by
Approved by - date
Date
08/08/2006
Material: Steel
Constrained comp ng
Side block
Quantity 2
Boeing block side

Top jaw section for furnace rig
Material: 5mm thick steel plate
Top section
100,00
74,00
200,00
22,50
R20
23,59
M10x1.5 - 6H
100,00
219,00
500,00
Ø15,00 THRU
550,00
42,00
450,00
150,00
200,00
150,00
200,00

Ø15,00 THRU
200,00
200,00
150,00
5,00
Base plate for furnace rig
Quantity 2
Material: 5mm thick steel plate
Base plate
11/07/2003
1 / 1

D
C
B
A
1
2
3
4
5
6
Pivot for furncae rig
Quantity 1
Material: Steel
Pivot
35.75
M24x3 - 6H
21.00
40.00
61.00
122.00

Designed by
Rob Easby
Checked by
Approved by - date
Date
17/01/2005
Material: Steel
Connector A
Connector A for load cell
Quantity 1
M24x3 - 6H
ø16.00
18,57
60,00
40,00
1,00
40.00

A
B
C
D
1
2
3
4
5
6
Ø20,00
13,99
1,00
66,00
M14x1.5 - 6g
14,00
27,00
Designed by
Rob Easby
Checked by
Approved by - date
Date
17/01/2005
Material: Steel
Connector B
Sheet
1 / 1
Connector B for load cell
Quantity 1

D
C
B
A
1
2
3
4
5
6
Designed by
Rob Easby
Checked by
Approved by - date
Date
17/01/2005
Connector A-B assembly
Assembly
Sheet
1 / 1
A-A (1 : 1)
A
A

Material: 15mm thick steel plate
Top jaw A
Top jaw A
Quantity 1
Designed by
Rob Easby
Checked by
Approved by - date
Date
06/09/2006
Sheet
1 / 1
60,00
15,00
542,10
300,00
15,00
499,60
300,00
150,00
333,59
237,76
264,90
392,50
300,00
436,60
Ø25,00 THRU
R42,50
Ø20,00 THRU
Ø12,00 THRU
15,00
155,00
155,00
15,00
400,00
157,50
700,00
400,00

Material: 15mm thick steel plate
Top jaw B
Top jaw B
Quantity 1
112,00
15,00
590,00
300,00
15,00
R12,50
500,00
15,00
55,00
125,00
285,00
165,00
25,00
50,00
492,50
339,40
300,00
254,03
425,00
Ø12,00 THRU
Ø20,00 THRU
129,00
129,00
15,00
15,00
15,00
400,00
700,00
157,50
400,00

Base plate for pool fire rig
Quantity 2
Material: Steel
Base plate
300,00
400,00
700,00
400,00
15,00

100,00
25,00
30,00
Ø25,00 THRU
90,19
1000,00
575,00
M4x0.7 - 6H
M4x0.7 - 6H
Ø12,00 THRU
55,00
15,00
50,00
25,00
10,00
Material: Steel
Extension bar
Extension bar
Quantity 2
06/09/2006

110,00
35,00
Ø25,00
M70X1,5-6H
R5,00
110,00
R5,00
R2,00
30,00
30,00
R5,00
Ø19,00 THRU
R5,00
Material: Steel
Gimble
Cylinder gimble
Quantity 1
Rob Easby
06/08/2008

Ø28,00
16,00
Ø25,00
Spacer for cylinder gimble
Quantity 1
Material: Steel
Spacer
06/09/2006

M14x1.5 - 6g
Ø50,00
50,00
30,00
38,53
2,00
2,00
26,00
M30x1.5 - 6H
Designed by
Rob Easby
Checked by
Approved by - date
Material: Steel
Load cell connector
Load cell connector
Quantity 2